

2012

Characterisation of the parameters influencing the storage and drainage of gas in coal

Raul Maria Melgarejo Florentin
University of Wollongong

UNIVERSITY OF WOLLONGONG

COPYRIGHT WARNING

You may print or download ONE copy of this document for the purpose of your own research or study. The University does not authorise you to copy, communicate or otherwise make available electronically to any other person any copyright material contained on this site. You are reminded of the following:

Copyright owners are entitled to take legal action against persons who infringe their copyright. A reproduction of material that is protected by copyright may be a copyright infringement. A court may impose penalties and award damages in relation to offences and infringements relating to copyright material. Higher penalties may apply, and higher damages may be awarded, for offences and infringements involving the conversion of material into digital or electronic form.

Characterisation of the parameters influencing the storage and drainage of gas in coal

A thesis submitted in fulfilment of the requirements for the award of the degree

Doctor of Philosophy

from

The University of Wollongong

by

Raul Maria Melgarejo Florentin, BE, MEngPrac (Mining)

School of Civil, Mining and Environmental Engineering

2012

AFFIRMATION

I, Raul Maria Melgarejo Florentin, declare that this thesis, submitted in fulfilment of the requirements for the award of Doctor of Philosophy, in the School of Civil, Mining and Environmental Engineering, Faculty of Engineering, University of Wollongong, is wholly my own work unless otherwise referenced or acknowledged. The thesis was completed under the supervision of A/Prof. N. I. Aziz and Dr. L. Nghiem and has not been submitted for qualification at any other academic institution.

Raul Maria Melgarejo Florentin

Dec 2012

ACKNOWLEDGMENTS

I thank my parents and members of my family for their enduring support in getting me to this stage of higher learning. Your love has made it possible for me to reach my dreams.

I thank my supervisors Associate Professor Naj I. Aziz and Dr. Long Nghiem for their continuing support through out this study period. A/Prof. Naj funded my studies from his research grants awarded to him by Broken Hill Propriety Billiton – Illawarra Coal Holdings Pty Ltd. His invaluable support, patience and guidance throughout the study period and his comments and advice contributed to the outcomes of this study. In particular his critical review of the thesis manuscript is appreciated. The assistance of Dr. Long, co-supervisor of the thesis in discussing the results and reading the draft, greatly appreciated. I also would like to thank the technical staff in the School of Civil, Mining and Environmental Engineering of their help. I especially wish to thank Alan Grant, Ian Laird, Bob Rowlan, and Fernando Escibano for their laboratory assistance, and other logistical supports. They were always there whenever I needed help.

Special thanks to Earth Data Pty for its support in performing the proximate analysis of the coal samples.

I am grateful to University of Wollongong and BHP Billiton for the opportunity of the scholarship which allowed me to pursue my PhD studies.

Thanks to Gloria Clark, Bill Clayton, Colin Hadfield and Ken McLain for editing this manuscript generously.

ABSTRACT

Adsorption and desorption characteristics of coal samples of the Bulli seam were examined with respect to coal particle size, gas type, and temperature. Adsorption and desorption tests were conducted by an indirect gravimetric method to determine the gas content in coal. Various coal particle sizes, 0.21 mm, 0.30 mm, 1.18 mm, 2.36 mm, 4.75 mm, 6.70 mm, 8.00 mm and 15 mm cubical blocks were examined in addition to the 54 mm diameter coal core. The coal samples were subjected to gas pressure increase, in steps of 500 kPa, up to 4 000 kPa. The coal samples were tested with N₂, CO₂ and CH₄ gas, as single and as mixed gases, at temperatures of 21, 24 and 28 °C. The reported results suggest that the adsorbed mass in coal depends strongly on gas type, sorption time, temperature, and particle size. Saturation time appears to be dependent on gas type but independent of particle size. The minimum saturation time with N₂ and CO₂ gas was found to be approximately two day (2 880 min) while with CH₄ gas it took one day (1 440 min) longer to reach an equilibrium pressure. In addition, there appears to be a hysteresis between adsorption and desorption curves in all the coals tested and with all three gases (N₂, CO₂ and CH₄) investigated. The residual adsorbed mass in coal at atmospheric pressure was found to be about 20-50%, of the maximum gas content at 4 000 kPa, depending on gas type. Experiments were also conducted to examine the effect of displacing the adsorbed CO₂ and CH₄ gases and their binary mixture in coal by the injection of N₂ gas.

To study the feasibility of removing the initially adsorbed gas from coal with another gas, experiments were conducted using an in-house built multi-function outburst

research rig. The results revealed that CO₂ gas desorption increased by almost 30% as a result of N₂ gas injection, which was about double that obtained without N₂ gas injection. This finding has a significant bearing in solving the drainage difficulties experienced at rich CO₂ gas concentration zones such as at West Cliff Colliery, area 5, where this study was focused.

PUBLICATIONS

Black, D, Aziz, N, Jurak, M and Florentin, R, 2009. Outburst Threshold Limits – Are They Appropriate?, in Proceedings of Coal Operators Conference, 12-13 February, Wollongong, NSW, Australia, pp. 185-192.

Black, D, Aziz, N, Jurak, M and Florentin, R, 2009. Gas Content Estimation Using Initial Desorption Rate, in Proceedings of Coal Operators Conference, 12-13 February, Wollongong, NSW, Australia, pp. 193-198.

Florentin, R, Aziz, N, Black, D and Nghiem, L, 2009. Sorption Characteristics of Coal, Particle Size, Gas Type and Time, in Proceedings of Coal Operators Conference, 12-13 February, Wollongong, NSW, Australia, pp. 208-216.

Black, D, Aziz, N and Florentin, R, 2010. Assessment of Factors Impacting Coal Seam Gas Production, in Proceedings 2010 International Coalbed and Shale Gas Symposium, 17-21 May, Tuscaloosa, Alabama, USA.

Black, D, Aziz, N and Florentin, R, 2010. Estimating Total Gas Content from Early Stage Gas Emission Data, in Proceedings 2010 International Coalbed and Shale Gas Symposium, 17-21 May, Tuscaloosa, Alabama, USA.

Florentin, R, Aziz, N, Black, D and Nghiem, L, 2010 a. Recovery of Stored Gas in Coal by Nitrogen Injection – A Laboratory Study, in Proceedings of Coal Operators Conference, 11-12 February, Wollongong, NSW, Australia, pp. 217-228.

Florentin, R, Aziz, N, Black D, Nghiem, L, and Bariš K, 2010 b. Recovery of Stored Gas in Coal by Nitrogen Injection – Strain Measurements, in proceedings of the 17th Congress of Turkey, 2-4 June, Zonguldak, Turkey, pp. 317-329.

Florentin, R, Aziz, N, Black, D and Nghiem, L, 2010 c. Binary Carbon Dioxide/Methane Adsorption on Fragmented Coals – A Laboratory Study, in Proceedings of the 17th Congress of Turkey, 2-4 June, Zonguldak, Turkey, pp. 369-381.

TABLE OF CONTENT

AFFIRMATION	i
ACKNOWLEDGMENTS	ii
ABSTRACT	iii
PUBLICATIONS	v
TABLE OF CONTENT	vii
LIST OF FIGURES.....	xvi
LIST OF TABLES.....	xx
LIST OF EQUATIONS	xxi
LIST OF SYMBOLS AND ABBREVIATIONS	xxii
I. CHAPTER ONE	24
GENERAL INTRODUCTION	24
I.1 INTRODUCTION	24
I.2 GAS ADSORPTION/DESORPTION IN COAL	26
I.3 STATEMENT OF THE PROBLEM	27
I.4 OBJECTIVES OF RESEARCH	28
I.5 THESIS OUTLINE	29
II. CHAPTER TWO	31
A REVIEW OF COAL SORPTION CHARACTERISTICS	31
II.1 INTRODUCTION	31
II.2 PHYSICAL STRUCTURE OF COAL	31
II.3 GASES IN COAL	35
II.4 GAS ADSORPTION/DESORPTION IN COAL	37
II.4.1 ISOTHERM PARAMETERS	40
<i>Errors in determining adsorption and desorption of coal</i>	56
II.4.2 GAS HYSTERESIS.....	58
II.4.3 GAS ISOTHERM	62
II.4.4 GAS INJECTION	66
II.5 GAS TRANSPORT IN COAL	68

II.6	SUMMARY.....	74
III.	CHAPTER THREE	76
	SINGLE GAS ADSORPTION	76
III.1	INTRODUCTION	76
III.2	EXPERIMENTAL PROCEDURE	76
III.2.1	APPARATUS.....	76
III.2.2	COAL SAMPLE PREPARATION	79
III.2.3	TESTING PROCEDURE	82
III.3	EXPERIMENTAL RESULTS	84
III.3.1.	NITROGEN	85
III.3.1.1.	GAS SATURATION TIME	85
	Pressure level	85
	Coal particle size.....	87
	Bath water temperature	88
III.3.1.2.	ADSORBED MASS.....	89
	N ₂ adsorbed mass.....	89
	Langmuir isotherm	90
III.3.1.3.	COAL LINEAR STRAINS	91
III.3.2.	CARBON DIOXIDE	92
III.3.2.1.	GAS SATURATION TIME	92
	Pressure level	92
	Coal particle size.....	93
	Temperature	94
III.3.2.2.	ADSORBED MASS.....	96
	CO ₂ adsorbed mass.....	96
	Coal particle size.....	98
	Saturation time.....	99
	Temperature	101
	Langmuir isotherm	102
III.3.2.3.	COAL LINEAR STRAINS	105
III.3.3.	METHANE.....	107
III.3.3.1.	GAS SATURATION TIME	107
	Pressure level	107

Coal particle size.....	108
Gas type	109
Temperature	110
III.3.3.2. ADSORBED MASS.....	111
CH ₄ adsorbed mass.....	111
Coal particle size.....	112
Saturation time.....	113
Temperature	115
Gas type	116
Langmuir isotherm	116
III.3.3.3. COAL LINEAR STRAINS	117
III.3.4. SUMMARY.....	120
Saturation time.....	120
Adsorbed mass	121
IV. CHAPTER FOUR	123
MIXED GAS ADSORPTION	123
IV.1 INTRODUCTION	123
IV.2. EXPERIMENTAL PROCEDURE.....	123
IV.2.1. APPARATUS.....	123
IV.2.2. COAL SAMPLE PREPARATION	124
IV.3. EXPERIMENTAL RESULTS.....	125
IV.2.3. BINARY MIXED GAS	125
IV.2.3.1. MIXED GAS SATURATION TIME	125
Pressure level	125
Coal particle size.....	126
Bath water and room temperature	127
IV.2.3.2. MIXED GAS COMPOSITION	129
Pressure level	129
Coal particle size.....	129
Bath water temperature	130
IV.2.3.3. MIXED GAS ADSORBED MASS	131
CO ₂ /CH ₄ adsorbed mass.....	131
Coal particle size.....	133

CO ₂ and CH ₄ acting independently versus CO ₂ /CH ₄ mixed gas	134
Bath water temperature	135
IV.2.4. TERNARY MIXED GAS.....	136
IV.2.4.1. MIXED GAS SATURATION TIME	136
Pressure level	136
Coal particle size.....	137
Bath water temperature	138
IV.2.4.2. MIXED GAS COMPOSITION	139
Pressure level	139
Coal particle size.....	140
IV.2.4.3. MIXED GAS ADSORBED MASS	141
Ternary mixed gas adsorbed mass	141
Coal particle size.....	143
Gas mixture and single gas.....	144
IV.2.5. SUMMARY.....	145
BINARY MIXED GAS.....	145
TERNARY MIXED GAS.....	145
V. CHAPTER FIVE	147
SINGLE GAS DESORPTION.....	147
V.1. INTRODUCTION	147
V.2. EXPERIMENTAL PROCEDURE	147
V.2.1 APPARATUS.....	147
V.2.2 TESTING PROCEDURE	148
V.3. EXPERIMENTAL RESULTS	148
V.3.1. NITROGEN	148
V.3.1.1. GAS SATURATION TIME	148
Pressure level	148
Particle size	149
V.3.1.2. ADSORBED MASS.....	150
Experimental adsorbed mass.....	150
Coal particle size.....	152
V.3.2. CARBON DIOXIDE	153
V.3.2.1. GAS SATURATION TIME	153

Pressure level	153
Coal particle size.....	155
Temperature	155
V.3.2.2. ADSORBED MASS.....	156
Experimental adsorbed mass.....	156
Coal particle size.....	157
Langmuir isotherm	159
Temperature	160
V.3.2.3. RESIDUAL GAS	161
V.3.3. METHANE.....	163
V.3.3.1. GAS SATURATION TIME	163
Pressure level	163
Coal particle size.....	164
Gas type	165
V.3.3.2. ADSORBED MASS.....	166
Experimental adsorbed mass.....	166
Coal particle size.....	167
Gas type	169
Langmuir isotherm	169
V.3.3.3. RESIDUAL GAS	170
V.3.4. SUMMARY.....	172
Saturation time.....	172
Adsorbed mass	172
VI. CHAPTER SIX	174
MIXED GAS DESORPTION	174
VI.1. INTRODUCTION	174
VI.2. EXPERIMENTAL PROCEDURE.....	175
VI.2.1. APPARATUS.....	175
VI.2.2. TESTING PROCEDURE	175
VI.3. RESULT AND DISCUSSION	177
VI.3.1. BINARY MIXED GAS	178
VI.3.1.1. MIXED GAS SATURATION TIME	178
Pressure level	178

Coal particle size.....	179
Bath water and room temperature	180
VI.3.1.2. MIXED GAS COMPOSITION	182
Pressure level	182
Coal particle size.....	183
Bath water temperature	184
VI.3.1.3. MIXED GAS ADSORBED MASS	184
Binary mixed gas adsorbed mass	184
Coal particle size.....	187
Saturation time.....	190
Temperature	191
VI.3.1.4. RESIDUAL MIXED GAS.....	192
VI.3.2. TERNARY MIXTURE.....	193
VI.3.2.1. MIXED GAS SATURATION TIME.....	193
Pressure level	193
Coal particle size.....	194
Room temperature	196
VI.3.2.2. MIXED GAS COMPOSITION	197
Pressure level	197
Coal particle size.....	198
Gas mixture	200
VI.3.2.3. ADSORBED MASS.....	201
Ternary mixed gas adsorbed mass	201
Coal particle size.....	202
Extended Langmuir isotherm	204
Gas mixture	205
VI.3.2.4. RESIDUAL GAS	207
VI.3.3. SUMMARY.....	208
Binary mixed gas.....	208
Ternary mixed gas	209
VII. CHAPTER SEVEN	211
ENHANCING GAS DRAINAGE BY N ₂ AND CO ₂ INJECTION.....	211
VII.1. INTRODUCTION	211

VII.2.	EXPERIMENTAL PROCEDURE.....	211
VII.2.1.	APPARATUS.....	211
VII.2.2.	SAMPLE PREPARATION.....	213
VII.2.3.	TESTING PROCEDURE	214
VII.3.	EXPERIMENTAL RESULT AND DISCUSSION	215
VII.3.1.	GAS COMPOSITION	215
VII.3.1.1.	REFERENCE TEST.....	216
	Saturation time.....	216
	Temperature	217
	Gas composition	218
	Gas flow	220
VII.3.1.2.	BINARY MIXED GAS	220
	Saturation time.....	220
	Gas composition	221
VII.3.1.3.	CARBON DIOXIDE	224
VII.3.1.4.	METHANE TEST.....	225
VII.3.2.	VOLUMETRIC CHANGES IN COAL	226
VII.3.2.1.	REFERENCE TEST.....	227
VII.3.2.2.	BINARY MIXED GAS TEST	228
VII.3.2.3.	CARBON DIOXIDE TEST	232
VII.3.2.4.	METHANE TEST.....	235
VII.3.3.	PERMEABILITY	238
VII.3.4.	NITROGEN	239
VII.3.4.1.	CARBON DIOXIDE	241
VII.3.5.	SUMMARY.....	243
	Gas composition	243
	Volumetric strain.....	244
	Permeability	244
VIII.	CHAPTER EIGHT.....	246
	CONCLUSIONS AND RECOMMENDATIONS	246
VIII.1.	CONCLUSIONS	246
VIII.1.1.	SINGLE GAS ADSORPTION/DESORPTION	246
	TIME.....	246

ADSORBED MASS.....	247
LINEAR STRAIN	248
VIII.1.2. MIXED GAS ADSORPTION/DESORPTION.....	249
BINARY MIXED GAS.....	249
TERNARY MIXED GAS.....	250
VIII.1.3. ENHANCING GAS DRAINAGE BY N ₂ AND CO ₂ GAS INJECTION	252
VIII.2. RECOMMENDATIONS	253
APPENDICES.....	255
Appendix 1 – Raw data form	255
Appendix 2 – Gas saturation degree.....	256
Appendix 3 – Soave-Redlich-Kwong Equation of state.....	258
Appendix 4 – Adsorbed mass spreadsheet calculation	260
Appendix 5 – Langmuir equation.....	263
Appendix 6 – N ₂ saturation time in adsorption – Sample B2-7 (4.75 mm).....	265
Appendix 7 – N ₂ saturation time in desorption – Sample B2-7 (4.75 mm).....	267
Appendix 8 – N ₂ adsorbed mass in adsorption and desorption.....	268
Appendix 9 – CO ₂ saturation time in adsorption – Sample B2-6 (0.30 mm)	269
Appendix 10 – CO ₂ saturation time in desorption – Sample B2-6 (0.30 mm)	271
Appendix 11 – CO ₂ sorption capacity in adsorption	273
Appendix 12 – CO ₂ adsorbed mass in desorption	278
Appendix 13 – CH ₄ saturation time in adsorption – Sample BD-2 (54.00 mm diameter).....	280
Appendix 14 – CH ₄ saturation time in desorption – Sample BE-2 (54.00 mm diameter)	282
Appendix 15 – CH ₄ adsorbed mass in adsorption	284
Appendix 16 – CH ₄ adsorbed mass in desorption	288
Appendix 17 – Binary mixed gas saturation time in adsorption – Sample BC-6 (4.75 mm).....	290
Appendix 18 – Binary mixed gas saturation time in desorption – Sample BC-6 (4.75 mm)	292
Appendix 19 – Binary CO ₂ /CH ₄ mixed adsorbed mass in adsorption.....	294
Appendix 20 – Binary CO ₂ /CH ₄ mixed adsorbed mass in desorption.....	296
APPENDIX 21 – Ternary N ₂ /CO ₂ /CH ₄ mixed gas saturation time in adsorption – Sample BK-6 (0.71 mm).....	300

APPENDIX 22 – Ternary N ₂ /CO ₂ /CH ₄ mixed gas saturation time in desorption – Sample BK-6 (0.71 mm)	302
APPENDIX 23 – Ternary N ₂ /CO ₂ /CH ₄ mixed adsorbed mass in adsorption	303
APPENDIX 24 – Ternary N ₂ /CO ₂ /CH ₄ mixed adsorbed mass in desorption	305
REFERENCES	308

LIST OF FIGURES

Figure I-1 – Mine plan view	26
Figure I-2 – Thesis outline flowchart	30
Figure II-1 – Core coal sample	32
Figure II-2 – Coal cleats system (after Harpalani and Chen, 1995)	33
Figure II-3 – Butt and face cleats (after Sereshki, 2005)	34
Figure II-4 – Adsorbed CH ₄ in coal (after Moffat and Weale, 1955)	41
Figure II-5 – CO ₂ and moisture adsorption in coal pores	45
Figure II-6 – Equilibrium moisture content of coals of varying rank	47
Figure II-7 – Linear volumetric strain (after Harpalani and Chen, 1995)	48
Figure II-8 – Langmuir-type strain model used by Robertson and Christiansen, 2005) ..	49
Figure II-9 – N ₂ , CO ₂ and CH ₄ gas strain curve profiles (after Robertson and Christiansen, 2005)	51
Figure II-10 – Induce strain versus adsorbed gas (after Kelemen <i>et al.</i> , 2006)	52
Figure II-11 – 50/50 N ₂ /CH ₄ mixed gas isotherms on wet Tiffany coal (after Fitzgerald <i>et al.</i> , 2005)	54
Figure II-12 – Comparison of CO ₂ and CH ₄ gas adsorption-desorption isotherm (after Harpalani <i>et al.</i> , 2006)	59
Figure II-13 – CO ₂ and CH ₄ gas adsorption-desorption (after Busch <i>et al.</i> , 2003)	60
Figure II-14 – Processes involved in the transport of coalbed CH ₄ gas (after Harpalani and Schraufnagel, 1990)	69
Figure II-15 – Gas flow through coals in the Bowen Basin – a new model (after Gamson and Beamish, 1992)	70
Figure II-16 – Preferential CH ₄ gas adsorption by coal – Steps 1 and 2 (after Crosdale, 1998)	71
Figure II-17 - Preferential CH ₄ gas adsorption by coal – Steps 3 and 4 (after Crosdale, 1998)	72
Figure II-18 - Preferential CH ₄ gas adsorption by coal – Steps 5 and 6 (after Crosdale, 1998)	72
Figure II-19 - Preferential CH ₄ gas desorption by coal – Steps 1 and 2 (after Crosdale, 1998)	73
Figure II-20 - Preferential CH ₄ gas desorption by coal – Steps 3 and 4 (after Crosdale, 1998)	73
Figure III-1 – Diagram of adsorption/desorption apparatus	77
Figure III-2 – Adsorption/desorption apparatus	78
Figure III-3 – Bomb and components	78
Figure III-4 – Pressure transducer calibrator	79
Figure III-5 – Crushed and cored coal samples	80
Figure III-6 – Experimental procedure flow diagram for single and mixed gas adsorption/desorption	82
Figure III-7 – Effect of pressure levels on N ₂ gas saturation time	85
Figure III-8 – Effect of particle sizes in N ₂ gas saturation time	87
Figure III-9 – Effect of temperature in N ₂ gas saturation time	88

Figure III-10 – N ₂ adsorbed mass in coal during adsorption	89
Figure III-11 – Langmuir isotherm for N ₂ gas during adsorption.....	90
Figure III-12 – Linear strains in coal during N ₂ gas adsorption.....	91
Figure III-13 – Effect of pressure level in CO ₂ gas saturation time	92
Figure III-14 – Effect of particle sizes in CO ₂ gas saturation time	93
Figure III-15 – Effect of temperature in CO ₂ gas saturation time.....	94
Figure III-16 – Effect of room temperature on bath water temperature	95
Figure III-17 – CO ₂ adsorbed mass from experimental data in adsorption	97
Figure III-18 – Effect of particle sizes on CO ₂ adsorbed mass	98
Figure III-19 – Adsorbed CO ₂ mass due to quick test	99
Figure III-20 – Effect of saturation duration on adsorbed CO ₂ mass.....	101
Figure III-21 – Effect of temperature on CO ₂ adsorbed mass	102
Figure III-22 – Adsorbed CO ₂ mass profile modelled by Langmuir.....	103
Figure III-23 – Linear strain profile in CO ₂ gas adsorption	105
Figure III-24 – Axial and radial strains in B3-1 sample	106
Figure III-25 – Linear strains and adsorbed CO ₂ in adsorption	107
Figure III-26 – Effect of pressure levels in CH ₄ gas saturation time	108
Figure III-27 – Effect of particle sizes in CH ₄ gas saturation time.....	109
Figure III-28 – Effect of gas type in saturation time	109
Figure III-29 – Effect of temperature in CH ₄ gas saturation time.....	110
Figure III-30 – CH ₄ adsorbed mass profile in adsorption	112
Figure III-31 – Effect of particle sizes on CH ₄ adsorption capacity	113
Figure III-32 – Effect of saturation time on CH ₄ adsorption capacity.....	114
Figure III-33 – Effect of temperature in CH ₄ adsorbed mass in adsorption.....	115
Figure III-34 – Effect of gas type in adsorption	116
Figure III-35 – Langmuir isotherm from CH ₄ experimental data	117
Figure III-36 – Axial and radial strain due to CH ₄ gas adsorption.....	118
Figure III-37 – Linear strains and CO ₂ sorption capacity in adsorption	119
Figure III-38 – Effect of gas type in linear strains in CH ₄ gas adsorption	119
Figure IV-1 – Gas sorption apparatus	124
Figure IV-2 – Effect of pressure levels in mixed gas saturation time	126
Figure IV-3 – Effect of particle sizes in mixed gas time	127
Figure IV-4 – Effect of bath water temperature on saturation time	127
Figure IV-5 – Effect of room temperature on saturation time.....	128
Figure IV-6 – CO ₂ and CH ₄ gas composition in mixed gas adsorption	129
Figure IV-7 – Effect of particle sizes in CH ₄ gas composition	130
Figure IV-8 – Effect of temperature in CH ₄ gas composition	131
Figure IV-9 – CO ₂ and CH ₄ adsorbed mass during mixed gas adsorption.....	132
Figure IV-10 – CO ₂ and CH ₄ adsorbed mass trend line in adsorption	132
Figure IV-11 – Mixed gas adsorbed mass during adsorption	133
Figure IV-12 – Single CO ₂ and CH ₄ versus CO ₂ /CH ₄ mixed gas adsorbed mass.....	134
Figure IV-13 – Effect of temperature on the mixed gas adsorbed mass	135
Figure IV-14 – Effect of pressure levels in mixed gas saturation time	136
Figure IV-15 – Effect of particle size on gas saturation time	137
Figure IV-16 – Effect of temperature on gas saturation time	138

Figure IV-17 – N ₂ , CO ₂ and CH ₄ gas composition during adsorption	139
Figure IV-18 – Effect of particle sizes in ternary mixed gas composition	140
Figure IV-19 – Ternary mixed gas adsorbed mass during adsorption	141
Figure IV-20 – Effect of particle sizes in ternary mixed gas adsorbed mass	143
Figure IV-21 – Effect of particle sizes in CO ₂ and CH ₄ gas adsorbed mass	144
Figure IV-22 – Effect of gas mixture in CO ₂ and CH ₄ gas adsorbed mass	144
Figure V-1 – Effect of pressure levels in N ₂ saturation time	149
Figure V-2 – Effect of particle sizes in N ₂ saturation time	150
Figure V-3 – Excess in N ₂ adsorbed mass in desorption	151
Figure V-4 – Langmuir isotherm from N ₂ experimental data.....	151
Figure V-5 – Effect of particle sizes in N ₂ adsorbed mass in desorption	152
Figure V-6 – Effect of pressure levels on CO ₂ gas saturation time	154
Figure V-7 – Effect of particle sizes on CO ₂ gas saturation time	155
Figure V-8 – Effect of temperature on CO ₂ gas saturation time	156
Figure V-9 – Excess on CO ₂ sorption capacity in desorption.....	157
Figure V-10 – Effect of particles size on CO ₂ adsorbed mass in desorption	157
Figure V-11 – Langmuir isotherm from CO ₂ gas experimental data	160
Figure V-12 – Effect of temperature on CO ₂ adsorbed mass in desorption	160
Figure V-13 – Enhanced CO ₂ gas desorption by vacuuming	161
Figure V-14 - Enhanced CO ₂ gas desorption by increasing temperature	162
Figure V-15 – Effect of pressure levels on CH ₄ gas saturation time	163
Figure V-16 – Effect of particle sizes on CH ₄ gas saturation time	165
Figure V-17 – Effect of gas type in gas saturation in desorption	166
Figure V-18 – CH ₄ adsorbed mass in adsorption and desorption	166
Figure V-19 – Effect of particle sizes on CH ₄ adsorbed mass in desorption	168
Figure V-20 – Core coal sample	168
Figure V-21 – Effect of gas type in adsorbed mass in adsorption/desorption	169
Figure V-22 – Langmuir isotherm from CH ₄ gas experimental data.....	170
Figure V-23 – Enhanced CH ₄ gas desorption by vacuuming	170
Figure V-24 – Enhanced CH ₄ gas desorption by increasing temperature.....	171
Figure VI-1 – Gas desorption apparatus and components	175
Figure VI-2 – Effect of pressure levels in mixed gas saturation time	178
Figure VI-3 – Effect of particle sizes in mixed gas saturation time.....	179
Figure VI-4 – Effect of temperature in mixed gas saturation time.....	181
Figure VI-5 – Effect of room temperature in the bath water temperature.....	181
Figure VI-6 – Mixed gas composition during desorption	182
Figure VI-7 – Free CH ₄ gas composition during desorption	183
Figure VI-8 – Effect of temperature in gas composition in desorption	184
Figure VI-9 – Binary mixed gas adsorbed mass during desorption	185
Figure VI-10 – Excess in CO ₂ and CH ₄ gas adsorbed mass during desorption	186
Figure VI-11 – Effect of particle sizes in binary mixed gas content	187
Figure VI-12 – CO ₂ and CH ₄ adsorbed mass during mixed gas desorption.....	188
Figure VI-13 – CO ₂ and CH ₄ gas content over time	191
Figure VI-14 – Effect of temperature on the adsorbed mass of the CO ₂ and CH ₄ components.....	191

Figure VI-15 – Effect of pressure levels in TMG saturation time	194
Figure VI-16 – Effect of particle sizes in TMG saturation time	195
Figure VI-17 – Effect of temperature in TMG saturation time	196
Figure VI-18 – Ternary mass gas composition during desorption	197
Figure VI-19 – N ₂ and CO ₂ gas composition over pressure	198
Figure VI-20 – N ₂ and CO ₂ gas composition over time	199
Figure VI-21 – Binary and Ternary mixed gas composition	200
Figure VI-22 – Ternary mixed gas adsorbed mass during desorption	201
Figure VI-23 – Excess in N ₂ , CO ₂ and CH ₄ gas content during desorption	202
Figure VI-24 – Effect of particles size in ternary mixed gas desorption	203
Figure VI-25 – N ₂ , CO ₂ and CH ₄ adsorbed mass during desorption	203
Figure VI-26 – Extended Langmuir N ₂ , CO ₂ and CH ₄ gas isotherms	204
Figure VI-27 – Single CO ₂ and CH ₄ gas versus their gas mixture adsorbed mass	205
Figure VII-1 - Multi-function outburst research rig (MFORR)	212
Figure VII-2 – Schematic drawing of MFORR	213
Figure VII-3 – Core coal sample	214
Figure VII-4 – Pressure drop profile during adsorption	216
Figure VII-5 – Effect of temperature on pressure drop profile	218
Figure VII-6 – CO ₂ and CH ₄ composition during desorption	219
Figure VII-7 – Gas flow during desorption	220
Figure VII-8 – Binary CO ₂ /CH ₄ composition during saturation	221
Figure VII-9 – CO ₂ and CH ₄ composition over time	222
Figure VII-10 - CO ₂ composition during N ₂ injection	224
Figure VII-11 – CH ₄ composition during N ₂ injection	225
Figure VII-12 – Perpendicular and parallel strains (Reference test)	228
Figure VII-13 – Perpendicular and parallel strains (CO ₂ /CH ₄ test)	229
Figure VII-14 – Axial load profile (CO ₂ /CH ₄ test)	230
Figure VII-15 – Perpendicular and parallel strain (CO ₂ test)	232
Figure VII-16 – Axial load profile (CO ₂ test)	233
Figure VII-17 – Perpendicular and parallel strain (CH ₄ test)	236
Figure VII-18 – Axial load profile (CH ₄ test)	237
Figure VII-19 – N ₂ permeability profile	239
Figure VII-20 – N ₂ permeability against axial load	240
Figure VII-21 – Axial and radial strains due to N ₂ flow through	241
Figure VII-22 – CO ₂ permeability profile	242
Figure VII-23 – CO ₂ permeability and linear strains	242
Figure 0-1 – Pressure changes against time	257

LIST OF TABLES

Table II-1 – Gas saturation duration	42
Table II-2 – Summary of coal particle sizes used in adsorption test	50
Table II-3 - Summary of gas type used in adsorption test	56
Table II-4 – Relative error calculations for isotherms fits (after Clarkson and Bustin, 2000)	64
Table III-1 – Details of coal samples tested for adsorption	80
Table III-2 – Relative density, moisture and ash content analysis of panels 519 and 520	81
Table III-3 – Petrography results of panels 519 and 520 coal (Saghafi and Roberts, 2008)	82
Table III-4 – Pressure fluctuations during N ₂ gas adsorption at a given pressure	86
Table IV-1 – Coal samples tested with mixed gas and proximate analysis.....	124
Table IV-2 – Saturation time during mixed gas adsorption	126
Table IV-3 – Mixed gas adsorbed mass and composition in adsorption	134
Table V-1 – Coal samples tested during desorption.....	147
Table V-2 – N ₂ adsorption capacity in adsorption/desorption	153
Table V-3 – CO ₂ sorption capacity in adsorption/desorption	158
Table V-4 – Excess on CO ₂ sorption capacity in desorption.....	159
Table V-5 – CH ₄ adsorbed mass in adsorption and desorption	167
Table VI-1 – Summary of mixed gas saturation time.....	180
Table VI-2 – Changes in adsorbed mass of CO ₂ and CH ₄ components in desorption ..	189
Table VI-3 – Mixed gas adsorbed mass in adsorption/desorption.....	190
Table VI-4 – Residual binary mixed gas in coal.....	193
Table VI-5 – Summary of TMG saturation time.....	195
Table VI-6 – Ternary mixed gas adsorbed mass in adsorption/desorption	206
Table VI-7 – Residual ternary mixed gas in coal	207
Table VII-1 – CO ₂ and CH ₄ composition without N ₂ injection	219
Table VII-2 - CO ₂ and CH ₄ composition with N ₂ injection	223
Table VII-3 – Summary of strain and stress (CO ₂ /CH ₄ test)	230
Table VII-4- Summary of strain and stress (CO ₂ test)	234
Table VII-5 - Summary of strain and stress (CH ₄ test)	238
Table 0-1.....	256

LIST OF EQUATIONS

$\theta_i = \omega_i L_i = \frac{B_i P_{yi}}{1 + \sum B_j P_{yj}}$	Extended Langmuir (1) ..	62
$\theta_i = \omega_i L_i = \frac{(B_i P_{yi}) \eta_{i1} + (B_j P_{yj}) \eta_j}{1 + \sum (B_i P_{yi}) \eta_{i1} + \sum (B_j P_{yj}) \eta_j}$	Loading ratio correlation (LRC) (2) ..	63
$1n t = i = 1n x_i n_i^\circ$	Total adsorbed mixed gas (IAS) (3)	65
$n_i = n t * x_i$	Adsorbed gas by components (4)	65
$V_{void} = V_{cell} - m_{sample} \rho_{solid} * 1 - w_c - m_{sample} \rho_{H2O} * w_c$	(5) ..	83
$m_{adsG} = m_{meas} - m_{void} = m_{meas} - \rho_{gas} * V_{void}$	(6)	83
$m_{adsA} = m_{adsG} * \rho_{ads} \rho_{ads} - \rho_{gas}$	(7)	84
$\theta_i = \omega_i L_i = \frac{B_i P_{yi}}{1 + \sum B_j P_{yj}}$	(8)	125
$K = \mu Q \ln r_0 r_i \pi l P_{O2} - P_{u2}$	Darcy equation (9)	239
(10) Pressure change $\Delta P = P_{t1} - P_{t0}$	256
(11) Time change $\Delta t = T_n$	257
(12) Pressure change in % $\%P = \frac{\Delta P}{P_2 P_1}$	257
(13) Soave-Redlich-Kwong EOS $P = \frac{RT}{(\bar{v} - b)} - \frac{a}{\bar{v}(\bar{v} + b)}$	258
(14) Parameter a $a = 0.42747 (RT_c^2 P_c)$	258
(15) Parameter b $b = 0.08664 (RT_c P_c)$	258
(16) Reduced temperature $TR = \frac{T}{T_c}$	258
(17) Parameter $\alpha = (1 + m \frac{1 - 2TR}{TR})^2$	259
(18) Parameter m $m = 0.048508 + 1.55171 \omega - 0.15613 \omega^2$	259
(19) Coal weight (gm) $W_{coal} = W_1 - W_0$	260
(20) Gas weight (gm) $W_{gas} = W_2 - W_1$	260
(21) Coal volume (cc) $V_{coal} = \frac{W_{coal}}{\lambda}$	261
(22) Free and adsorbed volume (cc) $V(f + a) = \text{col AN} \rightarrow P \text{ real sheet}$	261
(23) Free bomb volume not taken by coal (cc) $V_{not coal} = V_0 - V_{coal}$	261
(24) Free gas volume (Ad) $V_1 = \text{column G} \rightarrow P \text{ real sheet}$	261
(25) Free gas volume (D) $V_1 = \text{column AN} \rightarrow P \text{ real sheet}$	261
(26) Volume of adsorbed gas in coal (cc) $V_4 = V(f + a) - V_1$	261
(27) Volume of adsorbed gas per gram of coal (cc/gm) $V_5 = \frac{V_4}{W_{coal}}$	261
(28) Langmuir equation $\text{adsorption rate} = \frac{d\theta}{dt} = k_{ap} (1 - \theta)$	263
(29) Desorption rate $\text{desorption rate} = \frac{d\theta}{dt} = k_d \theta$	264
(30) Desorption constant $k_{ap} \frac{1 - \theta}{\theta} = k_d$	264
(31) Surface coverage $\theta = \frac{K p_1}{1 + K p_1}, K = \frac{K_a K_d}{K_d}$	264
(32) Langmuir equation $PV = P_{VL} + \frac{P_{LVL}}{P}$	264

LIST OF SYMBOLS AND ABBREVIATIONS

<i>K</i> = Permeability to gas (Darcy)	(1)	239
<i>l</i> = Height of the sample (cm)	(2)	239
<i>Q</i> = Rate of flow of gas (cc/sec)	(3)	239
<i>P0</i> = Absolute pressure in the chamber (bars)	(4)	239
<i>r0</i> = External radius of sample (cm)	(5)	239
<i>Pu</i> = Absolute pressure at the outlet (bars)	(6)	239
<i>ri</i> = Internal radius of sample (cm)	(7)	239
<i>μ</i> = Viscosity of tested gas, centipoise	(8)	239
<i>ΔP</i> = pressure change in the time interval	(9)	257
<i>t1</i> = pressure at final time of the interval	(10)	257
<i>t0</i> = pressure at initial time of the interval	(11)	257
<i>T</i> = sorption period	(12)	257
<i>n</i> = number of segments, equal to 8	(13)	257
<i>P2</i> = final pressure	(14)	257
<i>P1</i> = initial pressure	(15)	257
<i>R</i> = universal gas constant	(16)	258
<i>T</i> = absolute temperature	(17)	258
<i>v̄</i> = specific molar volume	(18)	258
<i>b</i> = volume correction	(19)	258
<i>α</i> = function (<i>ω</i> , <i>T</i>)	(20)	258
<i>a</i> = molecular interaction parameter	(21)	258
<i>TR</i> = reduced temperature	(22)	258
<i>Tc</i> = critical temperature	(23)	258
<i>Pc</i> = critical pressure	(24)	258
<i>ω</i> = acentric factor	(25)	259
<i>δ</i> = gas density (gm/cc)	(26)	260
<i>λ</i> = coal density (gm/cc)	(27)	260
<i>Vbomb</i> = bomb volume (cc)	(28)	260
<i>W0</i> = empty bomb weight (gm)	(29)	260
<i>W1</i> = weight of bomb and coal (gm)	(30)	260
<i>W2</i> = weight of bomb and coal and gas (gm)	(31)	260
<i>Wcoal</i> = weight of coal (gm)	(32)	260
<i>Wgas</i> = weight of gas (gm)	(33)	260
<i>Vcoal</i> = coal volume (cc)	(34)	260
<i>V(f + a)</i> = volume of free and adsorbed gas	(35)	260
<i>Vnot coal</i> = free bomb volume not taken by coal (cc)	(36)	260
<i>V0</i> = actual volume of bomb (cc)	(37)	260
<i>V1</i> = free gas volume (cc)	(38)	260
<i>V3</i> = free gas volume in bomb with coal sample (cc)	(39)	260
<i>V4</i> = volume of gas adsorbed in coal (cc)	(40)	260
<i>V5</i> = gas volume adsorbed in 1 gm of coal (cc/gm)	(41)	260
<i>R1</i> = ratio of free gas volume over bomb volume	(42)	260

$d\theta$ = differential coverage of the surface	(43).....	263
dt = differential time	(44).....	264
ka = adsorption constant	(45).....	264
p = gas pressure	(46).....	264
θ = surface coverage	(47).....	264
kd = desorption constant	(48).....	264
VL = maximum amount of gas stored by coal	(49).....	264
PL = pressure at half the Langmuir volume	(50).....	264

I. CHAPTER ONE

GENERAL INTRODUCTION

I.1 INTRODUCTION

In 2008-2009, with an annual export capacity exceeding 261 mt, and sales of around \$A 55 billion, Australia is considered to be one of the world's major coal exporters. The total annual export of coal in Australia amounts to 28% of total world trade in hard coal, which is around 941 mt. Major markets in 2008-2009 were Japan (40%), South Korea (16%), Taiwan (10%), China (10%) and India (9%). In 2008-2009, the 56% of total saleable coal production of 333.6 mt came from Queensland while 41 % came from NSW. The other states, Western Australia, South Australia, and Tasmania contributed with 3%. Underground coalmines represented 25% (81.7 mt) of national coal production. In 2007-2008, there were 60 coal mines in NSW (29 underground and 31 open cut), producing approximately 138 mt of saleable coal. The total underground coal production in NSW represented around 51 mt (37%). In 2009-2010, the total coal production from Australian longwall mines was around 106 mt.

The productivity of underground operations is influenced by the depth of the coal seam and geological conditions. Also, the presence of gas and the ease with which it can be drained influences the productivity of an underground operation. Gas drainage maximises underground operations while simultaneously minimising the occurrence of gas outbursts stemming from ground stress and sorbed gases present in high quantities and at high pressures in coal seams and surrounding stratifications. According to Sereshki (2005), the productivity in underground mining with reduced risk of outbursts can match that of open cut operations. This is now a reality and according

CHAPTER ONE

General introduction

to production statistics for 2008 several underground operations with effective gas drainage system achieved coal production in excess of 4 mt, with one mine's raw coal production being in the order of 8 mt (Cram, 2008).

An integral understanding of gas sorption in coal is extremely useful because it helps in the design of underground coal mine ventilation and gas drainage systems. Coal seams with gas content and gas desorption rates either improve or alleviate measurements in mine safety. Gas drainage reduces the gas content in coal seams and minimises the risk of an outburst by diluting the liberated gas through the ventilated air.

The complexity and effectiveness of gas drainage systems varies from boreholes discharging to the atmosphere via ventilation fans, to boreholes connected to surface drainage plants, with subsequent utilisation of the drainage gas. In regions such as the Illawarra where mines operate at depths of 450-500 m under surface access constraints, the use of Underground to Inseam UIS drilling is used as underground gas drainage drilling. It is common in gassy mines such as the Bulli seam to have an intensive UIS drilling program ahead of any mining development, although drilling about 100 000 m per annum can cost in the order of \$4-6 million. However, although recent studies found that intensive UIS gas drainage programs were effective in 50% of the cases they did not reduce the gas content. In these instances it is common practice to drill more holes per given area, albeit with a consequent increase in costs.

Three Australia mines, Appin, West Cliff, and Tower collieries, actively utilised methane gas to generate power, well before the introduction of government schemes and incentives for utilising coal mine gas (Black and Aziz, 2009). The content of gas in coal is an important parameter in any evaluation of the extent of gas in a coal seam. The more

CHAPTER ONE

General introduction

knowledge available on gas adsorption/desorption only improves the understanding of gas storage and flow in coal seams because it minimises the number of holes that need to be drilled. Accordingly, a gas adsorption/desorption test was carried out on sample of coal taken from West Cliff Colliery, Area 5, and panels 519 and 520 (Figure I-1).

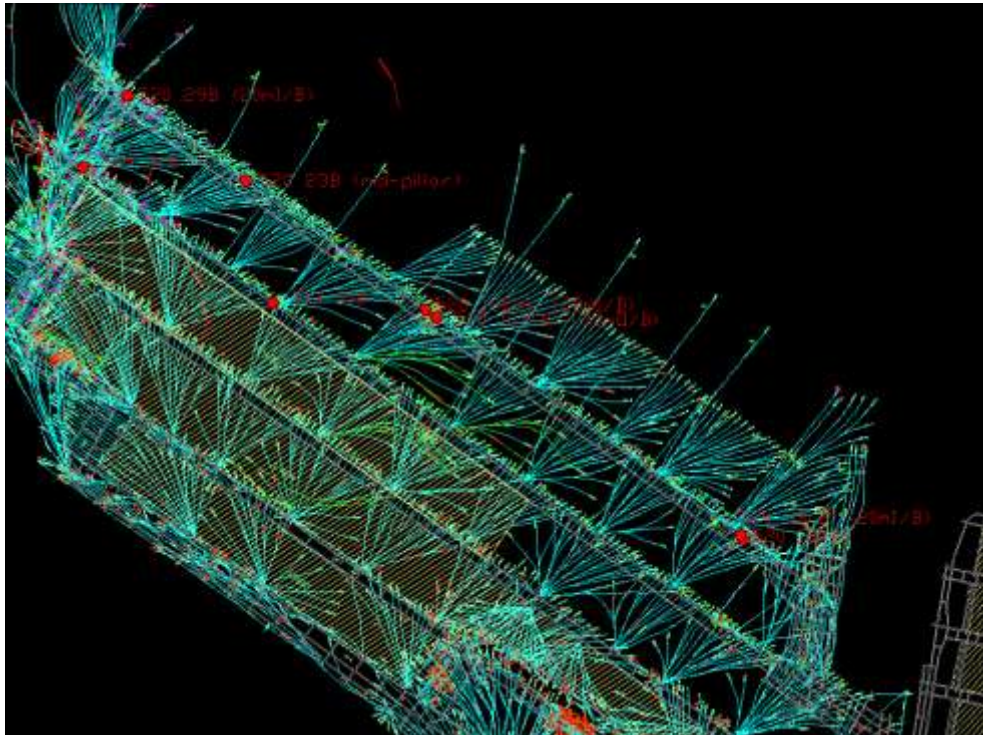


Figure I-1 – Mine plan view

This mine is located in the southern coal fields of New South Wales from where high quality coal is extracted from the 2.5m thick Bulli seam situated at an average depth of 500 m.

I.2 GAS ADSORPTION/DESORPTION IN COAL

Although gas adsorption on solids has been studied in the laboratory for a very long time, it is only in the second half of the 20th century that tests on the intensity of porous media have been done, and more specifically on coal samples. Faster development of mining techniques has given the impetus necessary to increase research into gas adsorption/desorption in coal. So too has other issues such as work

CHAPTER ONE

General introduction

place safety, stemming from an increase in the risk in mining operations mainly associated with an increase in CH_4 and CO_2 emissions, and drainage and coal/gas outbursts.

Gas adsorption/desorption tests in coal are currently carried out in powder, fragment, and core samples. The gases used are mainly He, N_2 , CO_2 , CH_4 , and their mixtures. Coal is usually saturated at different pressures, from as little as a few kPa up to several hundreds of MPa. Coal samples are saturated for a few min or hours and sometimes for several months. Time is the most variable of the parameters involved in gas adsorption/desorption in coal. Consequently, the different environments of gas adsorption/desorption tests, and also the variety of parameters used, mostly lead to different results, which prevents any an accurate comparison between laboratories.

In addition, the experimental databases are not always available for researchers at regional or basin level which means it is almost impossible to take advantage of previous studies.

I.3 STATEMENT OF THE PROBLEM

Improving our knowledge of how gas in coal behaves during adsorption/desorption will help to develop and conduct an effective gas drainage system, especially in seams where high stresses and low permeability make drainage technically and economically difficult. An assessment of the parameters influencing the effectiveness of gas drainage such as its pressure, content, and permeability, among others, would be critical for any computer model in simulating the adsorption/desorption mechanism and transport of gas in coal. Most of these simulation models depend on how accurate the assessment of gas was, the gas storage capacity of the coal, the mechanisms involved in its adsorption/desorption, and transporting it from coal matrices to the drainage network

CHAPTER ONE

General introduction

system. Thus, it is important to have more knowledge of coal gas adsorption/desorption and the parameters involved in this phenomenon, especially when it is used as an alternative to enhancing drainage by N_2 or CO_2 gas injection. For example, a study of N_2 gas injection is critical in solving the drainage difficulties experienced in rich CO_2 gas concentration zones.

Despite some standardisation in measurements on the gas content in coal among laboratories around Australia, mainly with respect to particle size and temperature, it is still necessary to define proper parameters such as saturation, duration, size of coal particles, and temperature, among others. Also, it would be very rewarding to establish a reliable and easily repeatable methodology for measuring the gas content in coal.

1.4 OBJECTIVES OF RESEARCH

The main objectives of this research work are:

- To evaluate the duration of gas saturation and its content in coal with respect to time, gas type, and their binary and ternary mixture, coal particle size, and temperature
- To establish the phenomenon of gas hysteresis in coal due to the processes of adsorption and desorption
- To determine the effectiveness of enhancing gas drainage in coal by N_2 and CO_2 gas injection
- To assess and quantify the residual gas content in coal as a result of the adsorption and desorption process
- To briefly evaluate the applicability of the Langmuir equation in tallying with the experimental data from gas adsorption and desorption using either single gases or mixed gases, and

CHAPTER ONE

General introduction

- To establish a new experimental procedure that increases the accuracy and repeatability of measurements.

Thus, the main purpose of this research work is to examine the adsorption/desorption behaviour of gases in coal, emphasising on the duration and saturation of the gas content, size of the coal particles, and the type and temperature of the gas.

Limited attention will be given to determining whether the Langmuir equation is accurate enough for modelling gas sorption, and whether the Soave-Redlich-Kwong equation of state (Soave, 1972; Redlich and Kwong, 1949) is applicable for characterising gas sorption in coal. The aim is also to establish a reliable and easily repeatable methodology for measuring the gas content in coal.

1.5 THESIS OUTLINE

The thesis covers eight chapters and is shown in the flowchart, Figure I-2. The structure of the thesis is as follows:

- Chapter 1 introduces the general purpose and objectives of the research work
- Chapter 2 reviews the gas sorption theory currently applied to gas drainage
- Chapter 3 includes the study of N_2 , CO_2 and CH_4 gas adsorption in powder and fragmented coal, in addition to 54.00 mm diameter samples of coal core. The dependency of the gas content is analysed as a function of gas saturation time, coal particle size, and gas type
- Chapter 4 describes the experimental work in binary CO_2/CH_4 (52/48) mixed gas adsorption in different sized particle of coal. There is also a detailed study on the ternary $N_2/CO_2/CH_4$ (34/33/33) mixed gas adsorption in coal. This study includes an analysis of the gas content in coal regarding the duration of its saturation, size of coal particles, and the type and composition of the gas

CHAPTER ONE

General introduction

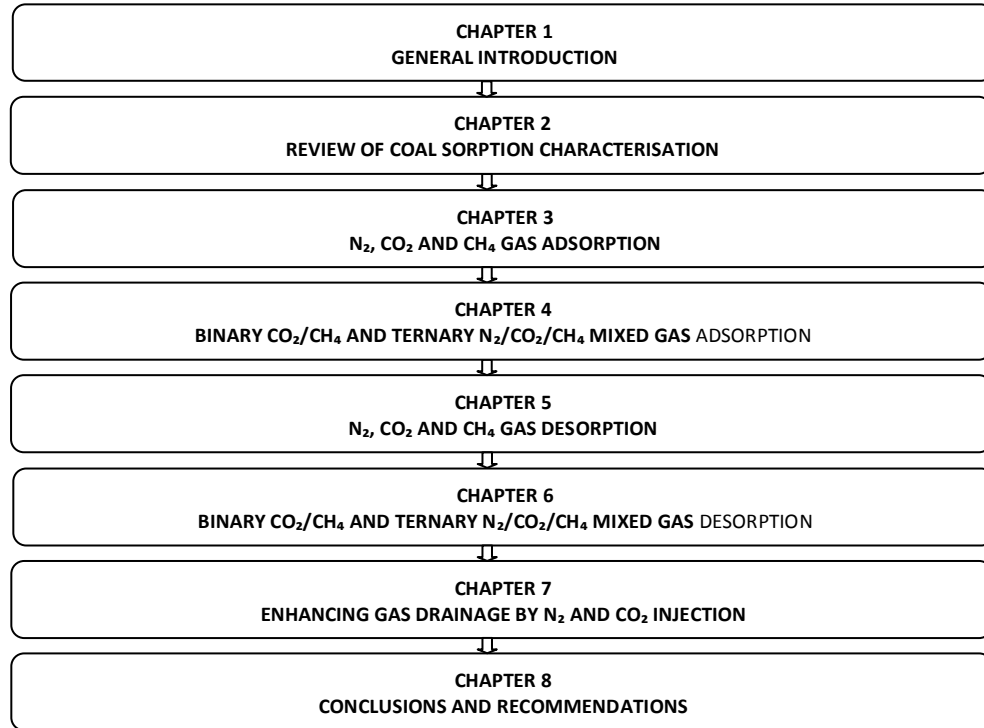


Figure I-2 – Thesis outline flowchart

- Chapter 5 outlines the study of N₂, CO₂ and CH₄ gas desorption in several coal particle sizes. Also, it describes the findings on residual gases in coal
- Chapter 6 presents the results of binary CO₂/CH₄ and ternary N₂/CO₂/CH₄ mixed gas desorption on several different sized particles of coal. It also compares the gas content in coal during desorption and adsorption
- Chapter 7 presents the results of the effectiveness of enhancing gas drainage in coal by injecting N₂ and CO₂ gas. The results are presented regarding axial load on coal, gas type, gas composition and volumetric changes.
- Chapter 8 summarises the findings of gas sorption in coal and makes recommendations for further research.

II. CHAPTER TWO

A REVIEW OF COAL SORPTION CHARACTERISTICS

II.1 INTRODUCTION

Advances in coal mining over the past 50 years are the direct consequence of new techniques, specifically in the area of extraction. These improvements were mainly achieved by the development of extraction equipment and haulage systems, and by improving the methods of extraction. This revolution was accompanied by either partial or full automation of these processes. However, this improvement in coal mining also raised significant challenges of safety and cost. The development of mining techniques associated with work safety and other issues related to gas hazards, have stimulated an interest in further studying gas adsorption/desorption in coal, as part of more complex studies on mine ventilation systems, coal/gas outburst, and gas drainage. As a result, it was necessary to gather accurate information on parameters such as adsorbed gas volume, emission rates, and gas desorption rates, and also study the enhancement of gas drainage by coal fracturing or N₂ gas injection. Accordingly, the phenomenon of gas adsorption and desorption in coal is reviewed and discussed in this chapter, with a special focus on three parameters; the size of coal particles, type of gas, and time of saturation.

II.2 PHYSICAL STRUCTURE OF COAL

Coal is a porous medium from the family of reservoir rocks but coal differs from conventional reservoirs due to the large volume of gas that it can store due to its large pore volume capacity. The gas in coal is stored mainly by being adsorbed into the pores

CHAPTER TWO

A review of coal sorption characterisation

large internal surface which is very large (20 to 300 m² per gram of coal). Figure II-1 shows a fractured core coal sample.



Figure II-1 – Core coal sample

According to Saghafi *et al.* (2007), the total volume of gas in coal can be divided in:

- Free gas: compressed in the pores. It is small compared to the total gas contained in coal;
- Adsorbed gas: on the internal surface of the pores. This amount of gas is about 90% of the total gas in coal;
- Absorbed gas: contained in closed pores or deeply in the solid matter.

The coal storage capacity and internal surface area are related to its porosity and distribution of its pore sizes. According to the International Union of Pure and Applied Chemists (IUPAC), the structure of the coal matrix can be classified in micro pores (less than 2 nm in diameters), meso pores (2 to 5 nm in diameter) and macro pores (more than 5 nm in diameter). Pore size depends on coal composition and rank. Faiz *et al.* (2007), reporting on the works of Moffat and Weale (1955), Mahajan and Walker (1978) and Janowsky (1984), stated that coals of lower rank were likely to be composed of higher volumes of larger pores, while bituminous coals were dominated by micro pores. In general, they stated that the total open porosity and internal surface area of coal decreased with an increase in rank, from high volatile bituminous (VR~0.7%) to medium volatile bituminous (VR~1.4%) and with further increases in rank

CHAPTER TWO

A review of coal sorption characterisation

they increased. Macro pore structure consists of a network of cleat systems. The micro and macro pores defined the coal as dual porosity rock (Harpalani and Chen, 1995).

Coal fractures and fissures in a network system are known as cleats (Figure II-2). Face and butt cleats are avenues for gas and water flow (Figure II-3). Face cleats are extensive and largely confined to the bright coal layer and are not continuous over all the coal seam. Butt cleats are discontinuous and orthogonal to the face cleats. The cleat porosity system is important in coal reservoir because most of the reservoir permeability comes from the cleat network. Bedding planes or surfaces which are not used to conduct gases or water, complement the cleat system.

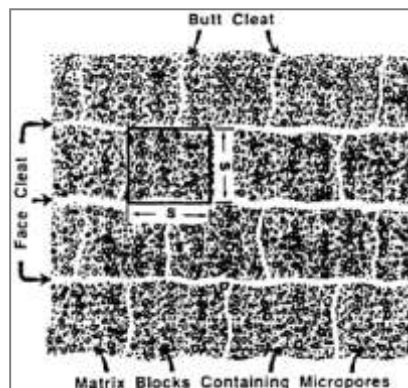


**Figure II-2 – Coal cleats system (after Harpalani and Chen, 1995)
(After Harpalani and Schraufnagel, 1990)**

The coal matrix contains very fine pore spaces which are referred to as micro pores. These micro pores do not contribute significantly to permeability but they can store large amounts of gas in adsorbed form (Shi and Durucan, 2003). The micro pores are the primary porosity system whereas the cleats are the secondary porosity system. They were caused by geological processes such as structural deformations, differential compaction and volume contraction. Coal cleats are extended fractures formed as a results of the stress generated by the volume shrinkage of coal matrix due to desiccation during thermal maturation (Nelson, 2000). Mazumder *et al.* (2006) defined

CHAPTER TWO

A review of coal sorption characterisation

the coal matrix as consisting of a three porosity system; micro pores, meso pores, and macro pores. High pressure allows a considerable amount of gas to be adsorbed into the coal by penetrating its molecular structure. In addition to this, a small amount of gas is stored as free gas in macro pores and fractures in the coal. The adsorbed volume of gas is related to the internal surface area, pressure, and temperature of the coal. The gas adsorption capacity increases asymptotically with pressure.

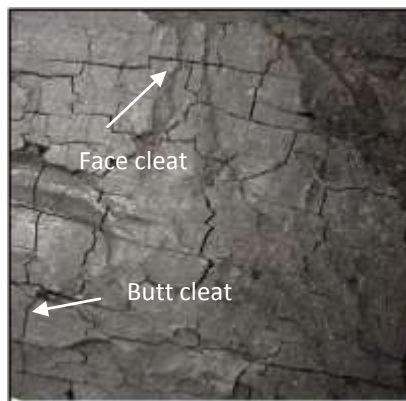


Figure II-3 – Butt and face cleats (after Sereshki, 2005)

Other important attributes of cleat geometry are spacing and width. Changes in cleat porosity are due to swelling and shrinkage. Swelling due to gas adsorption, closes or decreases the width of the cleats, causing a significant reduction in permeability (Mazumder *et al.*, 2006). However, coal shrinkage due to gas desorption opens or widens the cleat. Gregg and Sing (1982) reported that gas adsorption is an exothermic process. Once the equilibrium pressure is reached, the sorption capacity decreases with an increase in temperature. Faiz (1992) found that the adsorption capacity of coal varied according to the physical and chemical properties of the gas. For example, a bituminous coal from the Sydney Basin could store about 1.5 to 2 times more CO₂ gas than CH₄ gas at a given set of pressure–temperature conditions, and this ratio could be even greater than 10 times for sub-bituminous and brown coals. Ciu *et al.* (2004)

CHAPTER TWO

A review of coal sorption characterisation

explained the higher capacity for CO₂ adsorption in coal in terms of molecular size. CO₂ molecules are smaller than CH₄ molecules and small molecules can reach finer pores. Thus, the adsorbed mass of CO₂ in coal is higher than CH₄. Furthermore, the CO₂ in low rank coals that contain high moisture contents (e.g. brown coal) may also be stored in solution, especially at high pressures.

II.3 GASES IN COAL

Faiz *et al.* (2007) reported that coals from parts of the Sydney Basin contained over 90% CO₂ and some up to 12% C₂H₆ (Faiz and Hutton, 1995; Faiz *et al.*, 2003) despite the gas in coal seams generally consisting of CH₄ and minor amounts of CO₂, C₂H₆, higher hydrocarbons (C₂₊) and N₂ (Smith and Pallasser, 1996).

Seam gas in Sydney Basin coals was derived from multiple sources, including:

- Thermogenic CH₄ and higher hydrocarbons formed from deep burial during the Jurassic and Early Cretaceous periods (Faiz and Hutton, 1997),
- Secondary biogenic CH₄ formed since the Late Cretaceous uplift (Faiz *et al.*, 2003);
- CO₂ derived mostly from intermittent igneous activity between the Permian and Tertiary periods (Faiz and Hutton, 1995).

According to Faiz *et al.* (2003) coal seam gases in the southern Sydney basin were derived from thermogenic, magmatic and biogenic sources. At the present day distribution of these gases is mainly related to geological structure, depth and proximity to igneous intrusion (Hargraves, 1963). With regard to the coal maturity, the coal from the Illawarra region measures range in rank from high to low volatile bituminous. The model of their thermal history indicates that these coal ranks were attained as a result of high palaeo heat flux (75 to 100 mWm⁻²) and deep burial (> 2 km). Also, Faiz *et al.* (2003) reported that according to the thermal history and gas

CHAPTER TWO

A review of coal sorption characterisation

generation modelling, the generation of coal seam gas in the Illawarra region was due to the following processes:

- Methane, ethane, higher hydrocarbons and CO₂ were generated due to increasing temperature in the Late Permian and Late Cretaceous;
- As a by-product of early coalification, considerable amounts of CO₂ and water were generated between the Permian and Early Cretaceous;
- The highest rate of CH₄ and hydrocarbons generation from the coal occurred during the Early to Middle Cretaceous.

The modelling indicated that the amount of thermogenic gas generated was considerably higher than the total gas sorption capacity of the coal.

According to Armstrong *et al.* (2006), the geological history suggested that the gases had many opportunities to migrate into the strata overlying the coal seams. This migration could be done through the permeable pathways due to the intrinsic permeability of the sediments, as well as via faults, dykes, and fracture systems. Thermogenic gases were allowed to escape and microbial agents were introduced through the coal fracture system. It was quite possible that the permeability was reduced due to a dominant compressive stress field and diagenetic processes. In the absence of a clear model of gas migrating into the overlying strata, the best strategy for understanding the occurrence of strata gas was to attempt to map it from the geophysical wire line logs. However the mapping became difficult if the drill holes post dated the mining induced changes to the gas contents. Armstrong *et al.* (2006) concluded by saying that “there is consent that the discontinuous nature of the gas

CHAPTER TWO

A review of coal sorption characterisation

reservoirs and the localised and qualitative nature of the data-sets reduces the ability to accurately quantify the size of the reservoir”.

II.4 GAS ADSORPTION/DESORPTION IN COAL

The phenomenon of gas sorption has been studied for over two centuries. The adsorption of gases, mostly in charcoal, was described as early as 1773 by C.W. Scheele and later on in 1777 by A.F. Fontana (Brunauer, 1945). Brunauer (1945) reported on the work of De Saussure in 1811 and his systematic measurement of gas adsorption on several adsorbents. One particular reference is rather significant from the point of view of sorption, in that De Saussure refers to easily condensable gases being adsorbed in the largest quantities by the adsorbent. Gases in the presence of solids can remain either as free or attached to the solid surface. When the interaction between solid and gas/vapour is weak, the result is the condensation of gases on the surface of the adsorbent, called physical adsorption, while the process of evaporating gas from a solid surface is called desorption. Also, Brunauer (1945) reported that the word adsorption defined as the molecules attached outside a solid surface, was first introduced by H. Kayser at the suggestion of E. du Bois-Reymond in 1881. The adsorption and desorption processes are classified into chemical (chemisorption) and physical sorption (physisorption) in function of which energies of interaction are involved. The chemisorption is a highly specific process compared to physisorption which is not specific. In chemisorption, the gas is attached to a specific site on the solid surface either by electron transfer or electron sharing involving monolayer coverage. Physisorption however, involves monolayer or multilayer surface coverage. The physisorption attraction is due to a permanent or induced attraction between the gas molecules and the atoms of the sorbent surface. This attraction involves minor changes

CHAPTER TWO

A review of coal sorption characterisation

between the gas and the sorbent which remains unchanged until relaxation of the substrate lattice occurs. There is no covalent bond between the gas molecules and the solid surface making the physical adsorption a reversible process. It is assumed that at low pressures the adsorption occurs as a monolayer and as multilayers at high pressures (Karge *et al.*, 2008). Kelemen and Kwiatek (2009) stated that the rate of gas adsorption for coal varies with the size of coal particles that are smaller than the fissure network of the coal. They found for dry coal at 30 °C that the relative adsorption amount varies as $\text{CO}_2 > \text{CH}_4 > \text{N}_2$ which is in agreement with the general behaviour observed for dry bituminous coal. Also, they reported that the amount of CO_2 adsorbed by all dry coal samples at 30 °C was greater than at 75 °C. This finding agreed with Busch *et al.* (2004) reporting that at low constant pressure the sorption capacity of coal for CO_2 increases with decreasing temperature. Also, Kelemen and Kwiatek (2009) reported on coal matrix shrinkage and swelling that there was a strong non linear correlation between strain and the quantity of gas adsorbed. They found that the coal matrix shrinkage/swelling coefficient increased with increasing adsorbate concentration. Sakurovs *et al.* (2008) reported in modelling the CO_2 and CH_4 sorption properties under supercritical conditions that the calculated sorption capacity of coal was strongly temperature dependent and consequently, inconsistent with the simple monolayer model like Langmuir. However, they said that a pore filling approach can explain this temperature dependence. They found that the measured surface sorption capacity tends to decrease with increasing temperature. Also, they pointed out that if activated diffusion were the cause of differences in surface sorption capacity, it should increase with increasing temperature. Sakurovs *et al.* (2008) reported in their paper

CHAPTER TWO

A review of coal sorption characterisation

that the sorption capacity of CO₂ was about 4-5 times greater than CH₄ (on a mass basis), even though the βE (where E is the heat of adsorption and β is an affinity coefficient for the gas to the substrate) values were similar indicating that the heat of sorption and sorption capacity were not necessarily correlated. The study suggested that the correlation between the heat of sorption onto a surface and the sorption capacity measured by different supercritical gases at a given temperature was not mandatory. Despite of CH₄ and CO₂ having similar heat of sorption, according to the results of using this model, the coal has greater sorption capacity for CO₂ than CH₄. The difference is attributed to the strong interactions between CO₂ molecules than between CH₄ molecules that also it can be accounted as partly responsible for the greater critical temperature of CO₂. Also, according to the model, more CO₂ was adsorbed by the coal than CH₄ at a supercritical temperature due to the size of the pore width to be filled. At this temperature, the pore width that CO₂ can fill was greater than the width of the pore that CH₄ can fill. In contrast to many models of enhanced coal bed methane assumptions, if the heats of adsorption of the two gases on coal are similar, it may be more difficult to replace CH₄ by CO₂ on coal surfaces. By increasing the temperature, the monolayer coverage by the gas became better approximated and the Langmuir model would fit the data more accurately at any given temperature. The adsorption capacity of CH₄ and CO₂ can only be compared by adsorption under subcritical conditions due to its temperature dependency. However, the CH₄ adsorption capacity under subcritical conditions could be underestimated because of the low critical temperature of the CH₄. Consequently, the likeliness of accessing the coal structure will be very limited due to the low kinetic energy of the

CHAPTER TWO

A review of coal sorption characterisation

CH₄ molecules. The temperature dependence of the adsorption capacity can be explained as a function of the maximum pore width. Below this value, the pore can be filled-in by adsorbed gas under supercritical condition. This pore width decreases as temperature increases above the critical temperature. The CO₂ adsorption by coal as a process of pore filling simplifies the assessment of coal-gas interaction suggesting that the CO₂ motion across the coal surface is free and there is no attraction to a specific site. However, the water is attracted to a specific site in coal, mainly exposed oxygen atoms due to its polarity (Allardice and Evans, 1971; McCutcheon *et al.*, 2003).

II.4.1 ISOTHERM PARAMETERS

Gas adsorption and desorption has been the subject of intense study by Seidle and Huitt (1995), Moffat and Weale (1955), Jolly *et al.* (1968), Harpalani and Chen (1995), Lama (1988), Busch *et al.* (2003) and many more. There are different opinions regarding test adsorption and desorption duration. Seidle and Huitt (1995) used the coal matrix strain equilibrium to measure the gas saturation. The test was carried out using the coal matrix shrinkage method with the coal samples (core samples of unknown size) being subjected to pressures up to 13,790 kPa (2,000 psi). They reported that when coal adsorption was carried out in CH₄ gas, the coal matrix strain took about three months to stabilise. However, when in desorption it took about ten days. The process of desorption from the sample was carried out in 1,379 kPa (200 psi) steps. With He gas however, the equilibrium time at each step was about three days and with CO₂ it took around four days. As a result, Seidle and Huitt (1995) concluded that longer equilibrium times would be required for matrix shrinkage tests. Moffat and Weale (1955), using only CH₄, found that both powdered coal and lumps of about 12.5 mm in size required the same time to reach an equilibrium pressure. At 100 MPa (1000

CHAPTER TWO

A review of coal sorption characterisation

atm.) the coal sample took less than one hour to reach a state of equilibrium. Moffat and Weale (1955) also observed that in the same sample, previously saturated, the CH₄ released in a given amount took almost two hours to reach the new pressure state of equilibrium.

Figure II-4 shows the adsorbed CH₄ in coal against pressure in several samples of coal. All the particles tested in gas adsorption measured 0.21 mm. Levine (1996) carried out linear and volumetric strain tests in samples of high volatile bituminous Illinois coal blocks several centimetres in length and width using CO₂ and CH₄ gas. He reported very long equilibration times caused by restrictions in the size of the coal sample. He noted that some samples took about 200 hrs to achieve equilibrium pressure. In larger samples it would require even longer to reach equilibrium. Busch *et al.* (2003) reported that samples of powdered coal < 0.20 mm in size usually reached equilibrium pressure at 45 °C and at pressures up to 25 MPa in approximately 15 min, during a volumetric gas adsorption test conducted with CH₄ and CO₂ gas.

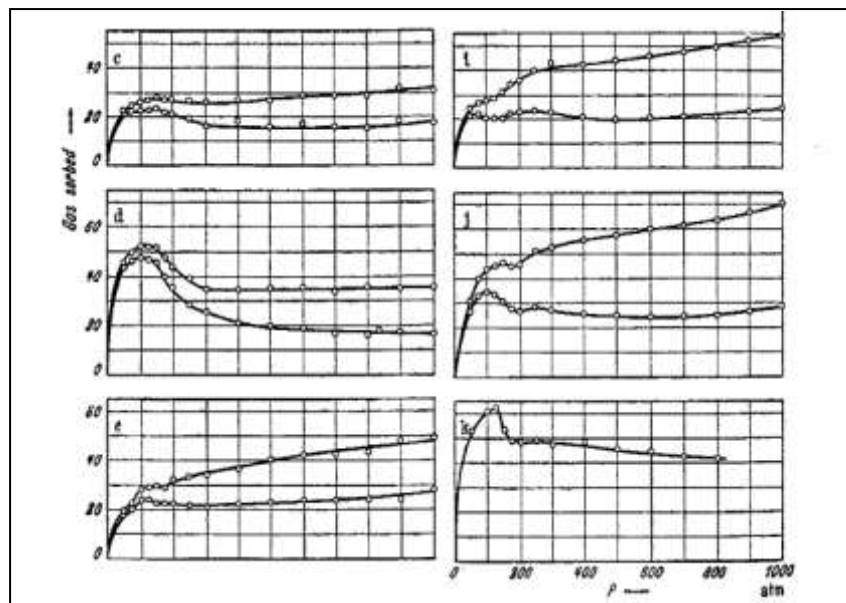


Figure II-4 – Adsorbed CH₄ in coal (after Moffat and Weale, 1955)

CHAPTER TWO

A review of coal sorption characterisation

Table II-1 summarises the saturation time reported by several researchers on adsorption and desorption tests. The table clearly shows that most of these tests were carried out over durations between less than 1 hr to more than 2 000 hrs.

Table II-1 – Gas saturation duration

Reference	Process	Time (hr)	Gas type	Size (mm)	Temperature (°C)	Pressure (kPa)
Seidle & Huitt (1995)	adsorption	2160	CH ₄	unknown	48	13,800
	desorption	240	CH ₄	unknown		
	desorption	72	He	unknown		
	desorption	96	CO ₂	unknown		
Moffat & Weale (1955)	adsorption	< 1	CH ₄	0.21 12.5	25	100,000
Levine (1996)	adsorption	200	CO ₂ , CH ₄	unknown	unknown	2,000
Busch et al. (2003)	adsorption	0.25	CO ₂ , CH ₄	< 0.20	45	25,000

Seidle and Huitt (1995) stated that unfortunately many of these studies were done at pressures and temperatures below those found in a coal seam and at different in situ humidity conditions, or that not enough information regarding the coal samples, petrography, or mineralogy such as ash content or mineral matter was provided. Thus the duration of saturation of different gases in coal could lead to different types of reactions independently of the process involved. The studies on gas adsorption often did not accurately report the time to reach saturation or the parameters used for deciding what the level of saturation was or should be. Therefore, comprehensive comparisons within these findings are not possible, and most of the time the outcome of the experiments are reduced to simple descriptions of laboratory procedures.

The presence of moisture on coal affects in several ways the measurements of gas adsorption. Coal density is complicated to measure in moist coal due to errors that can be accounted as a result of the presence and the volume occupied by the water. In general, water tends to reduce the adsorption capacity of coal. However, accurate

CHAPTER TWO

A review of coal sorption characterisation

estimates of gas adsorption required that isotherms be measured at equilibrium moisture. The sorption capacity for both CO₂ and CH₄ in moist coal was significantly lower than in dry coal. The reduction in the adsorption capacity was dependent on the coal rank having a great affect on low rank than high rank coals. Coal has a certain critical moisture content beyond which further moisture does not affect the adsorption capacity. This limiting moisture content was dependent on the coal rank and the injected gas, and corresponds approximately to the equilibrium moisture point. This equilibrium moisture point is achieved by exposing the coal to about 40-80% of relative humidity. The loss of adsorption capacity due to moisture can be explained by volumetric displacement of CO₂ and CH₄ by the water. CO₂ capacity was reduced by about four times greater than CH₄ for each 1% increase in moisture, at below the limiting moisture content (Day *et al.*, 2008). Levy *et al.* (1997) reported that an Australian bituminous coal at moisture levels below 4%, the CH₄ capacity decreased linearly with increasing moisture. Krooss *et al.* (2002) found that the CH₄ sorption capacity of the coal at equilibrium moisture was 25% lower than dry coal. He also found that the CO₂ capacity of moist coal was lower than that of the dry coal but their moist coal isotherms showed unusual maxima and minima which were interpreted as an effect of CO₂ induced swelling enhanced by the presence of moisture. The association of moisture with coal is complex even without any presence of gas. Water coexists in coal in different physical states and may vary from few percent in high rank coal to more than 70% in brown coals and lignite. According to Busch *et al.* (2007), the moisture itself may represent an important storage reservoir for CO₂, especially in low rank coals. However, Day *et al.* (2007) also found very little variation in the affinity of

CHAPTER TWO

A review of coal sorption characterisation

CO₂ with rank in dry coals. The adsorption of water in coal occurs by hydrogen bonding at oxygenated primary sites. Water is adsorbed in preference at these primary sites and could also form clusters around them. The oxygen content of the coal defines the amount of water to be adsorbed but for CO₂ and CH₄ the situation is unclear and the nature of the binding sites is not well defined (McCutcheon *et al.*, 2003). The traditional approach of gas adsorption is explained by the Langmuir model which is a monolayer surface coverage. However, in recent years other models such as Dubinin–Astakhov and Dubinin–Radushkevich appeared to better tally with the experimental data (Sakurovs *et al.*, 2007). This suggests that the supercritical gas adsorption occurs as pore filling. The pore can be fully saturated when the gas is at a supercritical state until a critical pore diameter is reached. Above this maximum pore diameter the pore is not fully filled. This model predicts that the density of the adsorbed is high at the surface and then progressively decreases at distances further away from the surface until reaching the density of the free gas. Therefore, narrow pores will be filled by the gas but for large pore diameters the pores would be partially filled because the gas is unable to condense under supercritical conditions (Figure II-5 a).

Water molecules are attached to polar sites, such as hydroxyl groups, on the coal surface which are represented as black marks in the figure. In this process the CO₂ and CH₄ capacity are reduced by physical displacement by the water. The monolayer coverage corresponds to the polar sites fully occupied by the water. Consequently, the sites remaining on the coal, which are the hydrophobic sites, continue to be available for adsorption of CO₂ and CH₄ (Figure II-5 b). The CO₂ and CH₄ adsorption capacity of

CHAPTER TWO

A review of coal sorption characterisation

the coal appear to be independent of the type of surface but the moisture capacity is related to the availability of the polar sites.

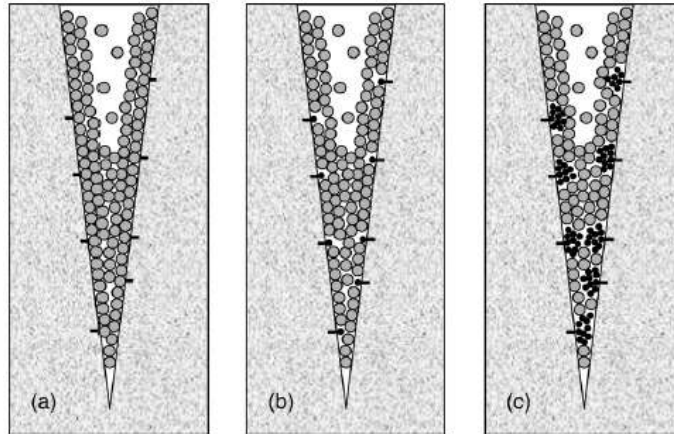


Figure II-5 – CO₂ and moisture adsorption in coal pores.
a) CO₂ only; b) CO₂ with water monolayer; c) CO₂ with water cluster
(after Day *et al.*, 2008)

The lack of clear correlation between the adsorption capacity for CO₂ and CH₄ and the rank of coal can be explained by the fact that the CO₂ and CH₄ adsorption capacity depend on the diameter of the pores, corresponding higher capacity for a large number of smaller pore diameter. Clusters of water molecules are likely to be formed around the polar sites by hydrogen bonding between adjacent water molecules when the moisture content is above the monolayer capacity (Figure II-5 c). These clusters are located in sites that could be occupied by gases. The unavailability of these sites reduces the adsorption capacity of CO₂ and CH₄. Adsorbed molecules of CO₂ could form a layer on the top of the adsorbed water but CH₄ is unlikely to be attached to the water. Thus, CH₄ will only occupy the hydrophobic sites not occupied by the water. According to Brennan *et al.* (2001), the interaction of coal with water is more complex than with non polar gases such as CH₄, Helium or CO₂ due to the weak dispersion of water with coal. The water tends to form hydrogen bonds with other adsorbed water

CHAPTER TWO

A review of coal sorption characterisation

molecules and surface chemical species. Also, there is a chemisorption interaction of the water with the coal mineral matter. The water molecules are strongly adsorbed on the solid surface by hydrogen bonds followed by the creation of water clusters and eventually pore filling. The filling of micro pores is progressive; first, the narrow micro pores are filled and then, the water molecules are adsorbed in the remaining micro porosity. The water molecules adsorbed in the porosity of carbon have a solid-phase structure throughout the whole range of micro pore size (Alcaniz-Mongue *et al.*, 2001). Also, an important control on water adsorption on coal is the pore size distribution which plays a key role in the observed energies of the water adsorption process (Salame and Bandosz, 1998). According to Hanzawa *et al.* (1998) and also Iiyama *et al.* (1997), the water molecules form an ordered assembly structure in the hydrophobic nanospace as observed by X ray diffraction of adsorbed water molecules in molecular sieving carbons. Bratek *et al.* (2002) reported that at high pressures, the amount of water adsorbed decreases with an increase in rank showing a clear correlation between the coal rank and the amount of adsorbed water (Figure II-6). The minimum adsorbed water was reported to be at about 1.2% of vitrinite reflectance (VRr). This parabolic behaviour is similar to the rank dependence of the micro pore volume. Clarkson and Bustin (1996) investigated the effect of lithotype, maceral and mineral contents on the micro pore capacity and size distribution for a medium-volatile and a high-volatile bituminous coal. They reported that the low pressure Dubinin micro pore capacities and Langmuir monolayer volumes at -0.15 °C increased with increasing total and structured vitrinite content and decreased with increasing inertinite and mineral matter content. With vitrinite, the increase in the number of micro pores caused the

CHAPTER TWO

A review of coal sorption characterisation

increase in micro pore capacity. The largest micro pore capacity was found in samples with high vitrinite and semifusinite contents likely to be due to the development of micro pores in semifusinite through burning. An increase in inertinite and mineral content led to an increase in micro pore heterogeneity.

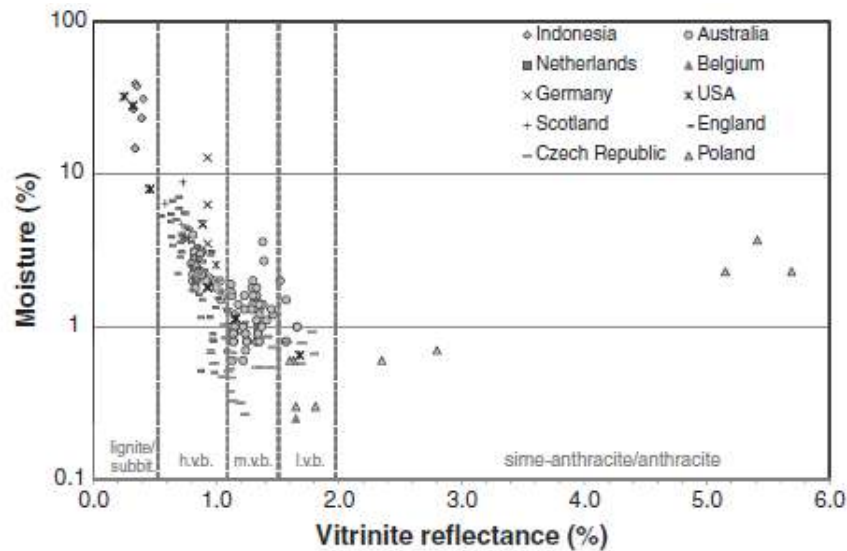


Figure II-6 – Equilibrium moisture content of coals of varying rank (after Busch and Gensterblum, 2011).

The gas capacity in bituminous coals is a function of the micro pore capacity and the size distribution. In meso and macro pore materials, the internal surface area is the primary factor controlling gas adsorption. The pores are filled with gas in multilayers. However, micro pores appear to be filled by volume filling. Thus, micro pore volume controls the gas adsorption for micro pore materials. The main parameter in evaluating the gas adsorption is the proportion of the total pore volume contributed by micro porosity. The proportion of micro pores generally increases with rank and micro pores are predominant at high rank coals. Macro pores are predominant in low rank coals (Gan *et al.*, 1972). They reported that the CO₂ surface area of the coals in their study decreased with increasing rank up to high volatile to medium volatile bituminous. Also, the composition of the coal is another important factor that affects pore size

CHAPTER TWO

A review of coal sorption characterisation

distribution and surface area. Faiz *et al.* (1992) reported that CO₂ and CH₄ Langmuir volumes decreased with mineral matter content. However, the relation with Maceral composition was not clear probably due to the masking effect of rank differences between coals studied. Crosdale and Beamish (1993) indicated that CH₄ adsorption was generally higher for high vitrinite coals than for inertinite coals. CO₂ adsorption followed a similar trend.

Swelling and shrinkage tests conducted by Harpalani and Chen (1995) found that CH₄ gas took nearly four months to reach strain equilibrium at increasing pressure, but only about a month in decreasing pressure. They suggested using smaller samples instead of 89 mm diameter cores to reduce the duration of the experiment. Also, Harpalani and Chen (1995) reported that the volumetric shrinkage was linearly proportional to the desorbed gas, as shown in Figure II-7, and only took place with desorption.

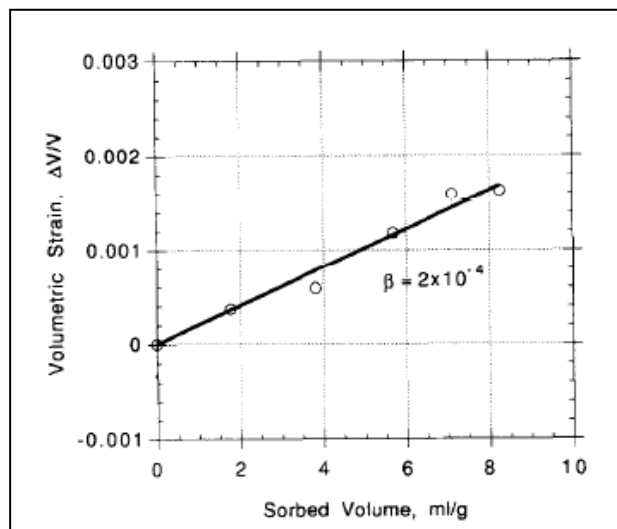


Figure II-7 – Linear volumetric strain (after Harpalani and Chen, 1995)

Harpalani (2005) reported adsorption measurements of CH₄ and CO₂ gas using pulverised samples of coal from the Illinois basin that were 0.42-0.15 mm in size. Harpalani reported very long desorption times for most Illinois coal, which was suggestive of low diffusion rates. Robertson and Christiansen (2005) reported that due

CHAPTER TWO

A review of coal sorption characterisation

to the difficulties associated with resistance-type strain gauges and the length of time required for the samples to reach equilibrium, there was very little data of sorption-induced strain available. They therefore measured the longitudinal strains stemming from gas adsorption in sub-bituminous coal from the Powder River Basin in Wyoming, and highly volatile bituminous coal from East-Central Utah using an apparatus based on the optical detection of strains over a shorter period of time instead of using strain gauges, which require larger samples and a longer period of time to reach equilibrium. Strain curves were generated with CO₂, N₂, CH₄, He and various mixtures of these gases at a constant temperature of 26.7 °C (80 °F).

Figure II-8 shows the Langmuir-type equation used by Robertson and Christiansen (2005) to model the strain data from pure gases.

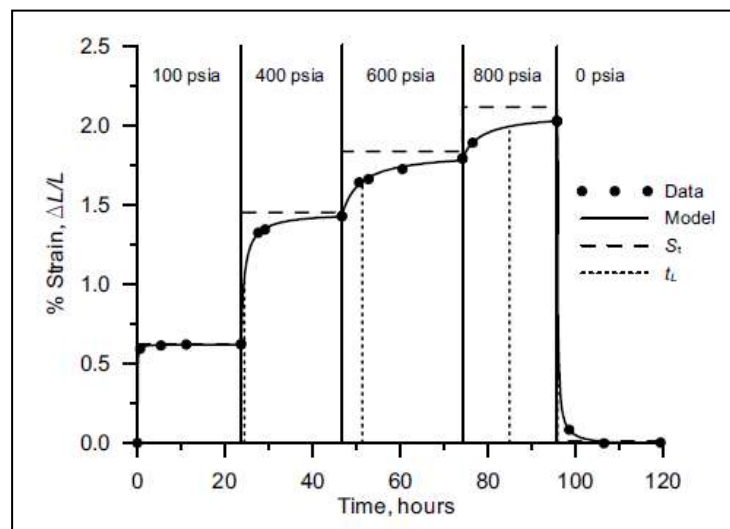


Figure II-8 – Langmuir-type strain model used by Robertson and Christiansen, 2005)

The graph suggests that the Langmuir-type equation used for modelling the induced strain on coal by Robertson and Christiansen (2005) appeared to be successful. Also Robertson and Christiansen (2005), in order to avoid the difficulties encountered by previous researchers and speed up the data collection process, made use of smaller

CHAPTER TWO

A review of coal sorption characterisation

samples (20x3x3 mm) to reduce the time required for equilibrium and hence, faster data collection. The results showed that with CO₂ gas the linear strain was stabilised quickly (0.032 hrs for 690 kPa) at low pressures, but at high pressure (around 5 500 kPa) equilibrium took longer (10.7 hrs). The data measured within each 24 hour period at each pressure point was modelled by using a Langmuir-type equation to extrapolate to infinite time.

Table II-2 summarises the report of the sizes of coal particles used by several researchers during gas adsorption. The table shows that the listed researchers did use samples that were dissimilar in size and shape. Some researchers used 89.0 mm diameter core samples for shrinkage tests while others used 20x3x3 mm cubic blocks.

Table II-2 – Summary of coal particle sizes used in adsorption test

Reference	Process	Gas type	Size (mm)	Temperature (°C)	Pressure (kPa)
Moffat & Weale (1955)	adsorption	CH ₄	0.21 12.5	25	100,000
Busch et al. (2003)		CO ₂ , CH ₄	< 0.20	45	25,000
Harpalani & Chen (1995)		CH ₄	89 mm	unknown	10,300
Harpalani (2005)		CH ₄ CO ₂	0.42-0.15	22.2	10,300 5,500
Robertson & Christiansen		CO ₂	20x3x3	26.7	5,500

Thus, the use of different shape and size particles may affect the results obtained and could lead to erroneous conclusions, and the use of different temperatures could be questioned. Some researchers used reservoir temperatures but others used an arbitrary temperature. These dispersed criteria for the samples of coal appeared to be the cause of a discrepancy regarding the induced coal strains. Seidle and Huitt (1995), and Harpalani and Schraufnagel (1990) suggested that the sorption induced strain varied linearly while Robertson and Christiansen (2005) reported that sorption-induced

CHAPTER TWO

A review of coal sorption characterisation

strain is not a linear function of the gas pressure (Figure II-9). Pekot and Reeves (2002) also suggested that, for high adsorbed gas concentration, the adsorption-strain relationship may become non-linear. Under these circumstances it is almost impossible to use and compare the results obtained from different sources.

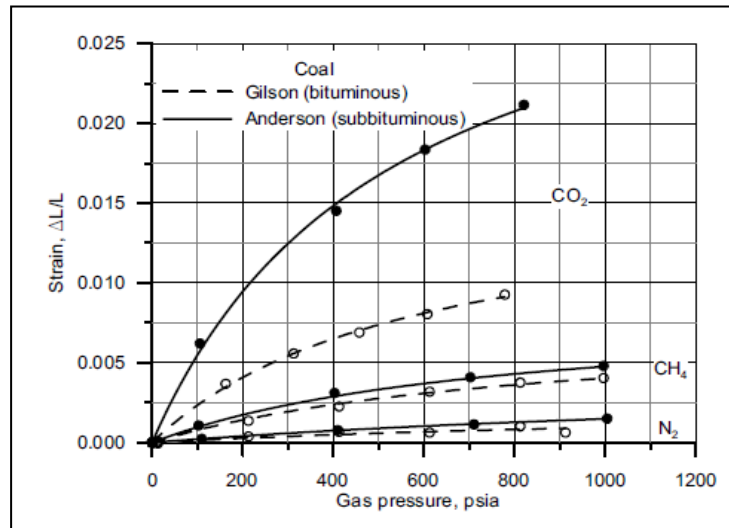


Figure II-9 – N₂, CO₂ and CH₄ gas strain curve profiles (after Robertson and Christiansen, 2005)

Kelemen *et al.* (2006) carried out swelling/shrinkage/sorption tests on three samples of bituminous Argonne premium coal with CO₂, CH₄ and N₂ gas at 23 and 75 °C, at pressure levels up to 1.6 MPa. They used 15x7x5 mm blocks and powder samples (0.074 to 0.15 mm) on strain measurements tests. Gas sorption measurements were made on 7x5x5 mm coal blocks. Swelling and shrinkage measurements were made using a pressurised dilatometer ($P \leq 2\,000$ kPa). Gravimetric gas sorption measurements and equilibrium time was fixed at one hour. They found that measurements on samples of block coal required far more time to reach equilibrium than powdered coal. At 23 and 75 °C the results indicated that both swelling and sorption were reversible with little adsorption hysteresis. Figure II-10 shows the relationship between induced strains against adsorbate concentration for N₂, CO₂ and

CHAPTER TWO

A review of coal sorption characterisation

CH₄ gas. The results suggest that the induced strain deviated marginally from a linear relationship with the amount of adsorbed gas.

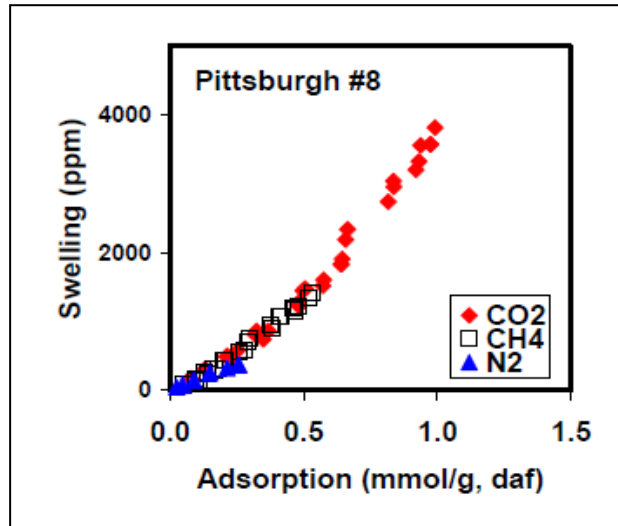


Figure II-10 – Induce strain versus adsorbed gas (after Kelemen *et al.*, 2006)

Kelemen *et al.* (2006) also reported that with CH₄ gas adsorption and desorption isotherms, the time to reach equilibrium was set to two hrs. The study indicated that data from samples of Pocahontas coal showed little or no hysteresis however, while desorption isotherms from samples of Pittsburgh and Blind Canyon coal appeared to be slightly above the adsorption curve. An increasing time from 2 to 5 hours to reach equilibrium resulted in better correspondence between the CH₄ adsorption and desorption. Strain measurements as a function of time were made in 7x5x5 mm blocks samples of coal at 1.6 MPa and 23 °C. Kelemen *et al.* (2006) found that with all the gases, swelling stabilised within five days. In powdered samples however, stabilisation using either CO₂ or N₂ gas took roughly one day, and five days for CH₄ gas. They also reported that the strain perpendicular to the bedding plane was 1.5 times the strain measured for powdered Pocahontas coal. Singh (1968) observed that coal could hold 1.4 to 2 times more CO₂ gas than CH₄ gas at about 345 kPa (50 psi) pressure and with

CHAPTER TWO

A review of coal sorption characterisation

N₂ gas achieving only 0.4 of CH₄ gas under the same conditions. However, Gunther (1965) reported that at a higher pressure these figures could be smaller. Recently, F. Van Bergen *et al.* (2009) carried out a swelling test in 1.0-1.5 mm³ size samples of unconfined coal exposed to CO₂, CH₄, and Ar gas. Each sample was tested for between 17 and 24 hours.

Mixed gas sorption in coal has been widely studied over the years by different researchers worldwide, and with varied results. Clarkson and Bustin (2000) studied the effect of coal moisture and composition on CO₂/CH₄ mixed gas adsorption characteristics. To analyse the isotherms they used four samples of medium volatile bituminous coal ranging from 0.25 mm to 4.74 mm in size, with CO₂ and CH₄ gas, and a mixture of both gases at 30 °C and up to 8 000 kPa pressure levels. The smaller sample was saturated with moisture at 30 °C while the larger sample was used dry. With CO₂ and CH₄ gas, equilibrium pressure was considered to be achieved after two hours, while twelve hours was enough time to conduct the whole experiment. With CO₂/CH₄ (75/25) mixed gases however, they found it took about five to seven days to reach equilibrium pressure at each pressure step.

Fitzgerald *et al* (2005) measured the CH₄, CO₂, N₂ and their binary and ternary gas mixtures adsorption on samples of wet Tiffany coal. They were measured at 54.45 °C (327.6 °K), at pressures up to 13.8 MPa, and an undetermined duration of gas saturation. Figure II-11 shows the 50/50 of N₂/CH₄ mixed gas isotherms against pressure on a sample of wet Tiffany coal at 54.45 °C (327.6 °K). The results suggest that the percentage of adsorbed N₂ acting individually was about 12% of the total adsorbed 50/50 N₂/CH₄ mixed gas. The adsorbed CH₄ gas was 88%. Thus, the sorption capacity of

CHAPTER TWO

A review of coal sorption characterisation

CH₄ was the higher than the N₂ in adsorption. They used particles of coal on a dry basis with the sizes distributed as follows: 0.85 to 1.70 mm (41-46%) and 0.43 to 0.85 mm (23-25%).

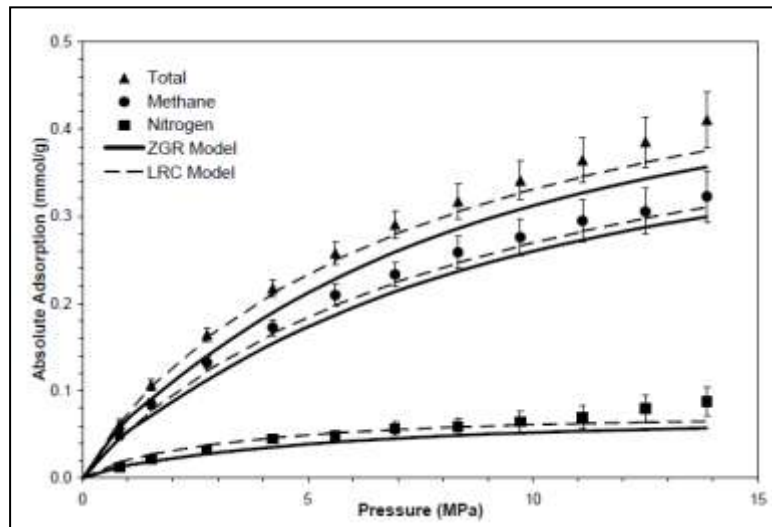


Figure II-11 – 50/50 N₂/CH₄ mixed gas isotherms on wet Tiffany coal (after Fitzgerald *et al.*, 2005)

Reeves *et al.* (2005) used eleven samples of coal from the Black Warrior, Cherokee, Forest City, Gulf Coast, Illinois, Northern Appalachian, Piceance, Powder River, and San Juan Basins and measured the single component CH₄, CO₂, and N₂ isotherms at pressures up to 34.5 MPa (5 000 psi) and temperatures between 18 to 68 °C (64 to 155 °F). In addition, they measured the binary and ternary component isotherms at 13.8 MPa (2 000 psi) and 54 °C (130 °F) on the sample from the San Juan Basin to compare the actual multi-component sorption to predictions based on single component data. They reported that, as expected, the gas storage capacity increased with coal rank and the highest adsorbed mass was with CO₂ and the lowest with N₂. CH₄ was between both. Crosdale (1998) carried out adsorption/desorption in samples of powdered coal (0.21 mm) from mines at Dartbrook and South Bulli, with CO₂ (up to 5 000 kPa), CH₄ (9 000 kPa) and 47.1/52.9 CO₂/CH₄ mixed gas at a bath water temperature of 30 °C and

CHAPTER TWO

A review of coal sorption characterisation

room temperature of 23.5 °C. Gas saturation time was set at up to three hours at each level of pressure. Pure gases were measured gravimetrically and mixed gases volumetrically. Crosdale (1998) reported that the adsorption rate depended on the size of the particle with significantly higher rates associated with finer particles. He also found that the content of CO₂ was very low compared to its single isotherm. The resultant shape of the CO₂ isotherm was almost linear and curved upwards at high pressures. He concluded that this shape was atypical for porous material such as coal and bore some resemblance to a Type II isotherm defined by Gregg and Singh (1982). The Type II isotherms were typical of gas adsorption by non porous solids where adsorption occurs as either a mono-layer or multi-layer. However, results from the mixed gas isotherms indicated that mono-layer adsorption probably does not occur and instead a process of pore-filling is responsible for the coal's adsorption properties. Crosdale (1982) found that the samples were more or less saturated with CH₄ gas in the presence of the mixed gas. He said that this result was not expected either intuitively or by using the Langmuir extended isotherm approach which would predict the CH₄ component to be about half the pure gas isotherm.

Table II-3 summarises the adsorption tests carried out by the listed researchers with respect to gas type. Adsorption tests carried out by most researchers were basically with N₂, CO₂, and CH₄ and their binary and ternary mixture. Unfortunately, most researchers performed their tests at different temperatures (22.2 to 68 °C) and different range of pressures (5 500 to 100 000 kPa), using coal particles of various shapes and sizes. This suggests that under these different laboratory environments, the

CHAPTER TWO

A review of coal sorption characterisation

results have limited use and cannot always be compared with each other with respect to time, size of coal particle, or type of gas.

Table II-3 - Summary of gas type used in adsorption test

Reference	Process	Gas type	Size (mm)	Temperature (°C)	Pressure (kPa)
Moffat & Weale (1955)	adsorption	CH ₄	0.21 12.5	25	100,000
Busch et al. (2003)		CO ₂ , CH ₄	< 0.20	45	25,000
Harpalani & Chen (1995)		CH ₄	89 mm	unknown	10,300
Harpalani (2005)		CH ₄ CO ₂	0.42-0.15	22.2	10,300 5,500
Robertson & Christiansen		CO ₂	20x3x3	26.7	5,500
Clarkson & Bustin (2000)		CO2/CH4	0.25-4.74	30	8,000
Fitzgerald et al. (2005)		N2, CO2, CH4 N2/CO2/CH4	0.43-1.70	54.45	13,800
Reeves et al. (2005)		N2, CO2, CH4 N2/CO2/CH4	unknown	18-68	34,500
		N2/CO2 CO2/CH4 N2/CH4		54	13,800

Errors in determining adsorption and desorption of coal

Potential sources of error in the determination of sorption in coal measured at low pressure were discussed by Ozdemir *et al.* (2003, 2004), Sakurovs *et al.* (2007), and Condon (2006). However, the assessment of the errors in the determination of sorption capacity at high pressure has not been done rigorously, according to Sakurovs *et al.* (2009). They reviewed in detail the probable sources of errors in the determination of the sorption capacity of coal. The authors found three sources of error in determining the free space volume. They are cell volume, coal mass and helium density of the coal. In the measurements of the free space volume, an accuracy of three digits is required in order to get high accuracy in the determination of the excess sorption capacity at high pressure. In the helium density determination three

CHAPTER TWO

A review of coal sorption characterisation

scenarios can occur; first, the given gas molecule being smaller than helium. Thus, the molecule can penetrate further into the coal to inaccessible locations that helium can not reach, leading to an overestimation of the calculated sorption. Second, helium reaching locations that the given gas can not penetrate. Thus, there is some space in coal that is accessible to helium but inaccessible to the given gas. This leads to an underestimation of the free space volume of the given gas. Finally, the given gas being dissolved into the coal (e.g. carbon dioxide) resulting in an overestimation of the calculated sorption. With respect to the adsorbed phase density, the study suggests that at high pressure the “adsorbed phase density” could even be higher than the density of the gas at the substrate surface. Sakurovs *et al.* (2009) reported for Hunter Valley coal a CO₂ density of 1320 kg m⁻³ which was significantly higher than liquid CO₂. The coal compressibility tends to decrease the volume occupied by the coal due to the injection of helium (St. George and Barakat, 2001). Consequently, the free space volume will increase making the measured sorption lower. Day *et al.* (2008) reported that the volumetric compression of an Australian bituminous coal was around 0.06 % at 15 MPa and 55 °C due to helium injection. An error of about 1% could be induced by a compression at 20 MPa if it is assumed that the compressibility changes linearly with pressure. In most of the cases this error can be neglected. The free space volume and consequently the measured adsorption could be affected by the effect of bulk space changes due to coal swelling. The swelling in carbon dioxide could be as much as 1-2% in bituminous coal and even greater for low rank coals. However, changes in the bulk volume of coal do not necessarily mean a decrease in the free space volume but an increase in internal volume that could be accessible to any gas. Measuring coal density

CHAPTER TWO

A review of coal sorption characterisation

by helium could potentially be affected by some slight adsorption of helium into coal. However, at the pressures used by a pycnometer, which is about one atmosphere at room temperature, the error may be neglected. In determining the gas density by any equation of state, the temperature must be measured with an accuracy of about 0.1 °C otherwise the adsorbed mass could be mismeasured, leading to significant errors in the adsorption capacity. Briefly, common sources of error among laboratories appeared to be due to errors in the free space volume and helium densities.

II.4.2 GAS HYSTERESIS

There is a growing interest in the study of CO₂ sorption in coal, as a single gas or as a gas mixed with CH₄. This interest stems from the current concern about reducing the green house effect globally as well as coal mining deposits that are difficult to drain. In particular the sorption of the binary CO₂/CH₄ gas presents an interesting challenge because the limited number of research publications point to formation on the isotherm hysteresis phenomenon in which there is a deviation of the gas profiles between adsorption and desorption isotherms. In general the desorption isotherms in both CO₂ and CH₄ are above the adsorption isotherms while the degree of hysteresis varies depending on various geological and environmental factors. Harpalani *et al.* (2006) studied adsorption/desorption in four samples of pulverised bituminous coal (0.15 to 0.42 mm) from the San Juan (45 °C) and Illinois Basins (23.5 °C) with CO₂ (up to 6 200 kPa) and CH₄ (up to 10 300 kPa) gas acting individually. Samples of pulverised coal were chosen to optimise the adsorption time which was set at 24 hrs. They stated that typically, the equilibrium time for single gas adsorption was not high. Harpalani *et al.* (2006) found that under similar conditions of temperature and pressure, coal

CHAPTER TWO

A review of coal sorption characterisation

prefers CO₂ rather than CH₄ gas. The preferential adsorption ratio varied between 2:1 and 4:1. That CO₂ had a greater affinity to coal than CH₄ is still not well understood.

Ettinger *et al.* (1966) explained that this preferential adsorption occurs because of a difference in the atmospheric boiling point. Gases with a higher boiling point attain higher adsorption in coal. The boiling point of CO₂ (-78.5 °C) is higher than CH₄ (-161.6 °C) so its affinity to coal is higher than CH₄.

However, Cui *et al.* (2004) explained the preferential CO₂ gas adsorption in coal in terms of the adsorption energy. Higher adsorption energy corresponds with higher gas adsorption in coal. CO₂ gas has higher adsorption energy than CH₄ gas and therefore its adsorption capacity is higher in coal.

Figure II-12 compares the CO₂ and CH₄ adsorption-desorption isotherm over pressure.

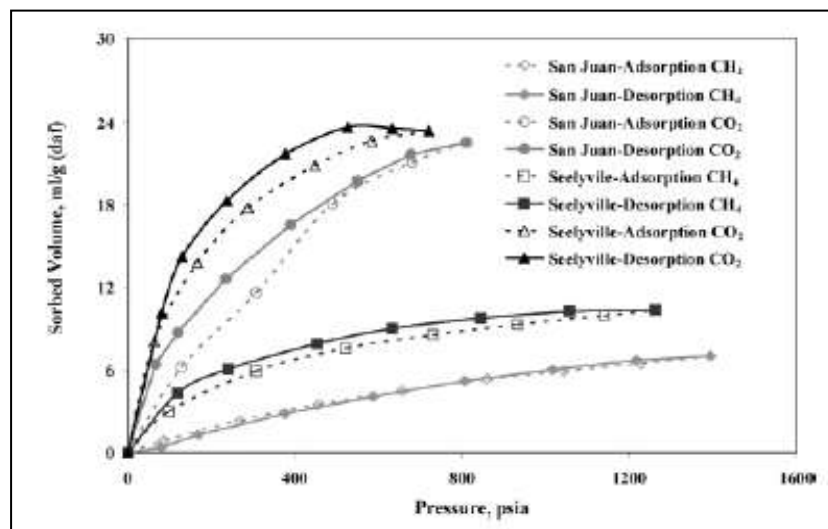


Figure II-12 – Comparison of CO₂ and CH₄ gas adsorption-desorption isotherm (after Harpalani *et al.*, 2006)

Harpalani *et al.* (2006) reported hysteresis of CO₂ and CH₄ in almost all the samples tested. The sorption capacity of CO₂ and CH₄ in coal during desorption was marginally higher than during adsorption at each level of pressure. According to Harpalani *et al.* (2006), gases such as N₂, CO₂, and CH₄ desorption isotherms should not deviate from

CHAPTER TWO

A review of coal sorption characterisation

their adsorption isotherms because adsorption/desorption is a physical and reversible process. This desorption hysteresis process may be attributed to changes in the properties/structures of coal and/or the capillary condensation in its micro-pores. Busch *et al.* (2003) measured CO₂ (up to 5 100 kPa) and CH₄ (up to 11 000 kPa) gas adsorption isotherms in samples of dry powdered coal (0.15 mm) at 22 °C.

Figure II-13 compares the CH₄ and CO₂ adsorption and desorption isotherm for the #3 sample of Pocahontas coal.

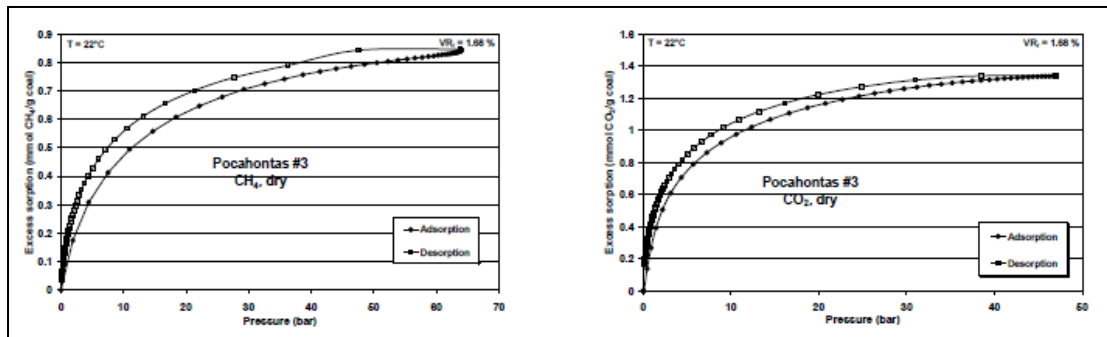


Figure II-13 – CO₂ and CH₄ gas adsorption-desorption (after Busch *et al.*, 2003)

Reporting on the sorption hysteresis, Busch *et al.* (2003) stated that the desorption isotherms of both CO₂ and CH₄ generally lay above the adsorption isotherms. The degree of hysteresis, i.e. deviation of sorption and desorption isotherms, varied irrespective of coal rank. The hysteresis effect indicated that the sorbent/sorbate system was in a metastable state, and that release of the gas from coal did not depend on a decrease in pressure corresponding to the values of the thermodynamic equilibrium. With respect to the mixed gas sorption in coal at 45 °C and up to 18 000 kPa, Busch *et al.* (2003) found that although preferential sorption of CO₂ appeared to be a regular case at high pressures of around 18 000 kPa, CH₄ may preferentially be adsorbed by certain coals in the low-pressure range (up to 4 000 kPa). More

CHAPTER TWO

A review of coal sorption characterisation

importantly, even for coals exhibiting preferential CH₄ sorption, a preferential desorption of CO₂ could be observed at high pressures. Ozdemir *et al.* (2004) measured adsorption and desorption isotherms of CO₂ on samples of dried Argonne premium coal. They reported that a small hysteresis was detected between the adsorption and desorption isotherms. Hysteresis was small or negligible for high rank coals but discernable for low rank coals. Goodman *et al.* (2004) measured the hysteresis from CO₂ desorption in three out of four separate tests carried out in different laboratories. In two laboratories, the experiments were performed at 22 °C in one and 55 °C in another. The CO₂ hysteresis depended on the rank of the coal; every test reported small or no hysteresis on higher ranked coals a large hysteresis on lower ranked coals. According to Goodman *et al.* (2004), the hysteresis was due to changes in the moisture content of the coal. Thus, different residual moisture contents in the coal after drying would be expected to play a role in the formation of hysteresis. Furthermore, hysteresis due to different residual moistures would be consistent with the previous discussion where one laboratory (Laboratory C) reported a lower capacity for adsorption. Other explanations include irreversible swelling of the matrix in the samples and CO₂ trapped in the ink bottle pores. Crosdale (1998) stated that it is apparent that when mixed gases are present, the adsorption isotherms of the single components cannot be reliably used, a mixed gas isotherm must be generated. In addition, it is required to generate a desorption isotherm due to the very large difference between the adsorption and desorption isotherm (hysteresis). Crosdale (1998) also found that with CH₄, hysteresis was either absent or very small, although the CO₂ component of the mixed gas showed a marked hysteresis compared to the

CHAPTER TWO

A review of coal sorption characterisation

pure CO₂ isotherm. From Crosdale (1998) to Harpalani (2006), the researchers commonly reported CO₂ and CH₄ hysteresis in coal during desorption. However, they attributed the reasons to different causes. Harpalani (2006) stated that gas hysteresis could not occur because physical sorption is a reversible process and therefore it may be attributed to changes in coal properties or to capillary condensation in the micropores. Busch (2003) concluded that hysteresis depended on coal rank. Ozdemir (2004) and Goodman *et al.* (2004) agreed with this and added that in high rank coal the hysteresis was almost negligible but was discernable for low ranks. However, Goodman *et al.* (2004) reported that the formation of hysteresis could be explained by the different residual moisture contents within the coal.

II.4.3 GAS ISOTHERM

Fitzgerald *et al.* (2005) used the extended Langmuir, Loading Ratio Correlation (LRC) and the Zhou–Gasem–Robinson (ZGR) two-dimensional Equation of State (EOS) to represent the total adsorption for pure, binary and ternary gas mixture systems.

The extended Langmuir model, which is the simplest model used to predict mixed gas adsorption isotherms, requires pure components of isotherm data for their predictions. The extended Langmuir model is given by the formula,

$$\theta_i = \omega_i / L_i = \frac{B_i P y_i}{1 + \sum B_j P y_j} \quad \text{Extended Langmuir (1)}$$

Where ω_i is the amount of component "i" adsorbed, L_i and B_i are Langmuir constants for "i", P is pressure, and y_i is the mole fraction of "i" in the gas phase.

Fitzgerald *et al.* (2005) stated that although the simplicity of the Langmuir model is attractive, the experimental data showed that it was inadequate to represent the behaviour of the mixtures of the gases CO₂, CH₄, and N₂. The combined Langmuir-

CHAPTER TWO

A review of coal sorption characterisation

Freundlick adsorption isotherm, expressed in terms of ω_i , yielded the loading ratio correlation (LRC) for mixtures:

$$\theta_i = \omega_i / L_i = \frac{(B_i P y_i)^{\eta_i}}{1 + \sum (B_j P y_j)^{\eta_j}} \quad \text{Loading ratio correlation (LRC) (2)}$$

The additional parameter η_i in the LRC lends more flexibility to the Langmuir model.

The results from Fitzgerald *et al.* (2005) suggested that:

- The LRC produced a better fit than the Langmuir correlation for the three gases studied
- The parameters of the LRC model obtained from the pure adsorption were used to predict the ternary mixture adsorption on wet Tiffany coal with poor results predicting pure adsorption
- Both the LRC and ZGR EOS were capable of predicting binary adsorption isotherms based on pure adsorption (as shown in Figure II-11) parameters within twice their experimental uncertainties
- The ternary predictions based on pure fluid parameters yielded three times the experimental uncertainties
- Further, for the present system, little improvement was realised by predicting the individual-component ternary isotherms based on parameters generated using both pure and binary adsorption data.

Clarkson and Bustin (2000) indicated that with CO₂ and CH₄ pure components on samples of dry coal on isotherm analysis, the Dubinin–Astakhov (Dubinin and Astakhov, 1971) (D-A) and Dubinin–Radushkevich (D-R) equations were clearly superior to the Langmuir equation for tallying with the experimental data. Also, the study found that

CHAPTER TWO

A review of coal sorption characterisation

errors resulting from using the Langmuir equation were larger for dry coal than from coal where the moisture had reached equilibrium.

Table II-4 shows the relative error calculations for isotherm fits on dry coal and samples of coal where the moisture had reached equilibrium. The table clearly indicates that the D-A equation fitted better than the Langmuir equation. The table also suggests that the Langmuir equation tallied better with coal where the moisture had reached equilibrium than with dry coal. Clarkson and Bustin (2000) found that the Ideal Adsorbed Solution (IAS) theory (Myers and Prausnitz, 1965) and the extended Langmuir model (Ruthven, 1984; Yang, 1987) differed substantially in their ability to predict how the adsorption of binary gas would react. They also reported that a comparison between model predictions and experimental data demonstrated that the IAS theory, in conjunction with the Dubinin-Astakhov single-component isotherm equations could predict the mixed gas desorption isotherms more accurately than the extended Langmuir.

Table II-4 – Relative error calculations for isotherms fits (after Clarkson and Bustin, 2000)

Relative error ^a calculations for isotherm fits												
Sample	Dry coal						Moisture-equilibrated coal					
	CH ₄ isotherm			CO ₂ isotherm			CH ₄ isotherm			CO ₂ isotherm		
	Langmuir	D-R	D-A	Langmuir	D-R	D-A	Langmuir	D-R	D-A	Langmuir	D-R	D-A
B2-11	5.16%	1.29%	0.18%	13.6%	12.0%	1.25%	1.79%	0.98%	0.83%	1.71%	1.47%	0.05%
C3-2	2.91%	1.76%	1.29%	9.76%	9.10%	2.05%	2.19%	0.44%	0.37%	1.48%	1.26%	0.00%
D3-3	3.78%	1.16%	0.19%	6.97%	4.00%	0.56%	2.89%	0.89%	0.81%	1.67%	1.13%	0.11%
B2-10	4.74%	1.63%	0.53%	8.41%	7.73%	1.23%	2.43%	0.72%	0.54%	1.63%	1.21%	0.39%

^aAverage relative error = $(100/N)\sum_{j=1}^N \text{abs}(V_{\text{calc}} - V_{\text{exp}})_j / V_{\text{exp}}$, where N = number of data points.

Stevenson *et al.* (1991) found that the IAS model could predict the binary and ternary mixed gas adsorption on dry coal quite adequately. The IAS theory assumed that the adsorbed mixed gases behaved like an ideal, adsorbed solution, and hence, was

CHAPTER TWO

A review of coal sorption characterisation

analogous to Raoult's law for bulk solutions. The amount of adsorbed mixed gas for an ideal solution is given by:

$$\frac{1}{n_t} = \sum_{i=1}^{n_c} \frac{x_i}{n_i} \quad \text{Total adsorbed mixed gas (IAS) (3)}$$

The amount of each component of the mixed gas is given by:

$$n_i = n_t * x_i \quad \text{Adsorbed gas by components (4)}$$

Hall *et al.* (1994) carried out adsorption tests with a variety of pure to mixed gas on samples of Fruitland coal. He indicated that all models predicting gas adsorption for pure gases performed similarly well. However, the IAS theory was more accurate than the extended Langmuir equation with mixed gases.

Reeves *et al.* (2005) reported that although the simplicity of Langmuir models were attractive, data showed that they could not represent the behaviour of mixtures of CO₂, CH₄, and N₂ gases adequately. In fact, errors greater than 100% were found when the extended Langmuir model was applied to data on the adsorption of N₂ from mixtures of N₂ and CO₂. All the theories used to evaluate predictions of mixed gas isotherms based on single components were inadequate in every case. Therefore, they suggested that new and more robust theories of mixed gas sorption using data for single components were required to predict mixed gas adsorption. Harpalani *et al.* (2006) reported that the experimental data were modelled using Langmuir, BET, and Dubinin-Polanyi equations. The accuracy of these models in quantifying coal-gas sorption was compared using an error analysis technique. The Dubinin-Radushkevich equation failed to model the coal-gas sorption satisfactorily. For CH₄, Langmuir, BET, and Dubinin-Astakhov (D-A), equations performed with a comparable accuracy, although the D-A equation performed much better than the other two for CO₂. Overall,

CHAPTER TWO

A review of coal sorption characterisation

the D-A equation fitted the experimental sorption data the best, followed by the Langmuir and BET equations. Since the D-A equation can derive isotherms for any temperature using a single isotherm, it provides added flexibility when modelling the variations in temperature from injection/depletion, and is therefore the model recommended for use. Ozdemir *et al.* (2004) measured adsorption and desorption isotherms of CO₂ on samples of dried Argonne premium coal. They found that the CO₂ isotherms were rectilinear and that this rectilinear form of data fitted poorly with the conventional adsorption equations. The rectilinear shape of the adsorption isotherms was related to the solubility of the CO₂ in the coal and to coal swelling. Different researchers used different equations for modelling single and mixed gas during adsorption/desorption in coal. The results were often diverse and particular for each situation. The fact that they used different equipment, experimental environments, size of coal particle, and saturation time producing dissimilar results that made it almost impossible to accurately model with just one particular equation. Thus, researchers used Langmuir, extended Langmuir, IAS theory, Dubinin-Astakhov, and Dubinin-Radushkevich equations, and many others with individual and sometimes opposing results.

II.4.4 GAS INJECTION

With increasing worldwide concern about Green House Gas (GHG) emissions and its reduction, significant interest is now directed toward finding a practical and economical way of enhancing the release of CH₄ from coal deposits and the subsequent recovery of this gas from both mineable and unmineable coal. CO₂ sequestration has been used successfully to recover CH₄ from coal measured rocks for some time now. The increased attraction of CO₂ to coal is commonly attributed to its

CHAPTER TWO

A review of coal sorption characterisation

affinity with CO_2 . As a result of CO_2 injection, the CH_4 gas is stripped from its monolayered adherence to the surface of the coal matrix and retained in its fracture space, which could then be readily driven out of coal by reducing the gas pressure. A major drawback in the application of CO_2 to CH_4 recovery is the hazard associated with an outburst of coal gas in underground coal mining. Therefore, this technique is limited to unmineable coal deposits. The storage of gas in general depends on the rank of the coal, especially in virgin seams. Higher rank coals such as bituminous and anthracite retain CH_4 in preference to other gases, but in coal seams such as the Bulli seam in the Sydney Basin, NSW, there are areas where the dominant seam gas is CO_2 rather than CH_4 . In fact, CO_2 and mixed gas CH_4/CO_2 have been found in a number of locations in Tahmoor, Metropolitan, Appin and West Cliff Mines. A typical site that is difficult to drain is at West Cliff Mine Area 5, where some sections of the longwall panels containing CO_2 are extremely difficult to drain, despite an extensive drilling programme. Field studies on the use of sand-propped hydraulic fracturing failed to increase the drainage of gas from such sites, although the technique was proven in other coal deposits, as reported by Mills *et al.* (2006). It was suggested that the highly stressed and low permeability of the coal was preventing CO_2 from being effectively drained. In recent years injecting N_2 to recover CH_4 had been trialled in a number of locations in the United State of America (USA) and Canada, with reported success at the Tiffany Project, San Juan Basin, USA. Reeves and Oudinot (2004) and Koperna *et al.* (2009), indicated that the recovery of CH_4 from coal has increased from 10-20 % after injecting N_2 . There has also been some growing interest in the possible use of a CO_2/N_2 mixture to enhance the recovery of CH_4 , particularly from mineable deposits of coal.

CHAPTER TWO

A review of coal sorption characterisation

According to Reeves and Oudinot (2004), injecting a mixture of gas could provide a synergy of production mechanisms which would lower the CO₂ in mine air. Clarkson and Bustin (2000) explained that accurate predictions of adsorbed gas during production required multi-component desorption isotherms using realistic compositions of initial gas reservoirs. According to Zuber *et al.* (1996), to increase the recovery of CH₄ during production, injecting non CH₄ gas may be used by either partially lowering the pressure of CH₄ in the free gas or by competitive adsorption.

Reznik *et al.* (1984) manifested that injecting CO₂ increased the in situ recovery of CH₄ in coal beds. Puri and Yee (1990) demonstrated that injecting N₂ increased the recovery of CH₄. Gunter *et al.* (1997) explained that reducing greenhouse gas emissions may be enhanced by dispersing anthropogenic CO₂ gas into coal seams. Knowing the mixed gas adsorption characteristics of coal is essential for any accurate assessment of enhanced recovery operations. Although some interesting research has been done in the past, most of it in the USA, more research under laboratory and in situ conditions is required, especially in Australia, using Australian coal seam parameters such as depth, temperature, main stresses, and pressure in order to gather results pertinent to the Australian environment.

II.5 GAS TRANSPORT IN COAL

Previous studies carried out by Curl (1978) and by Gray (1987), assumed that CH₄ was stored as a free gas in the fractures and large pores, and as adsorbed gas on the internal surfaces of the coal (Figure II-14). The adsorbed gas in coal is about 90-98%, while the remaining 2-10% is free gas in the open pores. Harpalani and Schraufnagel (1990) and King and Ertekin (1989) explained that present models of CH₄ flow through a coal seam indicate that it must diffuse through the pore structure of the matrix to the

CHAPTER TWO

A review of coal sorption characterisation

cleats, and then through the cleats due to the pressure gradient. This diffusion of CH_4 gas is modelled by Fick's Law and the free flow is modelled using Darcy's Law.

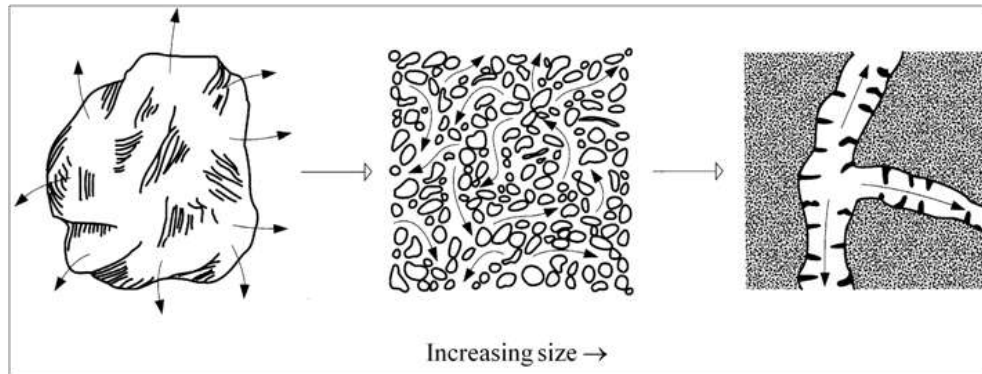


Figure II-14 – Processes involved in the transport of coalbed CH_4 gas (after Harpalani and Schraufnagel, 1990)

According to Gamson and Beamish (1992), in this model of CH_4 flow, gas transport is driven by two factors. Firstly, diffusion of CH_4 depends on the distance between the face and butt cleat spacing that defines the size of the coal matrix. Secondly, the amount of gas flowing through the cleat depends on the width, length, continuity, and permeability of the cleat. Although this CH_4 flow model may apply to predominantly bright coal seams with open and no mineralised cleats, studies indicate that the transport of gas in coal in the Bowen Basin is much more complex. Gamson and Beamish (1992) proposed a new CH_4 flow model where there may be four steps involved in the flow through the coal seam due to the varieties of micro-fractures and micro-cavities instead of two, as well as the different gas adsorption exhibited by bright and dull coals. They suggested diffusion at the micro-pore level and laminar flows at the macro-fracture or cleat level. Thus, a four tier model was proposed that incorporated CH_4 flow in both bright and dull coals (Figure II-15):

- Step 1 - Diffusion from and through the micro-pores to micro-fractures (in bright coal) and micro-cavities (in dull coal);

CHAPTER TWO

A review of coal sorption characterisation

- Step 2 - Diffusion and CH_4 flow through micro-fractures and micro-cavities partly blocked by diagenetic minerals such as clay, quartz, pyrite, or carbonates. Consequently, the movement of CH_4 on the size of the pores and how their remaining connections in the infill. At this level, movement of CH_4 is likely to involve a dual mechanism of diffusion and flow;

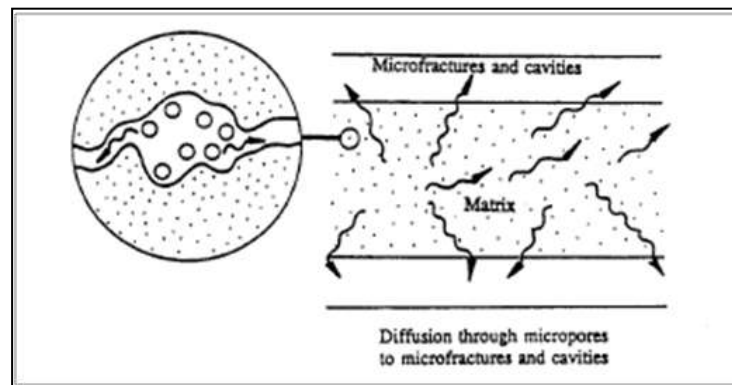


Figure II-15 – Gas flow through coals in the Bowen Basin – a new model (after Gamson and Beamish, 1992)

- Step 3 - Flow through open, non-mineralised micro-fractures (in bright coal) and micro-cavities (in dull coal). Micro-fractures and cavities are relatively large (0.05-20 μm wide) thus, the transport of CH_4 would primarily involve Darcy's laminar flow.
- Step 4 - Gas movement through cleats and joints to the well base. Because the open cleats are generally large, laminar flow is expected in most movements of gas. However, in the Bowen Basin, cleats are generally in-filled by clay minerals which mostly form a tight seal.

Crosdale (1998) carried out adsorption/desorption test in samples of coal from mines at Dartbrook and South Bulli. He reported that during adsorption, CH_4 occupied many of the available adsorption sites before CO_2 gas, this gas preventing large quantities of CO_2 gas from being adsorbed. This rapid access to the adsorption sites is due to the

CHAPTER TWO

A review of coal sorption characterisation

smaller molecules of CH_4 mass diffusing quickly into the pores. During desorption however, CH_4 is released more readily from the coal and is replaced by CO_2 that has a greater affinity with coal. Therefore, CO_2 gas is preferentially retained by the coal during desorption.

Crosdale (1998) explained the preferential adsorption of CH_4 during this process by the following steps:

1. The coal is evacuated (Figure II-16);
2. The mixed gas reaches the coal by Darcy flow through the larger pores (pore diameter $> 20 \text{ \AA}$);

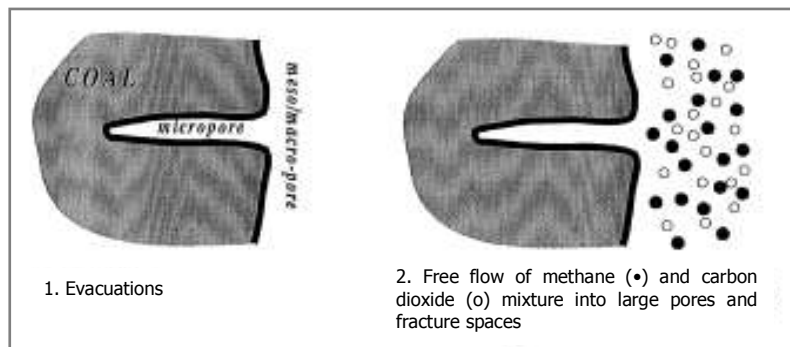


Figure II-16 – Preferential CH_4 gas adsorption by coal – Steps 1 and 2 (after Crosdale, 1998)

3. The mixed gas finds the coal surface open at the large fractures. Mono-layer and multi-layer adsorption may occur because the space is sufficient (Figure II-17). However, most of gas adsorption occurs in the small pores (pore diameter $< 20 \text{ \AA}$);
4. The mixed gas the small pores and the Knudsen process operates. In this environment the rate of diffusion is inversely proportional to the molecular weight (lighter CH_4 diffuses more rapidly). CO_2 stays on the surface of the coal longer, which retards its progress into the fine pore system due to its larger coefficient of adsorption;

CHAPTER TWO

A review of coal sorption characterisation

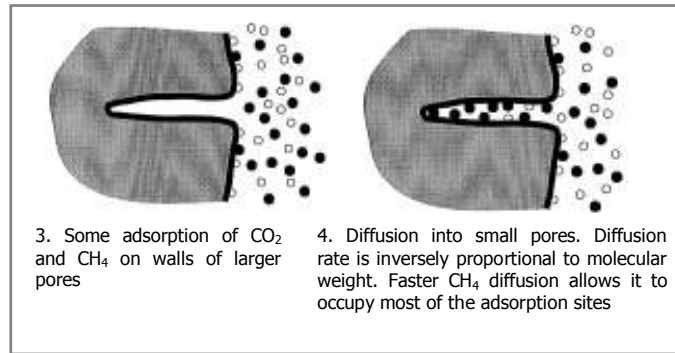


Figure II-17 - Preferential CH₄ gas adsorption by coal – Steps 3 and 4 (after Croisdale, 1998)

5. CH₄ gains access to the fine pores before the CO₂ arrives. Pore site accesses are blocked by the CH₄ which prevents the CO₂ from reaching them. Thus, most of the pore sites are occupied by the CH₄ component of the mixed gas and the mixed gas isotherm will approximate the pure CH₄ isotherm (Figure II-18);

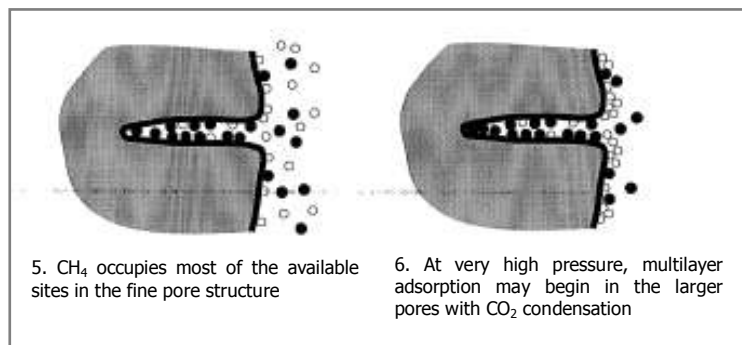


Figure II-18 - Preferential CH₄ gas adsorption by coal – Steps 5 and 6 (after Croisdale, 1998)

6. This process continues as pressure is increased. At very high pressure, the CO₂ will begin to condense and multi-layering will occur in the larger pore spaces.

The mixed gas desorption is explained as follows:

1. This initial state is the same as the final adsorption state (Figure II-19);
2. Gas flows from the larger pores by Darcy flow due to the drop in pressure. As a consequence of the free gas concentration, gas will desorb from the surfaces of

CHAPTER TWO

A review of coal sorption characterisation

the coal. The coal retains the CO_2 because of its greater affinity. Thus, the CH_4 will diffuse out of the very fine pore structure first, and then the CO_2 ;

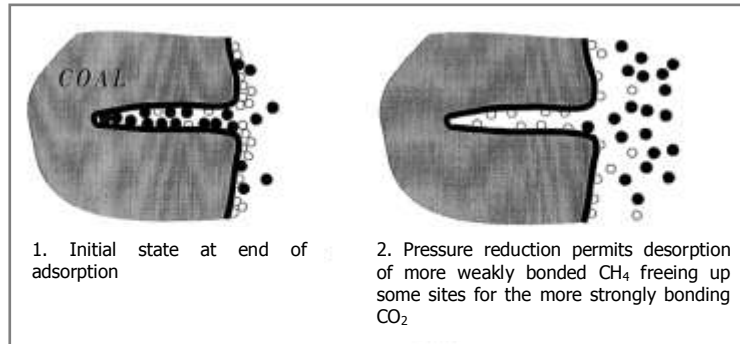


Figure II-19 - Preferential CH_4 gas desorption by coal – Steps 1 and 2 (after Crosdale, 1998)

3. As the pressure drop continues, CO_2 can now enter the desorption sites previously blocked by the CH_4 . By this mechanism, neither the CH_4 nor the CO_2 components of the mixed gas from the desorption isotherm will be related to the pure gas isotherm (Figure II-20);
4. Eventually, the gas pressure and concentration of CH_4 will be low enough for the sudden desorption of CO_2 .

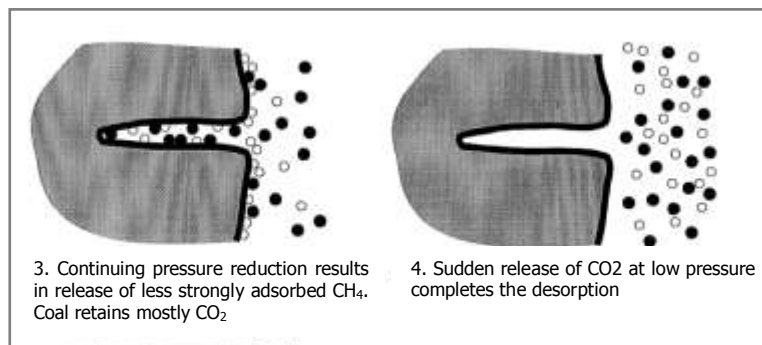


Figure II-20 - Preferential CH_4 gas desorption by coal – Steps 3 and 4 (after Crosdale, 1998)

Florentin *et al.* (2010 c) however, reported that in the earlier stages of adsorption, coal adsorbed CO_2 preferentially, but over time the CH_4 from the CO_2/CH_4 mixed gas was recovered at the expense of the CO_2 .

CHAPTER TWO

A review of coal sorption characterisation

II.6 SUMMARY

In this chapter, some of the available information about the behaviour of gas adsorption and desorption in pulverised, fragments, and samples of core coal were reviewed. The studies were done at a wide range of pressures (5 500 to 100 000 kPa) and temperatures (22.2 to 68 °C), at different conditions of in situ humidity, while information regarding the coal petrography or mineralogy such as ash content or mineral matter was not provided. Particle sizes from 0.21 mm to about 89.00 mm were tested on many types of equipment. It was found that the researchers often did not accurately report the gas saturation time or the parameters used for deciding the level of gas saturation. Therefore, comprehensive comparisons among these findings were not always possible, which meant that the outcome of these experiments was mostly reduced to a simple description of laboratory procedures. Thus, the use of quite different parameters in the tests affected the results in relation to gas content, permeability, gas hysteresis and induced strains, among others, which could at least lead to erroneous conclusions. It was also found that different researchers used different equations to model single gases and their binary and ternary mixture during adsorption and desorption in coal. The results were often diverse and specific to every situation. The use of different equipment, experimental environments, size of coal particles, and saturation time, produced dissimilar results that made it almost impossible to model accurately with one particular equation. Thus, researchers used Langmuir, extended Langmuir, IAS theory, Dubinin-Astakhov, Dubinin-Radushkevich equations and many others with individual and sometimes opposing results. Several adsorption and desorption tests were carried out on coals under laboratory conditions and in situ conditions (and more importantly, under Australian mining conditions)

CHAPTER TWO

A review of coal sorption characterisation

using parameters of Australian coal seams such as depth, temperature, main stresses, and pressure, in order to obtain results within the Australian mining environment. As a result, the isotherm test and its environment were reviewed to standardise the procedures and calculations in order to make them simpler and easier to compare with each other.

III. CHAPTER THREE

SINGLE GAS ADSORPTION

III.1 INTRODUCTION

A gas adsorption test was carried out on particles of coal ranging from 0.21 mm to 54.00 mm diameter. This study covered only the effect of gas saturation time, size of particle, and the type and temperature of the gas, in order to understand the process of N₂, CO₂ and CH₄ adsorption. While there appears to be enough information about gas adsorption in pulverised samples of coal, most of the tests were made on particles less than a few hundred microns and only few tests were made on sizes larger than a millimetre. Accordingly, tests were carried out to measure the adsorbed gas in different fragments of coal and on core samples. The effect of gas saturation time was systematically studied to compare its influence on the sorption capacity over long and short periods of time. Additionally, coal swelling was measured on several 54.00 mm diameter core coal samples with N₂, CO₂ and CH₄. Two pairs of strain gauges (lateral and radial) were attached to the core sample to study the effect of sorption capacity in coal swelling.

III.2 EXPERIMENTAL PROCEDURE

III.2.1 APPARATUS

The apparatus used to determine the volume of adsorbed gas in coal by an indirect gravimetric method consisted of a modified version of the original apparatus previously described by Lama and Bartosiewicz (1982) and later by N.I. Aziz and W. Ming-Li (1999). This apparatus has since been further modified by adding a pressure

CHAPTER THREE

Single gas adsorption

transducer to each pressure vessel, commonly known as a bomb. And the number of bombs was increased from 5 to 17.

Figure III-1 shows a diagram of the adsorption/desorption apparatus. The main components consist of:

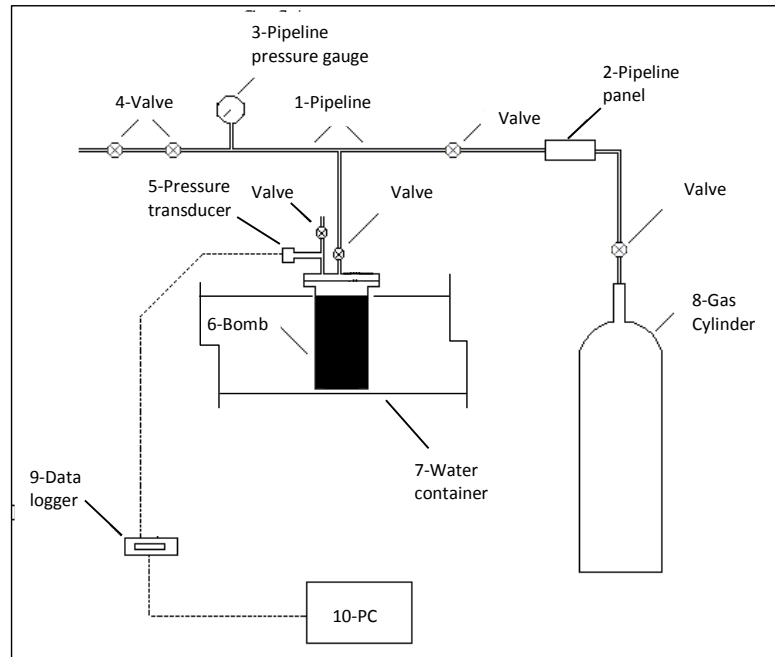


Figure III-1 – Diagram of adsorption/desorption apparatus

- Pipeline (1); 6 pipelines conduct He, Ar, N₂, CO₂, CH₄ and mixed gas from the gas cylinders (8) to the bombs (6).
- Pipeline panel (2) consists of 6 valves which regulate the inlet pressure of each gas.
- Pipeline pressure gauge (3); the pressure in pipelines is monitored by the pressure gauge.
- Valves (4); each pipeline has a couple of safety valves.
- Pressure transducers (5) are used to monitor pressure in the bombs.
- Bombs (6); the whole adsorption/desorption apparatus consists of 17 bombs.
- A bath water container (7) maintains the bombs at a constant 24 °C by a system of heater and stirrer.

CHAPTER THREE

Single gas adsorption

- A gas cylinder (8); 6 cylinders are kept outside the laboratory in a safety cage.
- A data logger (9) is used to collect data from the pressure transducers.
- PC (10) is used to gather the data.

Figure III-2 shows a picture of the adsorption/desorption apparatus described above.



Figure III-2 – Adsorption/desorption apparatus

Figure III-3 shows a picture and diagram of a typical bomb and its main components, i.e. (1) a pressure transducer, (2) an outlet valve, (3) and an inlet valve (4).

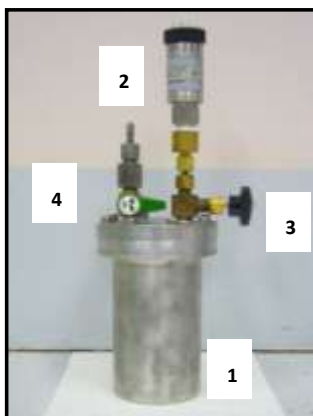


Figure III-3 – Bomb and components

Complementing the adsorption/desorption apparatus are the gas chromatography and a digital scale. The pressure transducers were calibrated before they can be used on a six monthly basis, although the scale must be calibrated daily.

Figure III-4 shows the equipment used to calibrate the pressure transducers at low and high pressure levels of 200 kPa and 5 000 kPa respectively. The pressure transducers

CHAPTER THREE

Single gas adsorption

were further subjected to different pressures by applying plates of weights that reflect the predetermined pressures.



Figure III-4 – Pressure transducer calibrator

III.2.2 COAL SAMPLE PREPARATION

Coal samples retrieved from the mine were received as lumps of approximately 30 kg in weight upon collection. They were wrapped in plastic bags and transported to the laboratory where they were stripped of wrapping and immersed in a tub of water. The coal lumps were crushed to a top size of 9.5 mm and then, they were sub sampled to a retained 0.21 mm (and passing through the immediately larger mesh size according to the listed mesh size), 0.30 mm, 0.71 mm, 1.18 mm, 2.36 mm, 4.75 mm, 6.70 mm, and 8.00 mm particles sizes. Cubes of 15.00 mm side size were prepared separately in addition to 54.00 mm diameter samples.

Table III-1 gives the details of samples collected from West Cliff Colliery, Area 5, panels 519 and 520. The preparation of 54.00 mm diameter samples (diameter/length of 1:1) was carried out according to the International standard for preparing and testing samples of rock core (ISRM, 1981). Samples of coal were kept in water until use in absence of a refrigerator which is the best way to maintain coal samples for long

CHAPTER THREE

Single gas adsorption

period without affecting its physical properties, and from preventing deterioration from environmental conditions (oxidisation). Each lump of coal was cast in concrete to help handling and coring. Once the sample was cored, some leftover lump of coal was also crushed to the desired sizes. Each sample was run only once, basically due to the long duration of each test.

Table III-1 – Details of coal samples tested for adsorption

Coal sample		Gas	Temperature	Sorption Duration	Coal sample		Gas	Temperature	Sorption Duration
Size	Quantity				Size	Quantity			
0.21 mm	1	CO ₂	24 °C	Saturation	4.75 mm	1	CO ₂	28 °C	Saturation
0.21 mm	2	CH ₄	24 °C	Saturation	4.75 mm	2	CH ₄	24 °C	Saturation
0.30 mm	2	CO ₂	21 °C	Saturation	4.75 mm	2	CH ₄	28 °C	Saturation
0.30 mm	3	CO ₂	24 °C	Saturation	4.75 mm	2	N ₂	24 °C	Saturation
0.30 mm	1	CO ₂	24 °C	2 hr	6.70 mm	2	CO ₂	21 °C	Saturation
0.30 mm	1	CO ₂	28 °C	Saturation	6.70 mm	4	CH ₄	24 °C	Saturation
0.30 mm	4	CH ₄	24 °C	Saturation	8.00 mm	2	CO ₂	24 °C	Saturation
0.71 mm	2	CO ₂	24 °C	Saturation	8.00 mm	1	CO ₂	24 °C	2 hr
0.71 mm	2	N ₂	24 °C	Saturation	8.00 mm	2	CH ₄	21 °C	Saturation
1.18 mm	3	CO ₂	24 °C	Saturation	8.00 mm	2	CH ₄	24 °C	Saturation
1.18 mm	3	CH ₄	24 °C	Saturation	15.00 mm	4	CO ₂	24 °C	Saturation
1.18 mm	1	N ₂	24 °C	Saturation	15.00 mm	3	CH ₄	24 °C	Saturation
2.36 mm	4	CO ₂	24 °C	Saturation	54.00 mm	4	CO ₂	24 °C	Saturation
2.36 mm	1	CO ₂	24 °C	2 hr	54.00 mm	9	CH ₄	24 °C	Saturation
2.36 mm	2	CH ₄	24 °C	Saturation	54.00 mm	2	N ₂	24 °C	Saturation
4.75 mm	2	CO ₂	24 °C	Saturation	Total	76	Coal samples		

Figure III-5 shows the crushed and cored samples being tested for gas adsorption. The samples were dried in an oven set at 105 °C for about 18-24 hrs before being used.

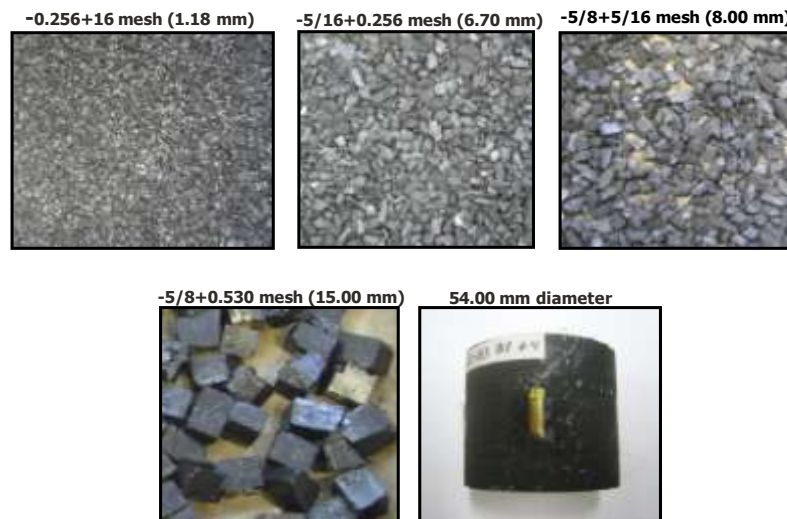


Figure III-5 – Crushed and cored coal samples

CHAPTER THREE

Single gas adsorption

The samples were kept at room temperature for about 24 hrs to adjust to the laboratory environment, especially the moisture content. This meant that their moisture content differed slightly from the dry coal. The test temperature was maintained constant by keeping the bombs in bath water at 24 °C. The room temperature was set at 24 °C with air conditioning.

Table III-2 shows the relative density, moisture and ash content from panels 519 and 520. The proximate analysis was undertaken in compliance with the procedure described in the Australian Standard TM (AS 1038.3).

Table III-2 – Relative density, moisture and ash content analysis of panels 519 and 520

Panel 520-B3				Panel 519-2122			
Sample	Relative Density	Moisture (%)	Ash (%)	Sample	Relative Density	Moisture (%)	Ash (%)
520B3-BA-2	1.41	1.2	8.3	5192122-BF-7	1.42	1.4	8.0
520B3-B1G-2	1.41	1.0	8.1	5192122-BB-5	1.42	1.2	8.0
520B3-B1G-3	1.42	0.9	8.3	5192122-B4-5	1.41	1.2	8.1
520B3-B1G-5	1.45	1.8	7.8	5192122-B1G-8	1.42	1.2	7.9
520B3-B2-2	1.41	0.9	7.9	5192122-B1G-10	1.42	1.4	8.0
520B3-B1G-100	1.42	0.9	7.9	5192122-BK-4	1.41	0.9	8.0
520B3-BH-2	1.42	1.1	8.2	5192122-B5-5	1.42	1.4	8.0
520B3-BK	1.39	1.0	7.9	5192122-B2-6	1.43	1.6	7.8
520B3-BC	1.43	1.0	8.6	5192122-BB-6	1.42	1.0	8.4
520B3-B5	1.43	1.0	8.6	5192122-BH-5	1.42	1.2	8.0
520B3-BF-4	1.42	1.0	7.8	5192122-B2-7	1.42	1.1	8.3
520B3-BB-2	1.42	1.0	8.1	5192122-BB-7	1.42	1.1	8.2
520B3-BF-3	1.42	1.2	8.3	5192122-B2-5	1.41	1.2	7.8
520B3-B6	1.41	1.1	7.9	5192122-B1G-9	1.43	1.2	8.8
520B3-B6-2	1.42	1.0	8.1	5192122-B6-4	1.41	1.1	7.9
520B3-BB	1.43	1.0	8.5	5192122-BF-6	1.42	1.1	9.0
520B3-B2-3	1.42	0.9	8.6	5192122-BF-8	1.43	1.3	8.5
520B3-B2-4	1.42	1.0	8.5	5192122-B5-7	1.42	1.2	8.4
520B3-B2-100	1.42	1.0	8.4	5192122-BC-5	1.42	1.3	7.9
520B3-B4-100	1.41	1.1	8.0	5192122-B4-6	1.43	1.4	8.4
520B3-BL	1.42	1.0	8.4	5192122-BK-5	1.43	1.1	8.7
520B3-BL-5	1.43	1.3	8.2	5192122-B1G-11	1.43	1.1	8.7
520B3-BA-100	1.43	1.2	8.5	5192122-B5-8	1.43	1.1	8.4
520B3-B4-3	1.42	1.1	7.6	51921-BC-7	1.42	1.1	8.2
520B3-BF	1.43	1.2	8.2				
520B3-B2-3	1.42	0.9	8.6				

Table III-3 shows the petrography measurements (Maceral analysis and Vitrinite reflectance) undertaken in samples from the same location to quantify their

CHAPTER THREE

Single gas adsorption

composition and rank, using the methodology based on Australian Standard (1998, 2000). The table is shown only as a reference due to the lack of information at this respect and it should be used carefully due to the highly coal heterogeneity. No petrography analysis was performed on the samples tested in adsorption and desorption.

Table III-3 – Petrography results of panels 519 and 520 coal (Saghafi and Roberts, 2008)

Sample ID (gas conditions)	Vitrinite reflectance (%)	Maceral (%)			Maceral (% mineral free)		
	Vitrinite	Liptinite	Inertinite	Mineral	Vitrinite	Liptinite	Inertinite
519-21B (Intermediate)	1.24	59.8	0.0	29.0	11.2	67.3	0.0
520-3B (CH ₄ rich)	1.28	41.6	0.1	55.3	3.0	42.9	0.1
519-31B (CO ₂ rich)	1.25	11.4	0.2	63.6	24.8	15.2	0.3

III.2.3 TESTING PROCEDURE

Figure III-6 shows a flow diagram for the preparation and experimental procedure for testing coal samples for individual and mixed gas.

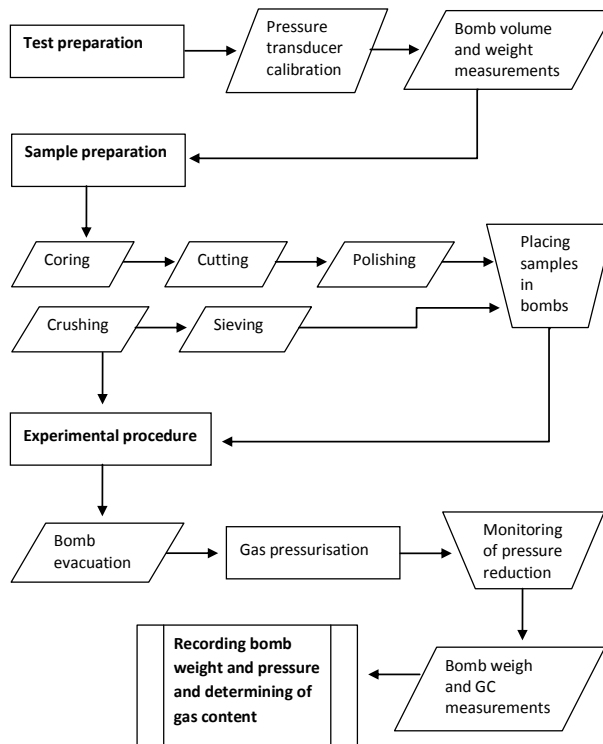


Figure III-6 – Experimental procedure flow diagram for single and mixed gas adsorption/desorption

CHAPTER THREE

Single gas adsorption

The volume and weight of the empty bombs were measured while preparing for the adsorption test, after which the sample was prepared as it was described previously. Each bomb was approximately 95% filled with coal, then sealed and placed under a vacuum for three, 20 minute periods to evacuate any undesired gas or air. After the cell was filled with coal, the void volume was measured by using Helium at the reference temperature of 24 °C since it is non adsorbent gas. Each bomb was pressurised in 500 kPa steps to a maximum of 4 200 kPa. At each step, adsorption parameters such as bomb weight, pressure, temperature, and composition of the gas (in the case of mixed gases) were measured/monitored daily until the pressure reached equilibrium. The pressure equilibrium was satisfied when its fluctuation was < 5% over a period of 18 hrs.

The experimental data is presented as Absolute adsorption measured by gravimetric method (Sakurovs *et al.*, 2009). This method is based on measuring the change in mass at increasing pressure steps in a sample vessel. The void volume is calculated by the following equation;

$$V_{void} = V_{cell} - \frac{m_{sample}}{\rho_{solid}} * (1 - w_c) - \frac{m_{sample}}{\rho_{H_2O}} * w_c \quad (5)$$

Where m_{sample} is the mass of the sample, w_c is the moisture content (as weight fraction), and ρ_{solid} is the solid density of the material. At each pressure step after adsorption was equilibrated, the mass of adsorbed gas was calculated on a Gibbs excess basis. The mass of adsorbed gas on a Gibbs excess basis is calculated by the following equation;

$$m_{ads}^G = m_{meas} - m_{void} = m_{meas} - \rho_{gas} * V_{void} \quad (6)$$

CHAPTER THREE

Single gas adsorption

Where m_{meas} is the measured change in mass of the sample, m_{void} is the mass of gas within the void volume, ρ_{gas} is the gas density and V_{void} is calculated from the previous equation. Then, this adsorption was expressed on the absolute basis where the void volume was adjusted for the presence of the adsorbed phase. The absolute adsorption is given by;

$$m_{ads}^A = m_{ads}^G * \left(\frac{\rho_{ads}}{\rho_{ads} - \rho_{gas}} \right) \quad (7)$$

Where ρ_{ads} is the adsorbed phase density.

The density of the adsorbed phase of the N₂, CO₂ and CH₄ were approximately taken as 0.808, 1.4 and 0.421 g/cm³ respectively, as suggested by Arri and Yee (1992). Finally, the adsorbed quantity was expressed in terms of m³/t at standard conditions (20 °C and 101.425 kPa). It was used the CO₂ equation of state (EOS) by Span and Wagner (1996) and the CH₄ EOS by Setzmann and Wagner (1991). Appendix 1 shows the spreadsheet used to monitor the pressure and weight of the bomb. Appendix 2 shows the calculations of fluctuating pressure over a period of time. The volume of adsorbed gas in the coal was also calculated by the Soave-Redlich-Kwong equation of state, as shown in Appendix 3. Also, the applicability of the Langmuir equation for modelling experimental data during adsorption/desorption was tested. The Langmuir equation, including a summary of the assumptions made by Langmuir (1918) are described in Appendix 5.

III.3 EXPERIMENTAL RESULTS

N₂, CO₂ and CH₄ adsorption on coal with respect to saturation time, adsorbed mass, and linear stress was studied.

CHAPTER THREE

Single gas adsorption

III.3.1. NITROGEN

III.3.1.1. GAS SATURATION TIME

Pressure level

Figure III-7 shows the drop in N₂ pressure over time on the 54.00 mm diameter core coal at 500 and 2 000 kPa. The graph shows that the sample achieved equilibrium (as defined previously, pressure fluctuations < 5%) at about 2 880 min (two days) at 500 and 2 000 kPa. However, from the graph it can be inferred that the samples were stabilised earlier at about 1 440 min then this equilibrium was broken due to some changes in the test environment which was likely due to a drop in the bath water temperature.

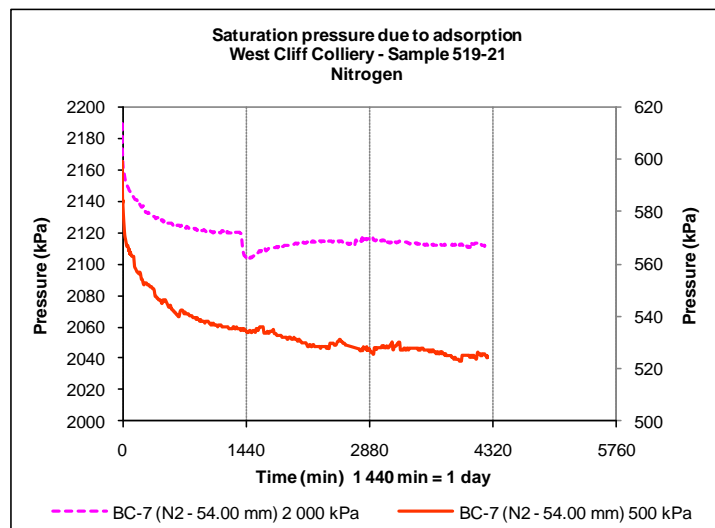


Figure III-7 – Effect of pressure levels on N₂ gas saturation time

These results suggest that N₂ saturation time was independent of the pressure levels. On the contrary, and as expected, N₂ saturation time was dependent on the environment conditions, in this case the temperature. Changes in temperature may have affected the speed of the free gas molecules movement increasing or decreasing the gas pressure in the vessel. At steady temperature the equilibrium should be reached in less than 1 440 min as it is shown in the pressure profile of the BC-7 sample.

CHAPTER THREE

Single gas adsorption

At 500 kPa however, the BC-7 sample took longer to stabilise due to some gas leakage indicated by the continuously dropping pressure over time.

Table III-4 shows the fluctuations in the percentage of the N₂ pressure in a given period of time in several samples at approximately 3 000 kPa pressure level, measured at different saturation time periods of 24 hrs, 36 hrs, 48 hrs, and 72 hrs respectively. The table shows that, at about 3 000 kPa most of the coal samples achieved the desired degree of N₂ saturation at 48 hours mark where in most of the samples the fluctuation in pressure was less than 5% in the last 20.3 hrs.

Table III-4 – Pressure fluctuations during N₂ gas adsorption at a given pressure

N ₂ equilibrium pressure at about 3 000 kPa in adsorption									
Coal		Gas pressure fluctuation less than 5% in the last							
Sample	Size (mm)	24 hours		36 hours		48 hours		72 hours	
		(hrs)	(%)	(hrs)	(%)	(hrs)	(%)	(hrs)	(%)
BE(1)	54.00	9.0	2.8	-	-	-	-	(NA)	(NA)
BD(1)	54.00	9.0	2.9	-	-	17.9	4.9	(NA)	(NA)
B3(1)	54.00	9.0	2.4	7.5	4.7	17.9	2.8	(NA)	(NA)
B1(1)	54.00	9.0	1.1	20.4	4.0	17.9	2.0	(NA)	(NA)
BD(B)	54.00	-	-	13.2	3.1	6.0	1.0	-	-
B3(B)	54.00	6.0	4.5	13.2	3.3	6.0	0.4	-	-
B1(B)	54.00	6.0	4.7	13.2	3.9	18.0	2.0	8.4	4.3
BD(C)	54.00	3.0	4.5	-	-	-	-	7.3	4.6
B3(C)	54.00	3.0	0.0	-	-	-	-	7.3	4.8
B1(C)	54.00	3.0	1.9	13.2	3.5	12.0	4.2	-	-
BE(D)	54.00	12.4	3.7	-	-	30.1	1.6	-	-
BD(D)	54.00	6.5	0.0	17.7	2.5	30.1	2.3	-	-
B3(D)	54.00	9.5	2.2	17.7	0.0	30.1	0.0	26.5	4.9
B1(D)	54.00	12.4	1.4	22.1	1.5	30.1	0.0	52.5	5.0
BC-7	54.00	11.1	3.7	20.9	3.5	33.7	4.1	(NA)	(NA)
B1G-12	0.71	10.2	4.2	-	-	15.2	1.3	31.4	3.8
B2-7	4.75	10.5	5.0	10.2	2.9	18.6	3.9	33.5	5.0
Average		8.1	2.8	15.4	3.0	20.3	2.2	23.9	4.6
Note:									
(-) Gas pressure fluctuation greater than 5%									
(NA) Gas adsorption duration less than that time									

The results satisfied the mark of a minimum fluctuation < 5% in the last 18 hrs, as defined in Appendix 2. These results also suggest that 2 880 min (two days) was enough time to reach an adequate level of saturation. However, a different estimation

CHAPTER THREE

Single gas adsorption

of the saturation time could also be done by changing the decider factor which is the equilibrium pressure achieved when pressure drops less than 5% in the last 2-6 hours of test. Appendix 6 shows the pressure profile of the B2-7 (4.75 mm) sample during adsorption at each 500 kPa step.

Coal particle size

Figure III-8 shows the profiles of the drop in pressure over time in three different particles size at 500 kPa of pressure.

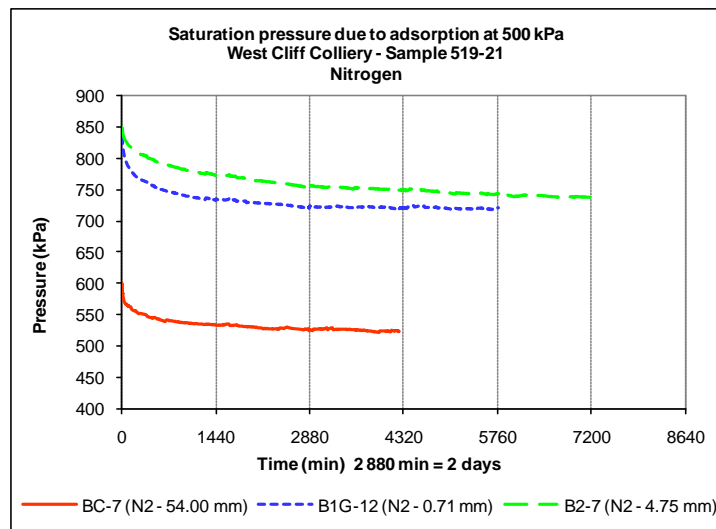


Figure III-8 – Effect of particle sizes in N₂ gas saturation time

These results suggest that every sample appeared satisfying the desired saturation level in about 2 880 min (two days). However, the 4.75 mm particle size required more time to achieve a similar degree of N₂ saturation than the other two samples likely due to some gas leakage denoted by the decreasing pressure profile. Note that each vessel was pressurised at different initial pressure level to achieve a final pressure of about 500 kPa. The results suggest that the duration of N₂ saturation appeared to be independent of the size of particle, a finding that agrees with the analysis of the data shown in Table III-4.

CHAPTER THREE

Single gas adsorption

Bath water temperature

Figure III-9 shows the drop in N₂ pressure over time during adsorption on a 0.71 mm particle size, and the changes in room temperatures RT 1 and RT 2 over time. Thermocouples RT 1 and RT 2 were located in the corner of the room, at about 8.0 m from the air conditioning and over the container of bath water, with approximately 2.0 m between them. The results suggest that there was some resemblance between the profile of the N₂ drop in pressure and the profile of the changes in room temperature, as shown by the circles.

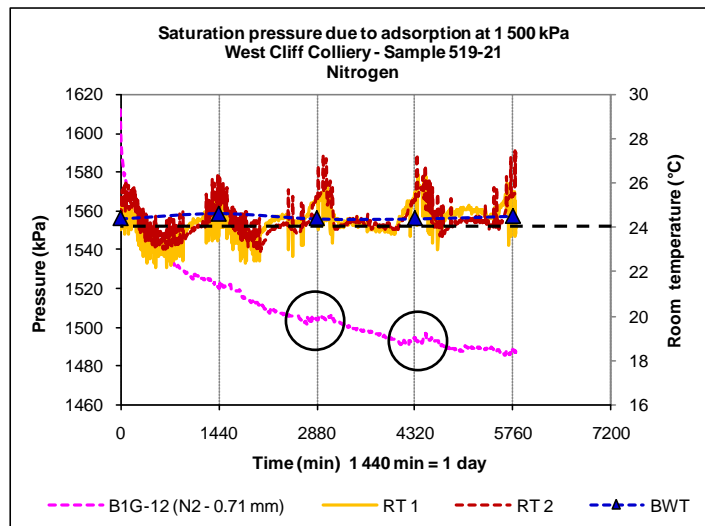


Figure III-9 – Effect of temperature in N₂ gas saturation time

The average RT 1 and RT 2 room temperatures over the test period were 24.4 and 24.6 °C respectively, which was close to the desired 24 °C temperature of the bath water (maintained almost steady at 24.5 °C). These results suggest that changes in room temperature slightly affected the temperature of the bath water, and consequently causing some marginal changes in the pressure of N₂. An increase in room temperature resulted in an increase in the pressure of N₂ which could trigger desorption rather than adsorption. A good practice will be to keep the bath water temperature few degrees (+5 °C) over the room temperature to avoid any influence on it.

CHAPTER THREE

Single gas adsorption

III.3.1.2. ADSORBED MASS

N₂ adsorbed mass

Figure III-10 shows the N₂ adsorbed mass profile from the experimental data in three different particles size on a dry and ash free (DAF) basis. The test pressure reached over 4 000 kPa. By comparing both samples on a DAF basis, the graph shows that the BC-7 sample (54.00 mm) achieved higher adsorbed mass of N₂ than the 4.75 mm particle size. Both samples had similar relative density (1.42) and moisture content (1.1 %) but slightly different ash content of 8.2 and 8.3 % respectively. The difference in adsorbed mass was about 11%.

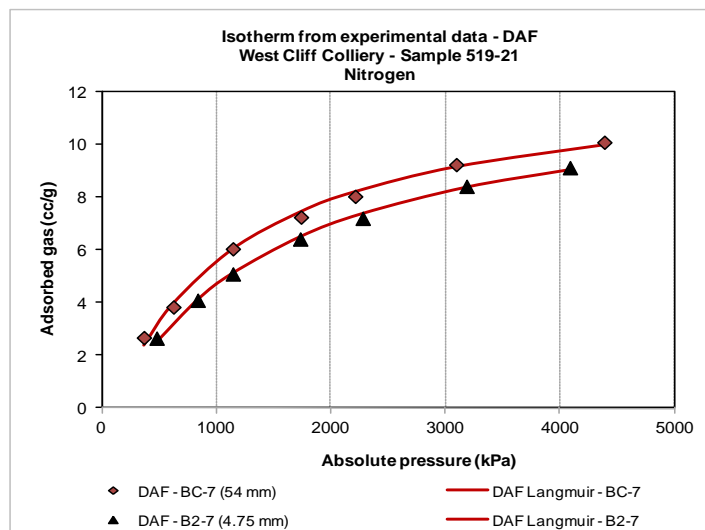


Figure III-10 – N₂ adsorbed mass in coal during adsorption

This result was unexpected, firstly because the 4.75 mm particle size have larger surface area than the 54.00 mm and secondly, the 4.75 mm sample was saturated longer than the 54.00 mm particle size (about 67 000 min against 30 270 min). It appeared that the N₂ was adsorbed largely in the micro structure of the 54.00 mm particle size rather than on the surface of the 4.75 mm sample. It seems that the coarse particle could not adsorb large quantities of N₂ gas because of the lack of micro structure, or the 4.75 mm sample was not well saturated. However, the results of the

CHAPTER THREE

Single gas adsorption

two samples were not sufficient to make a definitive conclusion on the N_2 adsorption behaviour. Another explanation could be that the 4.75 mm particle size was in some way deteriorated by oxidation due to the process of sample collection, management, and storage.

The study indicates that the adsorbed mass of N_2 in coal could depend eventually on the particle size; the larger the particle size the higher the adsorbed mass of N_2 . Appendix 8 shows the adsorbed mass of N_2 gas (Experimental and Langmuir isotherms) of all the samples tested in adsorption.

Langmuir isotherm

Figure III-11 shows the Langmuir isotherm for sample B2-7 due to the adsorption of N_2 .

The maximum sorption capacity of N_2 at about 4 100 kPa was 9.1 cc/gm, at the standard condition of 20 °C and 101.325 kPa.

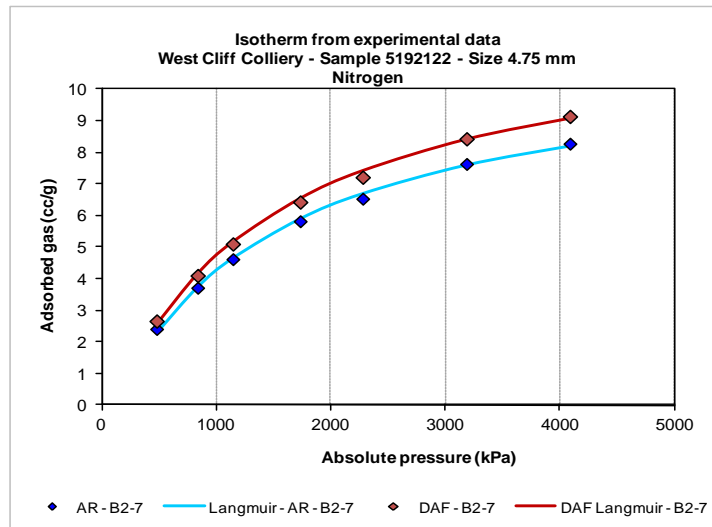


Figure III-11 – Langmuir isotherm for N_2 gas during adsorption

This suggests that the adsorbed mass of N_2 on coal from the experimental data can be modelled by the Langmuir equation with good degree of accuracy. Langmuir parameters PL and VL were 1.46 kPa and 12.286 cc/g respectively. The low PL value

CHAPTER THREE

Single gas adsorption

indicates that most of the coal sample pores due to adsorption were filled with N_2 at low pressure.

III.3.1.3. COAL LINEAR STRAINS

Axial and lateral deformation of core coal samples were monitored by two pairs of strain gauges mounted on the sample axially and laterally. Bombs were charged with N_2 to about 3 400 kPa of pressure.

Figure III-12 shows the linear strain due to swelling on five, 54.00 mm diameter samples adsorbing N_2 over time. The results indicate that in every sample, the axial strain (parallel to the longitudinal axis and denoted by the letter A) was greater than the radial strain. These results agreed with those obtained by St. George and Barakat (2001) when testing swelling in coal samples. The ratio of axial to radial strain varied from 1.05 (BE sample) to 1.95 (B4 sample). This different in ratios was likely due to differences in the physical properties of the samples as well as in the competency of the samples. The range of relative densities, moistures and ash contents measured were about of 1.43-1.40, 1.6-0.9 and 9.0-7.8 respectively.

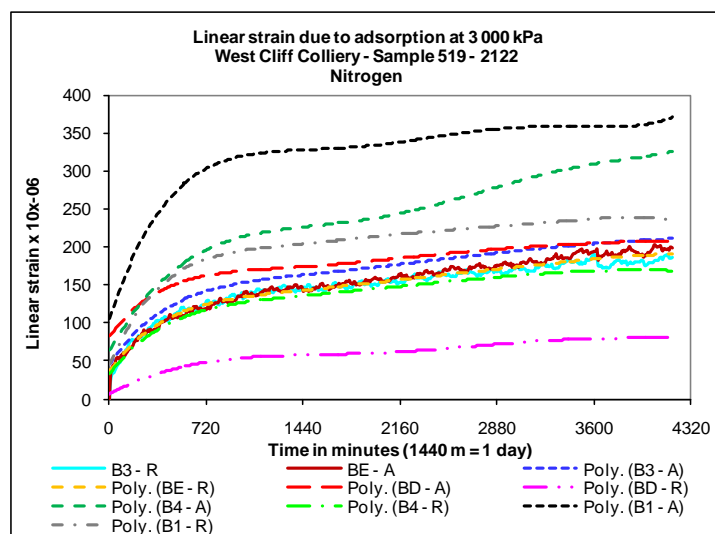


Figure III-12 – Linear strains in coal during N_2 gas adsorption

CHAPTER THREE

Single gas adsorption

III.3.2. CARBON DIOXIDE

III.3.2.1. GAS SATURATION TIME

Pressure level

Figure III-13 shows the drop in pressure over time at 500 and 3 000 kPa due to the adsorption of CO₂. The 500 kPa pressure level was chosen because at this level the surface and matrix of the coal appeared to have enough spots available to adsorb the gas molecules. The 3 000 kPa level was chosen on the basis that at this high pressure, the surface and matrices of the coal were expected to be almost filled with gas molecules. It is therefore seemed worthwhile to analyse the adsorption of CO₂ at these two pressure levels. The results suggest that at 500 kPa the CO₂ gas stabilised at about 2 880 min mark. The graph also shows that to reach the equilibrium pressure at about 500 kPa, the coal sample has to be injected with sufficient volume of CO₂ (pressure at about 1 000 kPa). This huge drop in gas pressure (50%) which meant large quantities of adsorbed CO₂ in coal, suggests that at low pressure, most of the CO₂ was adsorbed readily on the surface of the coal and very little on the matrices.

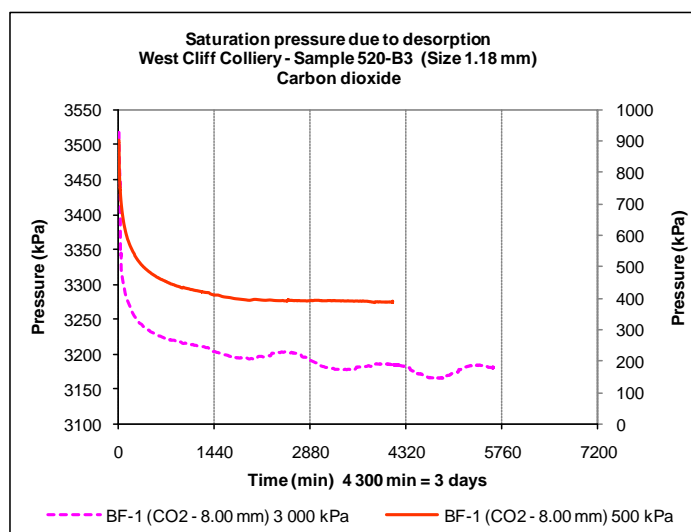


Figure III-13 – Effect of pressure level in CO₂ gas saturation time

CHAPTER THREE

Single gas adsorption

At the 3 000 kPa pressure level, the equilibrium state was achieved in about 2 880 min however the sample appeared to continue adsorbing CO₂ over time which is likely due to diffusion, as evident by the fluctuations in pressure. These results also indicate that the longer the saturation time the lower the equilibrium pressure level. The study indicates that the CO₂ saturation time was dependent on the level of the applied pressure; the lower the pressure, the shorter the saturation time. Longer saturation time may cause lower equilibrium pressure. This in part could be attributed to the CO₂ affinity to coal. Appendix 9 shows the drop in pressure of the B2-6 (0.30 mm) sample during adsorption, at each 500 kPa increment.

Coal particle size

Figure III-14 shows the drop in pressure over time from several samples during adsorption at a reference pressure of about 500 kPa. The samples were run for different periods of saturation to analyse the adequate saturation time for each particle size.

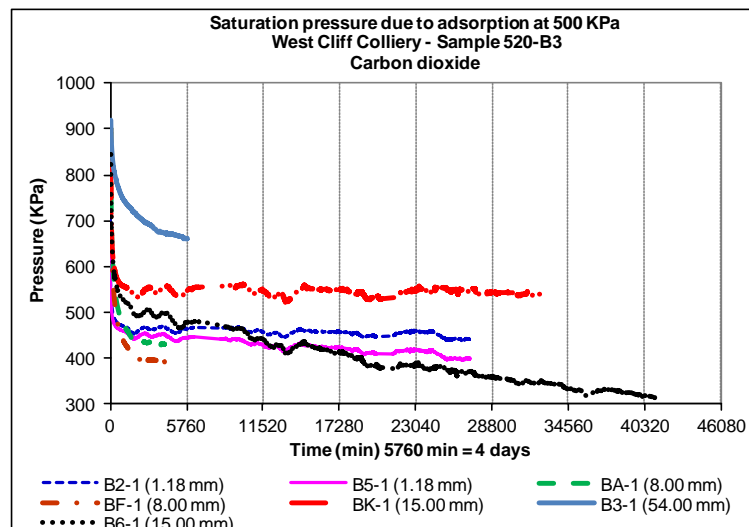


Figure III-14 – Effect of particle sizes in CO₂ gas saturation time

The graph shows that most of the samples of fragmented coal achieved equilibrium in about 2 880 min (two days) with CO₂. At this level of saturation time, the samples

CHAPTER THREE

Single gas adsorption

appeared to be well saturated (fluctuations in pressure < 5%), but at 5 760 min (four days) of saturation time of the sample B3-1 (54.00 mm) did not appear saturated enough to reach an acceptable level of equilibrium. The profile of sample B6-1 appears to be a typical example of a drop in pressure due to gas leakage. Over time, even very small gas leakages can easily be detected by analysing the pressure drop profile. The comparative study of different size particles saturated with CO₂ suggests that saturation time appeared to be independent of their sizes, although only fragmented samples were considered. However, the saturation time with CO₂ in 54.00 mm or larger (e.g. coal lumps) sample could depend on the particle size. The relative lack of results on this size makes difficult to reach a definite conclusion.

Temperature

Figure III-15 shows the drop in pressure over time in powder (size < 1.00 mm) and fragmented (54.00 mm > size > 1.00 mm) coal samples tested at temperatures of 21 and 24 °C. The coal samples B2-6 and B4-5 tested at temperatures of 21 and 24 °C, required less than 1 440 min to achieve satisfactory degree of CO₂ saturation.

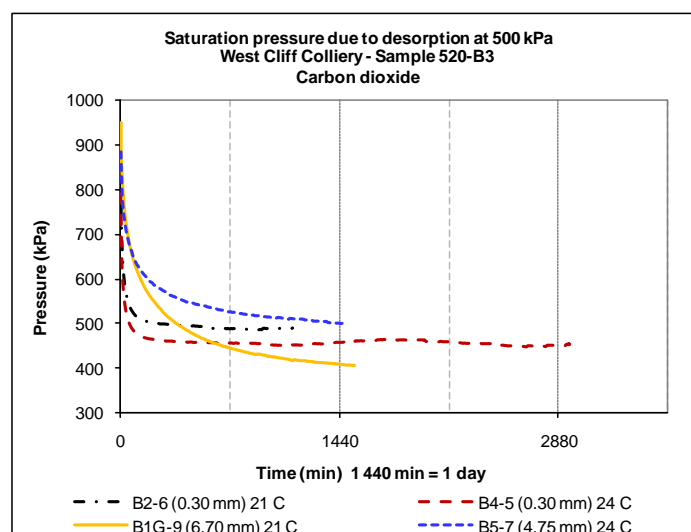


Figure III-15 – Effect of temperature in CO₂ gas saturation time

CHAPTER THREE

Single gas adsorption

The results indicate that CO₂ saturation time appeared to be independent of the temperature of the bath water for particles < 1.00 mm. In fragmented samples (size > 1.00 mm) however, the CO₂ saturation time took longer than 1 440 min to achieve the same saturation level than the powdered samples. The graph shows that regardless of the temperature, the shortest saturation time was with samples of powdered coal (size < 1.00 mm). The study suggests that CO₂ saturation time appeared to depend on the size of coal particles (considering sub groups of powder and fragmented coal samples) rather than the bath water temperature. It seems that small variations in temperature (2-5 °C) did not affect the adsorption process especially in the same sub group of particle size.

In addition, Figure III-16 shows both the bath water and room temperature profiles over time. Temperature could be considered one of the main sources of error in the measurement of the adsorbed gas in coal.

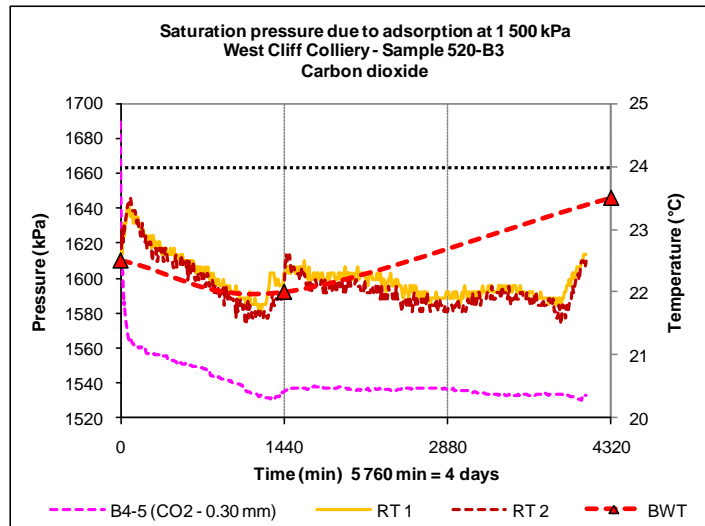


Figure III-16 – Effect of room temperature on bath water temperature

According to Sakurovs et al. (2009), the accuracy of the temperature measured in the system has to be better than 0.1 °C to avoid excessive errors in calculated sorption capacities. Thus, the influence of room temperature on the bath water and

CHAPTER THREE

Single gas adsorption

consequently in the behaviour of CO₂ during adsorption was analysed for sample B5-4. The graph shows that both the bath water and room temperatures were below 24 °C over the whole period. The result indicates that the difference between peaks in the bath water temperature over the period was 1.0 °C. These results suggest that changes in room temperature affected the temperature of the bath water. The graph also shows that drop in CO₂ pressure appeared to follow the same trend as room and bath water temperatures. The results suggest that CO₂ adsorption behaviour appeared to be marginally influenced by changes in room temperature. However, these changes in the test temperature could lead to important errors in the measurements of the CO₂ (or any gas) adsorbed mass.

III.3.2.2. ADSORBED MASS

The adsorbed mass of CO₂ gas in several samples of coal was measured at test temperatures of 21 and 24 °C. Few samples were tested at 28 °C. The results are presented in as received and DAF basis.

CO₂ adsorbed mass

Figure III-17 shows that the maximum CO₂ adsorbed mass (DAF) over pressure on 2.36 mm size particles during adsorption was 31.4 cc/gm at about 4 200 kPa. As expected the graph shows an increasing trend in the adsorbed mass of CO₂ over pressure. The coal sample appeared to have achieved full saturation at pressures of about 4 200 kPa. The Langmuir parameters PL and VL (DAF basis) were estimated to be 0.40 MPa and 33.82 m³/t, respectively. This adsorbed mass was 43% lower than similar sample from the same location as reported by Saghafi and Roberts (2008). They reported the Langmuir parameters PL and VL to be 2.71 MPa and 59.47 m³/t, on similar coal samples. Saghafi and Roberts (2008) also reported the sorption capacity for CO₂ and

CHAPTER THREE

Single gas adsorption

CH₄ gases of three samples from the same number of locations, from rich CH₄ (panel 520-3B), intermediate (panel 519-21B) and rich CO₂ (panel 519-31B) area. Although, a sample from panel 520B3 area was found to be rich in CH₄ (94%) with measured gas content of about 10.4 m³/t, they reported that this sample showed the largest gas storage capacity for both CH₄ and CO₂ gases.

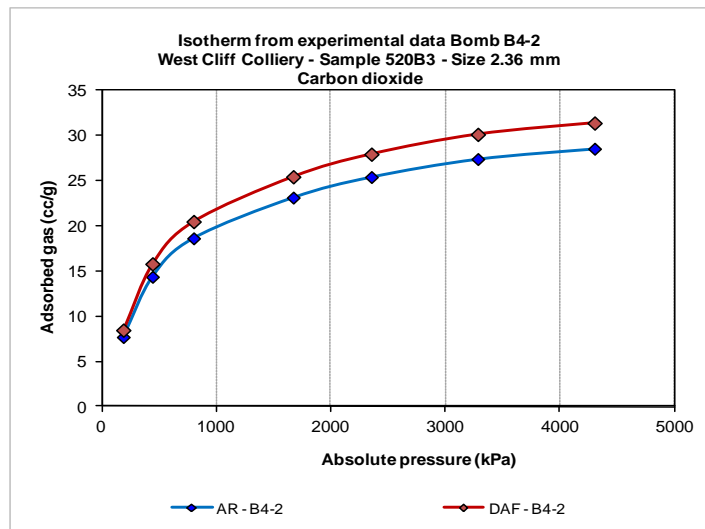


Figure III-17 – CO₂ adsorbed mass from experimental data in adsorption

The results of the proximate analysis were compared in order to understand the cause of such underestimation in adsorption capacity. The study estimated the helium density, moisture and ash content of the sample B4-2 in 1.41, 1.1 and 8.0 respectively. The average proximate analyses of more than 25 samples from similar location were 1.42, 1.1 and 8.21 respectively. However, Saghafi and Roberts reported for one sample from similar location as 1.43, 1.3 and 5.6 in helium density, moisture and ash content respectively.

The overestimation in ash content (with almost similar results in helium density and moisture) increases in little percentage the underestimation in adsorbed mass (DAF basis) rather than decreases it. Thus, the difference in ash content could not be accounted as the main reason of the underestimation in the CO₂ adsorption capacity.

CHAPTER THREE

Single gas adsorption

Poor sample collection, management and sampling could lead to errors in measuring sorption capacity in coal. Also, errors in void volume estimation, helium density determination, estimation of adsorbed phase density, temperature, mass determinations, equipment accuracy, and gas leakage are some of the possible common sources of errors in adsorbed mass measurements. Further discussion in more details of the likely errors involved in the adsorbed mass estimation will be examined in this study.

Coal particle size

Figure III-18 shows the adsorbed mass of CO₂ during adsorption at each 500 kPa increment up to about 4 200 kPa, in particles ranging from 0.21 mm to 15 mm in size.

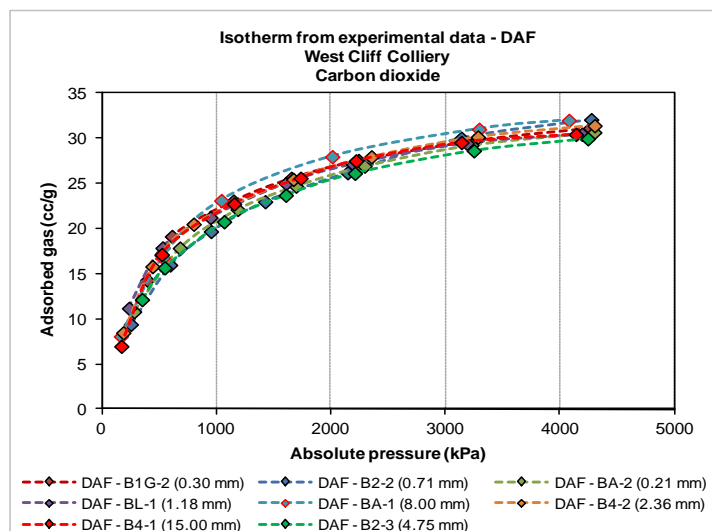


Figure III-18 – Effect of particle sizes on CO₂ adsorbed mass

The CO₂ adsorption capacity was analysed with respect to the size of coal particle. The results show that the sample BA-1 appeared to achieve the highest CO₂ adsorption capacity (DAF basis) with 32.00 cc/g at about 4 100 kPa. The lowest amount of adsorbed CO₂ was on sample B2-3 with 30.00 cc/g at about 4 200 kPa. These amounts of adsorbed CO₂ mass were lower in about 40-45% than similar coal samples from the same location reported by Saghafi and Roberts (2008). The maximum adsorption

CHAPTER THREE

Single gas adsorption

capacity (DAF basis) was estimated to be about 31.00 ± 1 cc/g. Average helium density, moisture and ash contents were estimated as 1.421, 1.1 and 8.2 for panel 520-B3, and 1.421, 1.21 and 8.2 for panel 519-21B. The graph showed a very high repeatability in the adsorbed CO_2 mass estimation (the results were almost identical). The study indicates that within experimental error, the adsorbed mass of CO_2 on coal samples from panels 519 and 520 appeared to be independent of particle sizes at pressures up to 4 200 kPa. Appendix 11 shows the profiles of CO_2 (Experimental and Langmuir isotherms) of all coal samples tested in adsorption.

Saturation time

Figure III-19 shows the adsorbed mass of CO_2 on coal at two different degrees of saturation; at equilibrium pressure according to the minimum saturation time (time variable with pressure fluctuations less than 5%), and at fixed period of two hours saturation time (quick test, denoted by QT).

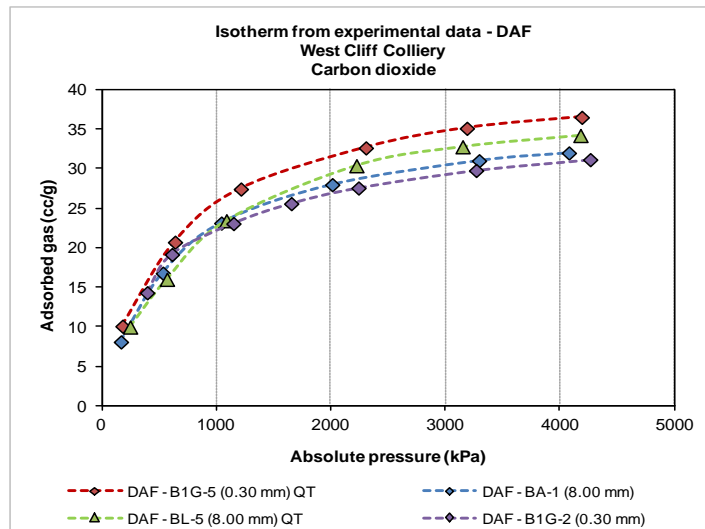


Figure III-19 – Adsorbed CO_2 mass due to quick test

In the quick test, the sorption capacity of CO_2 was measured every two hours independently of the degree of saturation achieved. The graph compares the adsorbed

CHAPTER THREE

Single gas adsorption

CO₂ mass (DAF basis) between two groups of samples, powdered (0.30 mm) and fragmented (8.00 mm). The graph shows that particles < 1.00 mm (powdered coal) the B1G-5 sample (QT) achieved marginally higher adsorption capacity of CO₂ (17%) than the B1G-2 sample over the entire range of pressure. Similarly fragmented samples readily saturated (BL-5) achieved a higher adsorbed CO₂ mass (7%) than the sample tested at equilibrium pressure (BA-1). Unexpectedly, the results show that the samples measured for the QT test achieved a higher CO₂ adsorption capacity than those measured at minimum saturation time. A likely explanation of this sorption behaviour is that in the quick test the experimental error could be larger due to firstly, an error in the void volume estimation and secondly, at the quick test, the gas pressure at each pressure step was higher than at equilibrium pressure (mainly because it did not achieve it) and consequently, the amount of free gas was also larger. Larger free gas and void volume estimation could lead to larger error in estimating the gas density. Thus, error in void volume estimation, and gas density estimation could lead to larger error in the adsorbed mass estimation because these two errors are added rather than being subtracted. The difference in adsorption capacity of about 7 and 17% could be within the experimental error. Comparing the adsorption capacity of samples BA-1 and B1G-2, it can be seen that both coal samples achieved almost identical adsorption capacity which is in agreement with the finding about the effect of coal particle size on adsorption capacity.

Figure III-20 shows the adsorbed mass of CO₂ over time in similar 15.00 mm cubic particles. Sample B4-1 was tested for about 28 800 min (10 days) while sample B6-1 for

CHAPTER THREE

Single gas adsorption

more than 100 800 min (70 days). Both samples achieved equilibrium at each of 500 kPa step.

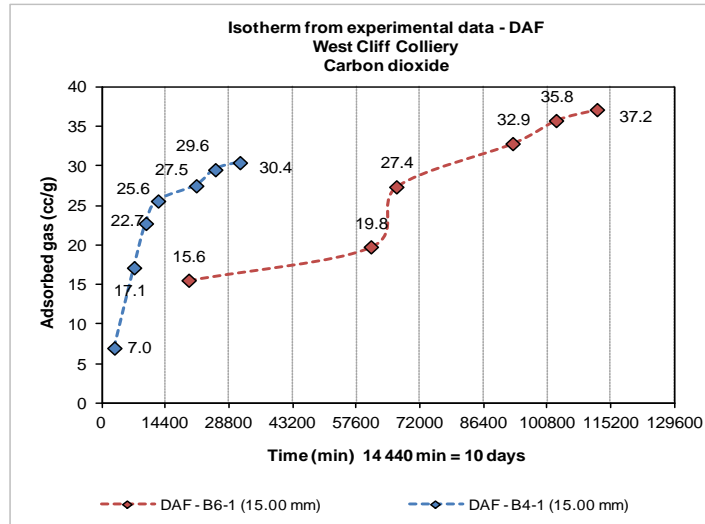


Figure III-20 – Effect of saturation duration on adsorbed CO₂ mass

The graph shows that the B6-1 sample achieved a higher CO₂ sorption capacity (37.2 cc/g) than the B4-1 sample (30.4 cc/g), at each step (measured at different periods of time). These results indicate that the adsorbed mass of CO₂ appeared to increase by about 22% for the five fold increase in saturation time. Thus, the result suggests that the longer the saturation time the higher the sorption capacity of CO₂. However, the difference between results appeared to be within the experimental error. Also, the longer the saturation time the larger the experimental errors especially those errors related to equipment accuracy and gas leakage.

Temperature

Figure III-21 shows the adsorbed mass of CO₂ over pressure in several samples tested at 21 and 24 °C temperature bath water. Room temperature was maintained steady at 24 °C. By analysing the effect of temperature regardless of the particle size, the results indicate that the highest CO₂ adsorption capacity was achieved in samples tested at 21 °C and the lowest was at 24 °C.

CHAPTER THREE

Single gas adsorption

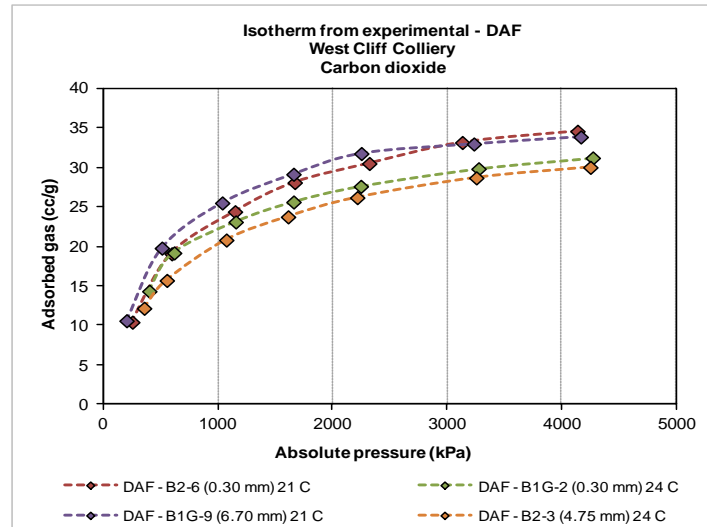


Figure III-21 – Effect of temperature on CO₂ adsorbed mass

The results indicate that the adsorbed mass of CO₂ depends on the temperature over the entire range of pressures. Also, the results show that within the experimental error the 0.30 mm particle sizes achieved almost identical CO₂ adsorption capacity than the 6.70 mm samples which was in agreement with previous finding with respect to particles size.

Langmuir isotherm

Figure III-22 shows the Langmuir and experimental data profiles over pressure from the adsorbed mass of CO₂ on coal. B2-3 and B1G-2 samples were tested up to 4 200 kPa of pressure. Langmuir parameters PL (MPa) and VL (cc/g) were 0.54, 33.45 and 0.46, 34.19 respectively. The Langmuir parameter VL accounts the maximum capacity of coal to store gas in the adsorbed phase and PL is the pressure corresponding to half of the maximum capacity (VL/2). The graph shows that the within experimental error the Langmuir equation tallied very well with the experimental data of CO₂ in coal. As discussed previously, the VL values were about 40-45% lower than those estimated by Saghafi and Roberts (2008).

CHAPTER THREE

Single gas adsorption

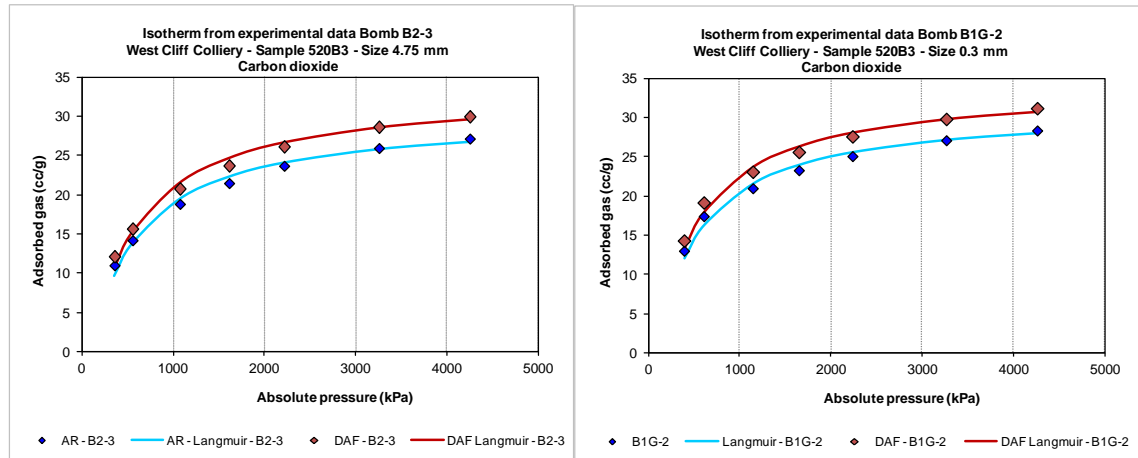


Figure III-22 – Adsorbed CO₂ mass profile modelled by Langmuir

The likely source of errors in gas sorption estimation can be summarised as follows:

- I. Sample collection: time of sample collection and subsequent testing. They was no information on how the samples were collected or chosen. Some of the lump of coal could have already suffered some deterioration/oxidisation.
- II. Sample storage: the samples were stored in a container with water until they were milled and sieved. The lack of water in some of the buckets could lead to sample deterioration/oxidisation. Storage in a fridge is a better practice.
- III. Sample preparation: Milling and sieving of the sample were conducted according to the good practice. However, the samples drying process was erroneously conducted at about 100 °C. This could oxidise (and deteriorate) in some degree most of the samples affecting the posterior proximate analysis and adsorbed mass estimation. This oxidation was likely more severe on the fine samples (particle sizes smaller than 1.00 mm). All the errors due to sampling can be minimised and also estimated by following the Pierre Gy's Sampling theory and sampling practice (Pitard, 1989).

CHAPTER THREE

Single gas adsorption

- IV. Void volume estimation: errors in the void volume estimation could be expected due to gas leakage and inaccuracy of the equipments such as scale, pressure transducers, and thermocouples. The volume of the system (cells, tubes and connectors) were measured once and then used for all cases.
- V. Gas density estimation: densities rely on temperature. Deficient measurement of temperature due to temperature fluctuations on the bath water could lead to errors.
- VI. Equipment calibration: the scale with four digit accuracy was not recalibrated along of the study. A daily check with two calibrated mass. Pressure transducers were calibrated using oil that could contaminate the samples despite of the caring of the process.
- VII. Gas leakage: gas leakage was frequent and efforts were made to minimise and control its occurrence with limited success.
- VIII. Other sources of errors such as CO₂ dilution, compressibility of coal, adsorbed phase density estimation, helium sorption, swelling, may have affected the estimation of the adsorbed mass.

This study could be affected in some measure by almost all the errors. Thus, the difference in adsorbed mass of 35-45% with respect to results on similar samples from the same location may be within the experimental error. The errors have affected all the samples and measurements equally. The lower estimated PL values of about 0.40-0.50 MPa compared with 3.05 MPa obtained by Saghafi and Roberts (2008) indicate clearly that the sample oxidation may have affected more severely on the results, particularly at higher pressure levels. It seems that at higher pressure levels the pore

CHAPTER THREE

Single gas adsorption

network was less accessed by the CO₂ gas and most of the gas was adsorbed mainly in the surface. The pore network (conducts) could be totally or partially blocked or damaged due to the coal oxidation making it inaccessible by the gas. According to Saghafi et al. (2007), the Langmuir parameter PL indicates the rate of gas adsorption onto coal. A lower PL indicates that coal would reach its maximum capacity rapidly and at lower gas pressure. Additional CO₂ sorption capacity profiles modelled with the Langmuir equation are shown in Appendix 11.

III.3.2.3. COAL LINEAR STRAINS

Figure III-23 shows the axial (denoted by suffix A) and radial (denoted by suffix R) strains over time due to adsorption of CO₂ on several 54.00 mm diameter samples of coal that were cored perpendicular to the bedding plane.

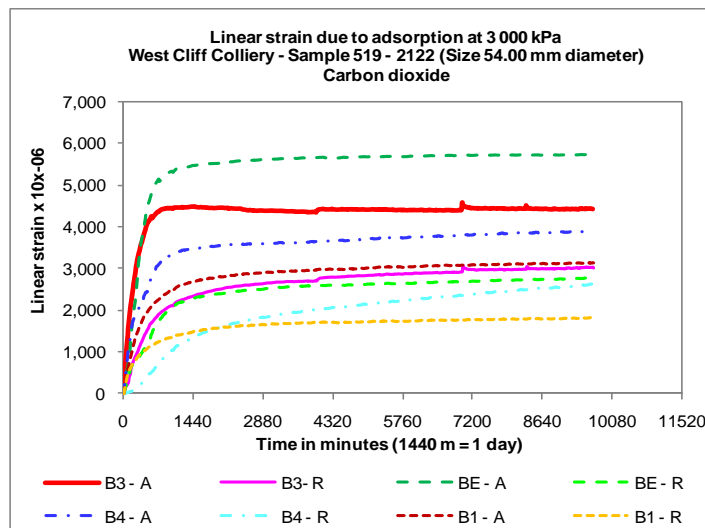


Figure III-23 – Linear strain profile in CO₂ gas adsorption

The bombs were charged with CO₂ up to about 3 300 kPa. The graph shows that the change in the axial (and also radial) strain after they reached their maximum level was almost negligible over time at about the 2 880 min mark (two days). At this point the samples appeared to achieve equilibrium (pressure fluctuations < 5%), which suggest that 2 880 min (two days) appeared to be sufficient time to achieve linear strain

CHAPTER THREE

Single gas adsorption

equilibrium. It was also found that the axial strain was greater than the radial in every sample tested with CO₂. The biggest axial/radial strain ratio was 2.1 in the BE sample and about 1.5 on average in the other samples. On average, the axial strain was 50-100% greater than the radial strain during CO₂ adsorption, which was similar to that obtained with N₂.

Figure III-24 shows the axial and radial strains measured over pressure on the 54.00 mm diameter samples of core coal.

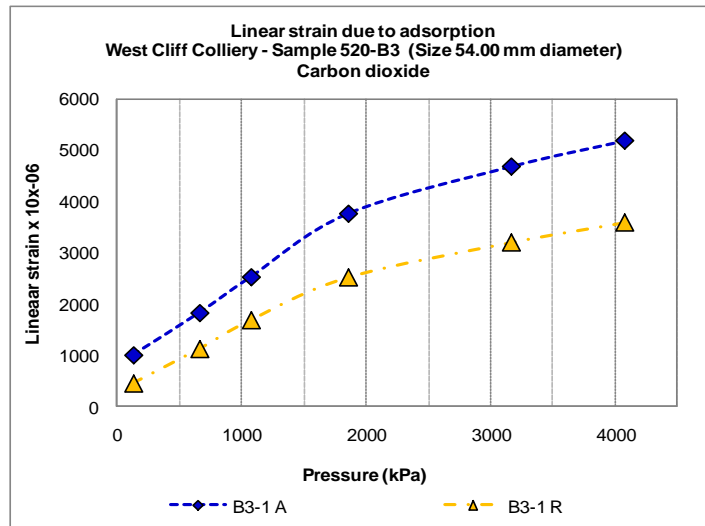


Figure III-24 – Axial and radial strains in B3-1 sample

Sample B3-1 was pressurised with CO₂ in 500 kPa steps up to 4 200 kPa reference pressure level, and the adsorbed mass of CO₂ on the same sample was then measured. As expected, the axial strain was greater than the radial strain at each step, but the difference between them increased with pressure, reaching a maximum axial/radial ratio of about 1.45. Thus, at high pressures the ratio of axial/radial strains was greater than at low pressures. This indicates that the axial and radial strains appeared to depend almost linearly on the pressure in such a way that the higher the gas pressure the greater the linear strain.

CHAPTER THREE

Single gas adsorption

Figure III-25 shows the axial and radial strains against the sorption capacity of CO₂ of the B3-1 sample. The graph shows that the linear strains followed an increasing trend line. The linear strains depended on the adsorbed mass of CO₂; the higher the adsorbed CO₂ the greater the axial and radial strains. As expected, the largest ratio of axial/radial strains (1.45) occurred at the maximum adsorbed mass of CO₂ (32.60 cc/g measured at about 4 200 kPa).

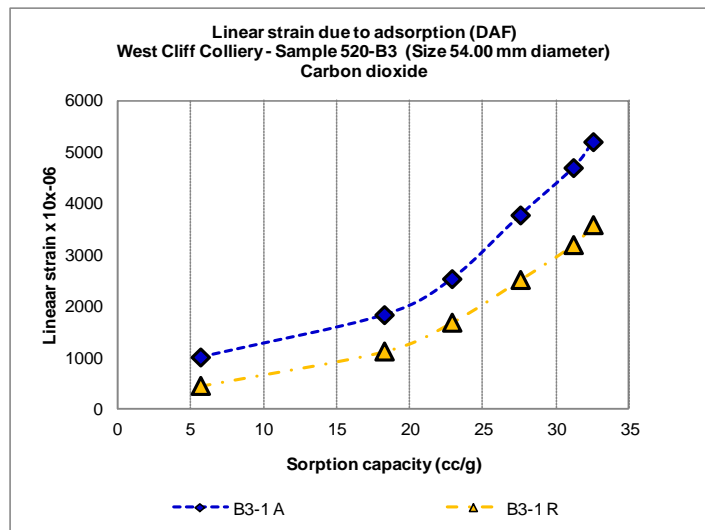


Figure III-25 – Linear strains and adsorbed CO₂ in adsorption

III.3.3. METHANE

III.3.3.1. GAS SATURATION TIME

Pressure level

Figure III-26 shows the drop in pressure over time of CH₄ during adsorption stage. Samples of coal were saturated with CH₄ in steps of 500 kPa, up to about 4 200 kPa pressure. The aim was to analyse how the level of gas pressure was affected by the saturation time. The graph compares the behaviour of CH₄ at two pressure levels; 500 (low level) and 3 000 kPa (high pressure level). At 500 kPa the equilibrium pressure occurred in around 4 320 min (three days) despite the pressure continuing to drop over time, as shown in the graph. It seems that the cell was slowly losing pressure due to

CHAPTER THREE

Single gas adsorption

the gas leakage. The result indicates that longer saturation time led to lower equilibrium pressure for the same volume of CH₄. The pressure profile shows that the pressure dropped almost 50% from the initial 750 kPa level to about 450 kPa final equilibrium pressure level.

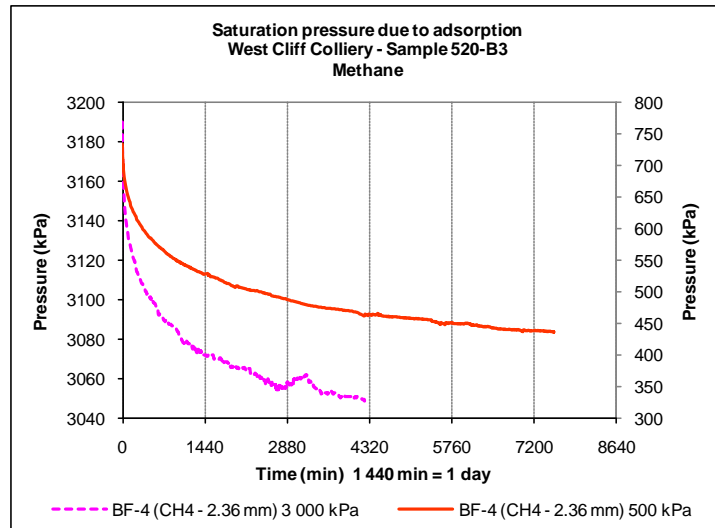


Figure III-26 – Effect of pressure levels in CH₄ gas saturation time

At 3 000 kPa, the equilibrium pressure was satisfied at around 4 320 min (three days). The results suggest that the saturation time of CH₄ appeared to be independent of the pressure levels. Also, the longer the saturation time the lower the resultant equilibrium pressure level. Moreover, 4 320 min was the minimum saturation time for fluctuations in pressure < 5%. Compared with the saturation time for CO₂, CH₄ took longer to attain saturation level similar to the CO₂.

Coal particle size

Figure III-27 shows the drop in pressure over time on several particles size during adsorption of CH₄ at pressure levels of 500 kPa. Particles tested ranged from 1.18 mm (fragmented coal) to 54.00 mm core coal. Every sample of coal appeared to achieve equilibrium pressure at around 5 760 min mark (four days), for fluctuations in pressure < 5%. This result suggests that saturation time of CH₄ appeared to be independent of

CHAPTER THREE

Single gas adsorption

the particle sizes. However, the graph shows that the samples were better stabilised when they were run over a longer period of time.

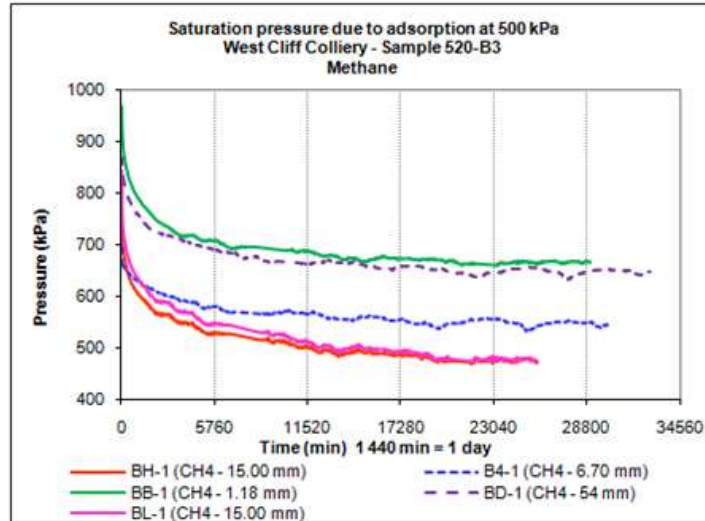


Figure III-27 – Effect of particle sizes in CH₄ gas saturation time

Appendix 13 shows drop in pressure of the BD-2 (54.00 mm) coal sample at each 500 kPa steps during adsorption of CH₄.

Gas type

Figure III-28 shows drop in pressure over time with respect to the type of gas. The graph shows that, regardless of particle size, N₂ and CO₂ appeared to require between 1 440 min to 2 880 min to adequately stabilise in pressure.

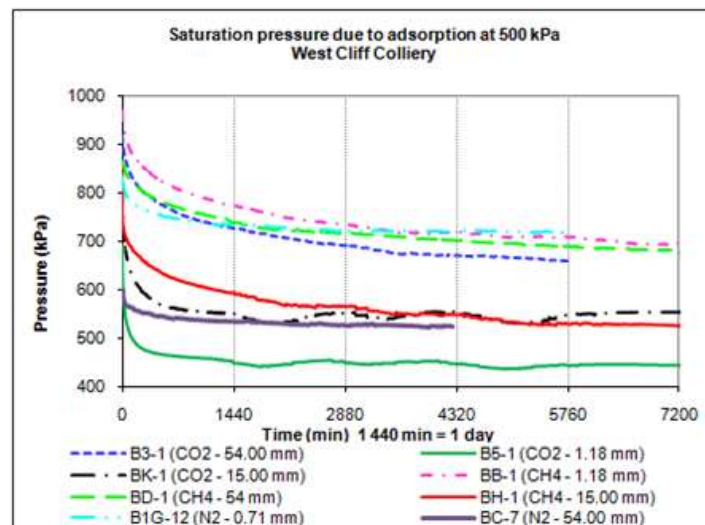


Figure III-28 – Effect of gas type in saturation time

CHAPTER THREE

Single gas adsorption

Meanwhile, CH₄ required at least 4 320 min (three days) to achieve a similar degree of saturation, which suggests that the saturation time of gas in coal appeared to depend on the type of gas. Saturation time of CH₄ took longer to attain the same degree of saturation as N₂ and CO₂. Also, the results suggest that regardless of the gas type and particle size the samples charged to lower initial pressure were better saturated, which was evident by the flat pressure profile at equilibrium or near equilibrium point.

Temperature

Figure III-29 shows the effect of the bath water and room temperature on the CH₄ pressure over time. The graph shows that the room temperatures RT 1 and RT 2 were on average below 24 °C over the entire test period. Also, the room temperature profiles indicate that during the first 1 440 min of the test, the bath water temperature was affected in almost 2 °C, below the desired 24 °C mark.

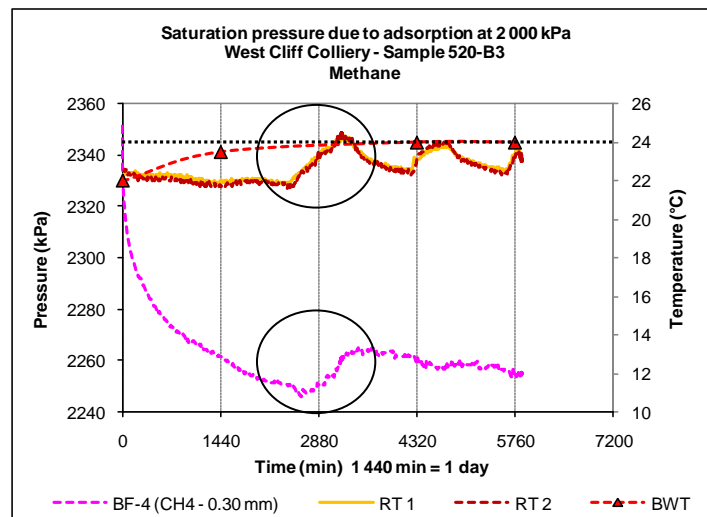


Figure III-29 – Effect of temperature in CH₄ gas saturation time

Meanwhile during the first 1 440 min, the room temperatures RT 1 and RT 2 were both maintained almost constant at about 22 °C. Apparently the bath water temperature was affected by the changes in the room temperature, although during the following days the bath water temperature (BWT) held steady despite some fluctuations in room

CHAPTER THREE

Single gas adsorption

temperature. This suggests that the drop in pressure did not appear to be affected by the changes in the bath water temperature, but by changes in room temperature, since the transducers were out of the water container. The circles on the graph show that an increase in room temperature meant firstly an increase in the pressure of CH₄, and then a slight CH₄ pressure fluctuation helped by the steady bath water temperature. This suggests that changes in the bath water temperature appeared to depend on changes in room temperature. Furthermore the pressure of CH₄ appeared more susceptible to changes in room temperature rather than changes in bath water temperature; an increase in room temperature meant an increase in the pressure of CH₄. This undesired effect can be avoided by increasing the bath water temperature in at least 5 °C above the room temperature and by covering (isolating) the pressure transducer.

III.3.3.2. ADSORBED MASS

CH₄ adsorbed mass

Figure III-30 shows the adsorption capacity of CH₄ over pressure from the experimental data, measured at each 500 kPa step up to 4 200 kPa pressure level. The maximum adsorption capacity of CH₄ of sample B5-1 (DAF) was around 16.5 cc/g at 4 200 kPa, which was about 50% of the adsorbed mass of CO₂ at similar pressure levels. This was in agreement with Saghafi et al. (2007) finding which reported that coal adsorbed two times (in volume) more CO₂ than CH₄ and five times than N₂. Langmuir parameters PL and VL (DAF basis) were estimated to be 0.89 MPa and 19.84 m³/t (same in cc/g). The estimated adsorbed mass was lower 28% than similar sample from the same location reported by Saghafi and Roberts (2008) on similar samples from the same location.

CHAPTER THREE

Single gas adsorption

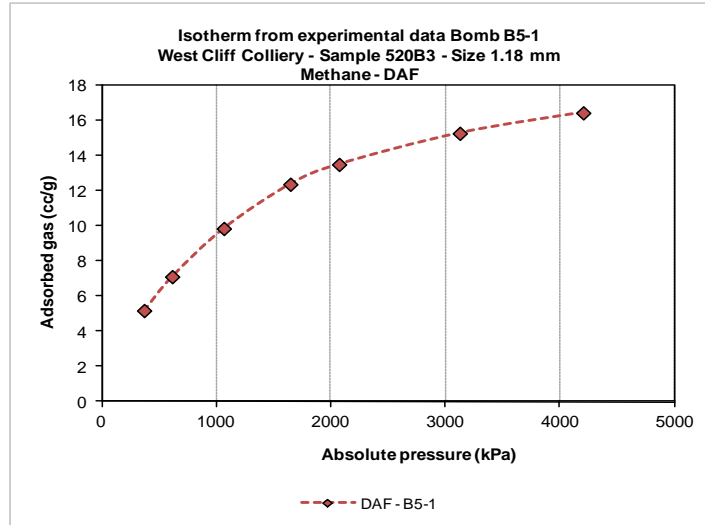


Figure III-30 – CH₄ adsorbed mass profile in adsorption

Similarly to those samples tested with CO₂, this lower adsorbed mass can be attributed to the experimental errors described previously, mainly due to coal oxidation or sample deterioration. The amount of adsorbed mass on sample B5-1 was among the average value of all the samples tested with CH₄. It seems that all the samples were affected equally by the same potential error.

Coal particle size

Figure III-31 shows the sorption capacity profiles of CH₄ over pressure obtained from the experimental data. Particles ranging from 0.21 mm to 54.00 mm diameter samples of core coal were tested during the adsorption of CH₄. By analysing the graph the results suggest that within experimental errors all the samples adsorbed similar amount of CH₄, around $18 \pm 2 \text{ m}^3/\text{t}$. The highest adsorbed mass of CH₄ was attained in the largest (15.00 mm) size particle, while the lowest amount of CH₄ was in the 54.00 mm diameter core coal. However, the majority of samples were within average. Despite the results were not conclusive, they suggested that the sorption capacity of CH₄ on coal was independent of the size of the coal particles. Additionally, the analysis of the result on the 15.00 mm cubes sample, it appeared to be the less affected by

CHAPTER THREE

Single gas adsorption

oxidisation or deterioration caused during the coal sampling and preparation. The cubes were prepared using the inner part of the core thus, the ageing effect was minimised. However, the core coal sample appeared to be strongly affected by the drying process making it less permeable to the gas.

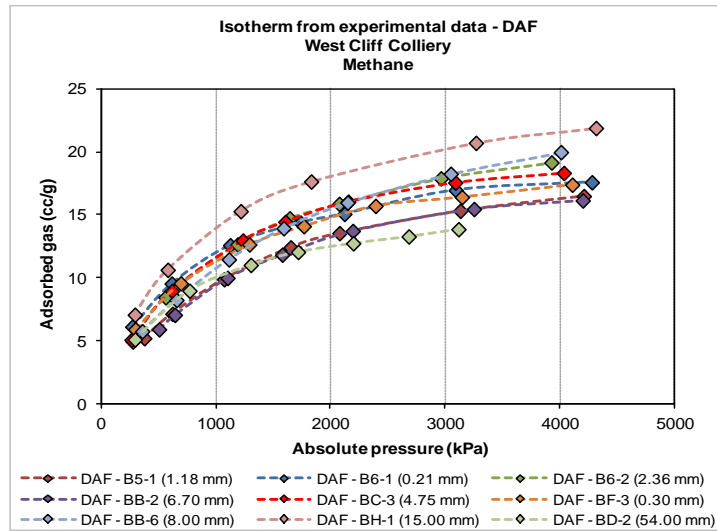


Figure III-31 – Effect of particle sizes on CH₄ adsorption capacity

Appendix 15 shows the CH₄ adsorption capacity (Experimental and Langmuir isotherms) of several samples of coal tested in adsorption.

Saturation time

Figure III-32 shows the adsorbed mass of CH₄ over time in two different particles size, powder (0.21 mm), and 15.00 mm cubical coal samples. By comparing the B6-1 sample with the BK-1 sample, the graph shows (as expected) that, for similar saturation time (e.g. for saturation time below 14 400 min) similar samples attained near equal adsorbed mass of CH₄. For longer saturation time, the BK-1 sample attained marginally more CH₄ than the B6-1 sample. Thus, the graph suggests that the adsorbed mass of CH₄ on identical particle sizes appeared to depend on the saturation time; the longer the saturation time the higher the sorption capacity of CH₄ in coal.

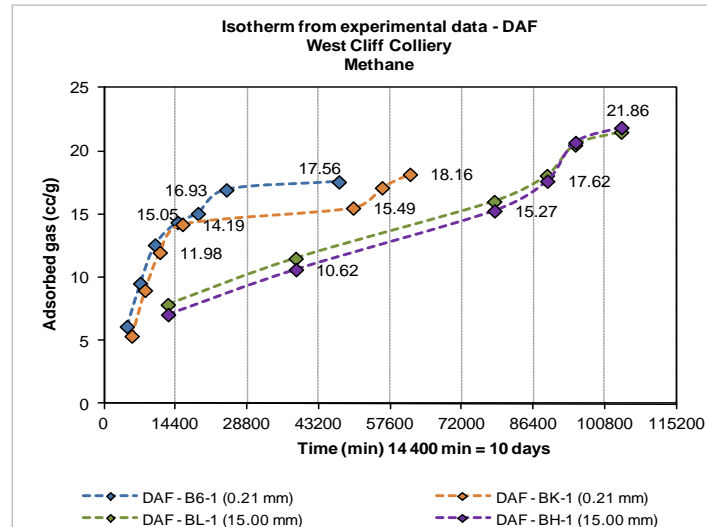


Figure III-32 – Effect of saturation time on CH₄ adsorption capacity

Also, the adsorption capacity on the 15.00 mm cubes shows that they achieved almost the same amount of CH₄ at each pressure step and saturation period. The graph indicates that identical particles size saturated for the same period of time achieved similar amount of CH₄. By comparing the 0.21 mm samples with the 15.00 mm size coal, the graph shows that the 15.00 mm cubes samples adsorbed marginally more CH₄ (20%) than the 0.21 mm particles size, a result that suggests that the adsorbed mass of CH₄ appeared to depend on the particle sizes; the larger the particles the higher the adsorption capacity of CH₄. Also, the graph shows that the cubic samples were saturated for almost 43 200 min (30 days) longer than the 0.21 mm particles size, which suggests that the adsorbed mass of CH₄ could be increased by increasing the saturation time. However, an increase of about 20% by extending the saturation period by more than 100% does not appear to be a great achievement. As it was said previously, the results may carry an experimental error of about 28% when comparing with similar samples from identical location. Thus, the increase in 20% on the adsorption capacity may be within the experimental error. This error was smaller due to the fact that the 15.00 mm samples were better prepared as it was stated in the

CHAPTER THREE

Single gas adsorption

section of the Coal particle size. Additionally, it was not unexpected that larger particle sizes running for very long period of time could achieve higher adsorption capacity due to mainly its larger pore network.

Temperature

Figure III-33 shows the adsorbed mass of CH_4 over pressure measured on samples at 21, 24, and 28 °C of bath water temperatures.

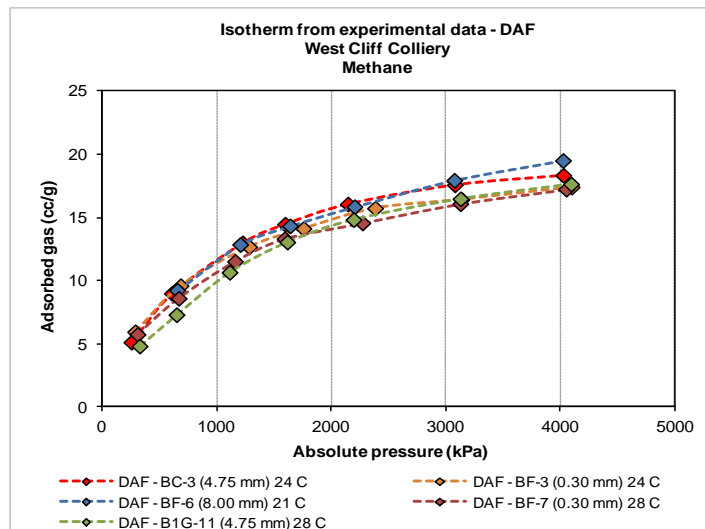


Figure III-33 – Effect of temperature in CH_4 adsorbed mass in adsorption

The results shows that regardless of the particle size, the highest adsorbed mass of CH_4 occurred at 21 °C while the lowest was at 28 °C, while the sample tested at 24 °C was in between. The similarity in sorption capacity could be attributed to the small differences in the temperature of the test and in the effect of the room temperature fluctuations (about ± 2 °C) on the bath water temperature. Also, experimental errors could have affected the sorption capacity of the samples. By comparing two samples (BC-3 and B1G-11) with identical sizes (4.75 mm), the highest sorption capacity was on the sample run at 24 °C (sample BC-3). Thus, the results indicate that the CH_4 sorption capacity on coal depend on the temperature; the lower the temperature the higher the adsorbed mass of CH_4 on coal.

CHAPTER THREE

Single gas adsorption

Gas type

Figure III-34 shows the adsorbed mass over pressure during adsorption on coal with respect to gas type. The results indicates that the adsorbed mass of CO₂ was the highest measured on coal and N₂ the lowest, while CH₄ was in between them.

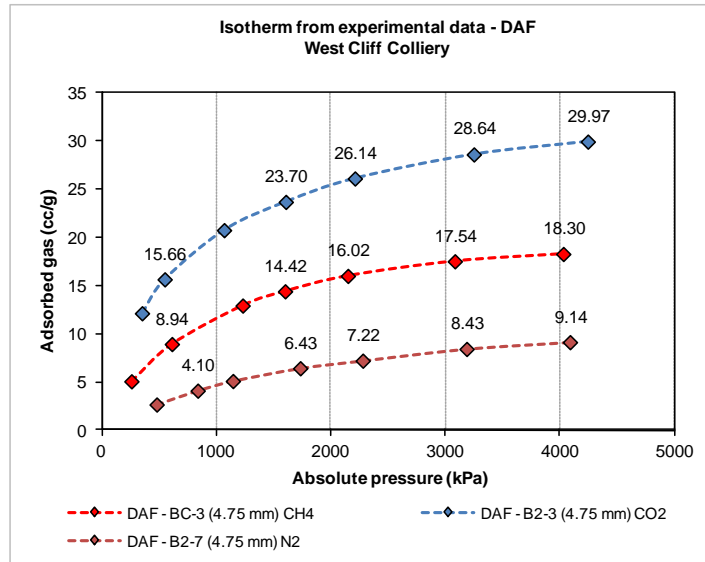


Figure III-34 – Effect of gas type in adsorption

The results show that at maximum pressures coal adsorbed 65% more CO₂ than CH₄ and 225% than N₂. Also, CH₄ adsorption capacity on coal was 100% higher than N₂. These ratios were lower than those ratios reported by Saghafi et al. (2007). They reported that coal adsorbed two times more CO₂ than CH₄ and five times more N₂. As it was discussed previously, it appears that the CO₂ adsorption capacity was strongly affected by the coal collection, storage, and sampling and also by the drying process done at temperature higher than 30 °C.

Langmuir isotherm

Figure III-35 shows the CH₄ isotherms of the BC-3 sample due to adsorption. Experimental data of the adsorbed mass of CH₄ on coal during adsorption was modelled using the Langmuir equation. The graph shows that the Langmuir equation

CHAPTER THREE

Single gas adsorption

appeared to tally well with the experimental data of the CH₄ sorption capacity during adsorption. It can be seen that the Langmuir equation modelled with good degree of accuracy the CH₄ adsorption capacity of coal.

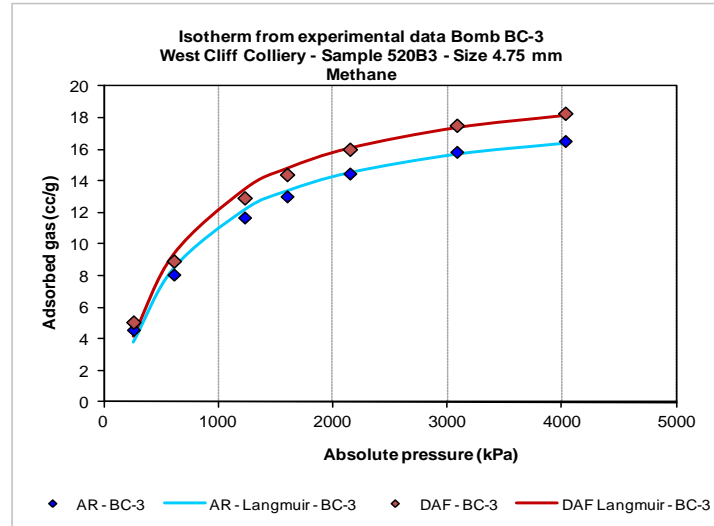


Figure III-35 – Langmuir isotherm from CH₄ experimental data

The results indicate that the Langmuir equation models very well the adsorbed mass of single gas (CO₂, CH₄ and N₂) on coal. Additional profiles of CH₄ modelled with the Langmuir equation are shown in Appendix 15.

III.3.3.3. COAL LINEAR STRAINS

Figure III-36 shows the linear strains (axial and radial) over pressure due to adsorption in two, 54.00 mm diameter core coal samples. The strains are denoted by the suffix 'A' for axial and 'R' for radial. The graph shows that the axial strains were greater than the radial strains in both samples at each 500 kPa incremental pressure step. Both samples show almost identical response to the swelling effect due to CH₄ adsorption. The axial strain in both samples was about $1\,700 \times 10^{-6}$ (0.17%) at 3 500 kPa while the radial strain was about $1\,200 \times 10^{-6}$ (0.12%). The results show that the strains increased with adsorption as CH₄ pressure increased. There is a linear relationship between the strains

CHAPTER THREE

Single gas adsorption

and the quantity of gas adsorbed. The increase in axial and radial strains clearly indicates that the samples swelled due to CH₄ gas adsorption. This swelling appeared to be reversed when the applied pressure was released and then the sample came back to its original condition.

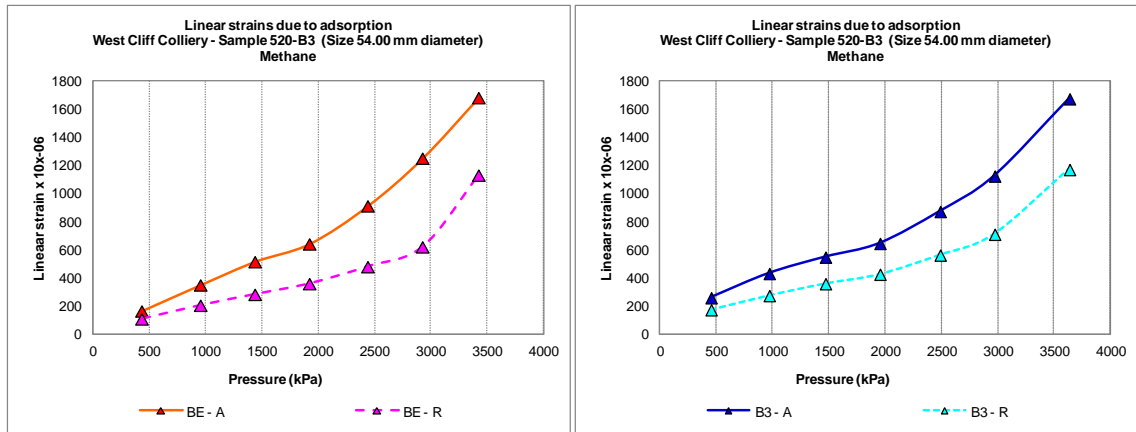


Figure III-36 – Axial and radial strain due to CH₄ gas adsorption

Eventually, incompetent samples could be partially damaged due to the swelling process, even at low pressures. At high pressure, samples could be fractured or the pore system could be damaged irreversibly. The sudden increase in radial strain shown as last point of the radial strain profile of sample BE-R suggests that the radial strain gauge was lost, either due to malfunction of the strain gauge or the fracture of the spot where the strain gauge was attached. Additionally, the average axial/radial strain ratio in both samples was about 1.42. The results suggest that the linear strains appeared to depend on the level of pressure; the higher the pressure the greater the linear strains.

Figure III-37 compares the CO₂ adsorption capacity on coal with the linear strains due to adsorption of CO₂ in the B3-1 coal sample. The graph shows that linear strain profiles due to CO₂ adsorption resembled the CO₂ isotherm profile. Both axial and radial strains increased with pressure which suggests that the linear strains were

CHAPTER THREE

Single gas adsorption

proportional to the quantity of CO₂ adsorbed; the higher the CO₂ adsorbed the greater the linear strains.

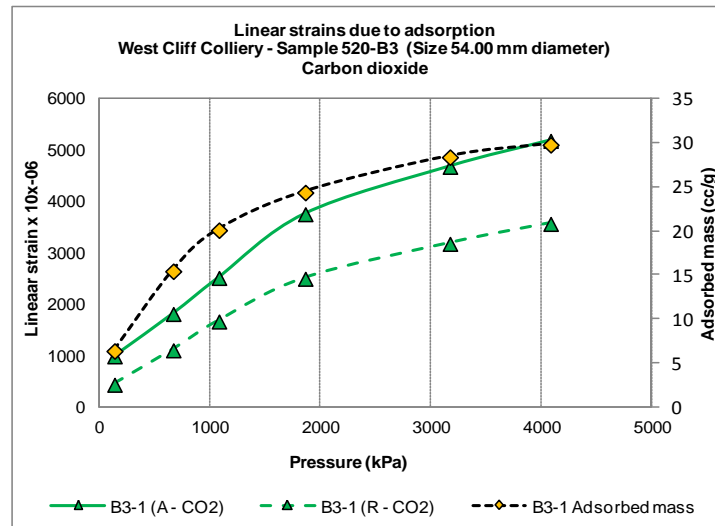


Figure III-37 – Linear strains and CO₂ sorption capacity in adsorption

Figure III-38 compares linear strain with the type of gas in two coal samples and as expected, linear strains stemming from adsorption of CO₂ were greater than those from adsorption of CH₄.

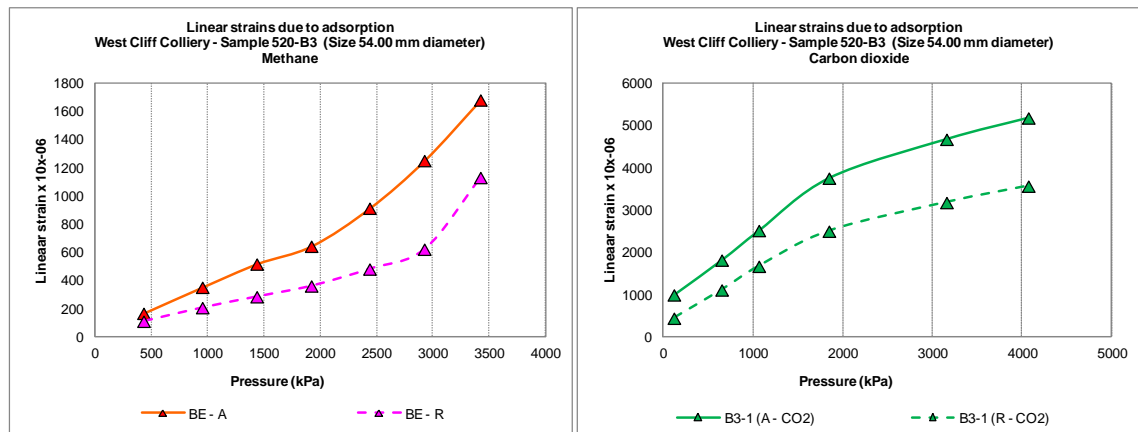


Figure III-38 – Effect of gas type in linear strains in CH₄ gas adsorption

The axial strain ratio of CO₂/CH₄ was about three times. This indicates that the adsorption of CO₂ caused more strain and swelling than CH₄, mainly due to the higher CO₂ adsorption capacity. St. George and Barakat (2001) reported that the expansion (volumetric strain) in a 52.5x45 mm core coal samples due to CO₂ adsorption was

CHAPTER THREE

Single gas adsorption

about 12 times higher than N_2 and eight times higher than CH_4 . Maximum volumetric swelling with CO_2 was estimated in about 1.7-1.9% by Day et al. (2008). Also, they reported that up to intermediate pressures swelling was roughly proportional to the amount of adsorbed CO_2 , but at high pressures the relationship was not longer linear, adsorption continued to increase but swelling did not.

III.3.4. SUMMARY

A sorption apparatus and a test procedure were established to gravimetrically measure the adsorption of gas in coal, and examine the changes in the properties of coal.

Saturation time

- Saturation time of N_2 and CH_4 appeared to be independent of the pressure levels, but saturation time of CO_2 seems to depend on the levels of pressure; the lower the pressure the shorter the saturation time,
- 2 880 min (two days) were sufficient for N_2 and CO_2 to achieve equilibrium pressure while CH_4 took one more day longer to achieve the same requirement with pressure fluctuation less than 5%. Saturation time of N_2 and CH_4 appeared to be independent of particle size. Saturation time of CO_2 was independent of the particle size with fragmented samples of coal but with 15.00 mm size or larger the saturation time with CO_2 may depend on particle size. More research is needed in larger particles size.
- The minimum saturation time obtained with respect to pressure levels also applies to particle sizes. Saturation time of gas in coal appeared to depend on the type of gas. CH_4 took longer than N_2 and CO_2 to achieve a similar degree of saturation.
- In general, changes in room temperature influenced bath water temperature. The saturation time of CO_2 appeared to be independent of bath water temperature as

CHAPTER THREE

Single gas adsorption

long as the changes were small. However, the pressure of N_2 and CH_4 appeared to be affected in higher degree for small changes in bath water temperature.

Adsorbed mass

- The adsorbed mass of CO_2 measured by quick test (QT), consisting of 120 min of saturation time at each 500 kPa step, was higher than those samples measured at minimum saturation time of two days. Sample deterioration could be attributed to this anomalous sorption behaviour. For very long saturation period, the adsorbed mass of CO_2 in coal appeared to depend on the gas saturation time. With CH_4 however, the longer the saturation time the higher the adsorption capacity on coal.
- The adsorbed mass of N_2 in coal could depend on the particle sizes. More research is needed in this respect. However, the sorption capacity of CO_2 and CH_4 up to 4 000 kPa, appeared to be independent of particle size. By analysing the adsorbed mass of CH_4 over time instead of pressure, its sorption capacity appeared to depend on time. Marginally higher adsorbed CH_4 mass was achieved by increasing the saturation time.
- Gas adsorption in coal depended on the type of gas. CO_2 was found to adsorb in coal 65% more than CH_4 and 225% more than N_2 . These lower values when comparing to other studies (Saghafi *et al.*, 2007) could be attributed to samples deterioration.
- Gas sorption depended on temperature. The lower the temperature the higher the adsorbed mass.

CHAPTER THREE

Single gas adsorption

- The experimental data obtained from single gas adsorption (N_2 , CO_2 and CH_4) can be modelled very well by the Langmuir equation.
- During N_2 , CO_2 , and CH_4 adsorption and due to swelling, the axial strains was larger than the radial strain,
- 2 880 min (two days) of CO_2 saturation time was sufficient to achieve equilibrium strains but CH_4 took longer,
- Axial and radial strains were almost linearly dependent on the pressure of gas; the higher the gas pressure the greater the linear strain. Also, the higher the adsorbed mass the greater the linear strains. Linear strain due to adsorption of CO_2 in coal was about three times greater than CH_4 .

IV. CHAPTER FOUR

MIXED GAS ADSORPTION

IV.1 INTRODUCTION

As part of the continuing research into mine gases and control of outbursts, studies were undertaken to examine the sorption of mixed gases (binary and ternary mixture). Particular emphasis was directed to characterise the adsorption in coal of mixed gases, their adsorbed mass, the accuracy of the extended Langmuir equation to model mixed gas adsorption, and the applicability of the Soave-Redlich-Kwong equation of state (Soave 1972, Redlich and Kwong 1949). Thus, N₂, CO₂, and CH₄ gas isotherms and the composition of mixed gas at steps of 500 kPa up to 4 000 kPa were studied on samples of coal from West Cliff Colliery, Area 5 under controlled laboratory conditions. The mixed gas adsorption in coal was characterised from the point of view of saturation time, particle size, gas mixture (binary and ternary), gas composition, and adsorbed mass.

IV.2. EXPERIMENTAL PROCEDURE

IV.2.1. APPARATUS

The adsorption apparatus used for the study was described in chapter 3, section 2.1. Figure IV-1 shows details of the sorption apparatus. The main gas chromatographer (GC) components were the gas detector and the bomb - gas sampling bag system. Before testing, the bag was attached to the GC inlet and small amount of gas samples were taken directly from the bomb to the plastic bag adapted for that purpose. Before each test, and on a six months basis, the pressure transducers were calibrated and the database updated (see calibration of pressure transducers in Appendix 18).

CHAPTER FOUR

Mixed gas adsorption

On daily basis, the scale was checked with calibrated weight and the GC was calibrated.

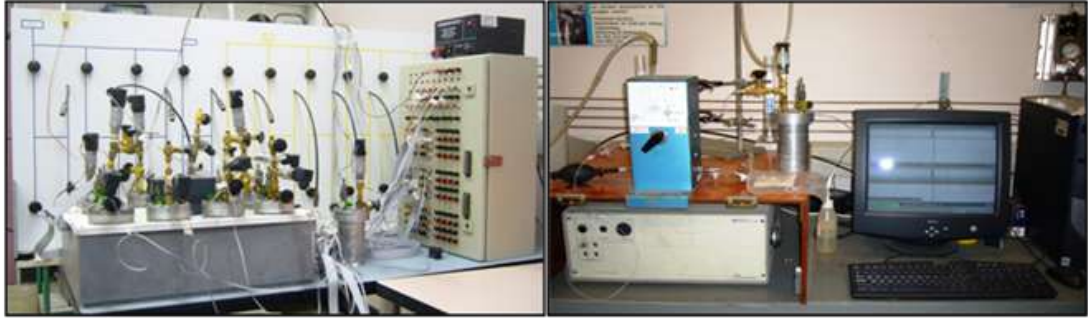


Figure IV-1 – Gas sorption apparatus

IV.2.2. COAL SAMPLE PREPARATION

A total of 44 coal samples from the Bulli seam at West Cliff Colliery, Area 5 (longwall panels 519-21, 519-2122 and 520-B3) were prepared and then tested in mixed gas adsorption. They were crushed/milled and mechanically sieved to obtain different particles size.

Samples tested with mixed gases				
Coal samples Size	Quantity	Temperature	Mixed gas	Sorption Duration
0.21 mm	1	24 °C	B	Saturation
0.30 mm	1	20-21 °C	B	Saturation
0.30 mm	5	24 °C	B	Saturation
0.30 mm	1	24 °C	B	2 hr
0.30 mm	1	24 °C	B	7 days
0.71 mm	3	24 °C	B	Saturation
0.71 mm	1	24 °C	T	Saturation
1.18 mm	5	24 °C	B	Saturation
1.18 mm	1	24 °C	T	Saturation
2.36 mm	3	24 °C	B	Saturation
4.75 mm	5	24 °C	B	Saturation
4.75 mm	1	28 °C	B	Saturation
4.75 mm	1	24 °C	T	Saturation
6.70 mm	1	24 °C	B	Saturation
6.70 mm	2	20-21 °C	B	Saturation
8.00 mm	5	24 °C	B	Saturation
8.00 mm	1	24 °C	B	2 hr
54.00 mm	4	24 °C	B	Saturation
54.00 mm	2	24 °C	T	Saturation
Total	44			
B --> 52/48 CO ₂ /CH ₄ Binary mixed gas				
T --> 31.8/33.4/34.8 N ₂ /CO ₂ /CH ₄ Ternary mixed gas				

Sample	Relative Density	Moisture (%)	Ash (%)
520B3-BA-6	1.41	1.1	8.2
520B3-BA-7	1.41	1.1	8.2
5192122-BB-7	1.42	1.0	8.2
520B3-B6-5	1.42	1.1	8.1
520B3-B6-6	1.42	1.1	8.1
520B3-B4-7	1.42	1.2	7.7
520B3-B5-4	1.43	1.1	8.5
520B3-BH-6	1.42	1.2	8.3
520B3-BH-7	1.42	1.2	8.2
520B3-BC-6	1.43	1.1	8.5
520B3-BL-7	1.43	1.2	8.2
520B3-BL-8	1.43	1.3	8.2
520B3-BK-6	1.40	1.1	8.0

Table IV-1 – Coal samples tested with mixed gas and proximate analysis

Tests were carried out on 54.00 mm diameter sample and various size fragments of coal, as shown in Table IV-1. Samples of coal were tested at equilibrium pressure and

CHAPTER FOUR

Mixed gas adsorption

also at two hrs and seven days of gas saturation. Chapter 3, section 2.2 and 2.3 describes the preparation, environment, and testing procedure of the samples.

IV.3. EXPERIMENTAL RESULTS

IV.2.3. BINARY MIXED GAS

Gas adsorption was carried out with mixed 52/48 CO₂/CH₄ in samples of coal, and the results were analysed for saturation time, and the composition and adsorbed mass of gas. Adsorbed mass and Langmuir equation are presented on “as received” basis. The extended Langmuir model used to predict mixed gas adsorption isotherms, require pure components of isotherm data for their predictions.

$$\theta_i = \omega_i/L_i = \frac{B_i P y_i}{1 + \sum B_j P y_j} \quad (8)$$

Where ω_i is the amount of component "i" adsorbed, L_i and B_i are Langmuir constants for "i", P is pressure, and y_i is the mole fraction of "i" in the gas phase.

IV.2.3.1. MIXED GAS SATURATION TIME

Pressure level

Figure IV-2 shows the drop in pressure against time in the 1.18 mm particle at 500 and the 3 000 kPa, taken as reference pressures. The results indicate that at 500 kPa the desired degree of saturation (time to each saturation with fluctuations in pressure < 5% over the period) was achieved between the 2 880 and 4 320 min mark, and a similar result was achieved at 3 000 kPa level.

At different levels of pressure the sample achieved a similar degree of saturation (time to reach saturation) over the same period of time, but at high pressure the graph shows some fluctuations in pressure drop that contrast with a smooth drop at low levels of pressure. These fluctuations could be attributed to changes in temperature.

CHAPTER FOUR

Mixed gas adsorption

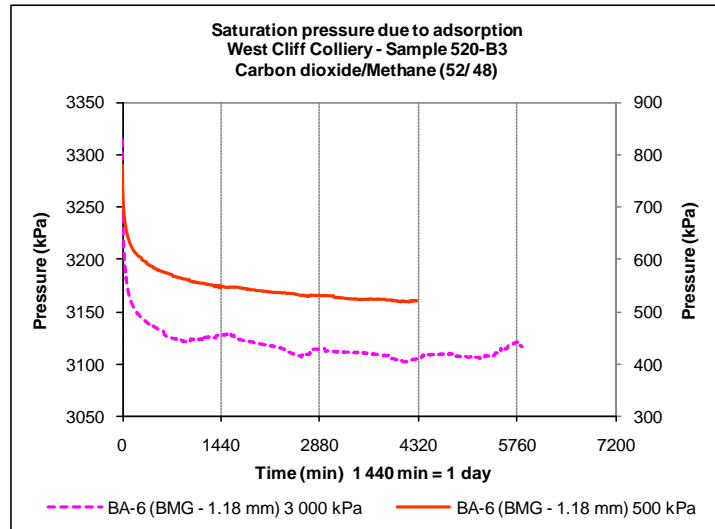


Figure IV-2 – Effect of pressure levels in mixed gas saturation time

Table IV-2 shows the saturation time (D) and the degree of saturation degree (SD) at each step in four representative size particles. The degree of saturation evaluated in the last 1 080 min (18 hrs) of saturation showed that the samples achieved adequate saturation around 2 880 min (two days), with the fluctuation in pressure being less than 5%, regardless of particle size or pressure level.

Table IV-2 – Saturation time during mixed gas adsorption

Samples	Saturation degree (SD) (%) - saturation duration (D) (minutes)															
	200 kPa		500 kPa		1000 kPa		1500 kPa		2000 kPa		3000 kPa		4000 kPa		Avg	
	SD	D	SD	D	SD	D	SD	D	SD	D	SD	D	SD	D	SD	D
B4-7 (8.00 mm)	1.2%	2506	3.6%	2533	2.5%	2549	0.1%	2833	3.1%	2575	0.8%	2816	3.0%	2630	2.0%	2635
BA-6 (1.18 mm)	1.3%	2461	3.0%	2457	1.9%	2433	1.0%	2848	3.0%	2494	2.1%	2810	1.2%	2630	1.9%	2590
B6-5 (4.75 mm)	1.8%	2548	2.7%	2742	2.4%	2425	1.7%	2544	2.4%	2625	0.6%	2898	5.0%	2604	2.4%	2626
BH-6 (0.30 mm)	0.5%	2506	2.6%	2633	3.0%	2665	1.2%	2572	2.0%	2520	0.9%	2874	5.0%	2599	2.2%	2624
Average	1.2%	2505	3.0%	2591	2.5%	2518	1.0%	2699	2.6%	2553	1.1%	2850	3.5%	2616	2.1%	2619

Coal particle size

Figure IV-3 shows the drop in pressure over time on several samples of fragmented coal ranging from 0.21 to 8.00 mm. In addition, 54.00 mm diameter samples were tested with a mixture of CO₂/CH₄ during adsorption to understand how saturation time was affected by different size particles. Most particle sizes achieved adequate saturation between 2 880 and 4 320 min. The result indicates that on average, it took a

CHAPTER FOUR

Mixed gas adsorption

minimum of 2 880 min (two days) for all particle sizes to attain an adequate degree of saturation. This suggests that saturation time seemed to be independent of particle size. Similar results were obtained with single gases.

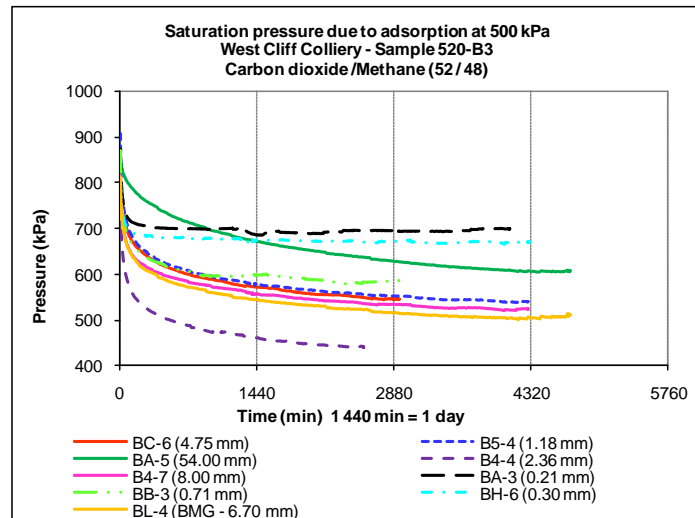


Figure IV-3 – Effect of particle sizes in mixed gas time

Also, the results suggest that the coal samples achieved equilibrium pressure but it was unclear (but very likely) whether or not composition equilibrium was attained.

Bath water and room temperature

Figure IV-4 shows the pressure drop profiles over time on samples tested at bath water temperatures of 21, 24 and 28 °C.

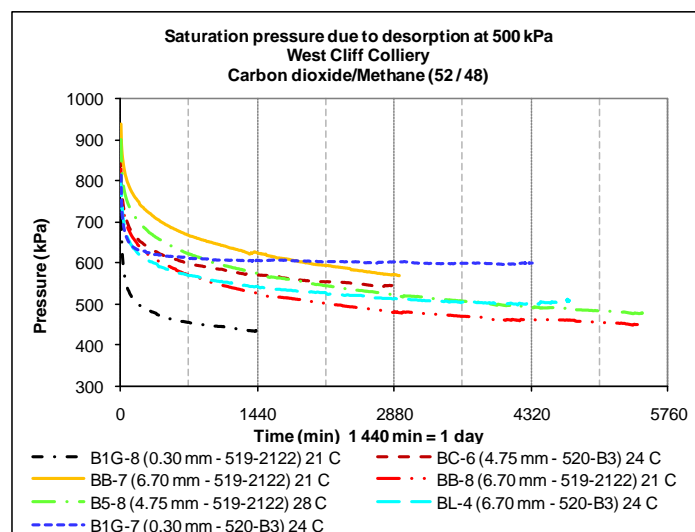


Figure IV-4 – Effect of bath water temperature on saturation time

CHAPTER FOUR

Mixed gas adsorption

Tests were carried out on powder (size < 1.00 mm) and fragmented samples (size > 1.00 mm and < 54.00 mm). The graph shows that both 0.30 mm samples reached equilibrium pressure at about 1 440 min. However, the sample tested at 24 °C attained equilibrium pressure quicker, in around 360 min. Particles of coal > 1.00 mm took about 2 880 min to attain equilibrium pressure which suggests that the saturation time of gas was similar at 21, 24 and 28 °C.

Figure IV-5 shows how changes in room temperature affected changes in the bath water temperature and the drop in pressure of the mixed gas during adsorption.

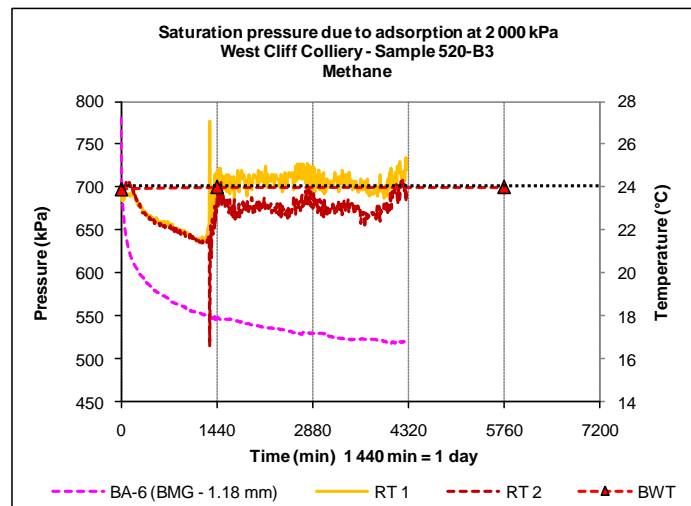


Figure IV-5 – Effect of room temperature on saturation time

The graph shows that in the first 1 440 min, the room temperatures measured in RT 1 and RT 2 dropped in more than two degrees, which shows that the bath water temperature (at 24 °C) was not affected by changes in room temperature. This indicates that these changes did not induce any changes in bath water temperature and consequently, in the pressure drop profile. However, bath water temperatures few degrees below or above to room temperature (acclimatised at 24 °C) could experience some undesired fluctuations in pressure, making more difficult to achieve equilibrium. Ideally, test temperature should be four degrees above room temperature.

CHAPTER FOUR

Mixed gas adsorption

IV.2.3.2. MIXED GAS COMPOSITION

Pressure level

Figure IV-6 shows the CH₄ free gas composition during mixed gas adsorption over pressure. At low pressure the 1.18 mm particle adsorbed CO₂ in a combined CO₂/CH₄ ratio of 3.4, decreasing gradually at increased pressure until it reached a ratio of 1.5 at about 4 000 kPa of pressure. CO₂/CH₄ ratios were calculated from GC analysis of a sampled gas.

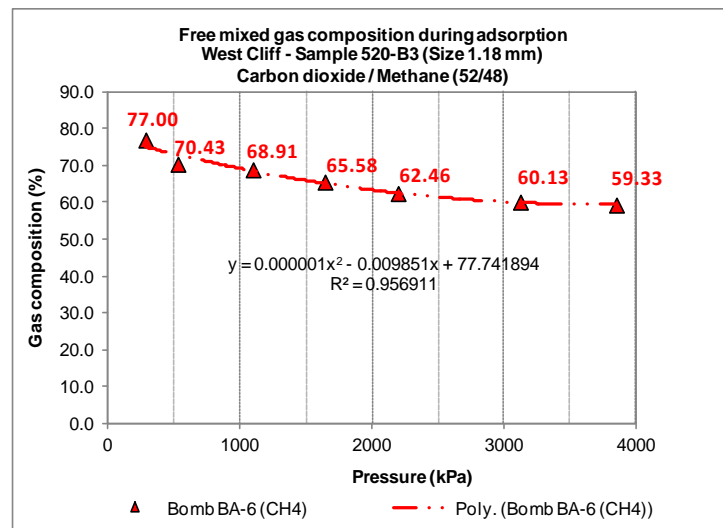


Figure IV-6 – CO₂ and CH₄ gas composition in mixed gas adsorption

This suggests that the CH₄ recovering at the expense of CO₂ may be slightly higher (CO₂/CH₄ ratio of 1.15) at much higher pressure levels (at about 4 950 kPa), as it is suggested by the trend of CH₄ free gas composition.

Coal particle size

Figure IV-7 shows the composition of free CH₄ over pressure in various particles ranging from 0.30 to 8.00 mm. The graph shows that for particles > 1.00 mm the composition of free CH₄ was marginally higher in the B6-5 sample (4.75 mm size particle). This suggests that in particles > 1.00 mm (fragmented coal) the composition

CHAPTER FOUR

Mixed gas adsorption

of free CH₄ appeared to be independent of particle sizes because overall, the lowest composition of free CH₄ was in the 0.30 mm particle.

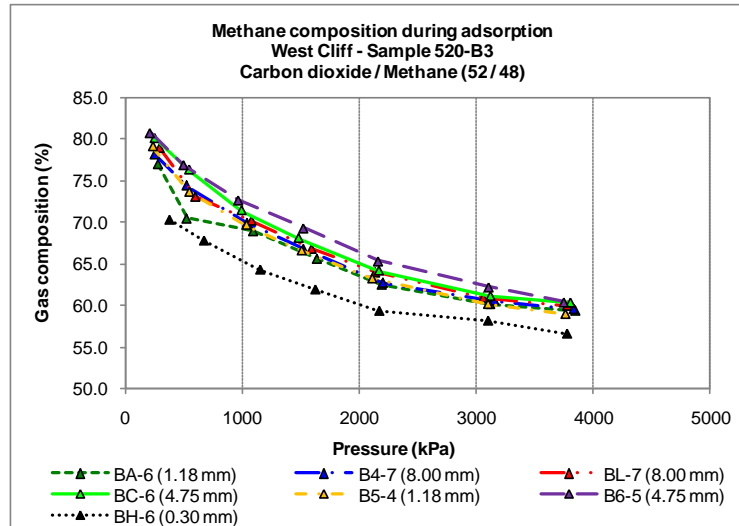


Figure IV-7 – Effect of particle sizes in CH₄ gas composition

This behaviour of CO₂ can be attributed to fact that smaller particles adsorb more CO₂ due to its larger surface area and greater affinity to coal. However, experimental error and sampling issues also could be the reason for this behaviour. It could not be found great differences in moisture and ash content among the samples. In average, the moisture and ash content in the samples showed in the graph were about 1.2% (ranged from 1.1 to 1.3%) and 8.2% (ranged from 8.1 to 8.3%) respectively. Relative density ranged from 1.41 to 1.43.

Bath water temperature

Figure IV-8 also shows the profile of CH₄ profile over pressure at 21 and 24 °C bath water temperatures. Although most samples were tested at 24 °C, the gas composition test was carried out also in two similar 6.70 mm samples tested at 21 °C in order to establish whether or not the CO₂/CH₄ composition was influenced by changes in bath water temperature. From these tests the highest composition of free CH₄ was attained with samples tested at 21 °C where free CH₄ depended on the bath water temperature

CHAPTER FOUR

Mixed gas adsorption

such that, the lower the bath water temperature the higher the composition of free CH_4 and consequently, the higher the adsorbed CO_2 . It appears that the lower the temperature the easier the CO_2 adsorption in CO_2/CH_4 mixed gas adsorption, which agreed with the findings with single CO_2 .

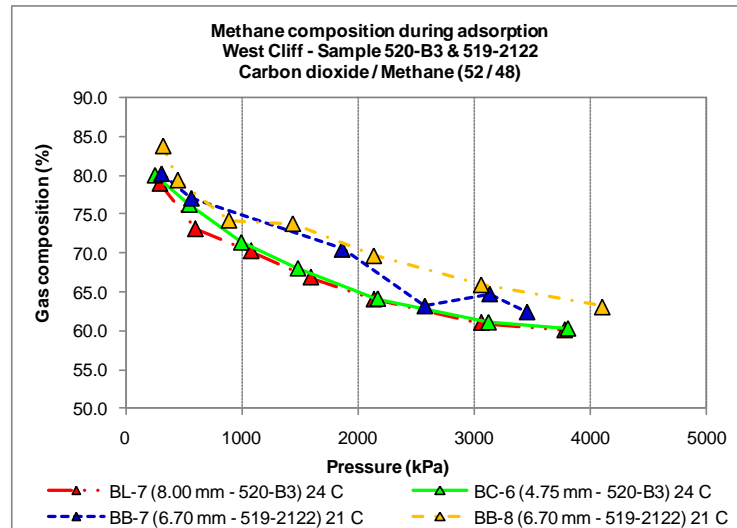


Figure IV-8 – Effect of temperature in CH_4 gas composition

IV.2.3.3. MIXED GAS ADSORBED MASS

CO_2/CH_4 adsorbed mass

Figure IV-9 shows the mixed gas isotherm on as received basis from experimental data in the 1.18 mm particle during adsorption. The CO_2 component attained higher adsorbed mass (almost three times) compared to the CH_4 component, at each level of pressure. Similar results were obtained during CO_2 and CH_4 gas adsorption as it was previously discussed in chapter 3. Coal adsorbed preferentially CO_2 than CH_4 . It is seen the same CO_2 affinity to coal observed when it was tested individually. The extended Langmuir equation was used to model the adsorbed mass of CO_2/CH_4 mixed gas from the experimental data. The graph shows it tallied very well with the adsorbed mass of binary mixed gas (acting as a whole) from the experimental data. Similar results were achieved using the extended Langmuir equation to model the CO_2 and CH_4

CHAPTER FOUR

Mixed gas adsorption

components. The results indicate that the extended Langmuir equation modelled very well the experimental data from adsorbed mass of CO₂/CH₄ mixed gas.

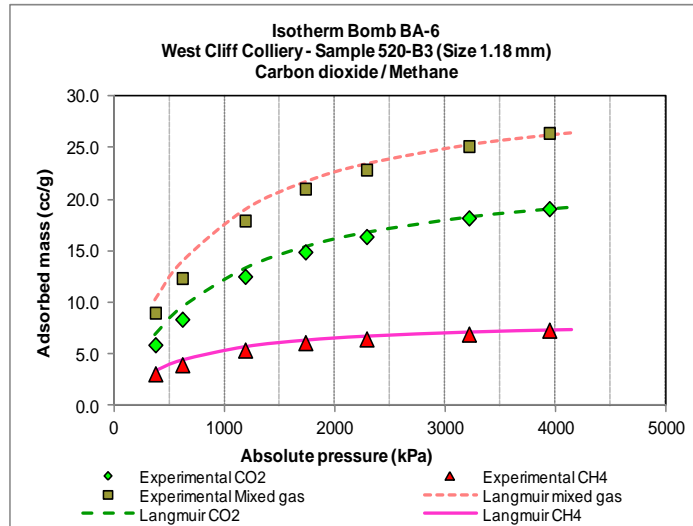


Figure IV-9 – CO₂ and CH₄ adsorbed mass during mixed gas adsorption

Figure IV-10 shows the trend of mixed gas adsorption over time in the entire range of pressure. The result indicates that the CO₂ and CH₄ components followed a polynomial trend, similar to the extended Langmuir equation trend.

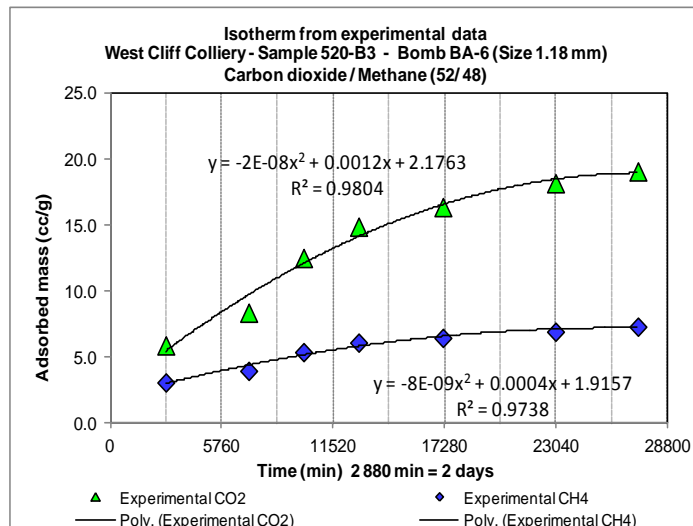


Figure IV-10 – CO₂ and CH₄ adsorbed mass trend line in adsorption

From the trend line it can be inferred that the CO₂ component adsorption rate over time was about three times greater than the CH₄ component adsorption rate (obtained from the coefficient of the 1st degree term, the 2nd degree term can be neglected).

CHAPTER FOUR

Mixed gas adsorption

This result agreed with the result obtained from the extended Langmuir equation.

Coal particle size

Figure IV-11 shows the CO₂/CH₄ mixed gas acting as a whole from the experimental data in particle sizes ranging from 0.30 to 8.00 mm, over pressure.

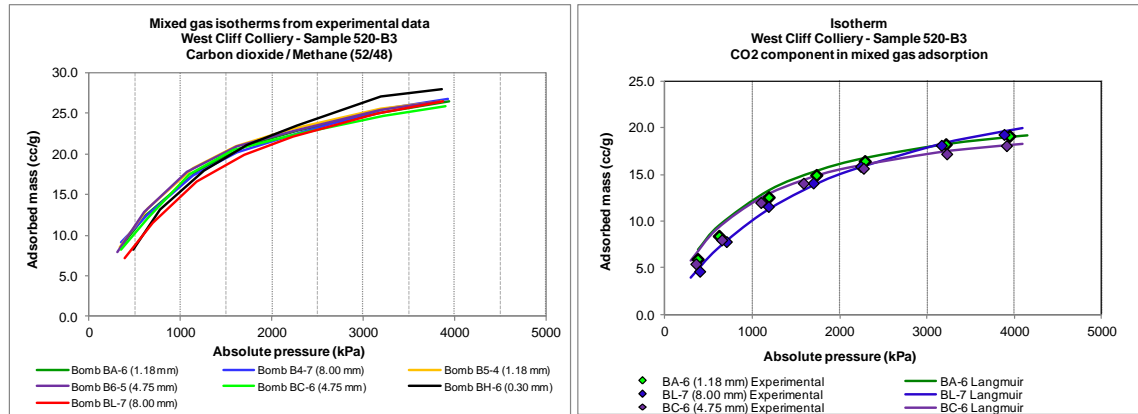


Figure IV-11 – Mixed gas adsorbed mass during adsorption

The graph shows that the CO₂/CH₄ mixed gas adsorbed mass was almost identical for all the samples. The results indicate that within experimental error, the mixed gas adsorption was independent of particle size over the entire range of pressure. Also, the graph shows that the CO₂ component adsorbed mass was very similar in the three particles sizes as shown in the graph. It appeared that in mixed gas adsorption, the CO₂ component adsorbed mass was independent of particle size. Similar result was obtained with CO₂ adsorption acting independently as it was discussed in chapter 3.

Table IV-3 summarises the changes in adsorbed mass and composition of gas in various particle sizes. The result shows that the total mixed gas adsorbed mass was in average 45% of the applied mixed gas mass. The changes in free CO₂ gas composition in the pressure range of 200-4000 kPa were in average 80%. This drop in the free CO₂ gas composition mainly can be attributed to the CH₄ recovery. The CH₄ recovery at expense

CHAPTER FOUR

Mixed gas adsorption

of the CO₂ suggests that CO₂ and CH₄ molecules competes each other for the same spot on the coal surface.

Table IV-3 – Mixed gas adsorbed mass and composition in adsorption

Bomb	Particle size (mm)	Sorption duration (min)	Applied mixed gas mass (gm)	Adsorbed mixed gas mass		Free gas composition					
				mass (gm)	percentage (%)	Carbon dioxide			Methane		
						Initial (200 kPa) (%)	Final (4 000 kPa) (%)	Change (%)	Initial (200 kPa) (%)	Final (4 000 kPa) (%)	Change (%)
BC-6	4.75	25,913	16.922	7.855	46.4%	19.91	39.75	99.6%	80.09	60.25	24.8%
BA-6	1.18	27,282	16.915	7.221	42.7%	23.00	40.67	76.9%	77.00	59.33	23.0%
BL-7	8.00	27,404	16.704	7.299	43.7%	21.06	40.00	89.9%	78.94	60.00	24.0%
B6-5	4.75	25,885	19.000	9.404	49.5%	19.31	39.59	105.0%	80.69	60.41	25.1%
B5-4	1.18	27,296	19.015	8.794	46.2%	20.94	41.10	96.3%	79.06	58.90	25.5%
B4-7	8.00	27,275	19.095	8.571	44.9%	21.94	40.47	84.4%	78.06	59.53	23.7%
BH-6	0.30	27,267	17.529	6.674	38.1%	29.64	43.45	46.6%	70.36	56.55	19.6%

Interestingly, the 0.30 mm sample shows smaller adsorbed mass and free gas composition changes. The smaller CH₄ gas recovery was achieved in the smaller particle size. The higher CO₂ adsorbed mass can be attributed to milling/crushing factor where the sample could be enriched in vitrinite and lowered in ash content.

CO₂ and CH₄ acting independently versus CO₂/CH₄ mixed gas

Figure IV-12 shows the CH₄ and CO₂ adsorbed mass acting independently and as a binary 52/48 CO₂/CH₄ mixed gas.

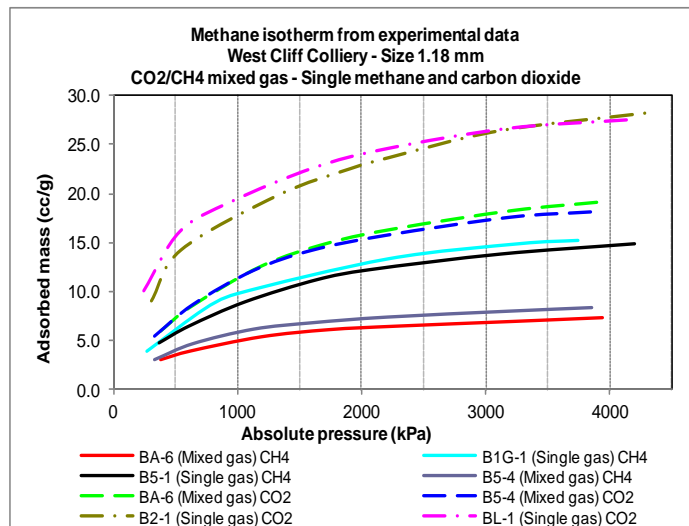


Figure IV-12 – Single CO₂ and CH₄ versus CO₂/CH₄ mixed gas adsorbed mass

CHAPTER FOUR

Mixed gas adsorption

By comparing the adsorbed mass of the single CO_2 adsorbed mass against the CO_2 component adsorbed mass of the CO_2/CH_4 mixed gas, it can be found that the single CO_2 (acting independently) was adsorbed almost two times greater than the CO_2 component of the mixed gas. Similar result was found by comparing the single CH_4 adsorbed mass to the CH_4 component of the 52/48 CO_2/CH_4 mixed gas adsorbed mass. The adsorbed mass ratio between single CO_2 against single CH_4 of about 2.0 was kept constant and equal to the ratio of the adsorbed mass of the CO_2 component against the CH_4 component of the CO_2/CH_4 mixed gas. This could be attributed to the almost identical gas composition of the gas mixture (52%/48%). Different gas composition could lead to different adsorbed mass ratio.

Bath water temperature

Figure IV-13 shows the profile of mixed gas at 21 °C (bath water temperature) and the designed test temperature of 24 °C.

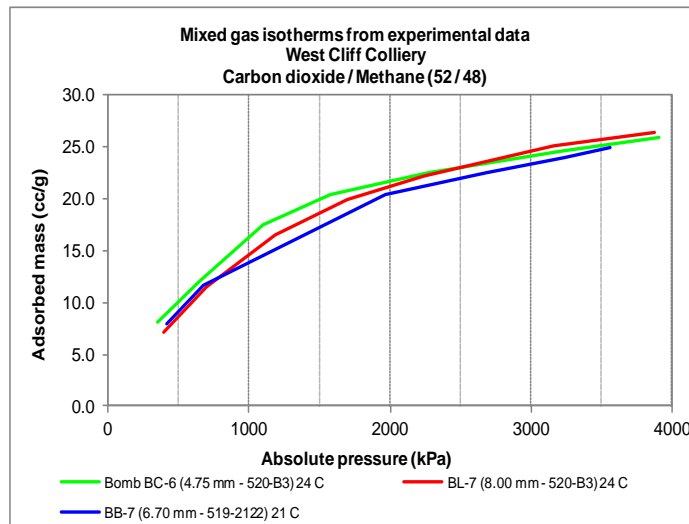


Figure IV-13 – Effect of temperature on the mixed gas adsorbed mass

Unexpectedly, the graph shows the adsorbed mass of the mixed gas at 21 °C was marginally lower than at 24 °C. This difference could have been caused by either experimental error or poor bath water temperature control or measurements

CHAPTER FOUR

Mixed gas adsorption

uncertainties which are expected to be important in mixed gas adsorption measurements.

IV.2.4. TERNARY MIXED GAS

A gas adsorption test was carried out in fragmented samples of coal ranging from 0.71 mm to 54.00 mm diameter. The gases were a ternary mixture of N_2 , CO_2 , and CH_4 in a ratio of 31.8/33.4/34.8 at bath water temperature of 24 °C.

IV.2.4.1. MIXED GAS SATURATION TIME

Pressure level

Figure IV-14 shows the drop in pressure against time in the 54.00 mm diameter sample at reference pressure levels of around 500 and 3 000 kPa. At 500 kPa the sample attained an adequate saturation of gas (gas pressure fluctuations < 5% over the period) at approximately 2 880 min (two days). At 3 000 kPa however, the sample required an extra 1 440 min (one day) of saturation for attain the required degree of saturation. Poor bath water temperature control could be the reason of this delay.

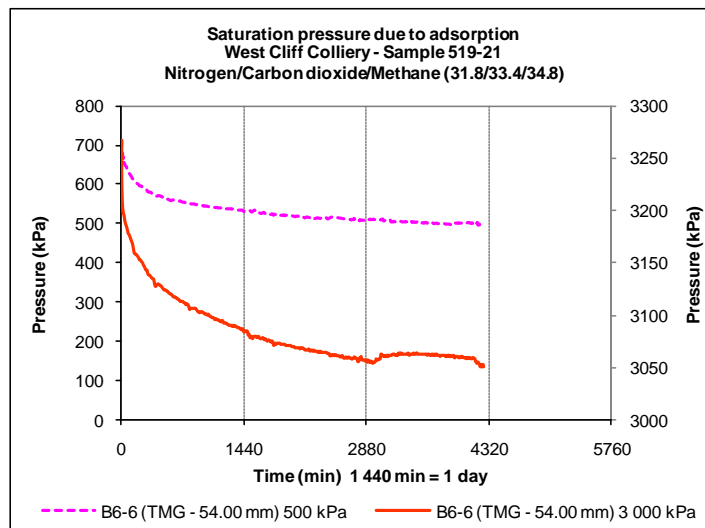


Figure IV-14 – Effect of pressure levels in mixed gas saturation time

From this result, saturation time appeared to be independent of the level of pressure. The minimum time required to attain an acceptable degree of pressure equilibration

CHAPTER FOUR

Mixed gas adsorption

appeared to be 4 320 min (three days). Similar minimum saturation time was reported with CH₄ acting independently suggesting that the CH₄ component of the mixture could drive the duration of the equilibrium pressure.

The CO₂ component seemed to achieve equilibrium pressure faster than the other components. The ternary mixed gas took 1 440 m longer to achieve equilibrium pressure than the binary mixture of gases. Also, it is expected longer saturation time with the ternary mixture of gases due to compositional equilibrium.

Coal particle size

Figure IV-15 shows the drop in pressure over time at reference pressures of 500 kPa in various size particles during adsorption of ternary mixed gas.

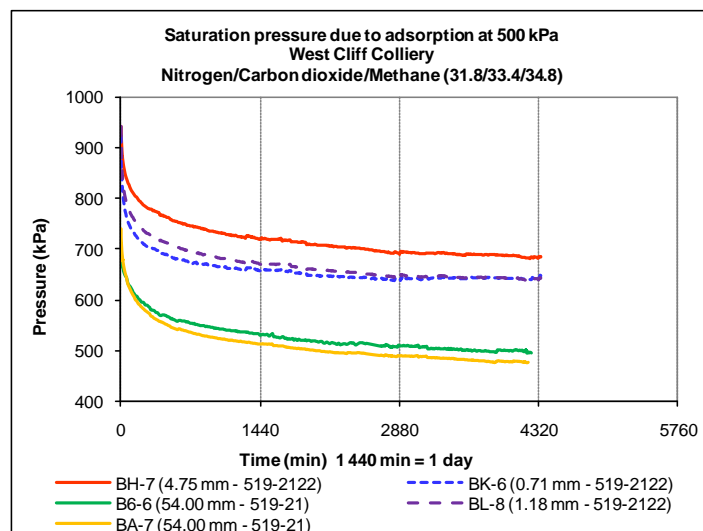


Figure IV-15 – Effect of particle size on gas saturation time

The graph shows that the profiles of pressure drop over time were similar to each other, which indicates that the samples attained a similar degree of saturation over the same period of time. It appeared that 4 320 min was enough to attain the degree of saturation required. This indicates that at 500 kPa reference pressure levels, saturation time was independent of particle sizes.

CHAPTER FOUR

Mixed gas adsorption

Similar behaviour could be expected at any pressure level. Similar results were found in the CO₂ and CH₄ acting independently as well as with the binary mixture of both gases. It appeared that pressure level did not play any decider role in the duration of the gas saturation. It could not be found in the literature any detailed study of the effect of the pressure level in the saturation time.

Bath water temperature

Figure IV-16 shows the changes in temperature over time. The graph shows that room temperatures RT 1 and RT 2 fluctuated between 22 and 26 °C over the period, while the bath water temperature established at 24 °C for the period remained unchanged according to the five bath water temperature reading done in four days.

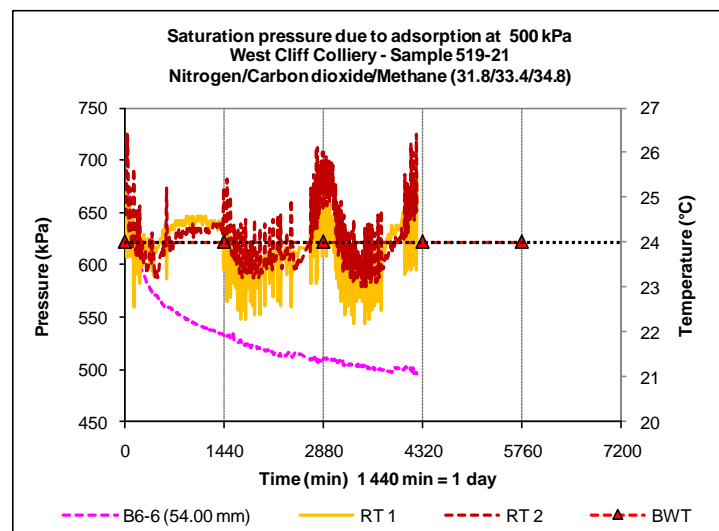


Figure IV-16 – Effect of temperature on gas saturation time

This means the bath water temperature and the pressure profiles of the ternary mixed gas were not affected by the changes in the room temperatures RT 1 and RT 2. The saturation time at 500 kPa during the ternary mixed adsorption appeared to be independent of changes in the room temperatures RT 1 and RT 2 for small fluctuations in temperature (2-3 degrees).

CHAPTER FOUR

Mixed gas adsorption

IV.2.4.2. MIXED GAS COMPOSITION

Pressure level

Figure IV-17 shows the composition of free N_2 , CO_2 , and CH_4 from the ternary mixed gas in the 0.71 mm size particle.

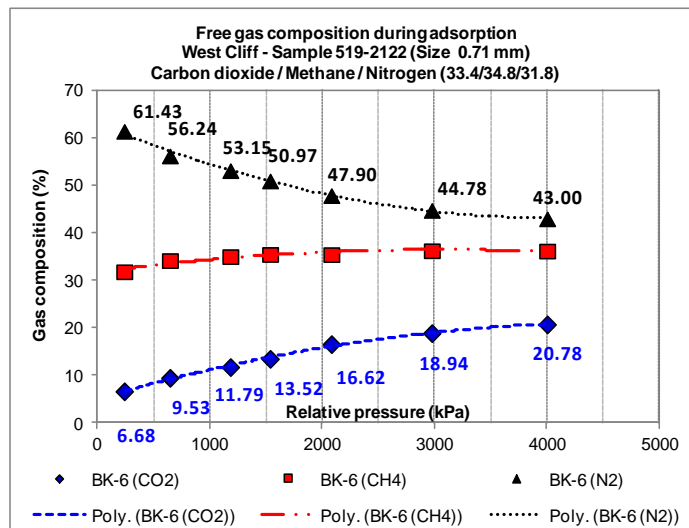


Figure IV-17 – N_2 , CO_2 and CH_4 gas composition during adsorption

The composition of free N_2 was the highest over the entire range of pressures, while the composition of free CO_2 was the lowest. As expected, the lower adsorbed gas in coal was N_2 while the higher was CO_2 . The CH_4 was in between of them and higher than N_2 . The affinity of CO_2 , CH_4 and N_2 to the coal acting independently was maintained with the mixture of them at component level. The changes in the gas composition over pressure were higher in CO_2 (about 210%) than N_2 gas (43%), and changes in free CH_4 (about 14%) over pressure were in between them. This suggests that the recovery of N_2 appeared to be mostly at the expense of CO_2 as the composition of CH_4 changed only marginally. This behaviour suggests that the CH_4 adsorption rate was almost constant over the pressure range. It appeared that CO_2 and CH_4 molecules did not compete over the same adsorption site. The composition of CH_4 however, compared to the CO_2/CH_4 binary mixed gas was strongly affected by the inclusion of N_2 in the

CHAPTER FOUR

Mixed gas adsorption

mixture, especially at low pressures, where the ratio of CH_4/CO_2 (4.8) increased by 100% compared to their binary mixture (2.4). At high pressure however, the ratio of CH_4/CO_2 increased about 30% (from 1.3 to 1.7) due to the composition of ternary mixed gas. The result suggests that the gas composition of the ternary mixture of CO_2 , CH_4 and N_2 depend (at least indirectly) on the pressure level. The gas diffusion into pores and matrix is a slow process. In the case of the CO_2 , it is retained longer on the coal surface and its progress is retarded into the fine pores due to its larger adsorption coefficient.

Coal particle size

Figure IV-18 compares the composition of N_2 , CO_2 , and CH_4 over pressure with respect to particle sizes, and indicates that within the experimental error the gas composition appeared to be independent of the particle size.

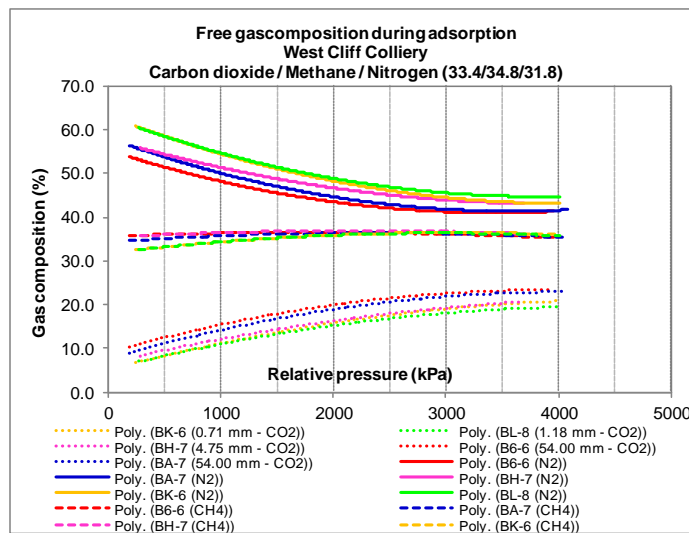


Figure IV-18 – Effect of particle sizes in ternary mixed gas composition

The CO_2 seemed to be adsorbed quicker than CH_4 and N_2 and it did not depend on the particle size. It smaller size allowed to the molecules access to the fines pores and adsorption sites. However, it seems that the CH_4 diffuses readily and deeper than CO_2

CHAPTER FOUR

Mixed gas adsorption

and N₂ due to its lighter molecular weight (diffusion rate is inversely proportional to the molecular weight).

IV.2.4.3. MIXED GAS ADSORBED MASS

Ternary mixed gas adsorbed mass

Figure IV-19 shows the profiles of ternary mixed gas in the 54.00 mm diameter sample of core coal during adsorption, at each 500 kPa step and up to 4 000 kPa. It was tested at a temperature of 24 °C.

The graph shows the profiles of N₂, CO₂, and CH₄ components from the experimental data where as expected, the highest adsorbed mass was the CO₂ component and the lowest was N₂. CH₄ was in between them and close to the 50% of a combined CO₂ and N₂.

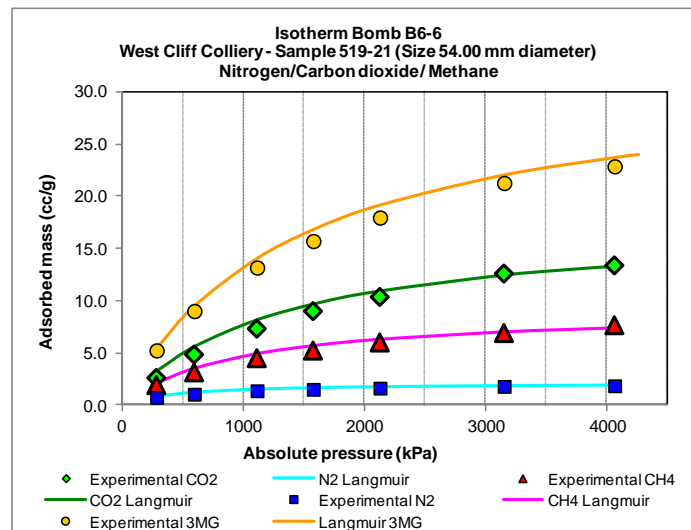


Figure IV-19 – Ternary mixed gas adsorbed mass during adsorption

The extended Langmuir equation was used to model the adsorbed mass of the ternary mixed gas components with good results, within experimental error. The graph shows that the extended Langmuir equation tallied well with the ternary mixed gas components from the experimental. This suggests that the extended Langmuir equation within experimental error can be used with relative success to model the

CHAPTER FOUR

Mixed gas adsorption

ternary mixed adsorption. However, Crosdale (1998) reported unsuccessful result in using the extended Langmuir model during binary mixed gas adsorption and his study suggested to use more complex model and additional research in the area of modelling mixed gases.

Similar results were reported by Clarkson and Bustin (2000) in their study on binary mixed gas adsorption. By comparing the ternary mixture components to the single CO₂, CH₄ and N₂, it was found that the CO₂ component adsorbed mass of the ternary mixture was about 45% of the single CO₂ adsorbed mass (B3-1 sample - 54.00 mm). However, the CH₄ component adsorbed mass was about 60% of the single CH₄ adsorbed mass (BD-2 sample – 54.00 mm). The N₂ component was about 20% of the single N₂ adsorbed mass (BC-7 sample – 54.00 mm). Now, comparing the CO₂ and CH₄ components from ternary mixture components to the CO₂ and CH₄ components from the binary mixture, it was found that CO₂ component adsorbed mass from the ternary mixture decreased in about 30% when comparing to the CO₂ component adsorbed mass from the binary mixture while the CH₄ component adsorbed mass remained almost the same. It appears that the N₂ component from the ternary mixture displaces more CO₂ molecules than CH₄ during the ternary mixed gas adsorption.

The total adsorbed mass from the ternary mixed gas was about 85% of the total adsorbed mass from the binary mixture of gases. The CO₂/CH₄ adsorbed mass ratio of the ternary mixture was about 1.8 comparing to the 2.4 from the binary mixture. The same 2.4 ratio was reported from the single gases acting independently. Also, the results suggest that the CO₂/CH₄ adsorbed mass ratio depend on the gas composition ratio.

CHAPTER FOUR

Mixed gas adsorption

The higher the CO_2/CH_4 composition ratio the higher the CO_2/CH_4 adsorbed mass ratio.

Coal particle size

Figure IV-20 shows the profile of ternary mixed gas of several particles ranging from 0.71 mm up to 54.00 mm. The total adsorbed mass among the samples of various sizes were very similar. Thus, the results suggest that within experimental errors the total adsorbed mass during the ternary mixed gas adsorption was independent of the particle size. This result agrees with the finding in CO_2/CH_4 binary mixed adsorption and CO_2 and CH_4 single gas.

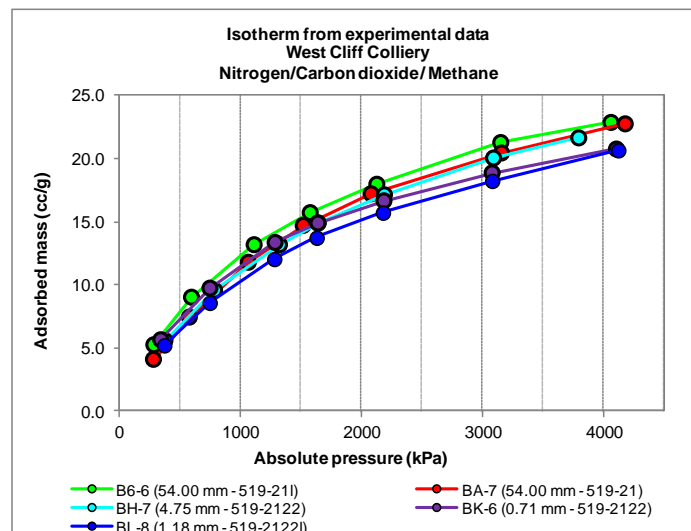


Figure IV-20 – Effect of particle sizes in ternary mixed gas adsorbed mass

Figure IV-21 analyses the adsorbed mass of the CO_2 and CH_4 component with respect to particle sizes during adsorption of ternary mixed gas. The graph shows that within experimental error the CO_2 and CH_4 components adsorbed mass were independent of the particle sizes. Similar results were obtained with the CO_2 and CH_4 components of the binary mixture of gases and the single CO_2 and CH_4 gases. The CO_2 and CH_4 components adsorbed mass were more related to their gas composition rather than their particle sizes.

CHAPTER FOUR

Mixed gas adsorption

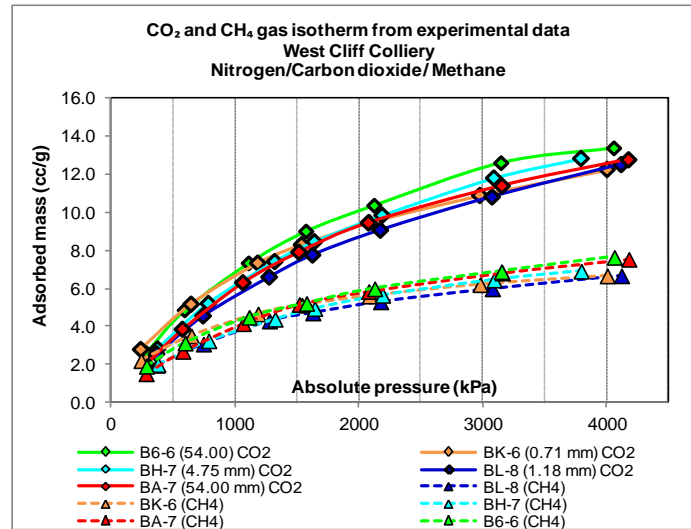


Figure IV-21 – Effect of particle sizes in CO₂ and CH₄ gas adsorbed mass

Gas mixture and single gas

Figure IV-22 compares the profiles of the single CO₂ with the same components from their binary and ternary mixture in similar particle sizes (4.75 mm).

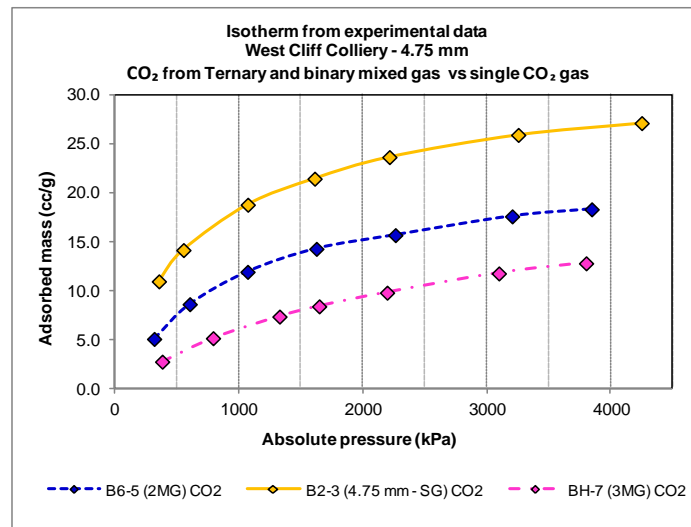


Figure IV-22 – Effect of gas mixture in CO₂ and CH₄ gas adsorbed mass

The graph shows that the CO₂ component adsorbed mass (about 18.3 cc/g) from the binary mixture was 69% of the single CO₂ at 4 000 kPa pressure level. The composition of CO₂ in the binary mixture was about 52%. However, the CO₂ component adsorbed mass from the ternary gas mixture (about 12.8 cc/g) was about 49% of the maximum single CO₂ adsorbed mass. The ratio of CO₂ in the ternary mixture was about 33.4%.

CHAPTER FOUR

Mixed gas adsorption

The result suggests that the drop in the CO₂ adsorbed mass appeared to be caused by the drop in its composition due to the binary gas mixture. The mixture was diluted in about 20% (from 52% to 33.4%) and the CO₂ component adsorbed mass dropped also 20% (from 69% to 49%). This indicates that the drop in CO₂ adsorbed mass due to its dilution in the gas mixture appeared to be proportional to its drop in composition. Similarly, the CH₄ adsorbed mass decreased in about 10% due to the same amount of dilution on the mixture. However, the N₂ component adsorbed mass decreased in about 1.1 times per each one percentage of N₂ dilution (77% of adsorbed mass drop for 68% of gas dilution).

IV.2.5. SUMMARY

BINARY MIXED GAS

- Gas saturation time was independent of the pressure level.
- 4 320 min (three days) was the minimum required to attain an adequate degree of saturation time independently of the pressure level, particle size, gas composition, and temperature.
- The adsorbed mass of CO₂ component was higher at each pressure level compared to the adsorbed mass of CH₄ component. The adsorbed mass of mixed gas was independent of particle size over the entire range of pressure. The adsorbed mass of single CH₄ and single CO₂ was higher than the CH₄ and CO₂ components from the binary mixed gas. The Langmuir equation tallied well with the adsorbed mass of binary mixed from the experimental data.

TERNARY MIXED GAS

- Saturation time was independent of particle sizes. 4 320 min (three days) was the minimum gas saturation time needed to attain an acceptable degree of

CHAPTER FOUR

Mixed gas adsorption

saturation independently of the pressure level, particle size, gas composition, and temperature.

- There was more N_2 in the composition of free gas over the whole pressure range while free CO_2 was the lowest. The recovery of N_2 was mostly at expense of the CO_2 . The composition of free N_2 , CH_4 and CO_2 was independent of particle size.
- The adsorbed mass of ternary mixed gas in coal was independent of particle sizes.
- The drop in single N_2 , CO_2 and CH_4 due to its dilution in the gas mixture (ternary or binary) was related to its composition.
- The Langmuir equation tallied well with the ternary mixed gas from the experimental data.

V. CHAPTER FIVE

SINGLE GAS DESORPTION

V.1. INTRODUCTION

After adsorption tests with N₂, CO₂ and CH₄ were completed, desorption tests on several samples of fragmented particles of coal were conducted as part of an integral study into these processes. The behaviour of gas in these samples was studied during desorption and changes in the adsorbed mass were established to compare and analyse with the volumes of gas obtained during adsorption. Particular attention was given to the hysteresis phenomenon, which in this study refers to the excess of adsorbed gas during desorption combined with adsorption. The effect of particle size, temperature, and type of gas in the adsorbed mass was studied over time. Finally, residual CO₂ and CH₄ in coal was measured at the end of the desorption test.

V.2. EXPERIMENTAL PROCEDURE

V.2.1 APPARATUS

The equipment used was the same as for other adsorption tests as described in Chapter 3, Section 2.1. The coal samples for desorption were prepared as described in Chapter 3, Section 2.2.

Table V-1 shows the particle size of the samples during desorption, with regard to particle size and type of gas. Type of gas is referred only for single gases.

Table V-1 – Coal samples tested during desorption

Gas type	Coal size (mm)							Total test
	54.00	15.00	8.00	6.70	4.75	1.18	0.30	
N ₂	1	NA	NA	NA	1	NA	NA	2
CO ₂	1	2	2	1	NA	2	1	9
CH ₄	2	2	1	NA	NA	1	NA	6
Total								17

CHAPTER FIVE

Single gas desorption

V.2.2 TESTING PROCEDURE

The adsorbed mass in coal during desorption was determined gravimetrically, as with adsorption. Pressure in the bombs was lowered from about 4 200 kPa to almost atmospheric pressure in steps of 3 500, 2 500, 1 500, 500 and 200 kPa, and the desorption capacity was subsequently determined at these levels. Residual gas in coal was measured in two samples, with CO₂ in one and CH₄ in the other and their drops in weight were measured daily, immediately after the bombs were vacuumed for 60 s.

V.3. EXPERIMENTAL RESULTS

Gas saturation time during desorption was analysed and validated against the minimum saturation time reported in adsorption in Chapter 3, sections 3.1.1, 3.2.1 and 3.3.1, with regard to pressure level, particle size, type of gas, and temperature. Adsorption capacity was analysed with respect to particle size, temperature (only for CO₂ and CH₄) and type of gas. The adsorbed mass in coal was calculated according to the procedure described in Chapter 3.

V.3.1. NITROGEN

Three samples of coal were tested in desorption with N₂ at temperature of 24 °C.

V.3.1.1. GAS SATURATION TIME

Pressure level

Figure V-1 shows the rises in pressure due to N₂ desorption over time, at about 500 and 2 000 kPa, respectively. The aim of this comparison was to determine whether the level of pressure influenced the duration to achieve equilibrium or not. The sample was saturated for the same period at both pressures. At 500 kPa the changes in pressure (due to desorption of N₂) were almost negligible at about 1 440 min mark, which indicates that the sample was already saturated, with fluctuations in pressure of less

CHAPTER FIVE

Single gas desorption

than 5% over time. Also, the graph shows that the sample released in few minutes a considerable volume of adsorbed gas increasing the pressure near to the final equilibrium pressure, at over 500 kPa.

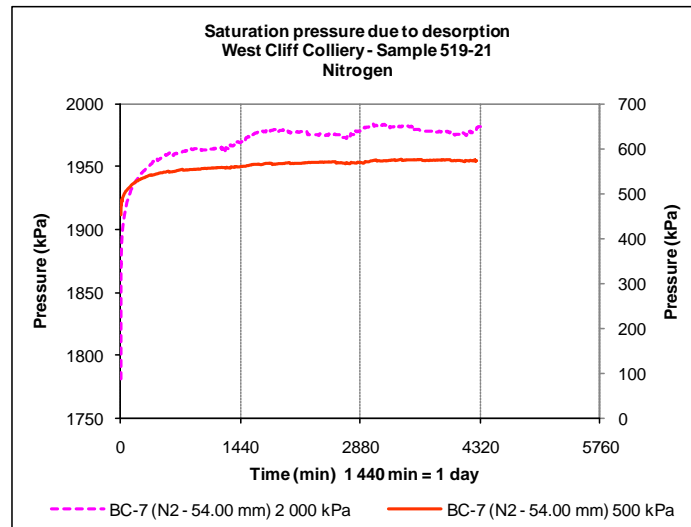


Figure V-1 – Effect of pressure levels in N₂ saturation time

At 2 000 kPa there were some minor fluctuations in pressure over the same period of time, although the level of pressure equilibrium was enough to consider that the sample was saturated to acceptable levels. The fluctuations in pressure seemed to be enhanced by a slow gas diffusion process. In this process, the sample re adsorbed and desorbed gas until it reached a new equilibrium stage. Comparatively, the sample appeared to achieve faster N₂ equilibrium pressure at 500 kPa than at 2 000 kPa over the same period. This suggests that N₂ saturation time during desorption appeared to be dependent on the level of pressure; the lower the pressure the faster to get equilibrium pressure.

Particle size

Figure V-2 shows the influence of particles size in N₂ saturation time. At 500 kPa, samples BC-7 and B1G-12 appeared to achieve equilibrium pressure in about 4 320 min (three days) despite their sizes varying from 54.00 mm diameter to 0.71 mm,

CHAPTER FIVE

Single gas desorption

respectively. The samples released in about 1 440 min sufficient gas to build up the pressure from 460 kPa near to its equilibrium. Then, the pressure fluctuated until achieving equilibrium due to gas re adsorption and desorption as a consequence of a slower desorption rate mainly driven by gas diffusion from the pores.

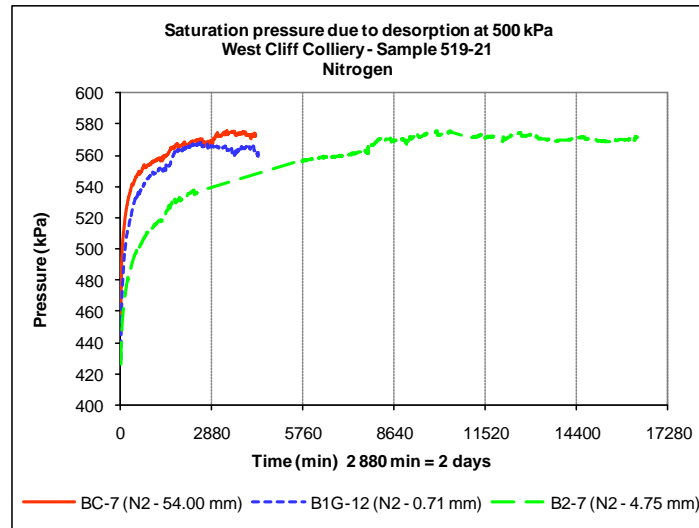


Figure V-2 – Effect of particle sizes in N₂ saturation time

The sample B2-7 was kept running for about 11 520 min mark (eight days) when it achieved fully equilibrium pressure despite that at 4 320 min the sample achieved similar equilibrium pressure that samples BC-7 and B1G-12. The results suggest that the saturation time (time to reach saturation) for similar saturation level appeared to be independent of particle size. Appendix 7 shows the drop in pressure of sample B2-7 (4.75 mm) during desorption, at each 500 kPa step down to almost atmospheric pressure.

V.3.1.2. ADSORBED MASS

Experimental adsorbed mass

Figure V-3 shows the adsorbed mass of N₂ over pressure, from experimental data during adsorption and desorption. The adsorbed mass of N₂ in coal during desorption was marginally higher at each pressure level than its corresponding adsorbed mass

CHAPTER FIVE

Single gas desorption

during adsorption. The excess of N_2 in the 4.75 mm size was about 2%. This excess of gas is commonly called hysteresis, which is probably was due to longer saturation time (adsorption plus desorption). However, this small excess of N_2 in desorption could be attributed to the experimental error.

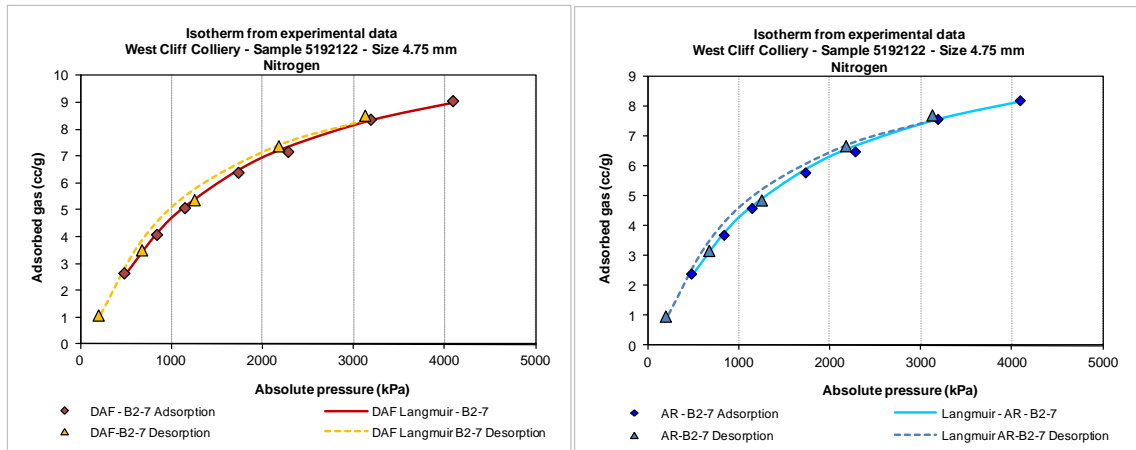


Figure V-3 – Excess in N_2 adsorbed mass in desorption

Figure V-4 shows the Langmuir equation compared with the experimental data of N_2 measured during desorption (as received and DAF basis).

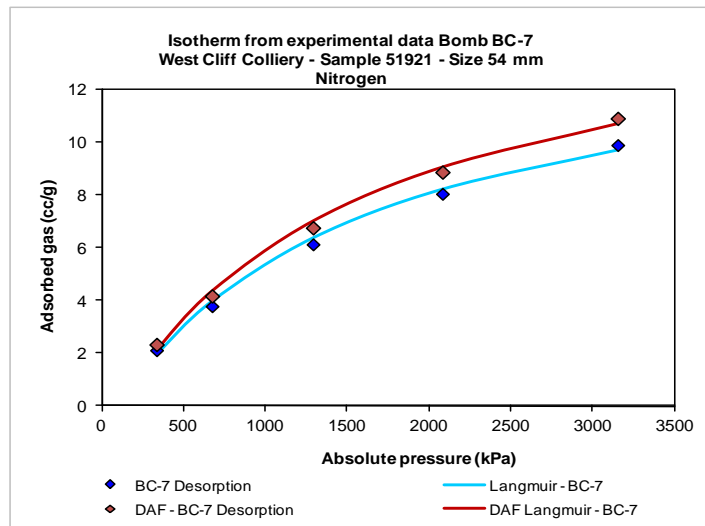


Figure V-4 – Langmuir isotherm from N_2 experimental data

The graph shows that within experimental error the Langmuir equation tally well with the N_2 experimental data. Thus, Langmuir equation accurately can be used in modelling the experimental data from N_2 desorption.

CHAPTER FIVE

Single gas desorption

Appendix 8 shows the adsorption capacity of N_2 (experimental and Langmuir isotherms) of several samples tested in desorption.

Coal particle size

Figure V-5 shows the adsorbed mass of N_2 against pressure in two particle sizes during desorption. The N_2 adsorption capacity was marginally higher in 54.00 mm diameter coal than 4.75 mm fragmented coal which suggests that during desorption, the adsorbed mass of N_2 appeared to depend on particle size. At high pressure, the adsorbed mass on the 54.00 mm sample was 25% higher than on the 4.75 mm. However, at low pressure this difference was almost negligible. It seems that at high pressure the difference in N_2 adsorption capacity can be attributed to the larger coal matrix of the 54.00 mm sample. Thus, larger coal matrix meant higher N_2 adsorption capacity in coal. The results suggest that the larger surface area on the 4.75 mm was not beneficial in the adsorbed mass process likely due to the lack of N_2 affinity to the coal.

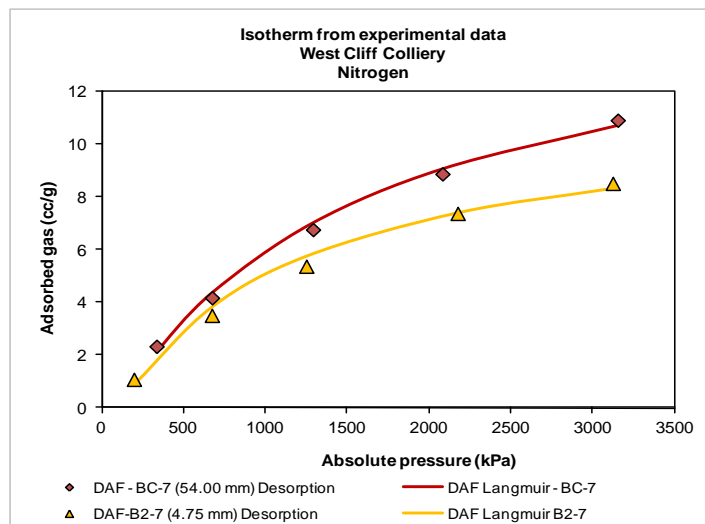


Figure V-5 – Effect of particle sizes in N_2 adsorbed mass in desorption

Table V-2 compares the adsorbed mass of N_2 in adsorption and desorption at several levels of pressure. Sample B2-7 showed that there was little difference in N_2 adsorbed

CHAPTER FIVE

Single gas desorption

mass at each step during adsorption and desorption. At 2 176 kPa in desorption, the N₂ adsorption capacity was almost 2.8% higher than the adsorption capacity during adsorption, even at a higher pressure (2 279 kPa). The adsorbed mass of N₂ in desorption, at any pressure level, was marginally higher than in adsorption. It seems that the saturation time (in adsorption plus desorption) could affect the N₂ adsorption capacity; the larger the saturation time the higher the N₂ sorption capacity.

Table V-2 – N₂ adsorption capacity in adsorption/desorption

Sample B2-7 (4.75 mm) - Nitrogen												
Pressure (kPa) Adsorbed mass (cc/g)	Adsorption							Desorption				
	479	837	1145	1733	2279	3186	4089	3124	2176	1250	673	196
	2.7	4.1	5.1	6.4	7.2	8.4	9.1	8.5	7.4	5.4	3.5	1.1

Comparatively, in N₂ adsorption was not clear the dependency of the particle size in the N₂ adsorption capacity but in desorption, the adsorbed mass of N₂ clearly depended on the particle size.

V.3.2. CARBON DIOXIDE

CO₂ desorption test was carried out in coal samples after adsorption test was concluded, at temperatures of 21 and 24 °C.

V.3.2.1. GAS SATURATION TIME

Pressure level

Figure V-6 shows the effect of pressure level in CO₂ saturation time during desorption. The pressure levels were analysed at 500 kPa (low pressure) and 2 500 kPa (high pressure). The pressure in the bomb was dropped from almost 1 500 kPa down to 400 kPa to achieve the desired equilibrium pressure of about 500 kPa. However, equilibrium was reached at about 800 kPa, in 8 640 min (six days). At that period mark the pressure of CO₂ appeared to increase over time due to continuing desorption. However, the fluctuations of CO₂ over time were minimal of about ±12 kPa in 1 440

CHAPTER FIVE

Single gas desorption

min (one day) which suggests that at low pressure in desorption, 2 880 min (two days) of saturation time appeared to be sufficient to achieve equilibrium pressure of CO₂ (fluctuations in pressure less than 5%). Alternatively, at higher pressure (2 500 kPa), the fluctuations of CO₂ over time were significantly higher (about ± 60 kPa), than at low pressure. The graph clearly shows that over time, CO₂ repeatedly passed through desorption followed by re-adsorption, which suggests that at high pressure the CO₂ took much longer to achieve adequate equilibrium pressure than at low pressure.

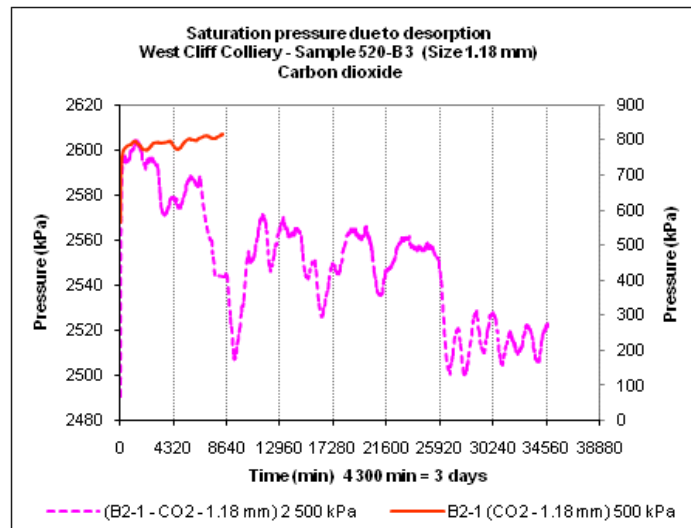


Figure V-6 – Effect of pressure levels on CO₂ gas saturation time

At high pressure (2 500 kPa), sample B2-1 was run for about 34 560 min (24 days) without achieving equilibrium pressure. At high pressure level large volume of CO₂ (adsorbed during adsorption) was release as a consequence of the pressure drop. Part of this large released volume was easily and quickly re adsorbed due to the great affinity of CO₂ to coal. Also, the pressure fluctuations appeared to be enhanced by some diffusion from the matrices. The results suggest that at high pressure the CO₂ equilibrium pressure was difficult to achieve due to fluctuations in pressure as a result of re adsorption of gas. In desorption, this process of equilibrium pressure took longer than in adsorption.

CHAPTER FIVE

Single gas desorption

Coal particle size

Figure V-7 compares the pressure profiles of CO₂ over time with respect to particles size. Fragmented coal (1.18 mm to 15.00 mm) and core samples (54.00 mm diameter) were analysed at 500 kPa (low pressure) from 1 440 min (one day) to 10 080 min (seven days), to monitor the fluctuations in CO₂ pressure over time. The graph shows that at low pressure, the coal samples appeared to reach adequate CO₂ equilibrium pressure during desorption in about 2 880 min (two days) despite some marginal fluctuations in pressure over time.

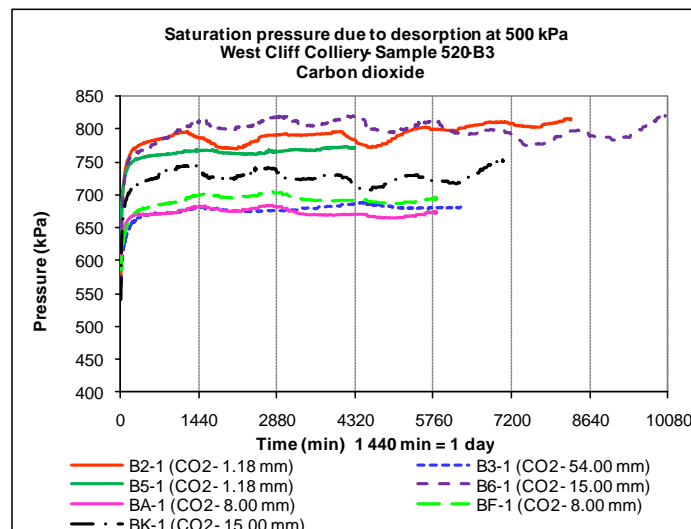


Figure V-7 – Effect of particle sizes on CO₂ gas saturation time

This result agreed with the minimum CO₂ saturation time reported in Chapter 3, section 3.2.1. The result suggests that fluctuations in CO₂ were cyclical over time and appeared to be independent of particle sizes. Appendix 10 shows the pressure drop profiles of sample B2-6 at each 500 kPa step down to almost atmospheric pressure.

Temperature

Figure V-8 shows the drop in the pressure of CO₂ over time in three samples at temperatures of 21 and 24 °C. The graph shows that sample B2-6 tested at 21 °C reached adequate equilibrium pressure in 1 440 min (one day), while the samples B5-1

CHAPTER FIVE

Single gas desorption

and BA-1 tested at 24 °C required at least 2 880 min (two days) to reach similar level of saturation. This level of saturation is indicated by changes in pressure over time; small changes in pressure indicate a high level of saturation or near saturation. This suggests that CO₂ saturation time appeared to be independent of temperature. However, the degree of CO₂ saturation was likely to be influenced by temperature, where a lower temperature meant a higher level of CO₂ saturation.

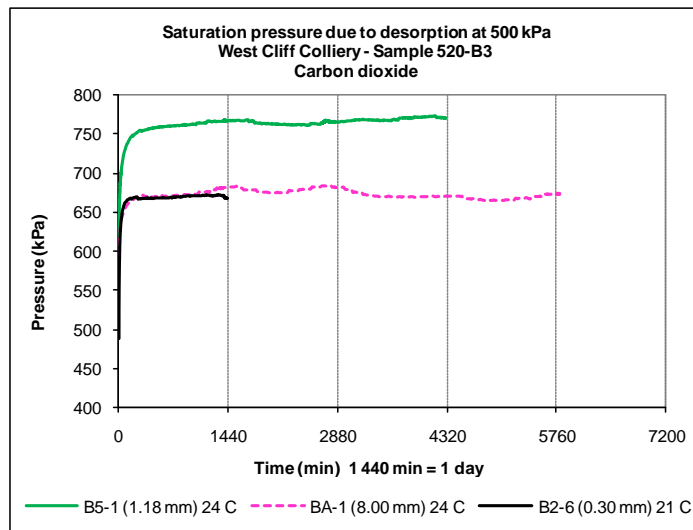


Figure V-8 – Effect of temperature on CO₂ gas saturation time

V.3.2.2. ADSORBED MASS

Experimental adsorbed mass

Figure V-9 shows the profile of CO₂ adsorption capacity in coal with respect to pressure in samples B2-6 during adsorption and desorption. The CO₂ adsorption capacity was measured at a temperature of 21 °C. Desorption in the B2-6 sample commenced from about 4 000 kPa down to almost 200 kPa in several steps. The results indicated that the adsorbed mass of CO₂ in coal was higher in desorption than adsorption. The excess CO₂ in desorption was probably due to an increase in saturation time (saturation time in adsorption plus in desorption). A longer saturation time allowed the adsorption of more CO₂ despite the process of desorption, which suggests the samples adsorbed CO₂

CHAPTER FIVE

Single gas desorption

even during desorption. Also, it appears that the diffusion process was improved by the time. The longer the saturation time the larger and deeper the volume of CO₂ transported by diffusion.

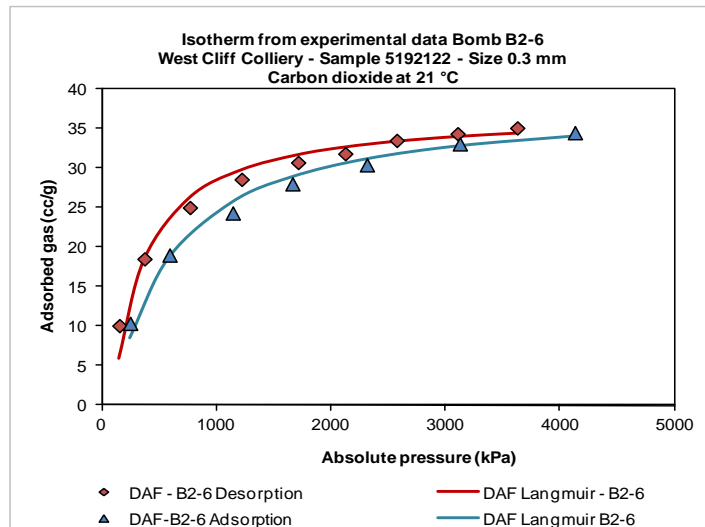


Figure V-9 – Excess on CO₂ sorption capacity in desorption

Coal particle size

Figure V-10 shows the experimental results of CO₂ adsorption capacity in desorption with respect to particle sizes.

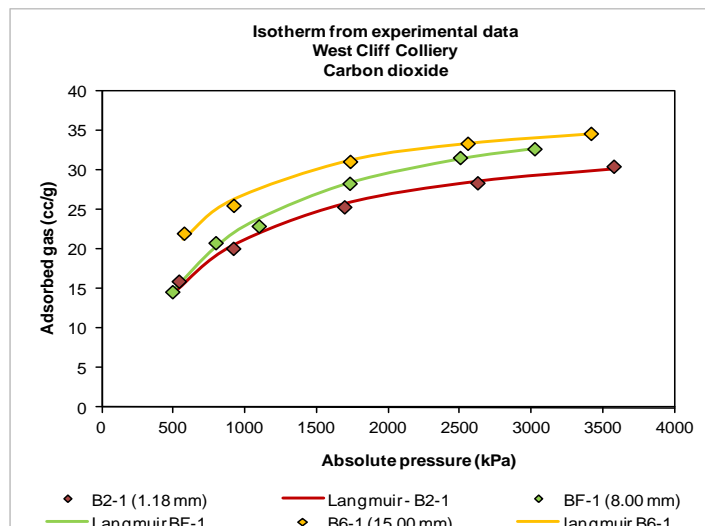


Figure V-10 – Effect of particles size on CO₂ adsorbed mass in desorption

Fragmented (1.18 mm < size < 15.00 mm) coal samples were tested at a temperature of 24 °C. The highest adsorbed mass of CO₂ was achieved in the B6-1 sample (15.00

CHAPTER FIVE

Single gas desorption

mm) over the entire range of desorption, while the lowest adsorbed mass of CO₂ was achieved in the 1.18 mm particles size. The results suggest that in desorption the adsorbed mass of CO₂ appeared to depend on the particle sizes in such a way that the larger the coal particle size the higher the CO₂ adsorption capacity. It seems that larger particle sizes with larger porous network allowed to CO₂ to be adsorbed in larger quantity. Mazumder et al. (2006) stated that high pressure allows a considerable amounts of gas to be adsorbed by penetrating the coal molecular structure. However, Harpalani et al. (2006) reported marginally CO₂ and CH₄ hysteresis in several coal samples. They also stated that gases such as N₂, CO₂ and CH₄ should not deviate from their adsorption isotherms because adsorption and desorption are a physical and reversible processes. They explained that the desorption hysteresis process can be attributed to changes in the properties of the coal and/or the capillary condensation in its micro pores.

Table V-3 compares the experimental data of CO₂ adsorption capacity in sample B2-6 during adsorption and desorption.

Table V-3 – CO₂ sorption capacity in adsorption/desorption

Sample B2-6 (0.30 mm) - Carbon dioxide														
Pressure (kPa)	Adsorption							Desorption						
	248	591	1144	1665	2315	3127	4132	3629	3108	2576	2126	1715	1221	770
Adsorbed mass (cc/g)	10.4	19.0	24.4	28.0	30.5	33.1	34.5	35.1	34.4	33.5	31.9	30.7	28.6	25.0

The result shows that the adsorbed mass of CO₂ in desorption was marginally higher than in adsorption. At about 3 100 kPa the adsorbed mass of CO₂ was about 34.4 cc/gm in desorption, and about 33.1 cc/gm in adsorption. The difference in adsorbed mass was 1.3 cc/gm (4%) and this was considered as an excess of CO₂ at that level of pressure. Also, the results indicates that the adsorbed mass of CO₂ was marginally higher in desorption than adsorption at almost every pressure step. At almost

CHAPTER FIVE

Single gas desorption

atmospheric pressure of 153 kPa (measured at equilibrium pressure) the excess in CO₂ was about 10.1 cc/gm. This remaining CO₂ gas in coal at almost atmospheric pressure level may be considered as residual CO₂ in coal due to adsorption-desorption.

Table V-4 shows the excess in CO₂ adsorbed mass in the 1.18 mm sample at several levels of pressure. The listed data was interpolated from the experimental data of CO₂ to make them easier to be compared. The results show that the highest excess of CO₂ was achieved at about 250-500 kPa. The CO₂ excess was about 15% higher. The result shows that the excess in CO₂ adsorbed mass in sample B2-1 (1.18 mm) was higher than in sample B2-6 (0.30 mm).

Table V-4 – Excess on CO₂ sorption capacity in desorption

Pressure (kPa) Adsorbed mass (cc/g)	Carbon dioxide															
	Adsorption						Desorption					Excess in sorption capacity				
	250	500	1000	2000	3000	4000	250	500	1000	2000	3000	250	500	1000	2000	3000
B2-1 (1.18 mm)	10.3	13.8	19.2	25.6	28.3	30.3	12.1	15.6	20.9	26.7	29.3	1.8	1.8	1.6	1.1	0.9

This result suggested that the excess in CO₂ adsorbed mass could depend on the particle size. As reported previously in section 3.2.2.1, the saturation time could be the factor influencing the excess of CO₂ in coal. This CO₂ excess was higher in larger particles with larger pore network system than in powdered coal, with substantially less pore space. Thus, the larger the particle size the higher the excess in CO₂ adsorbed mass.

Langmuir isotherm

Figure V-11 shows the Langmuir isotherm and experimental data profiles of CO₂ against pressure, in desorption. Similar to adsorption, the Langmuir equation was used to model experimental data of the content of CO₂ measured in desorption. The graph shows that within experimental error the experimental data was tallied very well with the Langmuir equation during desorption. Thus and similar to CO₂ adsorption,

CHAPTER FIVE

Single gas desorption

Langmuir equation can be used to model CO₂ adsorption during desorption with high accuracy.

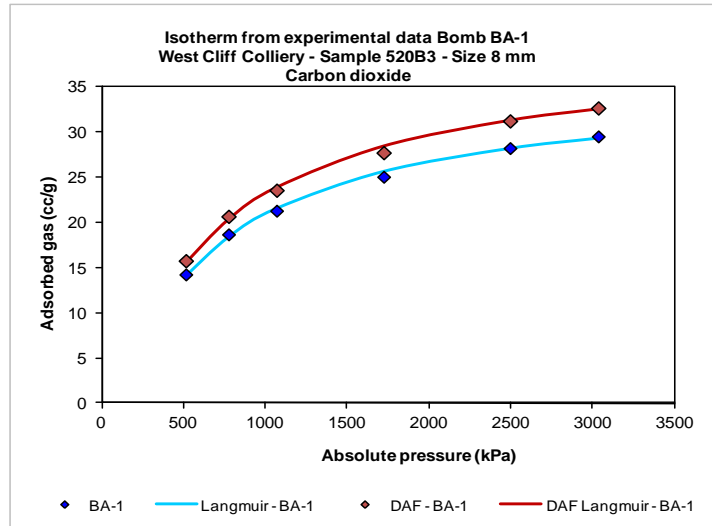


Figure V-11 – Langmuir isotherm from CO₂ gas experimental data

Temperature

Figure V-12 shows the CO₂ profile in desorption, in samples tested at temperatures of 21 and 24 °C. The adsorbed mass of CO₂ in samples B2-6 was measured at 21 °C while samples B2-1 and B5-1 were measured at 24 °C.

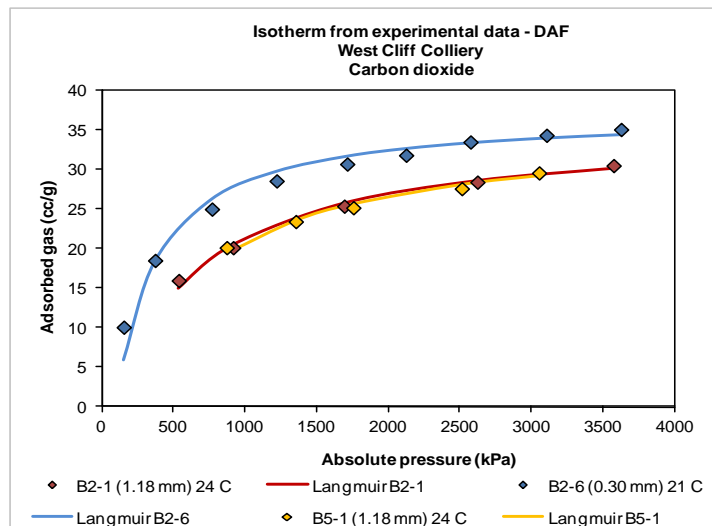


Figure V-12 – Effect of temperature on CO₂ adsorbed mass in desorption

The graph shows that the highest adsorbed mass of CO₂ was achieved in samples tested at temperature of 21 °C. The result indicates that CO₂ adsorbed mass during

CHAPTER FIVE

Single gas desorption

desorption depended on the temperature; the lower the temperature the higher the adsorbed mass of CO₂. Similar results were obtained in coal samples tested during adsorption. Additionally, the results show that similar coal particles size (B2-1 and B5-1 samples) at similar temperatures, achieved similar adsorbed mass of CO₂.

V.3.2.3. RESIDUAL GAS

In this study, residual CO₂ is defined as the gas remaining (or trapped) in coal at atmospheric pressure; it is any gas at atmospheric pressure that cannot be removed by vacuuming.

Figure V-13 shows the adsorbed mass of CO₂ against pressure due to enhancing desorption by vacuuming.

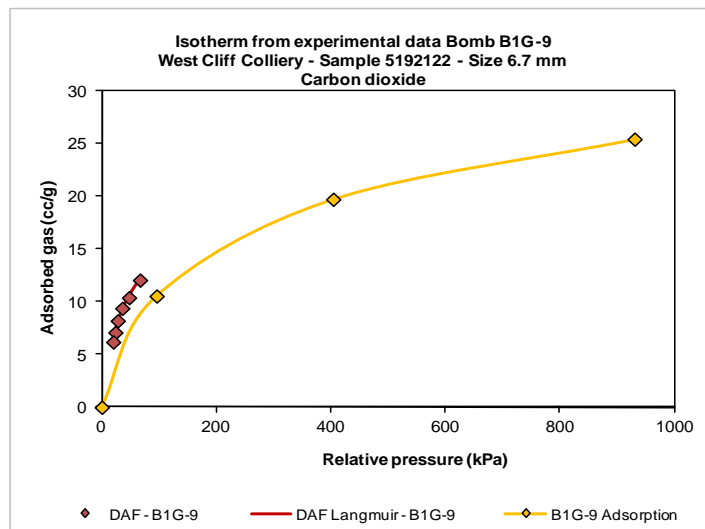


Figure V-13 – Enhanced CO₂ gas desorption by vacuuming

Adsorption and desorption on coal was initially tested at a bath water temperature of 21 °C. By comparing the adsorbed mass of CO₂ in coal (10 cc/gm) at near atmospheric pressure (70 kPa) during desorption, with a maximum of CO₂ (35 cc/gm) in adsorption at about 4 000 kPa (Figure V-9), the results show that the adsorbed mass of CO₂ dropped by about 71% in desorption due to the release of the pressure. However, 29% of the CO₂ remained in the coal and proved difficult to remove by the conventional

CHAPTER FIVE

Single gas desorption

method of pressure release. Figure V-13 shows there is still an excess of CO₂ in coal (about 6.0 to 10.0 cc/gm), at pressures below 70-80 kPa. The fact that at near atmospheric pressure the CO₂ molecules were removed only by vacuuming suggests that most CO₂ was located in the matrices or somewhere very deep in the coal structure. The results show that the adsorbed mass of CO₂ in sample B1G-9 was reduced by almost 50% in 8 640 min (six days) due to six vacuuming sessions of 60 s, every 24 hours. In order to enhance the CO₂ desorption rate of sample B1G-9 at atmospheric pressure even further, the temperature was increased to 28 °C.

Figure V-14 shows the adsorbed mass of CO₂ against pressure at 28 °C, where desorption of CO₂ was stimulated by 60 s of vacuuming, in 18 steps every 24 hrs.

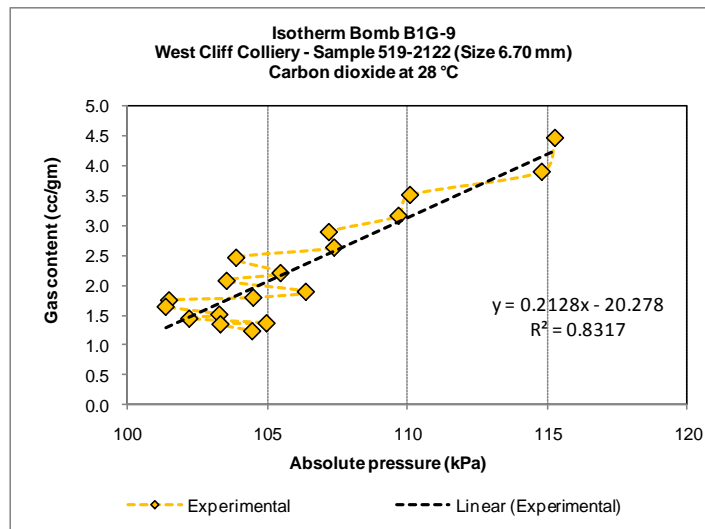


Figure V-14 - Enhanced CO₂ gas desorption by increasing temperature

Thus, the adsorbed mass of CO₂ was reduced by 80%, from 5.0 cc/gm to about 1.00 cc/gm, in 25 920 min (18 days). However, the strategy of increasing the temperature to 28 °C to stimulate desorption, took three times longer than the previous process at 21 °C. In sample B1G-9, the minimum adsorbed mass of CO₂ in coal was 1.24 cc/gm, at near atmospheric pressure. The total period of vacuuming was performed as 24 steps for 60 s every day. This minimum adsorbed mass of CO₂ in coal at atmospheric

CHAPTER FIVE

Single gas desorption

pressure, now called the residual adsorbed mass of CO₂ in coal, represented about 3.5% of the maximum adsorbed mass of CO₂ achieved, at about 4 000 kPa reference pressure. In the laboratory it was impossible to obtain, by any other mechanism, a lower adsorbed mass of CO₂ in coal than its residual gas content.

V.3.3. METHANE

The CH₄ desorption test in fragmented and core samples of coal followed immediately after the CH₄ adsorption test was concluded. In desorption, the adsorbed mass of CH₄ was measured gravimetrically in particles size varying from 1.18 mm to 15.00 mm in addition to 54.00 mm diameter samples.

V.3.3.1. GAS SATURATION TIME

Pressure level

Figure V-15 shows the effect the levels of pressure have on CH₄ saturation time in desorption. The pressure drop of sample BH-1 was analysed at the 500 and 2 500 kPa levels, respectively. Both levels were considered to represent the behaviour of CH₄ at both high and low pressures.

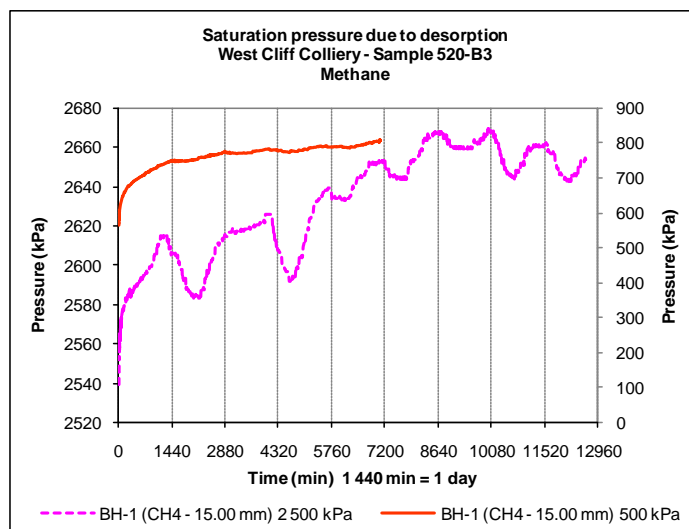


Figure V-15 – Effect of pressure levels on CH₄ gas saturation time

CHAPTER FIVE

Single gas desorption

At a near equilibrium pressure of 800 kPa, the sample appeared to achieve a satisfactory level of saturation (fluctuations in pressure < 5% over the period) between 2 880 (two days) and 4 320 min (three days). However, the graph shows that the pressure still increased over time which meant that full equilibrium pressure was not yet achieved. Full equilibrium pressure was considered to be when fluctuations in pressure were equal to zero over the period. These results suggest that in desorption and a low pressure levels, 4 320 min (three days) appeared to be sufficient to achieve an adequate level of CH₄ saturation, which agrees with a minimum saturation time of CH₄ of 4 320 min (three days) in adsorption. At an equilibrium pressure of about 2 600 kPa the graph shows that more than 11 520 min (eight days) were not enough time to achieve equilibrium pressure because fluctuations in pressure were more than the maximum acceptable level of 5%. Fluctuations of CH₄ bore some resemblance to the drop in CO₂ shown in Figure V-6. At high pressure (above 2 000 kPa), the graph shows that the sample did not achieve equilibrium pressure. This indicates that the saturation time of CH₄ appeared to depend on the level of pressure, which was similar to those results obtained with CO₂. The higher the level of pressure the longer the saturation time of CH₄ in desorption which was similar to those results obtained with CO₂.

Coal particle size

Figure V-16 shows saturation time with regard to particle size during desorption of CH₄ at a reference pressure of 500 kPa. Most samples appeared to achieve acceptable levels of CH₄ saturation between 2 880 min (two days) and 4 320 min marks (three days) despite some small but appreciable fluctuations in pressure over time. However,

CHAPTER FIVE

Single gas desorption

there were almost zero fluctuations in some of the largest particles of coal (samples BD-1 and BL-1), at about the 4 320 min mark of saturation time.

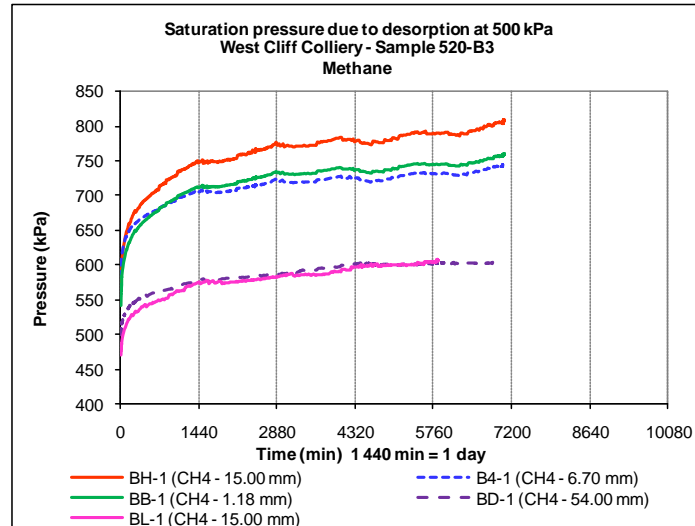


Figure V-16 – Effect of particle sizes on CH₄ gas saturation time

This discrepancy can be attributed to the fact that CH₄ saturation time appeared to depend on the level of pressure, as stated previously, rather than particle size. The result indicates that both saturation time and degree of saturation with CH₄ in desorption, appeared to be independent of particle size. The variations on the final pressure of each sample were attributed to different amounts of gas released.

Gas type

Figure V-17 shows the combined N₂, CO₂ and CH₄ profiles over time in fragmented and core coal samples, at about 500 kPa pressure level. The results suggest that during desorption, N₂ and CH₄ appeared to achieve the desired levels of equilibrium pressure between 2 880 min (two days) and 4 300 min marks (three days). However, CO₂ appeared to require less time of saturation (between 1 440 min and 2 880 min) to achieve a similar level of CH₄ saturation. The study indicates that in desorption, the saturation time appeared to depend on the type of gas, such that N₂ and CH₄ appeared

CHAPTER FIVE

Single gas desorption

to take longer to achieve saturation than CO₂, but both N₂ and CH₄ appeared to require similar saturation time to obtain an adequate saturation of gas.

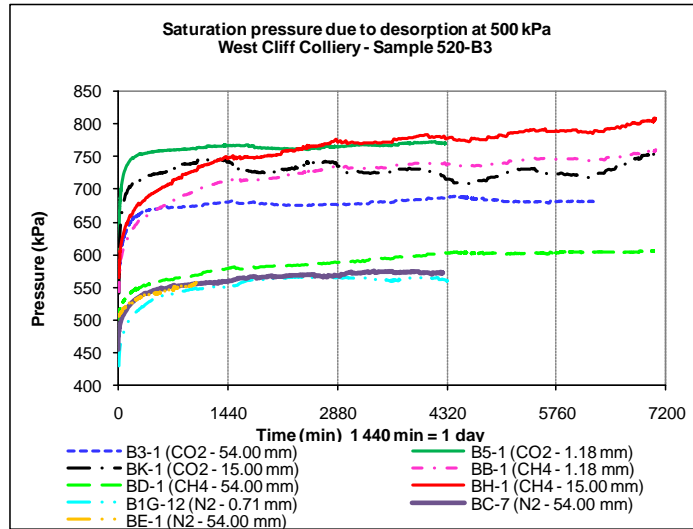


Figure V-17 – Effect of gas type in gas saturation in desorption

V.3.3.2. ADSORBED MASS

Experimental adsorbed mass

Figure V-18 shows the adsorbed masses of CH₄ (DAF basis) in coal during adsorption and desorption in two samples, BB-1 (1.18 mm) and BH-1 (15.00 mm).

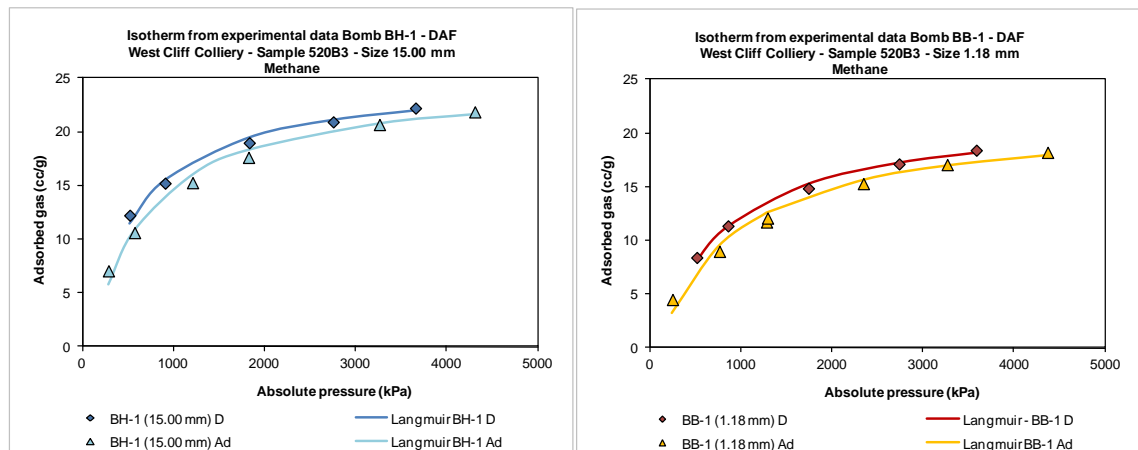


Figure V-18 – CH₄ adsorbed mass in adsorption and desorption

The suffix 'Ad' on a tested sample names means adsorption and 'D' means desorption.

The results indicate that in both samples the CH₄ adsorbed mass in desorption appeared to be higher than in adsorption. There was a clear excess of CH₄ in

CHAPTER FIVE

Single gas desorption

desorption (hysteresis) compared to adsorption, probably due to a longer saturation as a result of the desorption process. This excess in CH₄ appeared to be marginally higher in larger particles size (15.00 mm). This suggests that with the same duration of gas saturation, the excess of CH₄ adsorbed mass appeared to depend on particle size, such that the larger the particle size the higher the excess of CH₄ adsorbed mass.

Table V-5 shows in detail the adsorbed volume per gram of coal by pressure levels during CH₄ adsorption and desorption in sample BL-1 (15.00 mm). The results show that at a similar pressure of 1 800 kPa, the adsorbed mass of CH₄ in desorption was marginally higher by almost 1.0 cc/gm compared to the adsorbed mass of CH₄ in adsorption. Thus, the excess of CH₄ adsorbed mass in desorption was higher in average 6% than in adsorption.

Table V-5 – CH₄ adsorbed mass in adsorption and desorption

Sample BL-1 (15.00 mm) - Methane												
Pressure (kPa)	Adsorption						Desorption					
	268	576	1176	1808	3261	4305	3062	2728	1817	1059	708	450
	7.8	11.5	16.0	18.1	20.5	21.5	20.9	20.5	19.0	16.6	14.5	12.3

Coal particle size

Figure V-19 shows the adsorbed mass of CH₄ against pressure, in desorption, with respect to particle size. It is compared three different particles, a small (1.18 mm), middle (15.00 mm) and large size (54.00 diameter core coal sample). The graph shows that the highest CH₄ adsorbed mass during desorption was achieved in the 15.00 mm particles size. Both samples BL-1 and BH-1 were saturated for similar period of time at each pressure step. The result shows that both 15.00 mm coal samples achieved very similar amount of adsorbed mass of CH₄. Thus, similar particles size saturated for similar periods of time achieved similar CH₄ adsorbed mass. The sample BB-1 (1.18 mm) achieved lower adsorbed mass of CH₄ comparing to the 15.00 mm coal sample.

CHAPTER FIVE

Single gas desorption

The result suggests that during desorption, for large period of saturation time the larger the samples the higher the adsorbed mass of CH_4 . On the contrary, in adsorption it was found that the adsorbed mass of CH_4 was independent on the particles size.

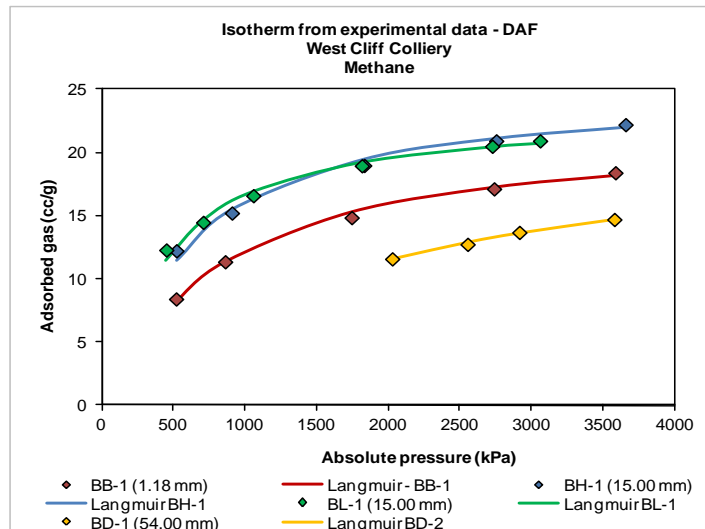


Figure V-19 – Effect of particle sizes on CH_4 adsorbed mass in desorption

However, the largest sample BD-2 (54.00 mm) achieved the lowest adsorbed mass of CH_4 during desorption. The bomb of the BD-2 sample did not leak gas over the entire experiment of adsorption and desorption despite being run longer than any other bomb. A possible explanation could be that the porous networks of some samples were partially blocked by reddish clay like substance that is clearly visible in Figure V-20. Also, it was found that the error in sampling due to oxidation and deterioration was more severe in the core coal samples than in the fragmented as it was stated in Chapter 3.



Figure V-20 – Core coal sample

CHAPTER FIVE

Single gas desorption

Gas type

Figure V-21 shows a combination of N₂, CO₂, and CH₄ over pressure with respect to type of gas, in adsorption and desorption, in two different particles size.

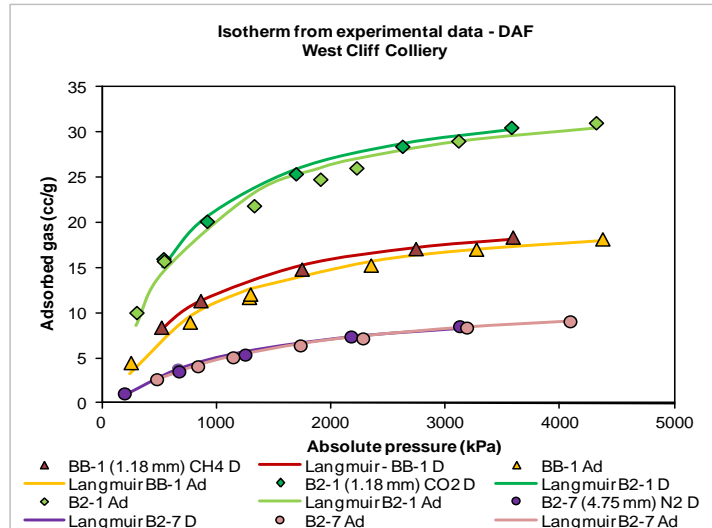


Figure V-21 – Effect of gas type in adsorbed mass in adsorption/desorption

The results show that in desorption the adsorbed mass of, CO₂ was the highest, N₂ was the lowest, and CH₄ was in between which was similar to those results during adsorption. The highest excess of adsorbed mass was with CH₄ while the lowest was with N₂. By comparing identical particles size (1.18 mm), the highest hysteresis due to desorption was found to be with CH₄. However, regardless particles size, the result shows that within experimental error, the hysteresis due to desorption appeared to depend on the gas type. The highest hysteresis was with CH₄; the lowest was with N₂ and CO₂ was between them.

Langmuir isotherm

Figure V-22 shows the Langmuir isotherm from sample BL-1 (15.00 mm) due to desorption of CH₄ in coal samples which suggests that the Langmuir equation tally very well with the experimental data of CH₄ measured during desorption. The Langmuir

CHAPTER FIVE

Single gas desorption

equation can be used to estimate the adsorbed mass of CH_4 during desorption, a similar result to those obtained for N_2 and CO_2 .

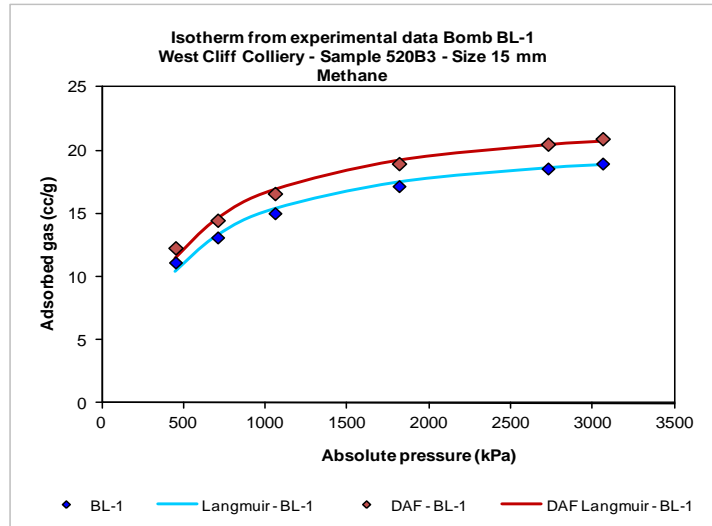


Figure V-22 – Langmuir isotherm from CH_4 gas experimental data

The Langmuir parameters P_L and V_L were 0.36 MPa and 23.30 cc/gm respectively which were similar to those values obtained during adsorption.

V.3.3.3. RESIDUAL GAS

Figure V-23 shows the adsorbed mass of CH_4 with pressure due to desorption after being vacuumed 60 s every 24 hours.

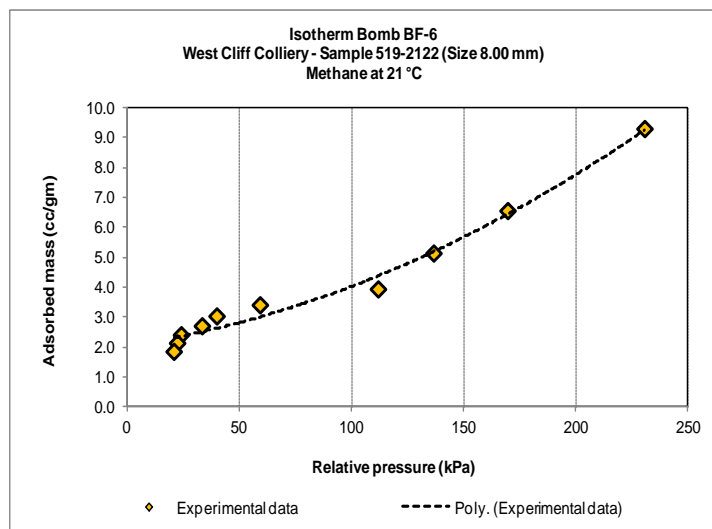


Figure V-23 – Enhanced CH_4 gas desorption by vacuuming

CHAPTER FIVE

Single gas desorption

The aim of the test was to study the speed of the CH₄ desorption from the coal sample at pressure levels near or below atmospheric pressure. After the CH₄ desorption test, the residual gas was measured in the 8.00 mm size particles. The sample BF-6 was tested in adsorption and desorption at a temperature of 21 °C. The results showed that still some CH₄ remained in the sample despite the long process of desorption of about 32 days. The fact that CH₄ was removed from the coal only by vacuuming suggests that most of the adsorbed CH₄ must have been located deep within the matrices. The graph shows that the adsorbed mass of CH₄ dropped more than 80% (in 9 steps of 24 hours each), from about 9.0 cc/gm to 1.5 cc/gm, at a desorption rate of about 0.03 cc/gm per kPa.

Figure V-24 shows the adsorbed mass of CH₄ with pressure due to desorption by vacuuming. At this stage, the bath water temperature was increased from 21 °C to 28 °C to test any improvement in the rate of desorption.

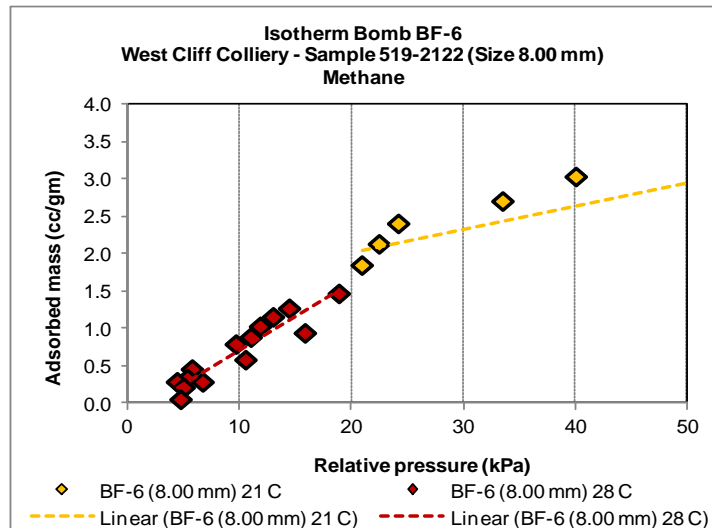


Figure V-24 – Enhanced CH₄ gas desorption by increasing temperature

At 28 °C the adsorbed mass of CH₄ dropped from 1.5 cc/gm to almost zero (0.05 cc/gm) in about 18 720 min (13 steps of 60 s vacuuming every 1 440 min), at a desorption rate

CHAPTER FIVE

Single gas desorption

of about 0.09 cc/gm per kPa. Comparisons of the rates of CH₄ desorption at temperatures of 21 and 28 °C suggests that as the temperature increases so too does the rate of adsorption. Residual CH₄ in sample BF-6, at atmospheric pressure, was measured in about 0.05 cc/gm after 22 steps of 60 s vacuuming every 1 440 min, this represents about 0.25% of the maximum amount of CH₄ measured at 4 000 kPa. Comparing with the residual CO₂ of 3.5%, the result indicates that CH₄ was easier to evacuate than CO₂ under the same process of vacuuming.

V.3.4. SUMMARY

Saturation time

- With N₂ and CO₂ gas, 2 880 min (two days) of saturation time (time to reach saturation) appeared to be adequate to obtain an adequate level of saturation level, although CH₄ took longer to achieve equilibrium pressure.
- With N₂ gas, saturation time appeared to be independent of the pressure level, while CH₄ saturation time appeared to depend on the pressure level. The higher the pressure the longer the CH₄ saturation time.
- Saturation time with N₂, CO₂ and CH₄ appeared to be independent of particle size while the degree of CH₄ saturation appeared to depend on particle size. The larger the particle the higher the degree of saturation.
- Saturation time depended on the type of gas. N₂ and CH₄ appeared to require a longer saturation time than CO₂, while N₂ and CH₄ appeared to be similar.

Adsorbed mass

- The adsorbed mass of N₂, CO₂, and CH₄ in desorption seemed higher than in adsorption, which appeared to be due to an increase in total saturation time (adsorption followed by desorption). The highest excess appeared to be with CH₄

CHAPTER FIVE

Single gas desorption

while the lowest was with N₂. The excess of CO₂ was between N₂ and CH₄ but was closer to the excess in CH₄,

- The excess in CO₂ and CH₄ appeared to depend on particle size, such that the larger the particle the higher the excess of CO₂ and CH₄.
- Although the adsorbed mass of N₂ was partially influenced by particle size it is not a convincing scenario, and hence more research is needed to confirm this statement. The adsorbed mass of CO₂ appeared to depend on particle size, such that the larger the particle the greater the volume of CO₂. However, the adsorbed mass of CH₄ appeared to depend on particle size for fragmented particles (1.00 mm < size < 54.00 mm).
- The adsorbed mass of gas in coal generally depended on the type of gas, with CO₂ being the highest and N₂ the lowest.
- The Langmuir equation tallied well with the experimental data of N₂, CO₂, and CH₄ profiles in desorption.
- Residual CO₂ in coal represented about 3.0% of maximum CO₂ (at 4 000 kPa) while residual CH₄ was lower, at about 0.25% of the maximum adsorbed mass of CH₄.

VI. CHAPTER SIX

MIXED GAS DESORPTION

VI.1. INTRODUCTION

There is a growing interest in the study of CO₂ sorption in coal either as a single gas or mixed with CH₄. This interest stems from the current climate of reducing the green house effect globally as well as mining coal from seams which are difficult to drain. In particular the sorption of binary CO₂/CH₄ and ternary N₂/CO₂/CH₄ gases present an interesting challenge as the limited research publications point to the formation of an isotherm hysteresis phenomenon where the profiles between adsorption and desorption isotherms deviate. In general the isotherms of desorption in CO₂/CH₄ are above the adsorption isotherms and the degree of hysteresis is variable and depends on various geological and environmental factors.

As part of a continuing research into mine gases and outburst control, the desorption of mixed gases was examined (binary and ternary mixture), with an emphasis on characterising the desorption and adsorbed mass of mixed gases, the accuracy of the extended Langmuir equation for modelling mixed gas desorption, and the applicability of the Soave-Redlich-Kwong equation of state (Soave 1972, Redlich and Kwong 1949). Accordingly this chapter is a further extension of the gas sorption study which examines the desorption characteristic of mixed gases in different size particles of coal. In particular, the focus of this study is to evaluate and quantify the residual gases in fragmented mined coal, particularly open cut mining.

CHAPTER SIX

Mixed gas desorption

VI.2. EXPERIMENTAL PROCEDURE

VI.2.1. APPARATUS

The equipment and components used to measure the composition of mixed gas was a gas chromatograph (GC), a gas sample bag system, and a PC for recording data (Figure VI-1). The sorption apparatus used in this study is described in Chapter 3, section 2.1.



Figure VI-1 – Gas desorption apparatus and components

Sampling was carried out directly from the inlet of the gas sample bag by connecting it to the bomb, which was in turn connected to the gas chromatographer. All the equipment was calibrated as described in Chapter 3, section 2.1 before testing commenced, including the pressure transducers (every six months), and the scale and gas chromatographer (daily).

VI.2.2. TESTING PROCEDURE

The apparatus used in the experimental study was checked regularly. The daily test procedure consisted of the following steps:

- Calibrate equipment (scale and gas chromatograph),
- monitor/control gas pressure stabilisation (if equilibrium pressure was achieved then increase the pressure),
- weigh the bombs,
- check gas composition (if necessary),

CHAPTER SIX

Mixed gas desorption

- check gas pressure (increase/decrease) (if necessary),
- check weight of bombs (if necessary), and
- Retrieve data.

The desorption test follows immediately after the mixed gas adsorption process has been completed. During desorption the adsorbed mass of gas in coal was determined gravimetrically at several decreasing pressure steps, starting from 3 500 kPa (reference pressure) down to atmospheric pressure. The binary mixed gas desorption test procedure can be summarised as follows:

- Desorption characteristics of 52/48 CO₂/CH₄ mixed gas carried out in two groups (A and B) of bombs containing different size particles of coal under a different desorption environment,
- From the last pressure step of the adsorption test, the pressure was reduced to the desired level with respect to the selected group.
 - In group A the pressure was reduced from about 4 000 kPa to the atmospheric pressure in steps of 200-300 kPa. At each step a test was run for 4-7 days regardless of the equilibrium pressure.
 - In group B the pressure was reduced in steps of about 500 kPa. At each step the test was run until equilibrium was reached.
- The composition of gas was measured in every sample on the basis of a step in pressure,
- The above steps were repeated until the pressure reached atmospheric level.

Group A consisted of three bombs, BH-6 (0.30 mm), BA-6 (1.18 mm) and B6-5 (4.75 mm), while group B contained bombs BC-6 (4.75 mm), B4-7 (8.00 mm) and BL-7 (8.00 mm).

CHAPTER SIX

Mixed gas desorption

mm). The reason for having group A experience small drops in pressure over time (200-300 kPa) was to compare it with the minimum time to reach saturation (due to equilibrium pressure and/or gas composition) carried out in previous investigations on desorption using individual gas, as discussed in Chapter 3, sections 2.4.1, 2.5.1, and 2.6.1, and also reported by Florentin *et al* (2009).

The second step of the desorption test was to monitor the residual mixed gas in coal.

The daily operational tasks can be summarised as follows:

- Weigh bombs,
- Vacuum bombs (60 s),
- Weigh bombs again. Repeat the steps until the gas released is almost negligible.

At this phase it is impossible to measure the composition of the gas due to the small volume collected.

The ternary mixed gas desorption procedure followed almost the same binary mixed gas procedure although the drops in pressure were raised to 1 000 kPa.

Data from desorption was channelled through a data logger to an online computer for processing. Information gathered includes, room temperature, bath water temperature, atmospheric pressure, room humidity, gas pressure of bombs (recorded every 480 s), composition and weight of gas.

VI.3. RESULT AND DISCUSSION

The duration of mixed gas desorption were compared with the minimum saturation time, as suggested for individual gas in Chapter 3, section 3.1. However, the results of mixed gas composition and mixed gas adsorbed mass were analysed for each individual

CHAPTER SIX

Mixed gas desorption

N₂, CO₂, and CH₄ gas, with respect to their levels of pressure, size of particles, type of gas and temperature.

VI.3.1. BINARY MIXED GAS

A mixture of CO₂ and CH₄ in a ratio of 52/48 was used in the binary mixed gas desorption test.

VI.3.1.1. MIXED GAS SATURATION TIME

Pressure level

Figure VI-2 shows the drop in pressure of the binary CO₂/CH₄ mixed gas over time at pressures of 500 and 3 000 kPa respectively.

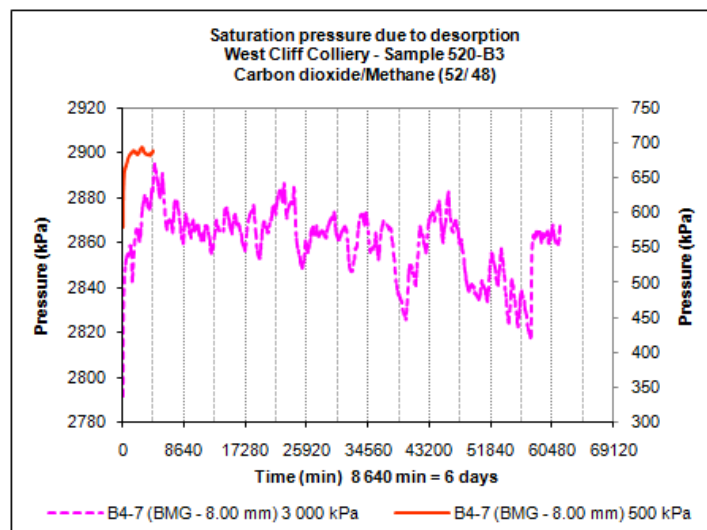


Figure VI-2 – Effect of pressure levels in mixed gas saturation time

At about 700 kPa the pressure fluctuations in the sample B4-7 were less than 5% during 2 880 (two days) and 4 320 min (three days), which matches the minimum time to reach saturation of 2 880 min suggested in Chapter 4, section 3.1. At higher pressure (about 2 860 kPa) however, the pressure fluctuations were considerably more vigorous in intensity and length than at low pressure. The graph shows that 60 480 min (42 days) of saturation time was not enough time to achieve adequate saturation of gas. The results suggest that during desorption and at high pressure, the sample took much

CHAPTER SIX

Mixed gas desorption

more than 4 320 min (three days) to reduce the fluctuations in pressure to the desired levels. This indicates that in desorption the mixed gas saturation time depended on the level of pressure. The higher the pressure levels the longer the time to reach saturation for mixed gas. The graph shows clearly that the sample did not achieve equilibrium pressure and likely compositional equilibrium as well. The graph however, did not indicate the cause of such disequilibrium. It could be due to poor temperature control, gas leakage and/or failure to achieve compositional equilibrium.

Coal particle size

Figure VI-3 shows the pressure profile over time during desorption in several particles ranging from 0.30 to 8.00 mm in size at 500 kPa of pressure.

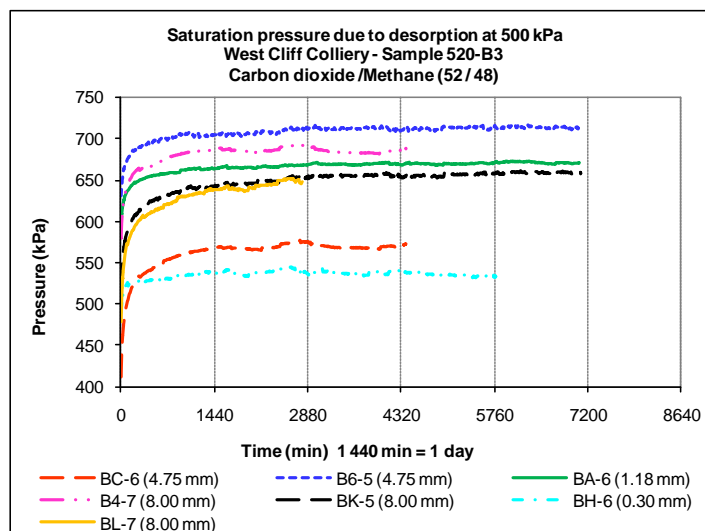


Figure VI-3 – Effect of particle sizes in mixed gas saturation time

The graph shows that an adequate level of saturation was achieved over at least 2 880 min (two days), independent of the size particle. However, it seems that fluctuations in pressure over the first 1 440 min in particles < 2.36 mm were flatter and therefore better saturated than the larger size particles. This finding suggests that the mixed gas saturation time appeared to be independent of the size of particles.

CHAPTER SIX

Mixed gas desorption

Table VI-1 summarises the mixed gas desorption duration at several levels of pressure for samples in group B (equilibrium pressure was pursued at each level). At pressures below 2 500 kPa, the results suggest that independent of particle size, the samples took about 2 880 min (two days) to achieve adequate equilibrium pressure.

Table VI-1 – Summary of mixed gas saturation time

Bombs (group B)	Pressure (kPa)	Average saturation		Pressure status
		(min)	(days)	
BC-6 (4.75 mm) BL-7 (8.00 mm) B4-7 (8.00 mm)	3500	60,468	42.0	1
	3000	61,506	42.7	1
	2500	14,667	10.2	2
	2000	10,052	7.0	2
	1500	7,323	5.1	2
	1000	7,076	4.9	2
	800	5,695	4.0	2
	500	4,409	3.1	2
	200	2,794	1.9	2
	Atmospheric	28,914	20.1	2, 3
Total		202,904	141	
1 --> Equilibrium pressure not achieved				
2 --> At equilibrium pressure				
3 --> Six steps at atmospheric pressure				

Note that the samples were run for longer than 2 880 min (two days) to monitor the behaviour of mixed gas over time. However, at pressures above 2 500 kPa, 42 days of saturation time was not enough to achieve equilibrium pressure. It was unclear why the samples could not stabilise the gas when under high pressure. It was likely that equilibrium was driven by the pressure and composition of the gas. Also, it seems that desorption and re adsorption could have happened making harder to achieve equilibrium.

Bath water and room temperature

Figure VI-4 shows the pressure profile over time in four particles tested during desorption at 21, 24, and 28 °C bath water temperatures. At about 500 kPa the four

CHAPTER SIX

Mixed gas desorption

samples required a minimal 2 880 min (two days) to achieve adequate saturation of gas, independently of the temperature. This indicates that the time of saturation with the binary mixed gas appeared to be independent of the bath water temperature.

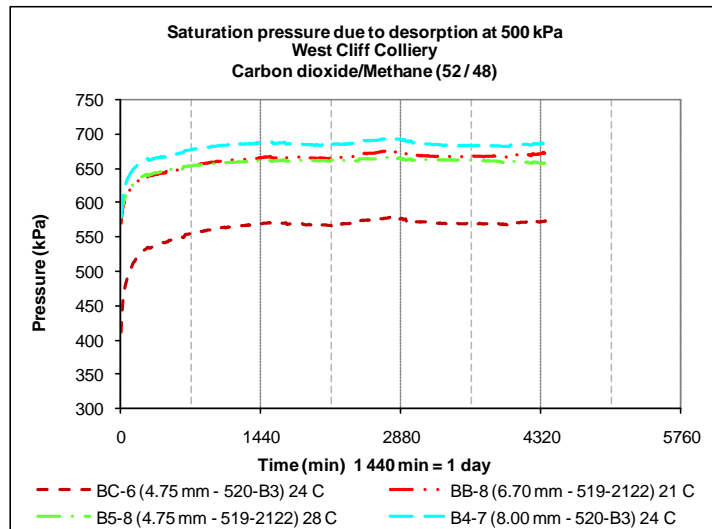


Figure VI-4 – Effect of temperature in mixed gas saturation time

Figure VI-5 shows how the bath water and room temperature affected the pressure profile of the mixed gas over time.

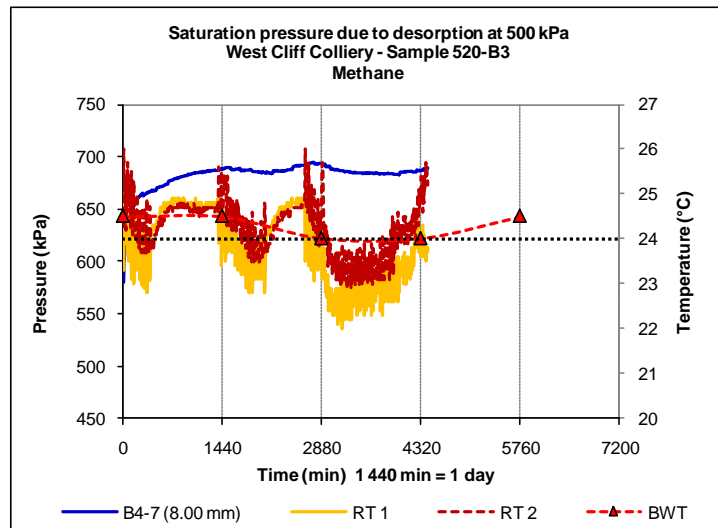


Figure VI-5 – Effect of room temperature in the bath water temperature

The graph shows fluctuations in room temperature of about ± 4 °C in RT 1 and RT 2 over that period. However, in the same period the room temperature had minimal impact

CHAPTER SIX

Mixed gas desorption

on the bath water temperature (fluctuations of about ± 0.5 °C). Consequently, minor changes in bath water temperature had an almost negligible affect on the gas pressure profile. This indicates that the pressure profile during desorption was independent of changes in room temperature, and that any fluctuation in pressure occurred at high pressure (see Figure VI-2) appeared to be independent of temperature changes in the room or the bath water.

VI.3.1.2. MIXED GAS COMPOSITION

Pressure level

Figure VI-6 shows the composition of CO₂ and CH₄ over pressure during desorption. The composition of the free mixed gas in samples of group A and B were measured at the equilibrium pressure at each incremental drop in pressure.

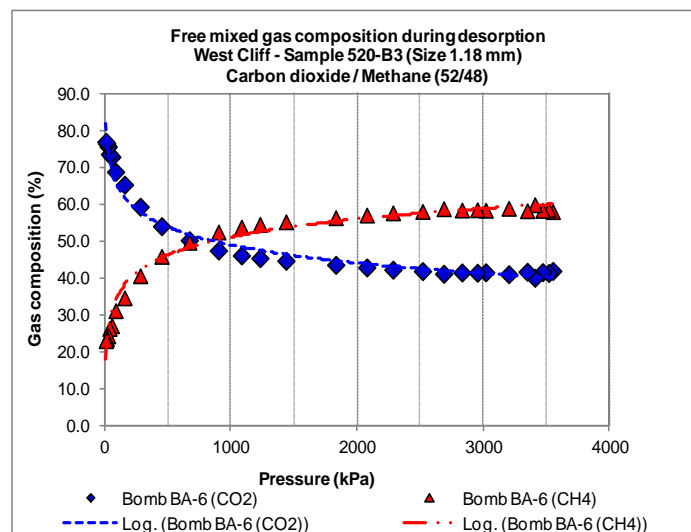


Figure VI-6 – Mixed gas composition during desorption

At about 3 500 kPa (1st pressure drop step), the free CH₄ was higher than the CO₂ in about 20%. This suggests that CH₄ diffused out easier than CO₂ that will be preferentially retained by the coal. Similar results were reported by Crosdale (1998).

The graph shows that the composition of free CH₄ was higher than the CO₂ for pressures above 750 kPa. Below this pressure mark, the pressure and also the CH₄

CHAPTER SIX

Mixed gas desorption

concentration was low enough that allowed the sudden CO₂ release. At pressures below 750 kPa the composition of free CO₂ was several times greater than CH₄, mainly due to the fact that all CH₄ may have been released at the start of the desorption process.

Coal particle size

Figure VI-7 shows the composition of free CH₄ over pressure for samples from group A and B. The result indicates that within experimental error the composition of free CH₄ in the mixture was independent of the particle size.

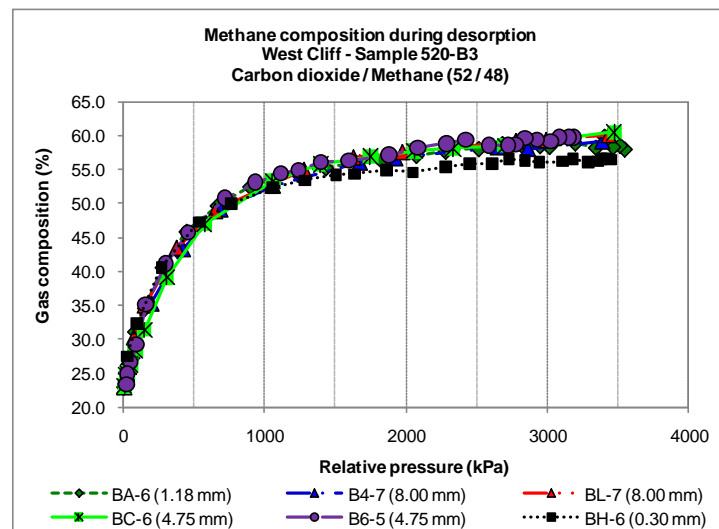


Figure VI-7 – Free CH₄ gas composition during desorption

This decrease in the composition of free CH₄ appeared to be linked with the behaviour of CO₂ (large adsorption coefficient and very slow diffusion from the fine pore structure) rather than CH₄. The drop in pressure and CH₄ concentration triggered the CO₂ desorption. Moreover the composition of CH₄ over pressure was similar in groups A and B, and changes in the composition of free CH₄ over pressure were independent of the drop in pressure. The composition of free CH₄ appears to remain unchanged during desorption, which suggests that desorption of mixed gas was not disturbed during sampling neither by the amount of gas collected (group B) nor the number of samples

CHAPTER SIX

Mixed gas desorption

of gas (group A). The free CH₄ profile suggest that compositional equilibrium could have been achieved despite that equilibrium pressure was not (especially in samples from group A where each pressure steps were run for fixed period without achieving equilibrium pressure).

Bath water temperature

Figure VI-8 shows the compositions of free CH₄ over pressure during desorption at bath water temperatures of 21, 24, and 28 °C. The graph shows that within experimental error the free CH₄ composition was independent of the bath water temperature.

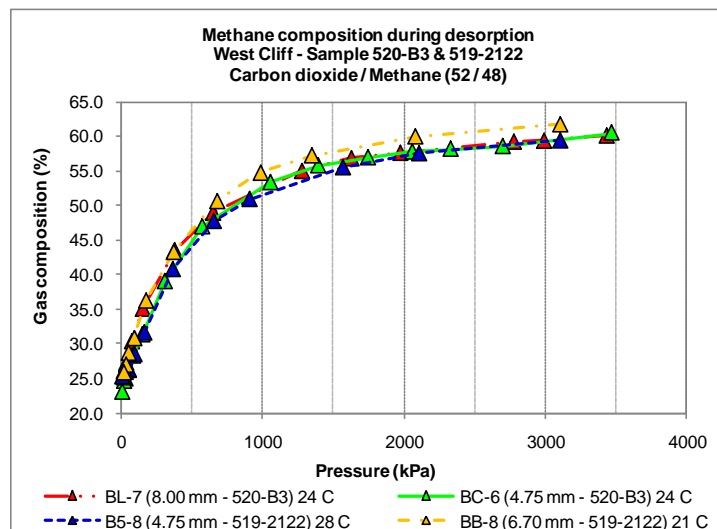


Figure VI-8 – Effect of temperature in gas composition in desorption

It appears that small changes in temperature did not affect the CH₄ behaviour during desorption. Desorption was triggered mainly due to changes in the pressure.

VI.3.1.3. MIXED GAS ADSORBED MASS

Binary mixed gas adsorbed mass

Figure VI-9 shows the adsorbed mass of CO₂/CH₄ mixed gas in the 1.18 mm particle from experimental data over pressure. The graph shows that the mixed gas acting as a whole decreased uniformly over pressure down to the 1 000 kPa level, while below this pressure mark the mixed gas lost almost 50% of its adsorbed mass. The same graph

CHAPTER SIX

Mixed gas desorption

also shows that the mixed gas during desorption (called Experiment D) was higher than during adsorption (called Experiment Ad). This excess of gas during desorption, called hysteresis, was already described in Chapter 5, section 3.1.2 (Individual gas desorption). Crosdale (1998) also reported in his work a strong hysteresis with mixed gas and he suggested that a mixed gas isotherm should be generated because adsorption isotherm of pure gas can not be reliably used when mixed gas is present.

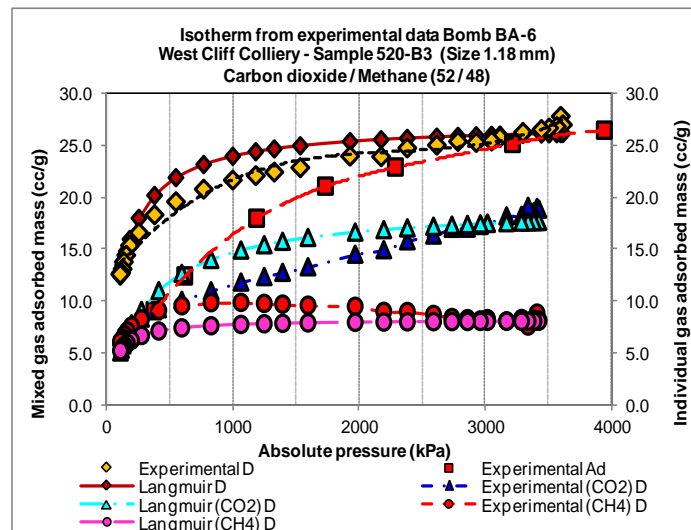


Figure VI-9 – Binary mixed gas adsorbed mass during desorption

The scenarios between CO₂ and CH₄ components were quite different; the CO₂ decreased steadily, slowly and almost linearly to around 250 kPa showing a strong dependency on pressure, while the CH₄ decreased almost instantaneously and then unexpectedly rebounded by increasing its adsorbed mass following a polynomial trend line to a maximum of 500 kPa, despite the drop in pressure. Below this level the adsorbed mass of CH₄ dropped by almost 50%. Furthermore, the adsorbed mass of CO₂ during desorption was higher than the CH₄ until it reached 500 kPa where the adsorbed mass of both was identical. At about 3 500 kPa however, the adsorbed mass of CO₂ was almost twice that of CH₄. Figure VI-9 also shows the extended Langmuir isotherm for CO₂ and CH₄ components and as a whole mixed gas. Despite the extended

CHAPTER SIX

Mixed gas desorption

Langmuir isotherms over estimate of the adsorbed mass of mixed gas in desorption, the behaviour of mixed gas during desorption was modelled well enough, while the results of the CO₂ and CH₄ components were uneven. The extended Langmuir equation over estimated the adsorbed mass of CO₂ considerably, and underestimated the CH₄. It appears that the behaviour of both CO₂ and CH₄ during desorption was caused by the gas filling the pores rather than multi-layer adsorption, which shows that the extended Langmuir equation did not model desorption of CO₂ and CH₄ very well. Described above is the excess of mixed gas during desorption, acting as a whole, but how this excess gas materialised was not suggested with respect to CO₂ and CH₄ acting individually.

Figure VI-10 shows the excess in CO₂ and CH₄ during desorption with respect to the adsorbed mass in adsorption. The graph shows that the CO₂ during desorption was marginally lower than in adsorption, and changes in the adsorbed mass of CO₂ in desorption were almost linear over pressure. The excess of CH₄ during desorption was significantly high which suggests that time could be a factor to take in account.

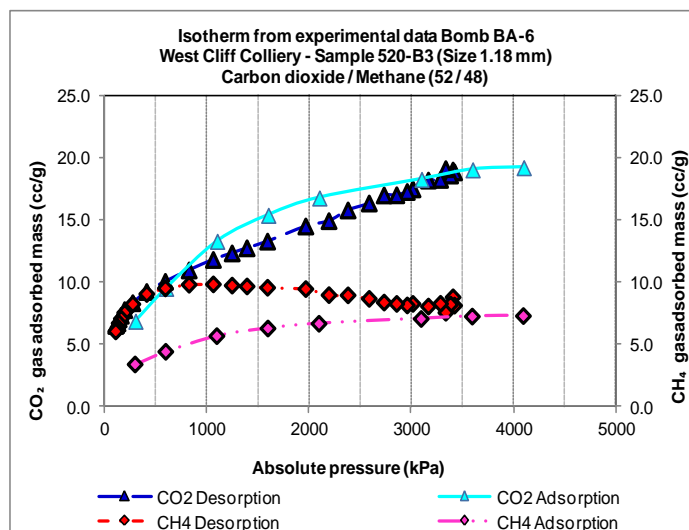


Figure VI-10 – Excess in CO₂ and CH₄ gas adsorbed mass during desorption

CHAPTER SIX

Mixed gas desorption

The longer the sorption process the higher the excess in CH_4 . Adsorption occurred even though pressure in the bomb was dropping. This increase in gas during desorption was thought to be due to the movement and rearrangement of molecules (especially CH_4) in coal structure (joints, the opening, cracks, and matrices). Molecules of CH_4 travelled deep inside the coal matrices over time, liberating spaces previously occupied. This rearrangement increased the volume of CH_4 molecules especially at low pressure moving from a free state to an adsorbed state, which indicates that the excess of mixed gas (acting as a whole) during desorption depended exclusively on an excess of CH_4 . Crosdale (1998) reported in the study of Lama (1988) that despite initial enrichment of CH_4 during mixed gas desorption the CH_4/CO_2 ratio increases again at later stages.

Coal particle size

Figure VI-11 shows the adsorbed mass of CO_2/CH_4 mixed gas acting as a whole over pressures up to 4 000 kPa during desorption in particles varying from 0.30 to 8.00 mm.

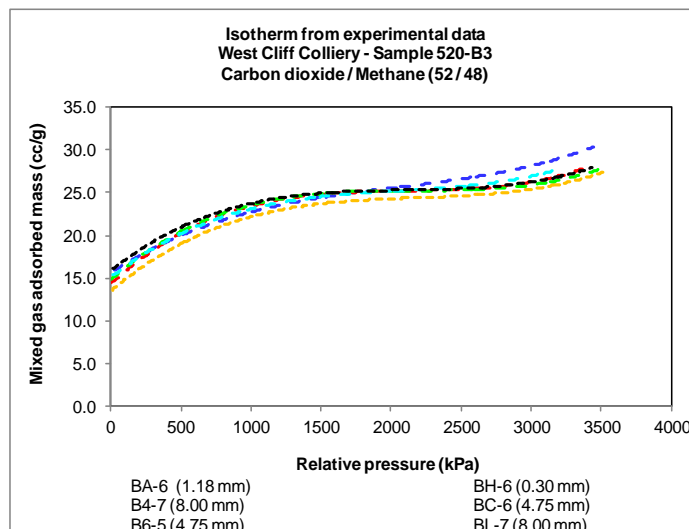


Figure VI-11 – Effect of particle sizes in binary mixed gas content

The graph shows that the adsorbed mass in desorption was independent of the particle size which was identical to the findings from the study on mixed gas in adsorption. The

CHAPTER SIX

Mixed gas desorption

large surface area and the great affinity of CO_2 for coal which is retained longer could be the reason why the mixed gas increased in adsorbed mass despite the drop in pressure. Also, this increase in mixed gas in desorption appeared to be due to the molecules of CO_2 being rearranged on the surface of the coal as a consequence of desorption and re-adsorption. At high pressures the composition of CH_4 (and also CO_2) changed marginally especially CO_2 during desorption, as shown in Figure VI-6. Thus, the adsorbed mass of mixed gas (and possibly CO_2 and CH_4 acting individually) was maintained high at high pressure. Note that desorption test was carried out immediately after the adsorption test. Also, in section 3.1.1 of this chapter, it was reported that the samples barely achieved equilibrium pressure at pressures above 2 500 kPa. The result indicates that the adsorbed mass of CO_2/CH_4 mixed gas acting as a whole appeared to be independent of particle sizes.

Figure VI-12 shows the adsorbed mass of CO_2 and CH_4 components over pressure.

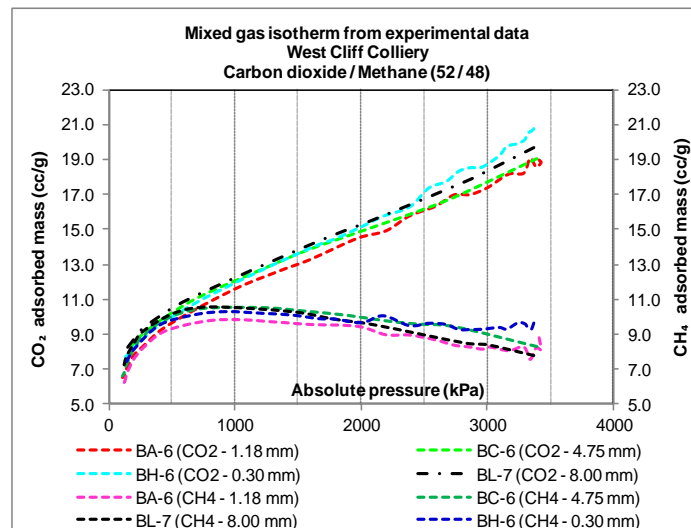


Figure VI-12 – CO_2 and CH_4 adsorbed mass during mixed gas desorption

The graph shows that at high pressure the adsorbed mass of CH_4 component, independently of particles size, was about 7.5 cc/g which was well below the average of 15 cc/g achieved by the single CH_4 . This figure shows that the CH_4 component has

CHAPTER SIX

Mixed gas desorption

released almost 50% of its adsorbed mass very fast and in very short time. However, the CO₂ component at high pressure appeared to be attached and retained by the coal longer mainly due to its affinity for coal. The release of the CO₂ adsorbed mass due to the pressure drop appeared to be done gradually and very slowly. The adsorbed mass of the CO₂ component at high pressure was about 75% of its adsorbed mass as a single gas. The CO₂ desorption appeared to achieve its maximum at low pressure in contrast to the CH₄ component that was at high pressure. The adsorbed mass of both CO₂ and CH₄ components during desorption were independent of the particles size. The desorption rate appeared to be caused mainly due to pressure drop.

Table VI-2 shows changes in the adsorbed mass of CO₂ and CH₄ components at two reference pressures of 3 500 (high pressure) and 500 kPa (low pressure).

Table VI-2 – Changes in adsorbed mass of CO₂ and CH₄ components in desorption

Sample	Particle size (mm)	Total gas content at		Total mass drop		CO ₂ content at		CO ₂ mass drop		CH ₄ content at		CH ₄ mass drop	
		3500 kPa (cc/gm)	500 kPa (cc/gm)	(cc/gm)	(%)	3500 kPa (cc/gm)	500 kPa (cc/gm)	(cc/gm)	(%)	3500 kPa (cc/gm)	500 kPa (cc/gm)	(cc/gm)	(%)
BH-6	0.30	30.398	20.891	9.507	31.3%	20.782	12.722	8.059	38.8%	9.617	10.170	-0.554	-5.8%
BA-6	1.18	27.767	19.535	8.232	29.6%	18.977	10.029	8.948	47.1%	8.790	9.506	-0.715	-8.1%
B6-5	4.75	27.586	20.468	7.118	25.8%	18.126	10.534	7.592	41.9%	9.460	9.934	-0.474	-5.0%
BC-6	4.75	27.344	21.605	5.739	21.0%	19.050	11.164	7.886	41.4%	8.294	10.441	-2.147	-25.9%
B4-7	8.00	27.484	20.289	7.194	26.2%	18.831	10.296	8.535	45.3%	8.653	9.993	-1.340	-15.5%
BL-7	8.00	27.451	20.842	6.609	24.1%	19.669	10.605	9.065	46.1%	7.782	10.237	-2.456	-31.6%

The table shows that the CO₂ component has dropped in adsorbed mass an average 40% from 3 500 kPa down to 500 kPa. The CH₄ component however, has increased its adsorbed mass. The CH₄ below 500 kPa has released almost 100% of its adsorbed mass. The causes of the CH₄ component being re adsorbed was already explained. The results show that the CH₄ component was released from coal easier and faster than the CO₂ component of the binary mixture.

CHAPTER SIX

Mixed gas desorption

Table VI-3 summarises the volume of adsorbed mass in adsorption and desorption of mixed CO₂ and CH₄ in sample BL-7 (8.00 mm). The adsorbed mass of the mixed gas (15.9 cc/g) acting as a whole near atmospheric pressure (135 kPa) in desorption was similar to that (16.2 cc/gm) at 1 200 kPa in adsorption. Most of the adsorbed mass at near atmospheric pressure was retained by the CO₂ component. The adsorbed mass of the CH₄ component (in adsorption) at 135 kPa was almost 70% higher than at 1 200 kPa (in desorption).

Table VI-3 – Mixed gas adsorbed mass in adsorption/desorption

Sample BL-7 (8.00 mm)																			
Gas content (cc/gm)	Absolute gas pressure in adsorption (kPa)							Absolute gas pressure in desorption (kPa)											
	400	700	1200	1700	2200	3160	3900	3500	3100	2900	2100	1700	1400	750	480	250	175	135	120
Mixed gas	9.7	13.6	16.2	18.8	21.4	25.0	28.2	27.5	26.7	26.2	25.1	24.6	24.0	22.2	20.8	18.6	17.0	15.9	15.0
CH ₄	3.4	4.5	4.6	5.0	5.8	6.8	7.7	7.8	8.4	8.5	9.5	9.9	10.3	10.6	10.2	9.2	8.3	7.7	7.2
CO ₂	6.2	9.1	11.6	13.7	15.6	18.2	20.5	19.7	18.3	17.7	15.6	14.7	13.7	11.6	10.6	9.4	8.6	8.2	7.7

Additionally, the adsorbed mass of the CO₂ component in adsorption was slightly higher than in desorption at each level of pressure, however the adsorbed mass of the CH₄ component was higher in desorption. It seems that the CH₄ component showed greater hysteresis than the CO₂ component.

Saturation time

Figure VI-13 shows the adsorbed mass of the CO₂ and CH₄ components over time during adsorption. The graph shows that the profiles of mixed gas acting as a whole and the CO₂ component decreased over time following an almost identical trend. It seems that the trend was defined by the CO₂ component behaviour. However, the CH₄ component marginally increased over time until the 172 800 min mark (at about 750 kPa, as shown in Figure VI-12), and then decreased following the same trend that the mixed gas as a whole and the CO₂ component. This time mark coincided with the 750 kPa mark at which was the maximum adsorbed mass of the CH₄ component during

CHAPTER SIX

Mixed gas desorption

desorption. By analysing the behaviour of CO_2 and CH_4 over pressure and time, they appeared to follow the same behaviour.

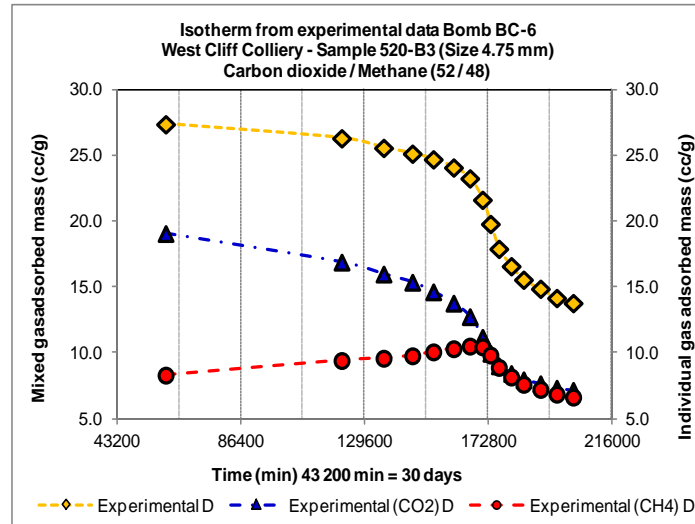


Figure VI-13 – CO_2 and CH_4 gas content over time

In this graph, it is clear that the CO_2 component desorbed gradually over time until the 172 800 min mark where the coal suddenly released most of the CO_2 adsorbed mass.

Temperature

Figure VI-14 shows the adsorbed mass of the CO_2 and CH_4 components at different bath water temperatures over pressure.

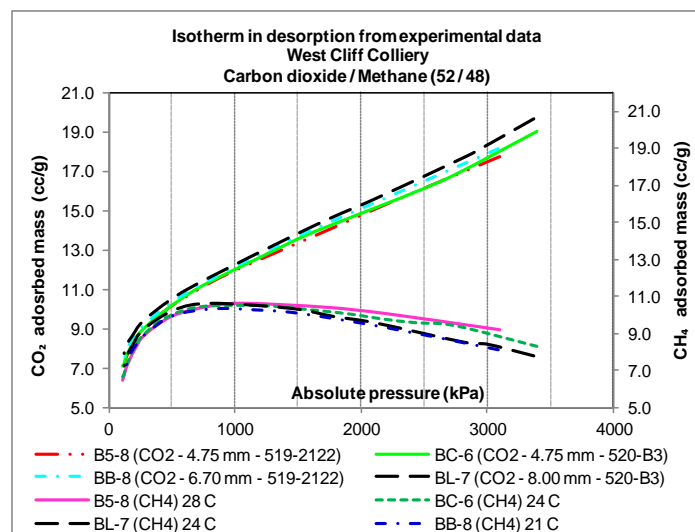


Figure VI-14 – Effect of temperature on the adsorbed mass of the CO_2 and CH_4 components

CHAPTER SIX

Mixed gas desorption

The result indicates that the CO₂ and CH₄ components did not change their behaviour (by comparing their profiles over pressure and time) during desorption due to the changes in the bath water temperature. Within experimental error, the graph shows that the CO₂ and CH₄ components of the mixed gas were independent of small changes in the temperature which was in agreement to the findings with the single CO₂ and CH₄ during desorption. Also, it appears that the small changes in temperature did not have a noticeable effect on the desorption behaviour of the CO₂ and CH₄ components.

VI.3.1.4. RESIDUAL MIXED GAS

After the mixed gas desorption test the residual gas was measured in particles ranging from 0.30 mm to 8.00 mm (group A and B) for almost 51 840 min (about 36 days), in fixed steps of 8 640 min (6 day). Due to the impossibility of measuring the composition of mixed gas close to atmospheric pressure, the adsorbed mass of the CO₂/CH₄ mixed gas was calculated assuming the last composition of mixed gas (at about 10 kPa of relative pressure) as steady mixed gas desorption and is designated as at atmospheric pressure. The dropped in mass was measured every six days after 60 s of vacuuming in order to evacuate all the released gas.

Table VI-4 shows the maximum adsorbed mass of the CO₂/CH₄ mixed gas in desorption (at about 4 000 kPa) and the remaining (residual) adsorbed mass of gas (at atmospheric pressures of 10 kPa). There was more residual mixed gas in the 4.75 mm particle (sample B6-5, group A) and least in the 0.30 mm (group A) particle size, and it was similar in samples from group B. This suggests that larger particles appeared to retain more residual mixed gas, which indicates that fragmented coals (sizes > 1.00 mm) retained more mixed gas than powder coals (sizes < 1.00 mm).

CHAPTER SIX

Mixed gas desorption

Table VI-4 – Residual binary mixed gas in coal

Sample	Size (mm)	Maximum Gas content (cc/gm)	Gas content at atmospheric pressure (cc/gm)	Residual (%)
BH-6	0.30	31.211	11.048	35.4%
BA-6	1.18	27.783	11.252	40.5%
B6-5	4.75	28.260	15.446	54.7%
BC-6	4.75	27.719	12.882	46.5%
B4-7	8.00	28.356	12.244	43.2%
BL-7	8.00	28.247	13.356	47.3%

VI.3.2. TERNARY MIXTURE

A mixture of N₂, CO₂, and CH₄ in ratios of 31.8/33.4/34.8 was used in the ternary mixed gas desorption test.

VI.3.2.1. MIXED GAS SATURATION TIME

Pressure level

Figure VI-15 shows the drop in pressure due to desorption of the N₂/CO₂/CH₄ Ternary Mixed Gas (TMG) over time at two pressures of 500 kPa (low pressure) and 3 000 kPa (high pressure), respectively. At about 600 kPa the coal sample appeared to attain equilibrium pressure in about 2 880 min (fluctuations in pressure < 5%), but the test was run for a longer period to examine the effect of time on the behaviour of gas desorption. The graph shows that although the sample was already saturated according to the test requirement (fluctuations < 5%), the pressure was still fluctuating over time. It appears that the level of gas saturation during desorption depended on the saturation time; longer saturation time assured a better equilibrium pressure and may be compositional equilibrium. The result suggests that at 500 kPa with ternary mixed N₂/CO₂/CH₄ the time required to attain an equilibrium pressure was similar to the saturation time with the binary CO₂/CH₄ mixed gas, in about 2 880 min. However, at about 3 000 kPa pressure mark the coal sample took longer to attain equilibrium

CHAPTER SIX

Mixed gas desorption

pressure, and in fact did not accomplish the requirement of a pressure fluctuation $< 5\%$ after 34 560 min (24 days) of the desorption test likely due to the inability to achieve compositional equilibrium which affected also the pressure equilibrium. Similar behaviour during desorption at high pressure was already mentioned with single CO_2 and CH_4 and CO_2/CH_4 mixed gases. This suggested that during desorption the increase in saturation time appeared to be caused by high levels of pressure fluctuations which indicates that the saturation time of ternary mixed gas depended on the pressure levels.

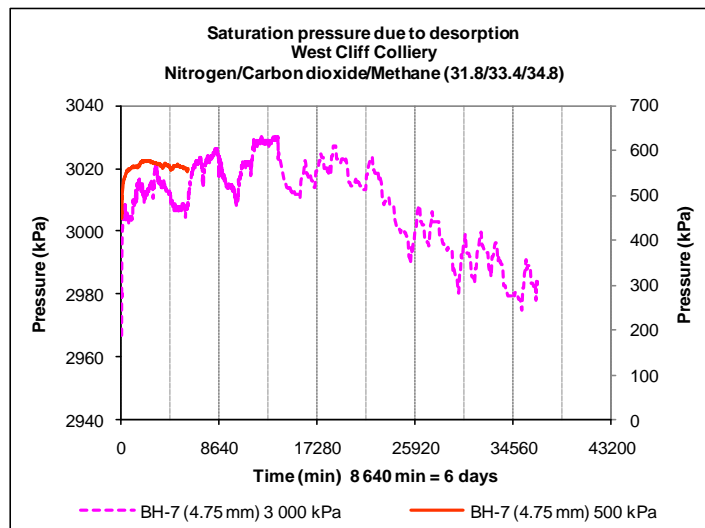


Figure VI-15 – Effect of pressure levels in TMG saturation time

The higher the pressure levels the longer the saturation time during desorption independently of the types of gas including their mixtures.

Coal particle size

Figure VI-16 shows the fluctuations in pressure over time in several core, fragmented (sizes > 1.00 mm), and powder (sizes < 1.00 mm) coal samples at about 500 kPa. All the particles reached equilibrium pressure in between 2 880 (two days) and 4 320 min (three days). The result suggests that the saturation time of ternary mixed gas during desorption seemed to be independent of particle sizes.

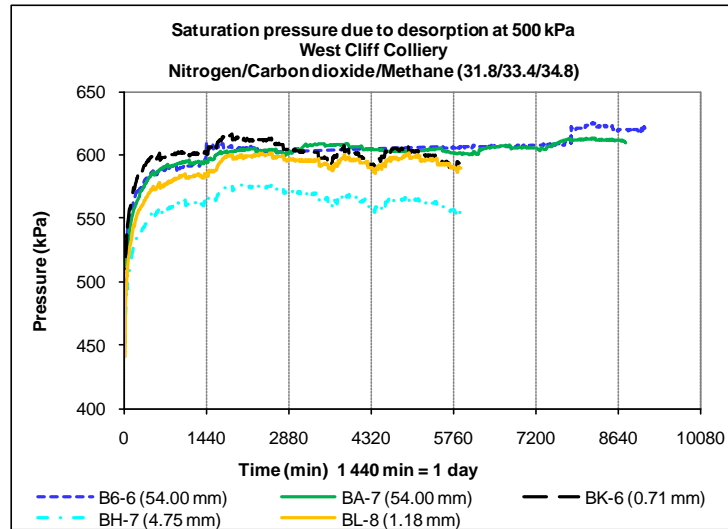


Figure VI-16 – Effect of particle sizes in TMG saturation time

Table VI-5 summarises the saturation time of the $N_2/CO_2/CH_4$ ternary mixed gas in desorption with respect to particle size.

Table VI-5 – Summary of TMG saturation time

Coal samples	Reference pressure (kPa)	Average saturation duration		Pressure status
		(min)	(days)	
BH-7 (4.75 mm) BL-8 (1.18 mm) BK-6 (0.71 mm)	3000	36,662	25.5	1
	2000	8,597	6.0	2
	1000	4,243	2.9	2
	500	5,880	4.1	2
	250	8,784	6.1	2
Atmospheric		27,019	18.8	2, 3
Total		91,186	63	
B6-6 (54.00 mm) BA-7 (54.00 mm)	3000	10,720	7.4	2
	2000	5,050	3.5	2
	1000	7,262	5.0	2
	500	8,935	6.2	2
	250	8,136	5.7	2
Atmospheric		19,692	13.7	2, 4
Total		59,795	42	
1 --> Equilibrium pressure not achieved				
2 --> At equilibrium pressure				
3 --> Three steps at atmospheric pressure				
4 --> Two steps at atmospheric pressure				

The samples of fragmented coal were run for about 92 000 min (63 days) in total during desorption. At pressures above 2 000 kPa, fluctuations in pressure during desorption were greater than the suggested 5% during the time period of about 37 000 min (26 days). The samples did not achieve equilibrium pressure above the 2 000 kPa pressure mark. This result was in coincidence with those obtained with single CO_2 and

CHAPTER SIX

Mixed gas desorption

CH₄ and their binary mixture during desorption. At pressures below 2 000 kPa the particles of fragmented coal reached equilibrium pressure at about minimum saturation time of 2 880 min (two days), although they were allowed to run longer in order to gain some understanding of the effect of time during desorption. The samples of core coal were run for about 60 000 min (42 days) and achieved equilibrium pressure over the entire range of pressure. The result suggests that during desorption the saturation time was depended on the pressure levels. At high pressure took longer than at low pressure to achieve equilibrium in pressure and composition.

Room temperature

Figure VI-17 shows the profiles of bath water and room temperature over time.

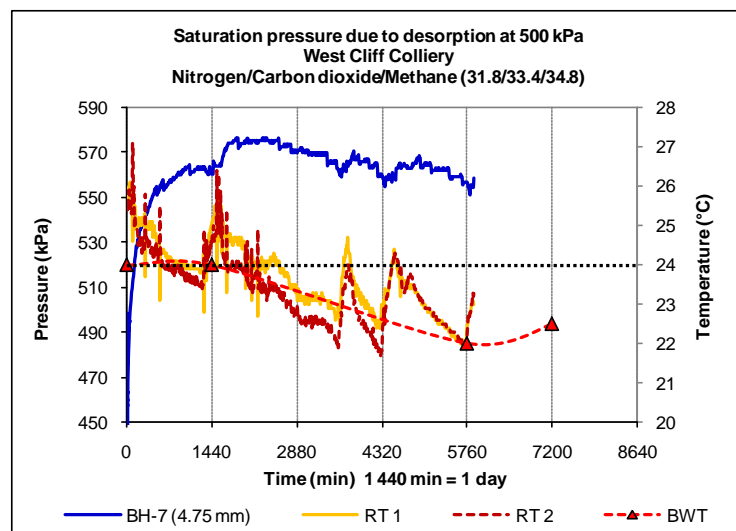


Figure VI-17 – Effect of temperature in TMG saturation time

The graph shows the effect of temperature on the behaviour of ternary mixed gas desorption. Both room and bath water temperatures fluctuated about two degrees Celsius over time which appeared to affect the pressure profile. Poor bath water temperature control could affect the pressure profile making it harder to achieve equilibrium. Low bath water temperature could be challenging to keep steady in the summer session as well as in winter.

CHAPTER SIX

Mixed gas desorption

VI.3.2.2. MIXED GAS COMPOSITION

Free compositions of N₂, CO₂, and CH₄ were measured in several samples during desorption at pressures ranging from 3 500 kPa down to atmospheric pressure. The level of free gas indicates the level of sorption for each N₂, CO₂ and CH₄ components.

Pressure level

Figure VI-18 shows the composition of N₂, CO₂, and CH₄ in sample BK-6 (0.71 mm) over pressure during desorption.

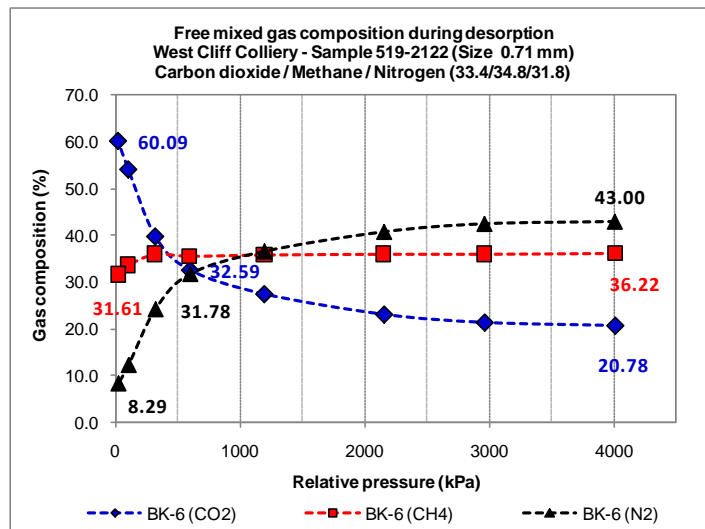


Figure VI-18 – Ternary mass gas composition during desorption

At high pressure (about 3 000 kPa), the composition of free CO₂ was the lowest (about 50% of the N₂) while the highest was N₂. The composition of free CH₄ was between CO₂ and N₂. The result indicates that at high pressure level the N₂ component was preferentially released while the CO₂ component was mainly retained by the coal. This result is in agreement with the finding with the binary CO₂/CH₄ mixed gas during desorption. The composition of free N₂ decreased consistently with the drop in pressure to reach its lowest value at atmospheric pressure. Meanwhile free CO₂ increased with pressure drop while free CH₄ suffered minor changes, especially above 300 kPa. At about the 600 kPa pressure mark the CO₂ component released most of its

CHAPTER SIX

Mixed gas desorption

adsorbed mass. Similar CO₂ components behaviour was previously reported with the binary mixed gas during desorption. The desorption process appeared to be exclusively driven by the drop in pressure. At nearly atmospheric pressure the composition of CO₂ was almost eight times greater than N₂, while the CH₄ only dropped about 5%. This result suggests that the CH₄ component was mainly released in the early stages of the desorption process. Similar CH₄ behaviour was described with the binary mixed gas in desorption. The result indicates that the CH₄ component desorbed easier, faster and mainly at high pressure. However, the CO₂ component was hardly released at high pressure and it was massively released at low pressure of about 600 kPa. The N₂ component appeared to be released gradually along with the drop in the pressure.

Coal particle size

Figure VI-19 shows the composition of free N₂ and CO₂ components versus pressure in several particle sizes (powdered, fragmented, and core coal samples) during desorption.

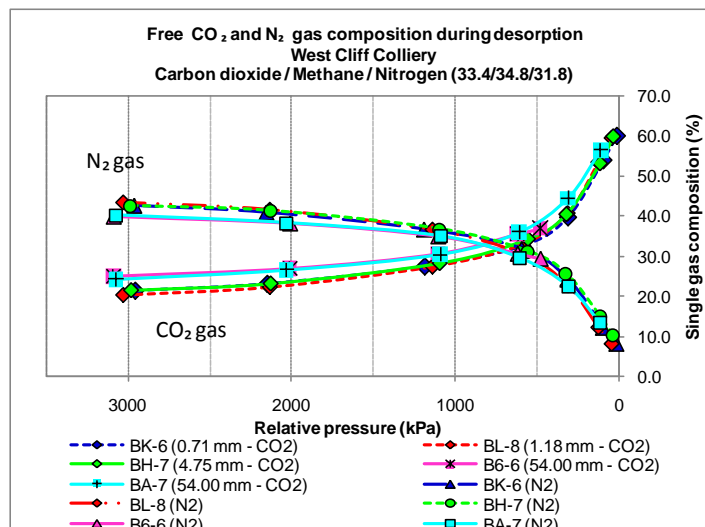


Figure VI-19 – N₂ and CO₂ gas composition over pressure

The result shows that within experimental error, the N₂ and CO₂ compositions during desorption were independent of particle size. The same is applied to the CH₄

CHAPTER SIX

Mixed gas desorption

component. This finding was in agreement with the CO₂ and CH₄ components of the binary mixed gas as well as the single CO₂ and CH₄ as they were described previously. Also, the results show that the CO₂ desorption at high pressure was slightly lower than the fragmented and powder samples in the 54.00 mm particle size. The drop in desorption of the CO₂ component at an early stage in the core coal sample could be caused in some measure by coal shrinkage due to the quicker desorption of the N₂ and CH₄ components making more difficult for CO₂ to diffuse from the matrix to the cleat. However, this coal shrinkage is expected not to be very important as it is well known that CO₂ is the larger cause of coal shrinkage.

Figure VI-20 shows the profiles of free N₂ and CO₂ compositions with time. The graph shows that the free N₂ and CO₂ compositions followed almost identical trend with time and with pressure (Figure VI-19). As it was previously suggested, the desorption process was driven by changes in pressure and as long as the pressure drops the coal will diffuse at constant rate over time.

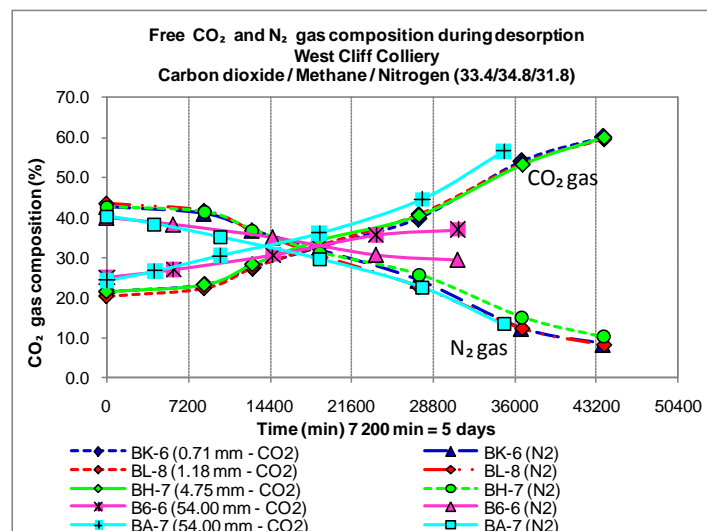


Figure VI-20 – N₂ and CO₂ gas composition over time

The graph also shows that in the first 7 200 min, the CO₂ did not change in its free composition which means very low mass release.

CHAPTER SIX

Mixed gas desorption

Gas mixture

Figure VI-21 compares both free CO_2 and CH_4 compositions during desorption as components of binary CO_2/CH_4 and ternary $\text{N}_2/\text{CO}_2/\text{CH}_4$.

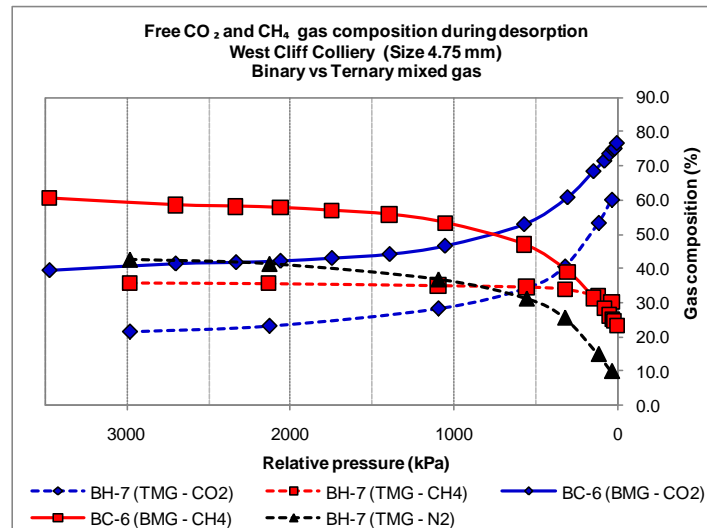


Figure VI-21 – Binary and Ternary mixed gas composition

The CO_2 composition from the binary mixture (CO_2/CH_4 ratio of 1.1) was higher (by about 28% at low pressure, and 45% at high pressure) compared to the CO_2 composition from the ternary mixture (CO_2/CH_4 ratio of 1.0). The profiles of both binary and ternary CO_2 followed an almost identical trend line over the entire range of pressure, although the binary CH_4 was higher (by about 61% at high pressure but lower by 18% at low pressure) than the ternary CH_4 . The ternary CH_4 trend line was totally different to the binary CH_4 . In the binary mixture the CH_4 component was released mainly at high pressure due to the pressure drop. In the ternary mixture however, the remained CH_4 component appeared to be gradually released over pressure and it seems to be less pressure dependent than in the binary mixture. The amount of CH_4 gradually released in the ternary mixture is very small. Most of the CH_4 component was already released at early stage. The initial gas composition did not appear to play important role in the desorption behaviour but than in the amount of mass release.

CHAPTER SIX

Mixed gas desorption

VI.3.2.3. ADSORBED MASS

Ternary mixed gas adsorbed mass

Figure VI-22 shows the profiles of mixed gas from the experimental data due to desorption and adsorption.

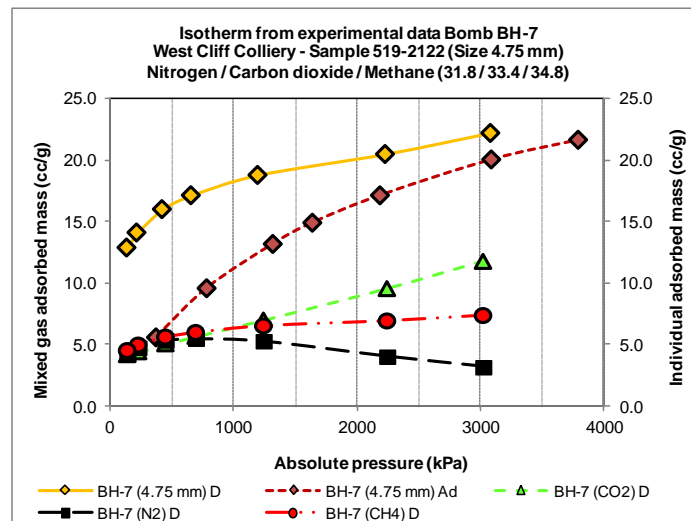


Figure VI-22 – Ternary mixed gas adsorbed mass during desorption

The adsorbed mass of the $N_2/CO_2/CH_4$ mixed gas was higher during desorption than adsorption, and the highest excess of mixed gas (about 7.3 cc/g) was attained at low pressure (at near atmospheric pressure). The result indicates gas hysteresis during desorption. Similar hysteresis was reported with the CO_2/CH_4 mixed gas and with the single N_2 , CO_2 and CH_4 . The graph also shows the profiles of N_2 , CO_2 , and CH_4 components over pressure while the test shows that at high pressure the adsorbed mass of CO_2 component was the highest in coal, N_2 was the lowest, and CH_4 was in between them. At low pressures, all the ternary mixture components appeared to retain the same amount of adsorbed mass that within experimental error it seems to be in around 4.5 (cc/g).

Figure VI-23 compares the profiles of N_2 , CO_2 , and CH_4 components of ternary mixed gas during desorption against the same components but during adsorption. The results

CHAPTER SIX

Mixed gas desorption

show a similar hysteresis as previously reported for single CO_2 and CH_4 and CO_2/CH_4 binary mixed gas due to desorption.

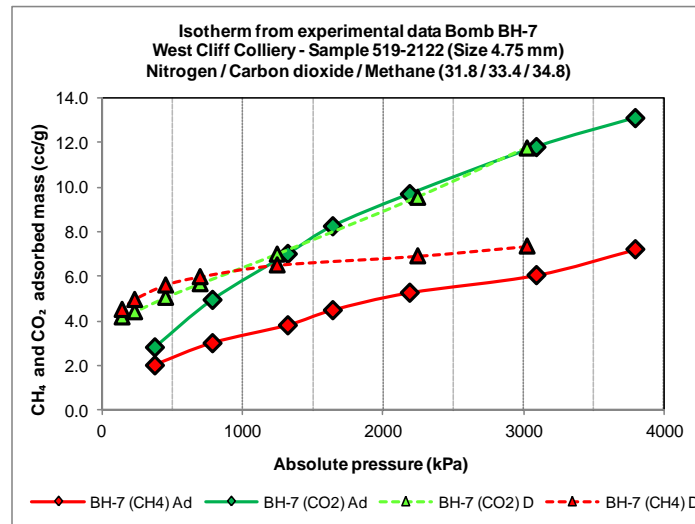


Figure VI-23 – Excess in N_2 , CO_2 and CH_4 gas content during desorption

The graph shows that the highest gas hysteresis was observed with the CH_4 component and the lowest was with CO_2 . Strong hysteresis developed between adsorption and desorption isotherms with both CO_2 and CH_4 components was reported by Crosdale (1998). This hysteresis could be caused by pore shape and capillary condensation.

Coal particle size

Figure VI-24 shows the adsorbed mass of ternary mixed gas against decreasing pressure on several samples of coal. Within experimental error, the adsorbed mass of ternary mixed gas as a whole was almost identical for all size particles over the entire pressure range. The result was in coincidence with the finding with single CO_2 , CH_4 and N_2 during both adsorption and desorption. Also, it is in agreement with the CO_2/CH_4 binary mixed in adsorption and desorption. The result shows that adsorbed gases during desorption behaved in a similar manner basically due to the changes in the desorption conditions that could be changes in pressure, volume or temperature rather than changes in particles size. The samples are very closely similar to each other

CHAPTER SIX

Mixed gas desorption

with almost identical relative density, moisture and ash content. Thus, it was expected that they would behave in similar manner under similar environmental condition in almost identical coal samples.

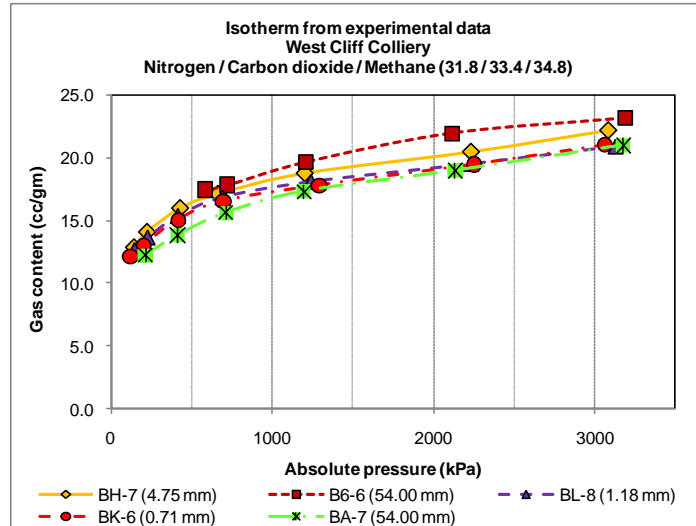


Figure VI-24 – Effect of particles size in ternary mixed gas desorption

Figure VI-25 shows the adsorbed mass of N_2 , CO_2 , and CH_4 components of the ternary mixed gas in desorption.

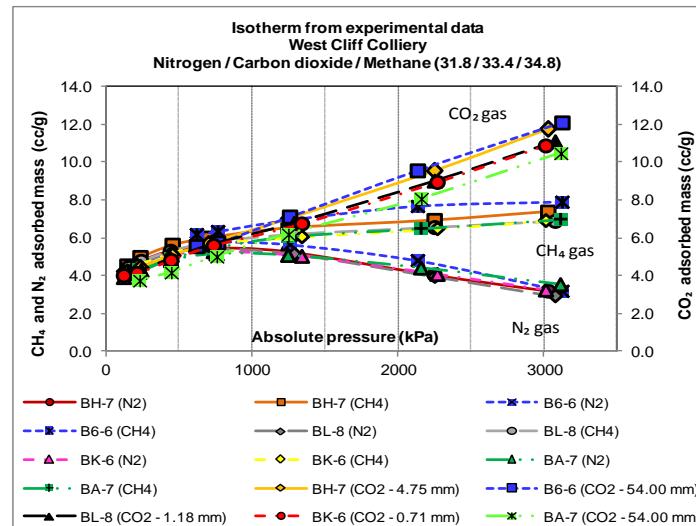


Figure VI-25 – N_2 , CO_2 and CH_4 adsorbed mass during desorption

The result shows that within experimental error the adsorbed mass of N_2 , CO_2 and CH_4 compositions were independent of particles size. At high pressure, the highest adsorbed mass was with the CO_2 component while the lowest was with the N_2

CHAPTER SIX

Mixed gas desorption

component. The N_2 and CH_4 components appeared to have lost most of their adsorbed mass at the earliest stage of the desorption process. Thus, it can be inferred that the easier gases to desorb were N_2 and CH_4 while the hardest was CO_2 . Also, the result shows that the adsorbed mass of N_2 , CO_2 and CH_4 components of the ternary mixture were poorly related to their pure adsorbed masses which was similar to the findings with the CO_2/CH_4 binary mixed gas. Clearly, the desorption process was driven by pressure drop and it was independent of the particles size.

Extended Langmuir isotherm

Figure VI-26 shows the extended Langmuir isotherms in desorption of the $N_2/CO_2/CH_4$ ternary mixed gas based on the experimental data.

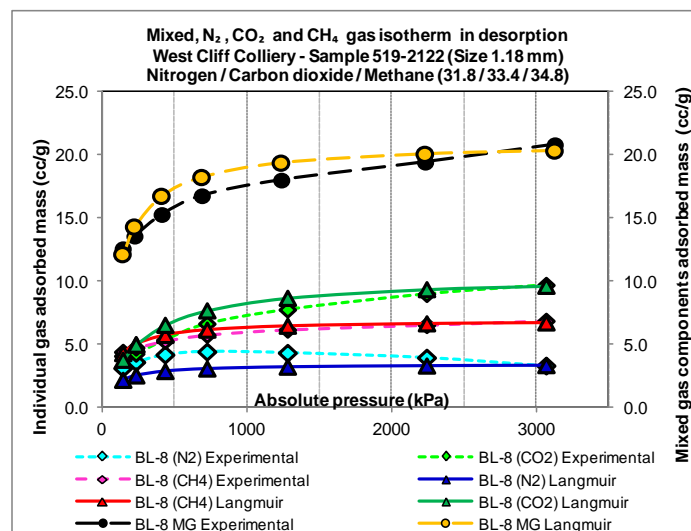


Figure VI-26 – Extended Langmuir N_2 , CO_2 and CH_4 gas isotherms

The graph shows the extended Langmuir isotherms of N_2 , CO_2 , and CH_4 components which appeared to tally reasonably well with the experimental data. However, the extended Langmuir seemed to over-estimate the adsorbed mass of the CO_2 component while the N_2 adsorbed mass appeared to be under estimated. Crosdale (1998) reported that for mixed gas isotherms there should be used a more complex model than the extended Langmuir equation. Also, Busch *et al.* (2006) reported that

CHAPTER SIX

Mixed gas desorption

“the application of the extended Langmuir model implies that separation factors are constant for all pressures because they correspond to the ratios of the Langmuir constants for the pure component isotherms”. They added that this assumption, however, is not necessarily accurate as reported by Clarkson and Bustin (2000). The extended Langmuir model generally predicts preferential CO₂ adsorption since the adsorption capacity for CO₂ is usually higher than CH₄. Therefore, the model can not represent the cases where CH₄ adsorption is preferential as reported by Crosdale (1999) and confirmed by Saghafi and Roberts (pers. comm., 2004).

Gas mixture

Figure VI-27 compares the adsorbed mass of CO₂ and CH₄ components during desorption from their binary and ternary mixed gas against the single CO₂ and CH₄.

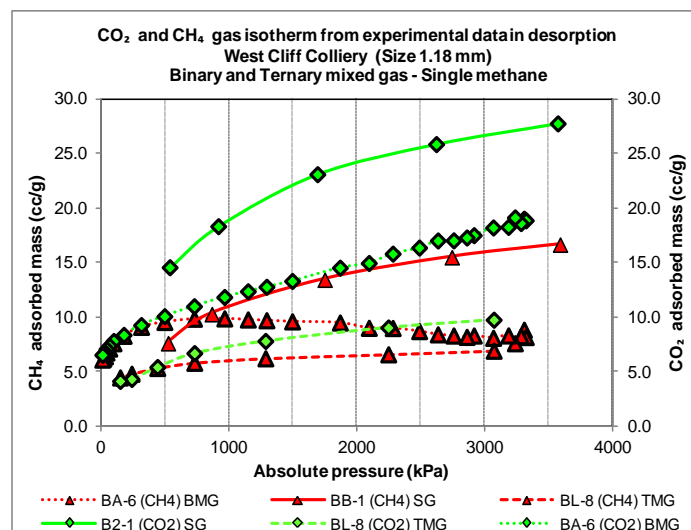


Figure VI-27 – Single CO₂ and CH₄ gas versus their gas mixture adsorbed mass

The result shows that at high pressure and for CO₂ the highest adsorbed mass in desorption was obtained with the pure CO₂ while the lowest was from its ternary mixed gas. The adsorbed mass of CO₂ from the binary mixed gas lay in between. This indicates that the maximum adsorbed mass of CO₂ in coal, as a single gas, dropped

CHAPTER SIX

Mixed gas desorption

about 40% due to a binary mixture of gas (CO_2/CH_4 ratio = 1.1), and by about 60% due to a ternary mixed gas (CO_2/CH_4 ratio = 0.96). Also, the result indicates that the adsorbed mass of the CO_2 mixed gas was poorly related to its pure CO_2 . At high pressure, the adsorbed mass of CH_4 in coal, as a single gas, was the highest while the CH_4 component from the ternary mixed gas was the lowest. The maximum adsorbed mass of CH_4 from the binary mixed gas was dropped to almost 47% in CH_4 adsorbed mass due to dilution. It appeared that adding N_2 into the mixture affected the CO_2 more than the CH_4 , which suggests that the adsorbed mass of CO_2 and CH_4 in coal depended on the composition of mixed gas. In the ternary mixture the lower the ratio of CO_2/CH_4 components (larger dilution) is, the larger the drop in adsorbed mass of the CO_2 and CH_4 components. However, the drop ratio in adsorbed mass did not appear to be directly related to their gas composition ratio.

Table VI-6 compares the ternary mixed gas adsorbed mass acting as a whole in sample BH-7 (4.75 mm) in adsorption and desorption to the N_2 , CO_2 , and CH_4 components at several levels of pressure. By analysing the mixed gas by components in desorption, the adsorbed mass of N_2 increased over the pressure drop, peaked at about 700 kPa and then decreased to atmospheric pressure.

Table VI-6 – Ternary mixed gas adsorbed mass in adsorption/desorption

Gas content (cc/gm)	Sample BH-7 (4.75 mm) - Ternary mixed gas													
	Absolute gas pressure (kPa)													
	Adsorption							Desorption						
	400	800	1300	1700	2200	3100	3800	3000	2200	1200	700	400	200	140
Mixed gas	5.8	9.1	11.9	14.0	16.1	19.4	22.7	22.2	20.5	18.8	17.1	16.0	14.1	12.9
N_2 (31.8)	1.0	1.1	1.1	1.4	1.2	1.6	2.4	3.2	4.0	5.3	5.5	5.3	4.7	4.2
CO_2 (33.4)	2.8	4.9	7.0	8.2	9.7	11.8	13.1	11.8	9.5	7.0	5.7	5.1	4.4	4.2
CH_4 (34.8)	2.0	3.0	3.8	4.5	5.3	6.0	7.2	7.4	6.9	6.5	6.0	5.6	5.0	4.5

CHAPTER SIX

Mixed gas desorption

However, the CO₂ and CH₄ components decreased all the way as the pressure dropped. By comparing the adsorbed mass at 1700 kPa (in adsorption) to the adsorbed mass at 200 kPa, the level of hysteresis achieved by the coal sample can be seen. The highest hysteresis was measured with the N₂ component.

VI.3.2.4. RESIDUAL GAS

The residual mixed gas in coal is realistically defined as the gas removed by vacuuming. For this test to be conducted, every experimental test on samples of coal was carried out at near atmospheric pressure of about 10 kPa.

Table VI-7 compares the adsorbed mass of mixed gas at atmospheric pressure against the maximum adsorbed mass of ternary mixed gas (at about 4 000 kPa in adsorption).

Table VI-7 – Residual ternary mixed gas in coal

Sample	Size (mm)	Adsorbed mass at atmospheric pressure (cc/g)	Maximum adsorbed mass (cc/g)	Residual (%)
BK-6	0.71	11.8	22.0	54%
BL-8	1.18	12.0	21.0	57%
BH-7	4.75	12.2	22.7	54%
BA-7	54.00	11.1	24.3	46%
B6-6	54.00	17.4	25.7	68%

The highest residual mixed gas was measured in sample B6-6 at 68% of its maximum adsorbed mass. Also, the lowest adsorbed mass of residual gas was measured in the 54.00 mm diameter particle. This unexpected result can be attributed to some gas leakage. Among the fragmented samples (1.00 mm < coal size < 54.00 mm) and within experimental error, the residual gas was similar in all the particle sizes suggesting that the residual was independent of the particle size. Comparatively, the residual gas in fragmented samples due to sorption of binary mixed gas was higher than residual gas with ternary mixed gas. This suggested that the higher proportion of CH₄ in the binary

CHAPTER SIX

Mixed gas desorption

gas mixture than the ternary gas mixture appeared to cause a variation in the volume of residual gas. The study suggests that increased residual mixed gas in fragmented coal was attributed to a higher proportion of CH_4 . The binary mixed gas test in desorption was run longer than the ternary mixed gas, which meant that saturation time could have also influenced the volume of residual mixed gas in coal. However, more research is needed at residual gas level.

VI.3.3. SUMMARY

Binary mixed gas

The study of the desorption characteristics of CO_2/CH_4 binary mixed gas from coal with respect to saturation indicates that:

- The saturation time depended on the level of pressure, such that the higher the pressure the longer it takes for mixed gas to saturate in desorption, and saturation time appeared to be independent of particle sizes and small changes in bath water temperature. CH_4 desorbed faster than CO_2 due to a drop in pressure. Free CO_2 and CH_4 components during desorption appeared to be independent of particle sizes over the entire range of pressure,
- The behaviour of mixed gas desorption was not disturbed by the amount of gas collected or the number of gas samples taken for composition and analysis in GC,
- The adsorbed mass of mixed gas in desorption was higher than during adsorption. At low pressure the adsorbed mass of CO_2 and CH_4 components were similar, but at high pressure there was almost twice as much CO_2 . This excess of mixed gas during desorption appeared to depend on the excess of CH_4 . The adsorbed mass of mixed gas appeared to be independent of particle sizes. The adsorbed mass of CH_4

CHAPTER SIX

Mixed gas desorption

component appeared to be pressure dependent while the CO_2 was also time dependent. The residual mass of mixed gas appeared to be influenced by the whole duration of adsorption/desorption. Larger particles appeared to retain marginally more mixed gas in coal (residual gas),

- The extended Langmuir equation appeared to model the adsorbed mass of CO_2/CH_4 mixed gas components well. However, the CO_2 and CH_4 appeared to be poorly related to their pure adsorbed mass.

Ternary mixed gas

- Ternary mixed gas saturation time in desorption depended on the level of pressure; at low pressure the samples reached equilibrium pressure at minimum saturation time but took longer at high pressure which was similar to the saturation time with binary mixed gas. Basically, the higher the pressure the longer the saturation. Saturation time appeared to be independent of particle sizes,
- At high pressure the composition of free CO_2 was the lowest and the highest was with N_2 gas. At atmospheric pressure however, the composition of free CO_2 was almost eight times higher than N_2 . The composition of free N_2 , CO_2 and CH_4 appeared to be independent of particle sizes. The composition of free N_2 and CH_4 appeared to depend on the pressure level; the lower the pressure the lower their compositions and the CO_2 component appeared to desorb slower than N_2 and CH_4 . The highest excess of mixed gas was achieved at near atmospheric pressure. For similar ratios of gas composition, the excess of gas depended on its type,
- At high pressures, there was more adsorbed mass of CO_2 component in coal than N_2 or CH_4 . The adsorbed mass of ternary mixed gas appeared to be independent of

CHAPTER SIX

Mixed gas desorption

particles size. The adsorbed mass of N_2 , CO_2 , and CH_4 components appeared to strongly depend on pressure. The adsorbed mass of N_2 recovering in desorption appeared mainly to be at the expense of CO_2 . The amount of adsorbed mass of CO_2 and CH_4 components in coal appeared to depend on the composition of mixed gas. The lower the ratio of CO_2/CH_4 the higher the drop in their adsorbed mass,

- The extended Langmuir equation can be cautiously used to estimate the adsorbed mass of ternary mixed gas in desorption; it could over or under estimate the adsorbed mass of their components,
- A higher proportion of CH_4 in ternary mixed gas appeared to cause more residual gas in fragmented coals.

VII. CHAPTER SEVEN

ENHANCING GAS DRAINAGE BY N₂ AND CO₂ INJECTION

VII.1. INTRODUCTION

CO₂ gas sequestration to recover CH₄ from coal measure rocks has been tried successfully for some time now. Injecting CO₂ strips the CH₄ from its monolayer and forces it to the surface of the coal matrix where it is captured between the fractures to be readily driven out of the coal by reducing the gas pressure. A typical site which is difficult to drain is West Cliff Mine Area 5, where some sections of the longwall panels containing CO₂ are extremely difficult to drain, despite an extensive drilling programme. It is suggested that the highly stressed and low permeability coal is preventing CO₂ from being effectively drained.

Little has been reported in literature about using N₂ to strip CO₂ from coal, particularly from underground coal mines, so a laboratory study was undertaken to examine the effect of displacing adsorbed gases in coal with injected N₂.

VII.2. EXPERIMENTAL PROCEDURE

VII.2.1. APPARATUS

To study the feasibility of removing or displacing adsorbed gas from coal with another gas, tests were carried out using an in-house built Multi-Function Outburst Research Rig (MFORR). This apparatus consists of a number of components which can be utilised for a number of investigations albeit it was initially built to study how gas influences the strength of coal. A description of this equipment, and its utilisation have been reported previously in various publications such as Lama 1995, Aziz, Hutton and Indraratna 1996 and Aziz and Ming 1999.

CHAPTER SEVEN

Enhancing gas drainage by N₂ and CO₂ injection

Figure VII-1 shows the integrated components of the MFORR. The apparatus includes:



Figure VII-1 - Multi-function outburst research rig (MFORR)

- A high pressure chamber which has a load cell for measuring the load applied to the samples of coal,
- The main apparatus support frame,
- A precision drill,
- A drill cutting collection system,
- A universal socket for loading a sample of coal vertically into the gas pressure chamber,
- Flow meters,
- A gas chromatograph (GC),
- A data acquisition system.

Figure VII-2 shows a schematic drawing of the apparatus. The pressure chamber is a rectangular prism of cast iron with a removable front and rear viewing plates. It measures 110 mm long x 110 mm wide x 140 mm deep. The viewing windows are 20 mm thick glass set into a cast iron frame. Access to the chamber is achieved by unbolting the steel frame at the front of the chamber. The chamber has packers

CHAPTER SEVEN

Enhancing gas drainage by N₂ and CO₂ injection

between the frame and the box and O-rings around the loading shaft at the top of the chamber which make it leak proof. Inside the chamber is a 40kN load cell which monitors the axial load. Two plates with locating lugs were used to hold a cylindrical specimen. Three flow meters were connected in series to measure the flow of the gas escaping from the coal inside the chamber. The individual flow rate of these meters was 0-100 mL/min, 0-2 L/min, 0-15 L/min, respectively. The composition of the discharged gases was measured by a gas chromatographer (GC).

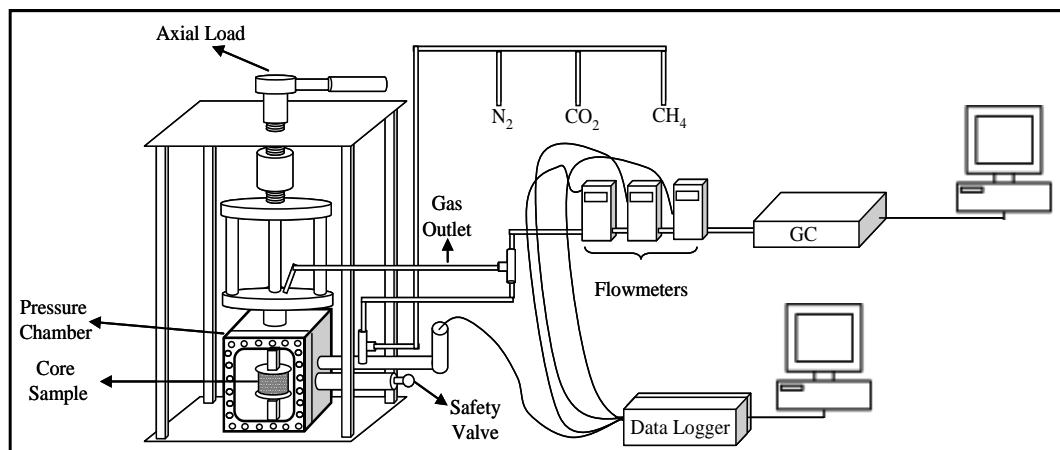


Figure VII-2 – Schematic drawing of MFORR

Thus the main features of the MFORR to study coal gas sorption include:

- Application of stress,
- Application of gas suction,
- Gas pressure confinement (gas flooding),
- Sample strain measurement, and
- Gas flow rate measurement.

VII.2.2. SAMPLE PREPARATION

Samples for this study were obtained from the Bulli Seam at West Cliff Colliery, Area 5. Bulk samples were taken from different locations along longwall panel 519, sealed in plastic bags and transported to the University of Wollongong mine gas laboratory.

CHAPTER SEVEN

Enhancing gas drainage by N₂ and CO₂ injection

Inside the laboratory the lumps of coal were cut into regular and manageable sizes and immersed in water to minimise the effect of adverse climatic conditions.

Figure VII-3 shows core coal samples 54 mm diameter by 50 mm high, already prepared for testing, and the graph showing the pressure chamber already holding a specimen.

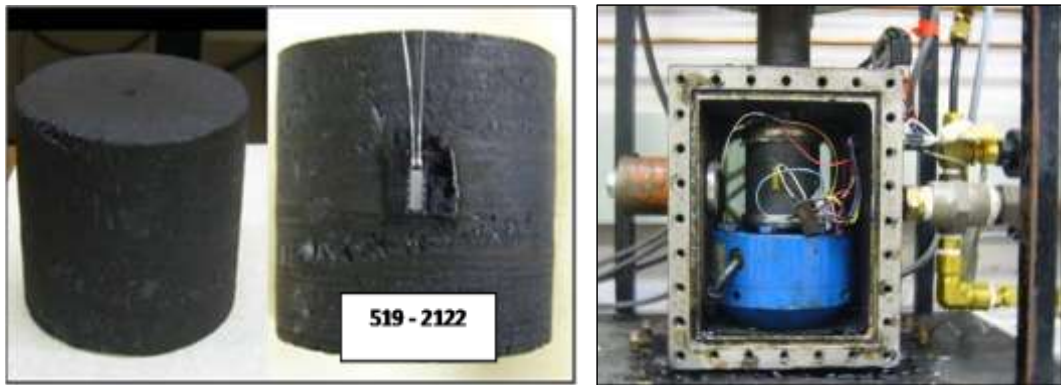


Figure VII-3 – Core coal sample

The samples of coal were prepared according to the International standard for rock core sample preparation and testing (ISRM, 1981). A 2 mm diameter hole was then drilled through each sample to drain the gas flowing through the core. Before the sorption test, each sample was fitted with axial and circumferential strain gauges to monitor volumetric changes during gas sorption and desorption.

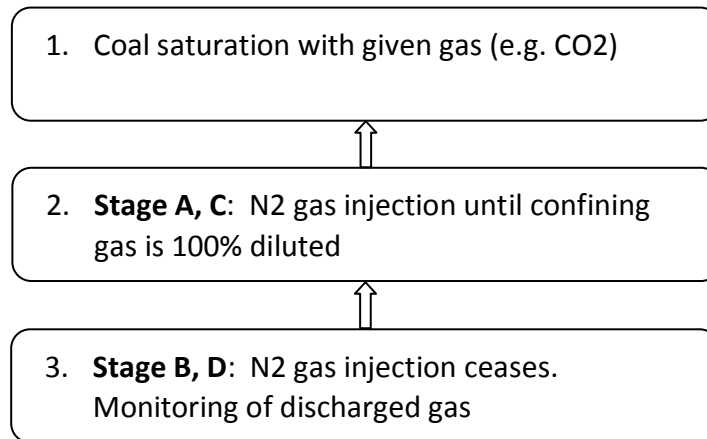
VII.2.3. TESTING PROCEDURE

Each sample used for the injection study was placed inside the high pressure chamber of the MFORR and sealed tight. The general procedure was to saturate the sample with a specific gas (e.g. CH₄) and then recharge it by injecting N₂. Three types of gas were used for the initial saturation phase, a mixture of CO₂/CH₄ (52/48), and CO₂ and CH₄, respectively. The experimental procedure was carried out in two stages, referred to A, B, C and D. In Stage A or C, N₂ was injected into the pressure chamber with a gas initially adsorbed at 3 200 kPa of pressure. The N₂ was maintained for a predetermined

CHAPTER SEVEN

Enhancing gas drainage by N₂ and CO₂ injection

period until the confining N₂ concentration measured by the GC was almost 100%. As a result of the N₂, the initial mixture of gas was reduced to almost zero. Stage B or D commenced when no more N₂ was injected.



The gas discharged (which was part free gas as a confining gas, and part adsorbed gas) from the samples was monitored for its rate of flow and composition. Every test was carried out under strict environmental and laboratory conditions and the room was maintained at a constant 22 °C throughout. This controlled environment was considered useful for producing coal bed CH₄ gas, CO₂ sequestration research, and for controlling outbursts of gas in coal mines.

VII.3. EXPERIMENTAL RESULT AND DISCUSSION

VII.3.1. GAS COMPOSITION

Before the N₂ gas injection test, a series of tests were carried out to examine the adsorption and desorption of the binary mixed gas (CO₂/CH₄) in coal subjected to axial and lateral confining pressures. Accordingly the following laboratory tests were carried out:

- Adsorption/desorption characteristics of binary CO₂/CH₄ mixed gas in coal (Reference test),

CHAPTER SEVEN

Enhancing gas drainage by N₂ and CO₂ injection

- Displacement characteristics of adsorbed binary mixed gases with N₂ gas injection (Binary mixed gas test),
- Displacement characteristics of adsorbed CO₂ gas with N₂ gas injection (CO₂ gas test), and
- Displacement characteristics of adsorbed CH₄ gas with N₂ gas injection (CH₄ gas test).

VII.3.1.1. REFERENCE TEST

Saturation time

During the first stage of this adsorption/desorption test, known as the reference test, the sample was charged with mixed gas up to 3 200 kPa. The coal was saturation by flooding the pressure chamber with mixed gas to the required pressure.

Figure VII-4 shows the fluctuations in pressure over a period of around 7 200 min, from the first level down to the final level of about 3 000 kPa.

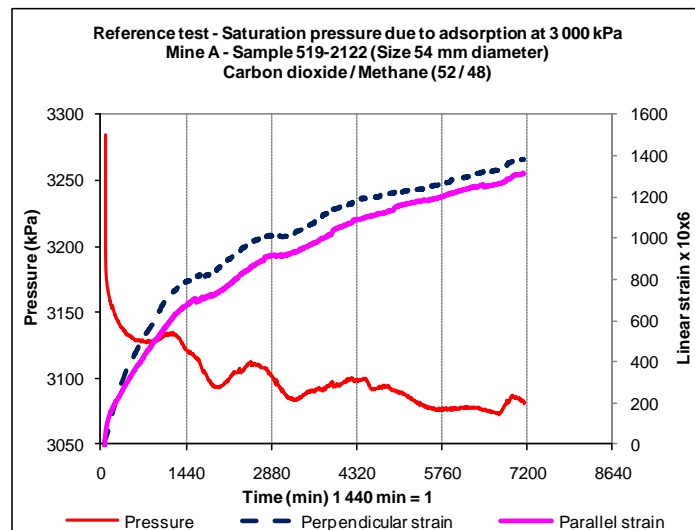


Figure VII-4 – Pressure drop profile during adsorption

The initial composition of CO₂/CH₄ was in a ratio of 52/48. The drop in pressure was typical of the 54.00 mm diameter core coal pressure profile during mixed gas adsorption. The saturation level (pressure fluctuations < 5%) was monitored for the

CHAPTER SEVEN

Enhancing gas drainage by N₂ and CO₂ injection

period suggested in Chapter 4, section 3.1.1 (Mixed gas saturation time). The graph also shows fluctuations in gas pressure over the period of pressurisation and saturation. This intermittent movement of gas in and out of the structure of the coal indicates that the sample was in a continuous state of adsorption and desorption, while the amplitude of adsorption was reduced as the coal approached full saturation. The results suggest that the amplitude of fluctuation in the adsorption profile showed how far the gas molecules are moving from the macro to the micro- pores in the coal structure. In the first step down of sorption shown in the graph (about 1 440 min), the sample was almost fully saturated mainly with CO₂ as was suggested in Chapter 4, section 3.1.2. The profiles of volumetric strain (swelling) confirmed that the sample never stopped adsorbing. In the following fluctuations the amount of CH₄ adsorbed gradually increased whereas the CO₂ decreased until both gases almost reached the same composition. However, to equalise the proportions of gases sorbed into the coal, it was necessary to run the experiment over longer periods. Thus, time was the deciding factor for the coal to adsorb CH₄ in the same amount as CO₂.

Temperature

Figure VII-5 shows how room temperature affected the pressure of the confining gas during the process of equilibrium. The graph shows that the room temperatures RT 1 and RT 2 rose from 22 to almost 27 °C (5 °C), although the average temperature fluctuated from 23 to 25 °C (2 °C). The graph also shows that the profile of the drop in pressure appeared to follow that of the room temperature profiles, which suggested that the level of equilibrium appeared to depend on the room temperatures such that as it decreased the equilibrium pressure decreased.

CHAPTER SEVEN

Enhancing gas drainage by N₂ and CO₂ injection

Similar results were previously reported in Chapter 4, section 3.1.1 (Mixed gas saturation time).

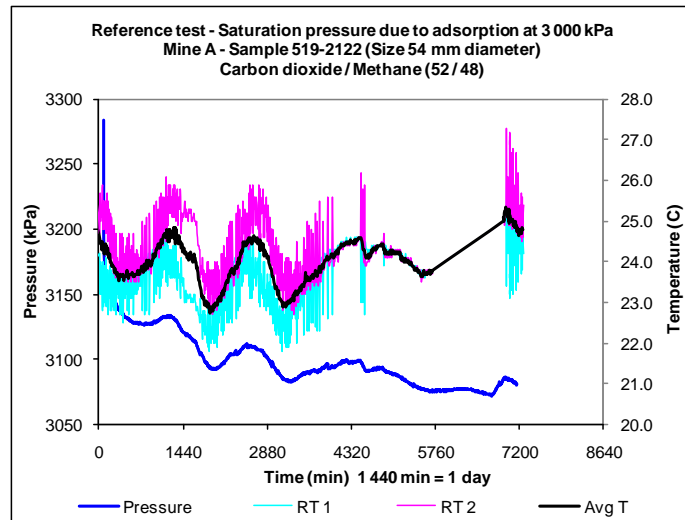


Figure VII-5 – Effect of temperature on pressure drop profile

The changes in room temperature affected gas adsorption and desorption by varying the equilibrium pressure in duration and value.

Gas composition

Figure VII-6 shows the changes in the composition of CO₂ and CH₄ over time. In the early stages the released gas was mostly due to pressure in the confining chamber while the latter part was a combination of both the confining chamber gas and desorbed gas from the sample. The results suggest that the initial ratio of 52/48 (CO₂/CH₄) changed to 51/49 during the first five days of saturation and when measured just before the confining gas was released, which indicates a differential component of adsorption in coal. The composition of CH₄ was marginally higher than the CO₂ during the early stages of adsorption, which was attributed to the preferential adsorption of CO₂ in coal (CO₂ affinity to coal) and the relatively short adsorption time. However, the percentages of mixed gas returned to the original 52/48 level after some 30 min of confining pressure when the bomb was dropped from 3200kPa to around 500 kPa. The

CHAPTER SEVEN

Enhancing gas drainage by N₂ and CO₂ injection

composition of mixed gas then reached a ratio of 56/44 (CO₂/CH₄) when the pressure in the chamber was almost at atmospheric level.

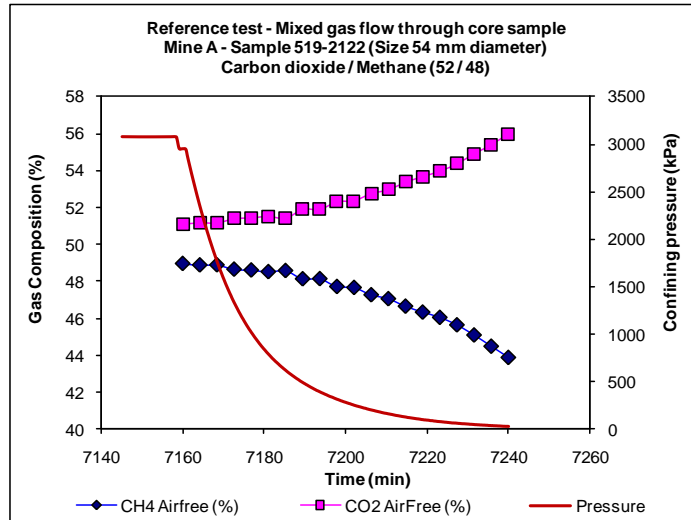


Figure VII-6 – CO₂ and CH₄ composition during desorption

Table VII-1 shows the CO₂ and CH₄ at the start and end of the test. The results indicate that at the initial stage of desorption the composition of desorbed CH₄ was greater than the desorbed CO₂. However, at the end of the test the composition of adsorbed CO₂ and CH₄ had both changed by about 7%.

Table VII-1 – CO₂ and CH₄ composition without N₂ injection

Reference test - Mixed gas				
% Desorbed gas			Period	CO ₂ /CH ₄ ratio
CO ₂	N ₂	CH ₄		
48.93%	-	51.09%	Start test	0.96
56.01%	-	43.88%	End test	1.28
7.08%	-	-7.21%	Change	

The composition measured at the GC was the sum of the confined and adsorbed gas. Confined gas refers to a combination of free confining chamber gas, and free gas in the cleat and fracture systems due to the flooded confined gas. At this short level of duration saturation (about five days) it was difficult to accurately predict the composition of adsorbed and free gases when they were released. Commonly, the gas measured at high pressure at the GC inlet was mostly composed of free gases that

CHAPTER SEVEN

Enhancing gas drainage by N₂ and CO₂ injection

passed through the sample of coal. Most of the desorbed gas (from openings and matrices) was likely to be measured at low pressure because it took longer to escape, so whether the 7% change in composition was due to desorption or the free gas that passed through the sample was not clear.

Gas flow

Figure VII-7 shows the various flow rates and declining gas pressure over time. The graph reveals that the movement of gas depended on a strong gas pressure. Both the discharge flow rate and declining pressure occurred at higher rates, particularly during the first 10 min of desorption where the pressure dropped to almost a third of its value. This appeared to happen because the sample of coal had many fractures. Similar results happened to other samples from the same location.

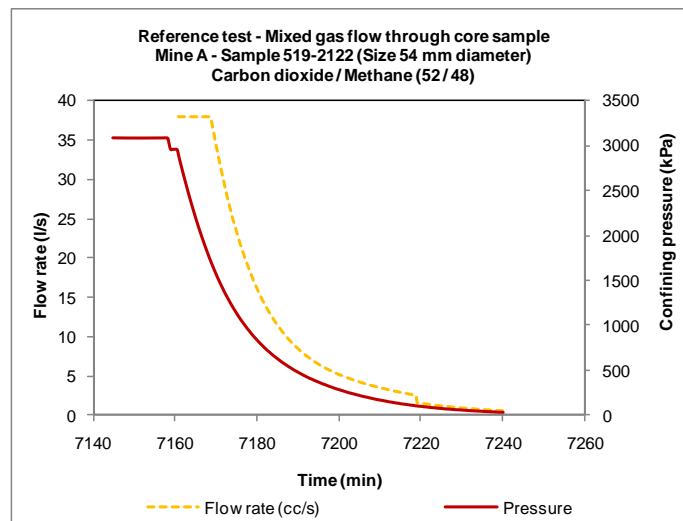


Figure VII-7 – Gas flow during desorption

At 3 200 kPa the maximum flow of gas through the sample was about 0.04 L/s (3.3 m³/D) and the maximum permeability of the cleat was approximately 11.7 mD.

VII.3.1.2. BINARY MIXED GAS

Saturation time

CHAPTER SEVEN

Enhancing gas drainage by N₂ and CO₂ injection

Figure VII-8 shows the results of the N₂ injection test carried out on a sample initially saturated with binary CO₂/CH₄ (52/48) gas. The saturation time for this sample was approximately 7 630 min (about 5.3 days). This period of charging was carried out just before the N₂ was injected.

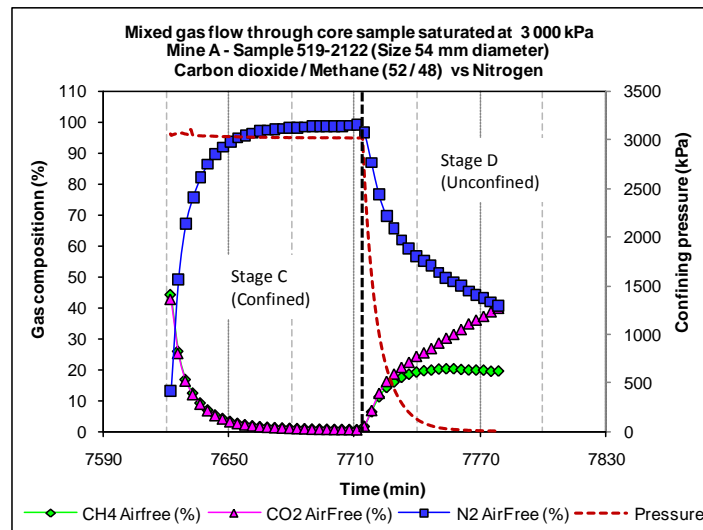


Figure VII-8 – Binary CO₂/CH₄ composition during saturation

As seen in the graph, as soon as N₂ was injected into the chamber in Stage C, its composition began to increase sharply. This rate of increase in N₂ occurred at the expense of the mixed CO₂/CH₄, and a near zero reduction in the composition of CO₂/CH₄ occurred 30 min after injection of N₂. At the same time the latter gas concentration increased to almost 100%. The decline in the rate of mixed gas was almost a mirror image of the increase in injected N₂, and as a result the combined gas pressure remained constant at approximately 3 200 kPa.

Gas composition

Figure VII-9 shows the profile of diluted CO₂/CH₄ over time. The results suggest that ratio at which this dilution occurred, when measured every fourth minute during the first 90 min of N₂ injection in Stage C, was marginally smaller than the initial 52/48 ratio. In the graph the CO₂ and CH₄ were plotted as free of air and N₂. The drop in the

CHAPTER SEVEN

Enhancing gas drainage by N₂ and CO₂ injection

ratio of CO₂/CH₄ occurred because the CO₂ was adsorbed into the coal during the early stage of saturation, as stated previously in Chapter 4, section 3.1.1 (Mixed gas saturation time).

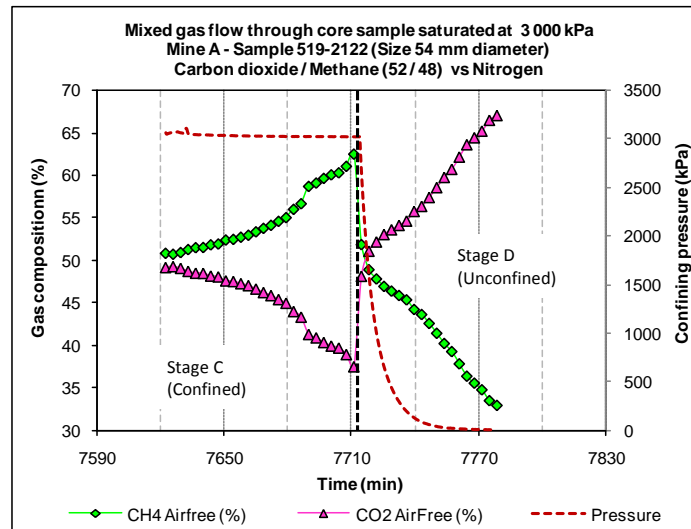


Figure VII-9 – CO₂ and CH₄ composition over time

The released gas was mostly free or confining gas. Once the injection of N₂ ceased the CO₂/CH₄ mixture gradually began to reappear, marking the beginning of stage D. The confining gas pressure dropped to almost zero some 40 min after the injection stopped. A comparison between the profiles of CO₂/CH₄ during stage C with the CO₂/CH₄ from the reference test (Figure VII-6) during stage A shows that when acting individually, each gas behaved quite differently in both cases. At unconfined stage D however, the CO₂/CH₄ acted as expected (stage B from reference test).

Table VII-2 summarises the results of the CO₂/CH₄ composition stemming from the injection of N₂. The results indicate that during the same period the level of CO₂/CH₄ increased and some 20 min later the proportion of discharged gas diverged with the CO₂ and almost doubled the discharge of CH₄. After approximately 30 min the CH₄ stabilised at about 19.5 %, while the CO₂ increased to almost 40.8%. The desorbed CO₂

CHAPTER SEVEN

Enhancing gas drainage by N₂ and CO₂ injection

increased by almost 16.2%, which was almost twice that obtained in the reference test (Table VII-1 - CO₂ and CH₄ without N₂ injection).

Table VII-2 - CO₂ and CH₄ composition with N₂ injection

CO ₂ /CH ₄ mixed gas and N ₂ injection					
% Desorbed			Period	Status	CO ₂ /CH ₄ ratio
CO ₂	N ₂	CH ₄			
44.1%	13.2%	42.6%	Start test		
50.9%		49.1%		N ₂ free	1.04
39.7%	40.8%	19.5%	End test		
67.1%		32.9%		N ₂ free	2.04
16.2%		-16.2%	Change		

Since the coal retained some gas in its matrices, the results suggest that these ratios could change over longer periods of testing. It is worth remembering that in stage C the CO₂ and CH₄ measured at the GC were mainly from free gases with a small amount from desorbed gases. In stage D however it was supposed that the measured CO₂ and CH₄ were mainly from the desorbed gases. Also, Figure VII-8 suggests that the CH₄ was due to molecules desorbing at a steady rate from the coal matrices. However, the profile of CO₂ appeared more likely to be due to molecules desorbing from openings, cleats, cracks, and fissures, which is where adsorbed gas is expected after a short period of adsorption. The profile of desorbed N₂ appeared to be due mostly to the free molecules passing through the sample and decreasing with the pressure. The results suggest that the N₂ appeared to displace the CO₂ due to an improvement in the concentration gradient, although the CH₄ appeared less affected by the injection of N₂ for the same reason. The study suggests that during CO₂/CH₄ adsorption most of the CH₄ was adsorbed in the coal matrices, while the CO₂ was preferably adsorbed in the macro pores with a small amount being stored in matrices because of the so called

CHAPTER SEVEN

Enhancing gas drainage by N₂ and CO₂ injection

affinity between CO₂ and coal. Thus, the CO₂ prevailed over the CH₄ in obtaining the sweetest spots available on the macro pores.

VII.3.1.3. CARBON DIOXIDE

Figure VII-10 shows the results of the N₂ injection test carried out on sample of coal saturated with CO₂. The saturation time of this sample was around 15 550 min (10.8 days). Afterwards it was injected with N₂ for about 110 min.

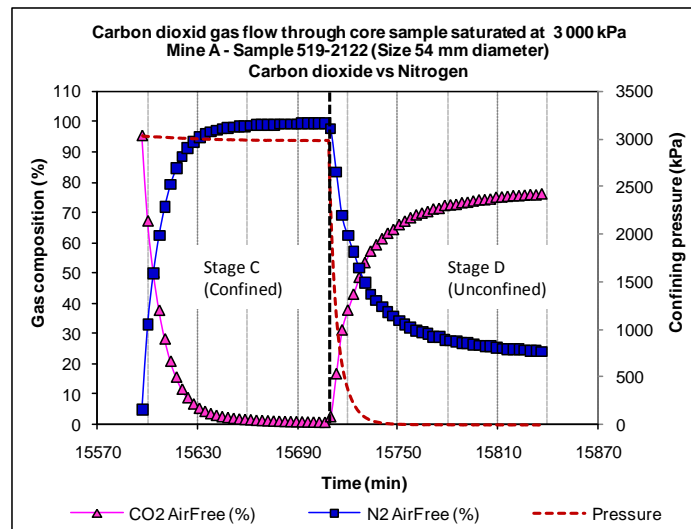


Figure VII-10 - CO₂ composition during N₂ injection

During the second phase (stage D), starting from 15 710 min, the results indicate that the CO₂ increased sharply from 0 to 50% in 20 min, at the same rate that the N₂ dropped. Thus, the 50 % composition point for the gas was achieved at the 15 730 min mark. The level of CO₂ from the gas flowing through the GC approached 75% after 215 min of GC analysis and testing, which suggests that the injection of N₂ gas appeared to have a significant influence on the displacement and removal of CO₂ from coal. During the early phase of stage D, the N₂ discharged was mostly free confining gas. Later on, and after the 15 800 minute, the small amount of N₂ released appeared to be mostly adsorbed gas. These results also suggest that any amount of released CO₂ appeared to be desorbed gas because the initially pure, free CO₂ confining gas was mostly diluted

CHAPTER SEVEN

Enhancing gas drainage by N₂ and CO₂ injection

during the N₂ injection process (Stage C) and it passed through the sample of coal. At about the 3 200 kPa level, the maximum amount of CO₂ flowing through the sample was about 0.04 L/s (3.3 m³/D) with a maximum cleat permeability of around 3.3 mD. This finding has a significant bearing on solving the drainage difficulties experienced at West Cliff Colliery Area 5, which has difficulty in draining the CO₂ rich zones.

VII.3.1.4. METHANE TEST

Figure VII-11 shows the results of the N₂ injection test carried out on the 54.00 mm diameter sample of core coal saturated with CH₄ for about 5 760 min (4.0 days). At about 3 200 kPa the maximum amount of CH₄ flowing through the sample was about 0.04 L/s (3.3 m³/D) with a maximum cleat permeability of about 2.5 mD. After saturation with CH₄, N₂ was injected for about 150 min. The results suggest that the removal of CH₄ was at best 20% after 90 min of testing. This composition of CH₄ was similar to that measured with the binary CO₂/CH₄ test from section 3.1.2 (Binary mixed gas test). These results from the enhancement of CH₄ desorption by injection of N₂ gas were insufficient, and appeared to be due to the short CH₄ saturation time.

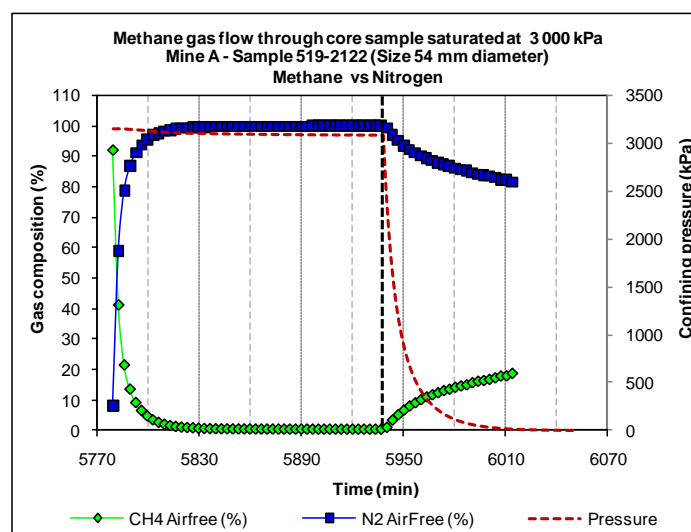


Figure VII-11 – CH₄ composition during N₂ injection

CHAPTER SEVEN

Enhancing gas drainage by N₂ and CO₂ injection

In any case, previous findings in either Chapter 4 or 6 suggest that the behaviour of CH₄ was not affected by the N₂ during the ternary N₂/CO₂/CH₄ mixed gas adsorption or/and desorption. Hence, using N₂ to recover CH₄ does not appear to be a viable method in the current laboratory environment.

VII.3.2. VOLUMETRIC CHANGES IN COAL

Gas is contained in coal either as free gas, within the cracks, fissures, and pores, or adsorbed in the coal matrices and in the interior surfaces of fissures and pores. Removing this gas is likely to cause volumetric changes such that shrinking or swelling will occur depending the way the adsorbed gas is displaced or removed. A laboratory study was undertaken to examine these volumetric changes as a result of displacing the adsorbed gases with N₂ injection. The adsorption and desorption characteristics of CO₂, CH₄, and the binary CO₂/CH₄ in coal by an injection of N₂ were studied with respect to the volumetric changes. The confining pressure in the gas chamber was maintained at about 3 200 kPa, thus creating a confining condition with lateral and vertical pressure acting on the sample of about a 4:1 to 2:1 ratio. The maximum pressure ratio was marginally greater than the stress in the ground in the Bulli Seam of the Southern coalfields of NSW. The following laboratory tests were carried out:

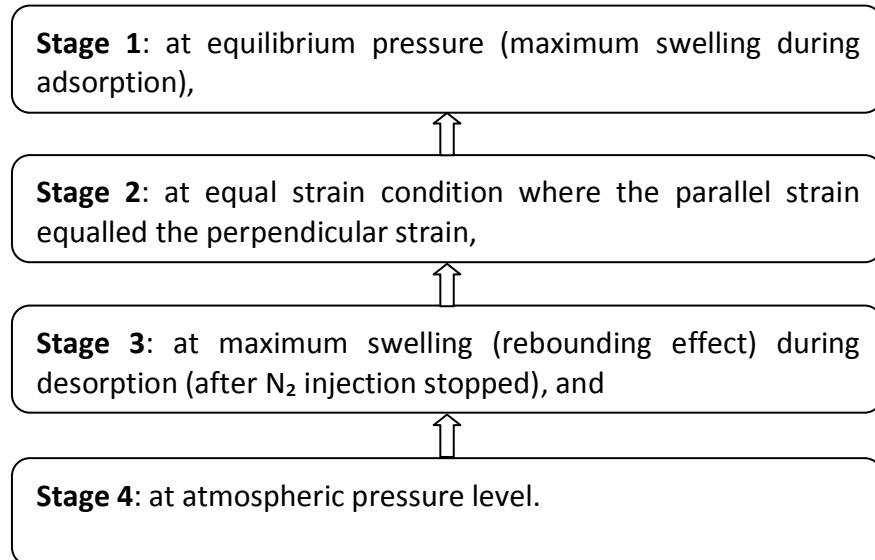
- Displacement characteristics of adsorbed mixed gases. Swelling and shrinkage characteristics of coal (reference test),
- Displacement characteristics of adsorbed mixed gases with N₂ injection. Swelling and shrinkage characteristics of coal,
- Displacement characteristics of adsorbed CO₂ with N₂ injection. Swelling and shrinkage characteristics of coal, and

CHAPTER SEVEN

Enhancing gas drainage by N₂ and CO₂ injection

- Displacement characteristics of adsorbed CH₄ with N₂ injection. Swelling and shrinkage characteristics of coal.

The tests were analysed at four different stages:



VII.3.2.1. REFERENCE TEST

The strain on the sample of coal was carried out under an initial axial load of 300 kg. This was equivalent to a stress level of 1.3 MPa acting perpendicular to the 54 mm diameter sample. The ratio of vertical to lateral pressure was 1:2.4. This was considered to be similar to the current ratio of stress in the Bulli seam.

Figure VII-12 shows the decrease in the parallel and perpendicular strains to the bedding planes, which indicated that the sample shrank volumetrically as it began to desorb its gas. The slope of the strain perpendicular to the bedding decreased almost linearly, basically due to gas desorption. This was not the case when the strain was parallel to the bedding, which actually increased while the confining pressure was reduced. Furthermore, decreases in the axial load, confining pressure, and perpendicular strain indicated that gas was desorbing from the coal. These volumetric changes occurred especially during the first 30 min of gas pressure drop, and until the

CHAPTER SEVEN

Enhancing gas drainage by N₂ and CO₂ injection

7 190 min mark (the confining pressure dropped from around 3 000 kPa to 500 kPa) which is the point where the parallel strain in desorption was at its maximum.

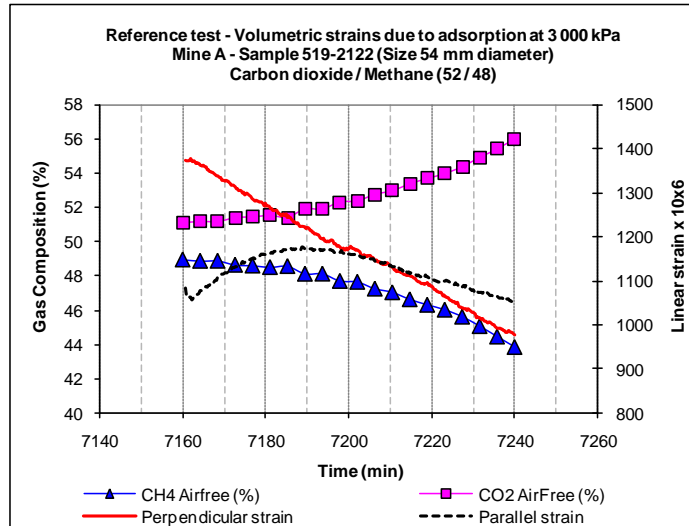


Figure VII-12 – Perpendicular and parallel strains (Reference test)

After this point, the matrix desorption was significant with the confining pressure almost zero. Thus both perpendicular and parallel strains decreased due to the coal shrinking probably to the level of its molecular structure.

VII.3.2.2. BINARY MIXED GAS TEST

An initial axial load of 1.96 kN (200 kg) was applied to the sample saturated with CO₂/CH₄. The axial load was equivalent to a stress level of 1.3 MPa acting perpendicular to the layers of the 54 mm diameter sample. The ratio of vertical to the lateral pressure was 1:2.4.

Figure VII-13 shows the profiles of perpendicular and parallel strain over time. The test was performed in two stages, first the sample was flooded with a 52/48 mixture of CO₂ and CH₄ to a pressure of about 3 300 kPa and left to saturate for more than 7 200 min (five days) until it reached the final and intended equilibrium pressure of about 3 080 kPa. The profiles of the perpendicular and parallel strain clearly show the coal swelling. In adsorption the perpendicular strain was greater than the strain parallel to the

CHAPTER SEVEN

Enhancing gas drainage by N₂ and CO₂ injection

bedding plane. At the state of equilibrium the maximum perpendicular strain was about 2 200 ppm and the parallel strain was about 1 500 ppm (1 ppm = 1 part in 10⁰⁶), a ratio of about 1.5:1. Before injecting N₂ the sample was placed under a 2.9 kN (300 kg) axial load.

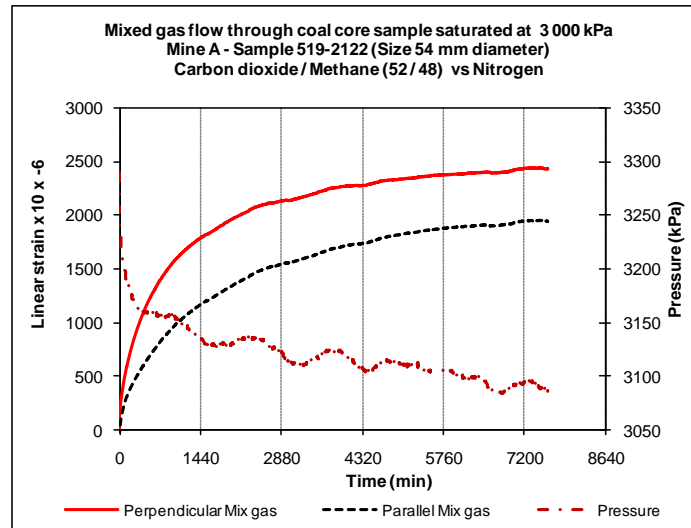


Figure VII-13 – Perpendicular and parallel strains (CO₂/CH₄ test)

At an equilibrium pressure of about 3 080 kPa the final axial load settled at about 3.58 kN (365 kg), which was almost 20% greater than the load applied initially. This increase in axial load was considered to be caused by the adsorption of gas from the coal. The second step was to inject N₂ into the gas chamber and maintain it at a constant 3 000 kPa. This was known as phase C of the N₂ injection into the gas chamber.

Figure VII-14 shows the profile of the axial load after N₂ had been injected into the gas chamber. The axial load followed the same trend as the perpendicular and parallel strain profiles, which indicated coal shrinkage. The axial load exerted on the sample was monitored every 5 min to measure the adsorption/desorption of gas with and without confining pressure.

Table VII-3 summarized the coal strains and stresses at four different stages of pressure in the chamber (S1, S2, S3 and S4). In general, the perpendicular strains

CHAPTER SEVEN

Enhancing gas drainage by N₂ and CO₂ injection

showed a decreasing trend due to a drop in pressure, and so too did the parallel strain.

This drop in pressure had a strong influence on the perpendicular strain.

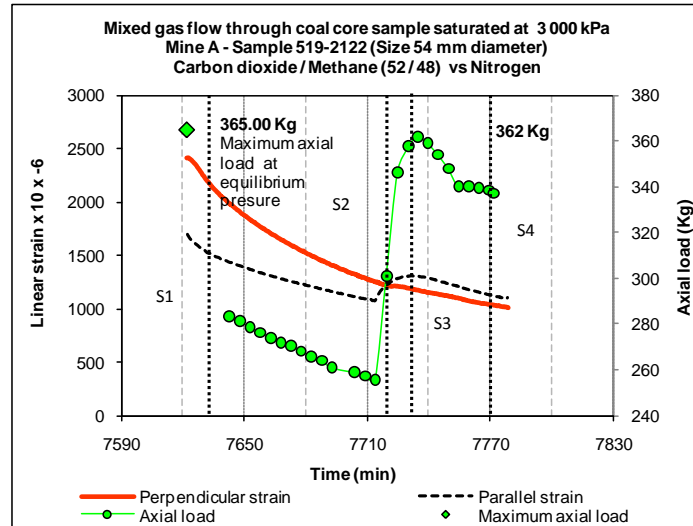


Figure VII-14 – Axial load profile (CO₂/CH₄ test)

The perpendicular strain was always expected to be greater than the parallel strain in a tri-axial or pseudo tri-axial environment, particularly during adsorption. However, during desorption the confining pressure played a dominant role retaining the lateral strain.

Table VII-3 – Summary of strain and stress (CO₂/CH₄ test)

Mixed gas and Nitrogen injection								
Stage	Time (min)	Axial load (kg)	Stress			Strain		
			Lateral/Axial ratio	Axial (MPa)	Lateral (MPa)	Axial/Lateral ratio	Axial ppm (10x-6)	Lateral ppm (10x-6)
S1	7631.50	365.0	1.95	1.59	3.1000	1.44	2216	1535
S2	7719.50	301.0	1.03	1.31	1.3600	1.00	1217	1222
S3	7730.50	357.6	0.23	1.56	0.3600	0.91	1192	1306
S4	7769.75	338.5	0.00	1.48	0.0013	0.92	1039	1126

In stage 1 (S1), known as the initial equilibrium stage, the results indicate that the perpendicular strain was greater than the parallel strain by about 45%. At pressures equal to atmospheric (stages S3 and S4) however, the parallel strain became marginally greater than the perpendicular. Stage S2 defined the point where the axial load reached its minimum value, the point immediately before the injection of N₂ stopped.

CHAPTER SEVEN

Enhancing gas drainage by N₂ and CO₂ injection

At this point the axial load decreased from its maximum value by almost 18% (i.e. from 365 kg to almost 300 kg), which suggested that injecting N₂ appeared to relax the coal somewhat. This level of relaxation was likely to depend of the duration of N₂ injection, such that the longer the duration the smaller the axial load; in other words, the (coal) structure relaxed even more. At about the 7 720 minute mark, the line on the parallel strain graph crossed over the perpendicular strain parallel to a bedding stress of around 1.36 MPa and at lateral/perpendicular stress ratio of about 1.0. A likely explanation of this increase in the parallel strain could stem from the drop in lateral confining pressure which made it unable to counterbalance lateral deformation in the coal. The results also suggest that the drop in axial load appeared to have no effect on the parallel strain. In stages S3 and S4, although the axial load was greater than the initial load, the perpendicular strain decreased rather than increased, probably due to the structure of the coal readjusting. The results also suggest that the previously adsorbed gases in the coal matrices appeared to produce uni-directional swelling as parallel strain. The lack of lateral gas pressure may have contributed to an increase in lateral strain. Note that after 100 min the N₂ injection was stopped and the axial load increased to 3.55 kN (362 kg), almost the same applied axial load, at a confining pressure of about 3 100 kPa (stage S1). At this point, however, the remaining confining gas pressure was only about 200 kPa. It is also worth mentioning that there was a differential confinement pressure/stress during this phase, known as phase D, when the N₂ injection had stopped completely and the coal sample was no longer subjected to consistent differential lateral/axial pressure. Equal vertical and lateral pressure confinements of about 1.3 MPa occurred over a very short period of time at around

CHAPTER SEVEN

Enhancing gas drainage by N₂ and CO₂ injection

the 7 720 minute mark (stage S2). At the end of the test the perpendicular and parallel strains were 1 000 ppm and 1 100 ppm respectively. Thus, despite the increase in axial load from 2.95 kN (300 kg) to 3.5 kN (357 kg), the parallel strain remained greater than the perpendicular strain.

VII.3.2.3. CARBON DIOXIDE TEST

Figure VII-15 shows the perpendicular and parallel strain over time due to CO₂ adsorption. The pressure in the gas chamber gradually lowered to a steady 3 000 kPa, however it occurred in a fluctuating cycle of adsorption and desorption within the molecular matrices of the coal, which was thought to be attributed to changes in the sorption environment (in this particular case, the temperature).

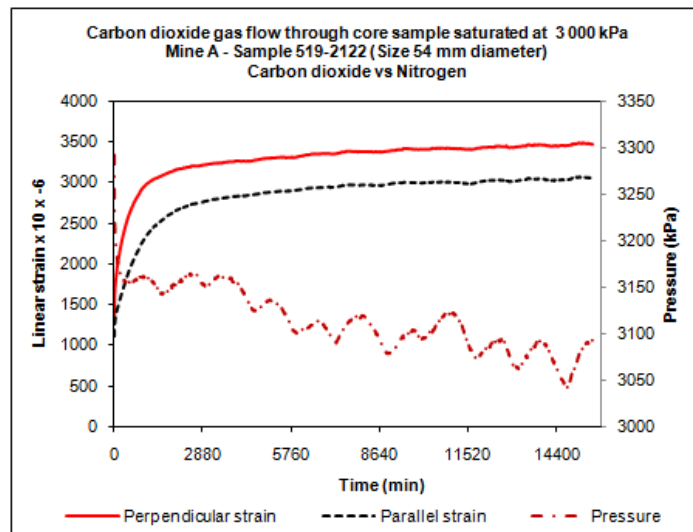


Figure VII-15 – Perpendicular and parallel strain (CO₂ test)

This change in gas pressure provided extra impetus to the coal-gas system to continue adsorption with the result that the sample adsorbed more gas. The trend line of the swelling profile was similar to that obtained with the CO₂/CH₄ test. However, the strains in coal due to CO₂ adsorption did not increase significantly compared to the mixed gas test, despite the fact that the sample was saturated for a longer time. At the 6 300 min mark, the perpendicular and parallel strains were around 3 500 ppm and

CHAPTER SEVEN

Enhancing gas drainage by N₂ and CO₂ injection

3 000 ppm, respectively, which were almost the same as those obtained at the end of the adsorption period (15 850 min) at equilibrium level. The maximum perpendicular/parallel strain ratio at the end of the adsorption period was about 1.2:1, almost 20% less than the same strain ratio obtained with the CO₂/CH₄ test. These results suggest that the coal appeared to adsorb the CO₂ better on the cleats, cracks, fissures, and surfaces, thus producing smaller perpendicular and parallel strains. However, the CH₄ component of the CO₂/CH₄ mixture adsorbed better into the coal matrices. Thus, the adsorbed CO₂ and adsorbed CH₄ components produced higher perpendicular and parallel strains due to the mixed CO₂/CH₄ adsorption.

Figure VII-16 shows the profile of the axial load over time due to CO₂ adsorption and desorption. The increase in axial loading from 3.92 kN (400 kg) to 4.27 kN (435 kg) was the result of CO₂ adsorption. This increase in the axial load was almost 10% less than the same ratio obtained from the mixed CO₂/CH₄ test.

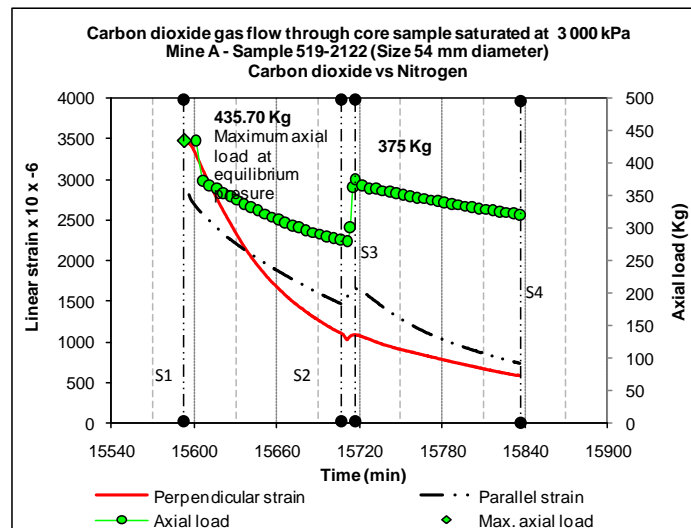


Figure VII-16 – Axial load profile (CO₂ test)

During desorption a maximum axial load of about 3.68 kN (375 kg) was achieved, which was possibly attributed to the coal body adjusting and rebounding, which was also reported in the mixed CO₂/CH₄ test (section 3.2.2). The graph also shows the

CHAPTER SEVEN

Enhancing gas drainage by N₂ and CO₂ injection

perpendicular and parallel strains stemming from the drop in pressure in the gas chamber. N₂ was injected for approximately 100 min from the 15 600 minute mark to the 15 700 minute mark, as shown in Figure VII-10. The duration of this injection was defined as a function of the degree of confined CO₂ dilution.

Table VII-4 summarised the strains and stresses in the coal in four different stages. In general, both parallel and perpendicular strains decreased when the pressure dropped. The results appeared to follow the same trend as found in the mixed CO₂/CH₄ test (section 3.2.2, Table VII-3).

Table VII-4- Summary of strain and stress (CO₂ test)

Carbon dioxide and Nitrogen injection								
Stage	Time (min)	Axial load (kg)	Stress			Strain		
			Lateral/Axial ratio	Axial (MPa)	Lateral (MPa)	Axial/Lateral ratio	Axial ppm (10x-6)	Lateral ppm (10x-6)
S1	15593.3	435.7	1.63	1.90	3.09	1.14	3469	3052
S2	15711.3	330.0	1.19	1.44	1.72	0.66	1023	1543
S3	15717.0	374.9	0.37	1.64	0.61	0.66	1084	1652
S4	15836.8	321.1	0.00	1.40	0.00	0.79	580	738

At equilibrium pressure (stage S1), the ratio of the perpendicular/parallel strain was about 1.1:1. The fact that the initial axial load increased by about 33%, from 2.94 to 3.92 kN, (from 300 kg in the mixed CO₂/CH₄ test to 400 kg in the CO₂ test) could be why this strain ratio was almost 20% less than that obtained in the mixed CO₂/CH₄ test. The axial load constrained the axial strain in the sample while the radial strain was unchanged. This happened because at about 3 000 kPa the confining gas pressure was kept constant in both tests. Because the axial load increased, the intersection where parallel and perpendicular strains met occurred when N₂ was being injected (at the 15 639 min mark). This contrasted with the intersecting point reported in the mixed CO₂/CH₄ test (Figure VII-14), where the N₂ injection was stopped completely. At the point of intersection the axial load was about 3.24 kN (330 kg), and the parallel stress

CHAPTER SEVEN

Enhancing gas drainage by N₂ and CO₂ injection

was about 3.0 MPa which produced a lateral/axial stress ratio of about 2.1. Note that this ratio was greater than the initial stress ratio (stage S1). At a similar confining pressure, the smaller the stress ratio the greater the strain ratio, which means that perpendicular strain will be greater than parallel strain. This increase in the perpendicular strain appeared to be linked to adsorbed CO₂. The results also suggest that a large perpendicular strain helps increase the content of CO₂ in coal. While N₂ was being injected (stages S2 and S3), the coal relaxed somewhat which lowered the axial load by more than 0.98 kN (100 kg). This drop in the axial load occurred while N₂ was being injected, and contrasted with the axial load dropping in the mixed CO₂/CH₄ test where it occurred after the N₂ injection was stopped. The results suggest that CO₂ desorption appeared to happen faster than in the mixed CO₂/CH₄ test due to displacement caused by the injection of N₂. In stage S2, S3, and S4, the axial load was smaller than the original loads because of desorption and consequently the perpendicular strain decreased in the same manner as the mixed gas test. In stage S3 and at the 15 717 min mark, a lateral confining gas pressure of about 600 kPa could not affect the parallel strain so the sample returned to its original shape.

VII.3.2.4. METHANE TEST

Figure VII-17 shows the perpendicular and parallel strains over time due to adsorption/desorption. These results suggest there was a sudden drop in gas pressure at the 1 710 min mark (1.2 days), probably caused by insufficient pressure in the chamber initially. The perpendicular and parallel strains showed the coal swelling was similar to that obtained with the mixed CO₂/CH₄ and the single CO₂ tests. These results suggest there were some similarities between the strain profiles and the mixed

CHAPTER SEVEN

Enhancing gas drainage by N₂ and CO₂ injection

CO₂/CH₄ test particularly, during the adsorption stage. The shape of the strain profile in the mixed gas test appeared to be greatly influenced by the CH₄ adsorption profile. At the 5 700 minute mark, the maximum perpendicular and parallel strains were 1 500 ppm and 1 200 ppm, respectively. The maximum perpendicular/parallel strain ratio was about 1.2:1, which was almost 20% less than the ratio obtained with the mixed CO₂/CH₄. This can be attributed to the fact that the amount of CH₄ adsorbed into the coal was much less.

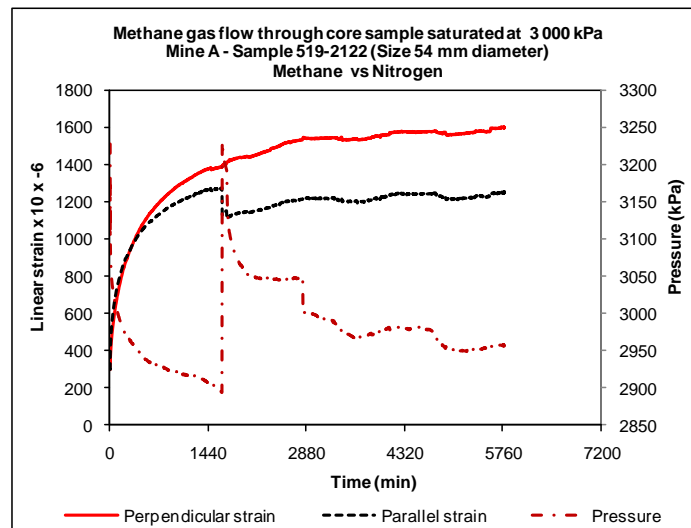


Figure VII-17 – Perpendicular and parallel strain (CH₄ test)

Figure VII-18 shows axial load over time due to the adsorption/desorption process. These results indicate an increase in the axial load of 0.72 kN (73 kg) on the sample, which represents a 40% increase to the 1.96 kN (200 kg) load applied initially. This increase in the axial load was almost 17% greater than the axial load obtained in the CO₂/CH₄ test. A relatively small applied axial load may have helped the coal to swell more, especially axially. A 2.9 kN (295 kg) axial load was measured at the 5 970 minute mark. This axial load meant there was a maximum axial load ratio of 1.5, almost 25% greater than that obtained in the CO₂/CH₄ test. The axial load obtained during desorption was probably due to some structural rebounding in the coal, as already

CHAPTER SEVEN

Enhancing gas drainage by N₂ and CO₂ injection

reported in section 3.2.2 (Binary mixed gas test) and section 3.2.3 (CO₂ test). The study suggests that this increase in the axial loads was caused by the same phenomenon. It was also found that an increase in the axial load (coal swelling) did not necessarily mean an increase in the gas content.

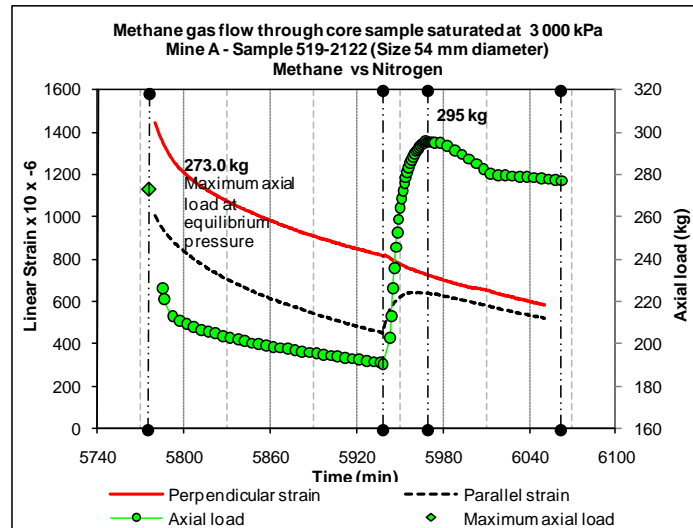


Figure VII-18 – Axial load profile (CH₄ test)

Table VII-5 summarises the coal strains and stresses at four different stages. The perpendicular strains decreased as the gas pressure dropped. The parallel strains decreased for the same reason but with CH₄ gas this drop was greater than the drop in the perpendicular strain. The initial axial load decreased by about 33% compared to the axial load in the CO₂/CH₄ test, from 2.94 to 1.96 kN (from 300 kg in the mixed gas test to 200 kg in the CH₄ gas test). The perpendicular strain was about 20% greater than the parallel strain at equilibrium pressure (stage S1), almost 25% smaller than that obtained in the CO₂/CH₄ test. In this test, the perpendicular strain was always greater than the parallel, and the maximum gap between them was at the 5 940 minute mark. At this point the perpendicular strain was almost 80% greater than the parallel. The axial load was around 190 kg and the ratio of lateral/axial stress was around 3.7. This ratio was even greater than that in stage S1. As with a previous test with mixed gas and

CHAPTER SEVEN

Enhancing gas drainage by N₂ and CO₂ injection

CO₂, the structure of the coal relaxed when N₂ was injected, this caused the axial load to drop by almost 85 kg. This occurrence during the injection of N₂ was in complete contrast with the same point in the mixed gas test when the N₂ injection was stopped and it was in a realistically unconfined condition of gas desorption (stage S2).

Table VII-5 - Summary of strain and stress (CH₄ test)

Stage	Time (min)	Axial load (kg)	Methane and Nitrogen injection					
			Stress			Strain		
			Lateral/Axial ratio	Axial (MPa)	Lateral (MPa)	Axial/Lateral ratio	Axial ppm (10x-6)	Lateral ppm (10x-6)
S1	5775.8	273.0	2.48	1.19	2.96	1.18	1478	1248
S2	5938.3	190.6	3.70	0.83	3.08	1.80	818	454
S3	5968.3	295.5	0.19	1.29	0.25	1.14	729	638
S4	6062.3	239.3	0.00	1.04	0.00	1.12	567	507

In stage S2, the axial load was smaller than the original axial loads due to desorption and consequently, the perpendicular strain was also smaller. Stage S3 shows an increase in parallel strain due to the CH₄ desorption, which is similar to an increase which occurred in the CO₂/CH₄ mixed gas test (when N₂ injection was stopped), but this increase was smaller than the perpendicular strain, and both strains were kept almost parallel and never crossed each other. The small axial load applied and lack of response from the CH₄ to the injection of N₂ could explain why there was no equal strain point.

VII.3.3. PERMEABILITY

A gas permeability test was carried out with N₂ and CO₂ on 54.00 mm diameter samples of core coal. A sample was confined with N₂ under levels of pressure from 500 kPa to about 3 000 kPa. However, the samples tested with CO₂ were confined at 500 kPa. The samples were subjected to axial loads of 0.98, 4.90, 7.35 and 9.80 kN (100, 500, 750 and 1 000 kg), at each level of pressure. Permeability was calculated using the following Darcy's equation, (Lama, 1995):

CHAPTER SEVEN

Enhancing gas drainage by N₂ and CO₂ injection

$$K = \frac{\mu Q \ln\left(\frac{r_0}{r_i}\right)}{\pi l (P_0^2 - P_u^2)} \quad \text{Darcy equation (9)}$$

$$K = \text{Permeability to gas (Darcy)} \quad (1)$$

$$l = \text{Height of the sample (cm)} \quad (2)$$

$$Q = \text{Rate of flow of gas (cc/sec)} \quad (3)$$

$$P_0 = \text{Absolute pressure in the chamber (bars)} \quad (4)$$

$$r_0 = \text{External radius of sample (cm)} \quad (5)$$

$$P_u = \text{Absolute pressure at the outlet (bars)} \quad (6)$$

$$r_i = \text{Internal radius of sample (cm)} \quad (7)$$

$$\mu = \text{Viscosity of tested gas, centipoise} \quad (8)$$

VII.3.4. NITROGEN

Figure VII-19 shows the permeability profile of N₂ gas at 0.98 kN (100 kg) of axial load over time.

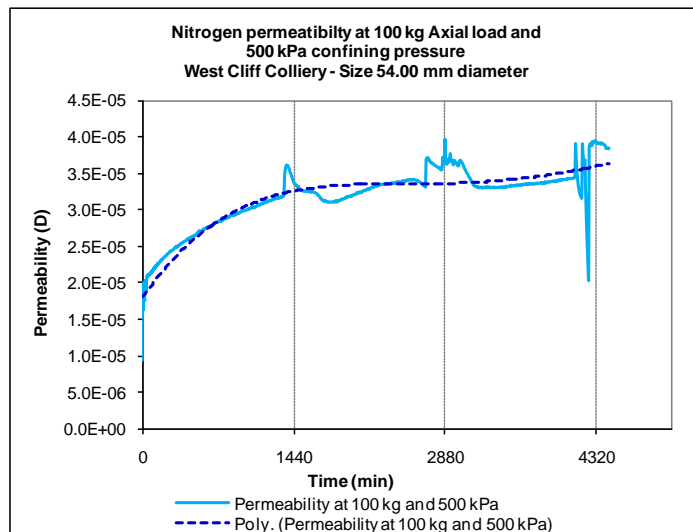


Figure VII-19 – N₂ permeability profile

CHAPTER SEVEN

Enhancing gas drainage by N₂ and CO₂ injection

The permeability of N₂ in samples of core coal from the West Cliff Colliery, Area 5 was tested at about 24 °C. This test was run for about 4 320 min and then stopped when the outflow of N₂ was confirmed as stabilised. The graph shows that the outflow of N₂ stabilised between the 1 440 and 2 880 min mark, measuring a permeability of about 0.000034 D (0.034 mD).

Figure VII-20 shows the results of the N₂ permeability from the whole experiment, with the graph showing its permeability against the axial load.

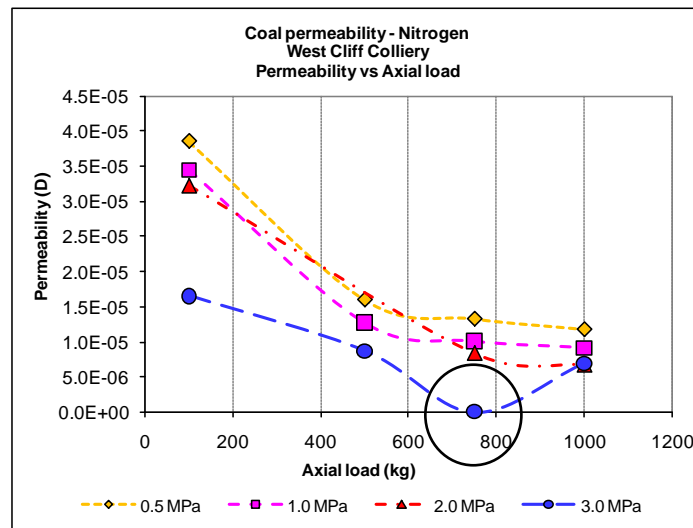


Figure VII-20 – N₂ permeability against axial load

The lowest permeability of N₂ was at 3.0 MPa of confined pressure while the highest was at 0.5 MPa, at each incremental step of axial load. However, the graph shows that the sample of core coal tested at a confining pressure of 3.0 MPa was crushed under a 7.35 kN (750 kg) axial load. These results suggest that the permeability of N₂ gas depended on the confining pressure such that the higher the confining pressure, the lower the permeability. The study also indicated that the maximum axial loads to be applied to the samples should be 7.35 kN (750 kg), as indicated by the circle on the graph. At the same confining pressure however, the results indicate that the

CHAPTER SEVEN

Enhancing gas drainage by N₂ and CO₂ injection

permeability of N₂ appeared to depend on the axial load such that the lower the axial load the higher its permeability in the sample.

Figure VII-21 shows the axial and radial strains against the N₂ confining pressure at several axial loads. The profiles of linear strains were similar over the 500 kPa incremental N₂ confining pressure. The study suggests that the axial load and radial strain did not appear to solely depend on the confining pressure, rather a combination of axial load and confining pressure.

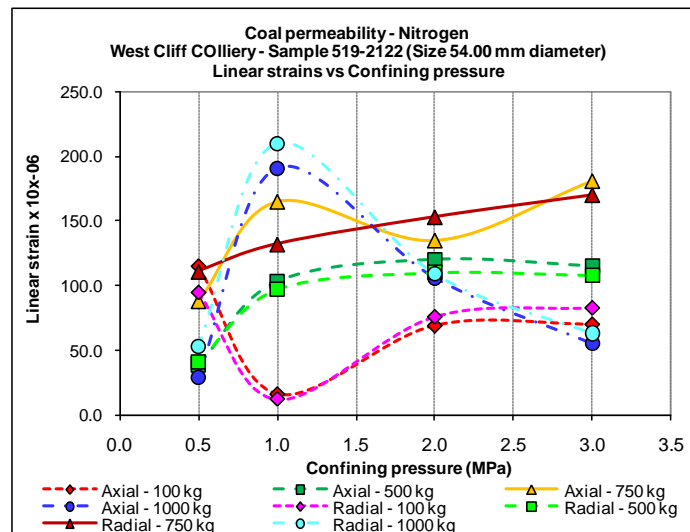


Figure VII-21 – Axial and radial strains due to N₂ flow through

VII.3.4.1. CARBON DIOXIDE

A permeability test of CO₂ was partially carried out in a sample of core coal only at 500 kPa of confining pressure due to some leakage problems with the pressure chamber. It was also found that the cored samples of coal were very friable and unable to be tested under a high axial load. However, this study revealed some interesting information despite the limited data. At saturation point the coal sample was subjected to zero axial load and 500 kPa of confining pressure. At this point, the core coal sample has experienced its maximum strains (radial and parallel). Figure VII-22

CHAPTER SEVEN

Enhancing gas drainage by N₂ and CO₂ injection

shows the permeability profile of CO₂ over time where the results show that 2 880 min was not sufficient to stabilise the outflow of CO₂ through the sample so the test was then stopped due to gas leakage.

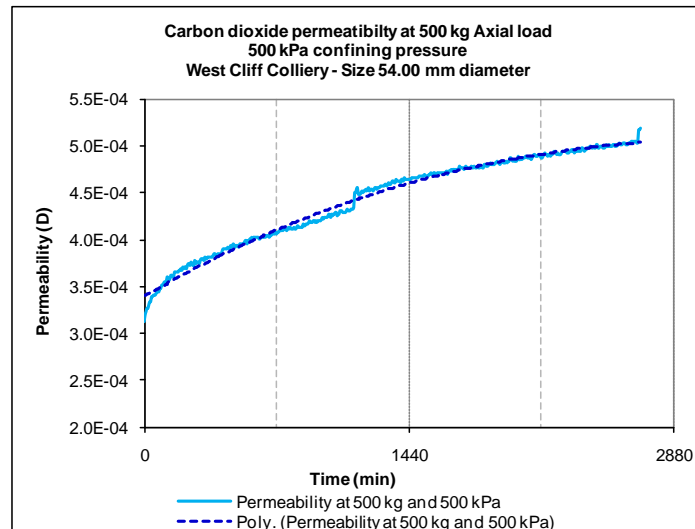


Figure VII-22 – CO₂ permeability profile

Figure VII-23 shows the CO₂ gas permeability and linear strains profiles at several axial loads and under 500 KPa of confining pressure. As expected the results suggest that the permeability of CO₂ depended on the axial load applied, the graph shows that the lower the axial load the lower the permeability, at the same confining pressure.

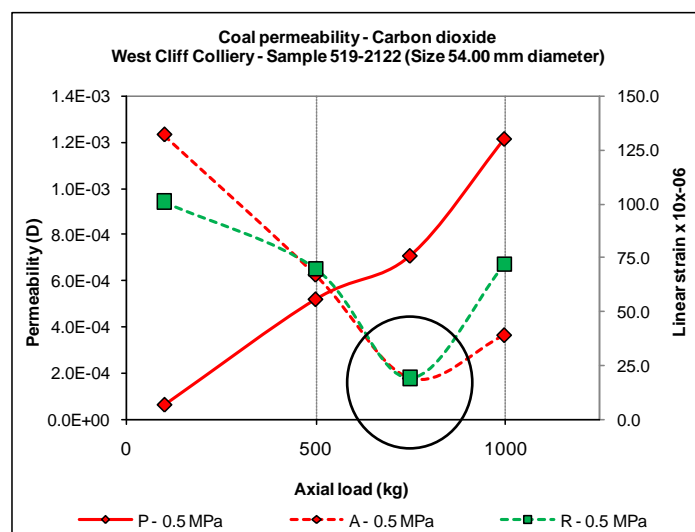


Figure VII-23 – CO₂ permeability and linear strains

CHAPTER SEVEN

Enhancing gas drainage by N₂ and CO₂ injection

This permeability behaviour is explained by the fact that at saturation point, the coal sample swells reaching its maximum strains. The coal swelling decreased cleats and conducts making more difficult the gas movement throughout the coal. Thus, coal swelling decreased coal permeability. At higher axial load however, the coal strains decreases to their minimum values due to an axial compression. At this point the coal sample regains its original shape and the cleat and conduct are made wider and the permeability is increased. This effect of opening the cleat and conducts up is similar to the coal shrinkage effect due to pressure drop. The increasing permeability trend was almost linear until the sample was broken which occurred at about 750 kg of axial load. At this point the permeability profile followed a steeper trend line up due to its fragmentation. Consequently, the permeability at 1000 kg was higher than expected. The results also show that the axial and radial strains followed the same strain trend over the axial load which indicates that the linear strains were dependent on the axial load. As expected, the sample should reach its maximum strains at zero axial loads. Thus, the lower the axial load the higher the linear strains. At about 1000 kg of axial load however, the linear strains unexpectedly increased. These abnormalities can be attributed exclusively to the failure of the sample.

VII.3.5. SUMMARY

Gas composition

The study of N₂ gas injected into coal with regard to its composition found the following:

- Coal appeared to adsorb more CO₂ than CH₄ in a confining environment and under axial load. At initial desorption the composition of desorbed CH₄ was greater than

CHAPTER SEVEN

Enhancing gas drainage by N₂ and CO₂ injection

that composition of CO₂, but at the end the composition of both gases changed approximately 7%,

- During the mixed gas test the rate of discharged CO₂ was almost double that of CH₄. The composition of CH₄ gas stabilised at 20 % after 30 min while the CO₂ increased to 40%. The composition of desorbed CO₂ acting individually increased by 16%, which was twice that obtained in the mixed gas test without injecting N₂,
- The N₂ that displaced the CO₂ was basically due to an improvement in the concentration gradient, although the CH₄ appeared to be affected less by the injection of N₂ gas for the same reasons. The removal of CH₄ after 90 min of testing was 20% at best. The injection of N₂ gas had a greater effect on the removal of CO₂ than on the removal of CH₄.

Volumetric strain

The study of N₂ injected into coal with respect to its volumetric changes indicates the following:

- An injection of N₂ changed perpendicular and parallel layering and bedding of the coal and it shrank uni-axially when this injection stopped. The perpendicular strain was greater than the parallel strain and appeared to be independent of the type of gas. The N₂ appeared to displace both CO₂ and CH₄, but it appeared to displace more CO₂ than CH₄ gas,
- An injection of N₂ appeared to relax the structure of the coal. As a result, the axial load dropped about 18% with a mixture of CO₂/CH₄, 24% with CO₂, and 30% with CH₄.

Permeability

The study of N₂ and CO₂ permeability in coal indicates that:

CHAPTER SEVEN

Enhancing gas drainage by N₂ and CO₂ injection

- The permeability of N₂ depended on the confining pressure such that the higher the confining pressure the lower its permeability. Its permeability also depended on the axial load such that in the sample, the lower the applied load the higher the permeability,
- At a similar confining pressure, the lower the axial load, the lower the axial strain and the higher the permeability of N₂, although the higher the axial load, the lower the axial strain and permeability. However, the permeability test with CO₂ was unfinished due to competency problems with the core samples.

VIII. CHAPTER EIGHT

CONCLUSIONS AND RECOMMENDATIONS

VIII.1. CONCLUSIONS

Accurate measurements of parameters such as adsorbed mass, permeability, and shrinkage are critical in the design of drainage systems and ventilation planes for coal mines. Safety and the emission of gas such as CH₄ rely on the assessment of such parameters. Accordingly, gas sorption characteristic tests were carried out in coal with a special focus on the adsorbed mass of gas with respect to particle size, time to reach saturation, temperature, and type of gas.

VIII.1.1. SINGLE GAS ADSORPTION/DESORPTION

TIME

- In adsorption, time to reach saturation of N₂ and CH₄ appeared to be independent of the pressure levels, but reaching saturation of CO₂ seems to depend on the levels of pressure; the lower the pressure the shorter the time to reach saturation.
- In desorption however, CH₄ saturation appeared to depend on the pressure level. The higher the pressure the longer the CH₄ saturation time.
- 2 880 min (two days) was sufficient time for both N₂ and CO₂ to achieve equilibrium pressure while CH₄ took one day longer.
- Saturation time for N₂ and CH₄ appeared to be independent of particle size.
- Time to reach saturation of CO₂ was independent of the particle size with fragmented samples of coal. However, the period of reaching saturation with 15.00 mm size or larger with CO₂ may depend on particle size.

CHAPTER EIGHT

Conclusions and recommendations

- More research is needed in larger particles sizes.
- The time to reach saturation in coal appeared to depend on the type of gas.
- In adsorption, CH₄ took longer than N₂ and CO₂ to achieve a similar degree of saturation while in desorption, N₂ and CH₄ appeared to require a longer time to reach saturation than CO₂, while N₂ and CH₄ appeared to be similar.

ADSORBED MASS

- The adsorbed mass of CO₂ measured by Quick Test (QT) was higher than those samples measured at minimum saturation time of two days. Sample deterioration could be attributed to this anomalous sorption behaviour.
- For very long saturation period, the adsorbed mass of CO₂ in coal appeared to depend on the gas saturation time. With CH₄ however, the longer the time to reach saturation the higher the adsorption capacity on coal.
- The adsorbed mass of N₂ in coal could depend on the particle sizes. More research is needed in this respect.
- However, the sorption capacity of CO₂ and CH₄ appeared to be independent of particle size.
- Gas adsorption in coal depended on the type of gas. CO₂ was found to adsorb in coal 65% more than CH₄ and 225% more than N₂. These lower values when compared to other studies could be attributed to sample deterioration.
- Gas sorption depended on temperature. The lower the temperature the higher the adsorbed mass.
- The experimental data obtained from single gas adsorption (N₂, CO₂ and CH₄) can be modelled very well by the Langmuir equation.

CHAPTER EIGHT

Conclusions and recommendations

- In desorption, the adsorbed mass of N_2 , CO_2 , and CH_4 seemed to be higher than in adsorption. The highest excess appeared to be with CH_4 while the lowest was with N_2 .
- The excess in CO_2 and CH_4 appeared to depend on particle size, such that the larger the particle the higher the excess of CO_2 and CH_4 .
- The adsorbed mass of CO_2 appeared to depend on particle size, such that the larger the particle the greater the volume of CO_2 . However, the adsorbed mass of CH_4 appeared to depend on particle size for fragmented particles.
- The adsorbed mass of gas in coal generally depended on the type of gas, with CO_2 being the highest and N_2 the lowest.
- The Langmuir equation tallied very well the experimental data of single N_2 , CO_2 , and CH_4 . The Langmuir equation appeared to be the easiest tool for estimating the adsorbed mass of single N_2 , CO_2 and CH_4 .
- Residual CO_2 in coal represented about 3.0% of maximum CO_2 while residual CH_4 was lower, at about 0.25% of the maximum adsorbed mass of CH_4 .

LINEAR STRAIN

- During N_2 , CO_2 , and CH_4 adsorption and due to swelling the axial strain was larger than the radial strain.
- 2 880 min (two days) of CO_2 saturation time was sufficient to achieve equilibrium strains but CH_4 took longer.
- Axial and radial strains were almost linearly dependent on the pressure of gas; the higher the gas pressure the greater the linear strain. Also, the higher the adsorbed mass the greater the linear strains.

CHAPTER EIGHT

Conclusions and recommendations

- Linear strain due to adsorption of CO₂ in coal was about three times greater than CH₄.

VIII.1.2. MIXED GAS ADSORPTION/DESORPTION

BINARY MIXED GAS

- The time to reach saturation was independent of the pressure level.
- 4 320 min (three days) was the minimum time required to attain an adequate degree of saturation independently of the pressure level, particle size, gas composition, and temperature.
- The adsorbed mass of CO₂ component was higher at each pressure level compared to the adsorbed mass of CH₄ component.
- The adsorbed mass of mixed gas was independent of particle size over the entire range of pressure.
- The adsorbed mass of single CH₄ and single CO₂ was higher than the CH₄ and CO₂ components from the binary mixed gas.
- The extended Langmuir equation tallied well with the adsorbed mass of binary mixed gas from the experimental data.
- In desorption, the saturation time depended on the level of pressure, such that the higher the pressure the longer it took for mixed gas to saturate, and time of saturation appeared to be independent of particle sizes and small changes in bath water temperature.
- CH₄ desorbed faster than CO₂ due to a drop in pressure.
- Free CO₂ and CH₄ components during desorption appeared to be independent of particle sizes over the entire range of pressure.

CHAPTER EIGHT

Conclusions and recommendations

- The adsorbed mass of mixed gas in desorption was higher than during adsorption.
- At low pressure the adsorbed mass of CO₂ and CH₄ components were similar, but at high pressure there was almost twice as much CO₂. This excess of mixed gas during desorption appeared to depend on the excess of CH₄.
- The adsorbed mass of mixed gas appeared to be independent of particle sizes.
- The adsorbed mass of CH₄ component appeared to be pressure dependent while the CO₂ was also time dependent.
- The residual mass of mixed gas appeared to be influenced by the whole duration of adsorption/desorption.
- Larger particles appeared to retain marginally more mixed gas in coal (residual gas).
- The Langmuir equation appeared to model the adsorbed mass of CO₂/CH₄ mixed gas components well. However, they appeared to be poorly related to their pure adsorbed mass.

TERNARY MIXED GAS

- Saturation time was independent of particle sizes.
- There was more N₂ in the composition of free gas over the whole pressure range while free CO₂ was the lowest.
- The recovery of N₂ was mostly at the expense of the CO₂.
- The composition of free N₂, CH₄ and CO₂ was independent of particle size.
- The adsorbed mass of ternary mixed gas in coal was independent of particle sizes.

CHAPTER EIGHT

Conclusions and recommendations

- The drop in single N_2 , CO_2 and CH_4 due to its dilution in the gas mixture (ternary or binary) appeared to be related to its composition.
- The extended Langmuir equation tallied reasonably well with the ternary mixed gas from the experimental data.
- In desorption, the time to reach saturation with the ternary mixed gas depended on the level of pressure; at low pressure the samples reached equilibrium pressure at minimum time but it took longer at high pressure which was similar to the saturation time with the binary mixed gas.
- Saturation time appeared to be independent of particle sizes.
- At high pressure the composition of free CO_2 was the lowest and the highest was with N_2 gas. At atmospheric pressure however, the composition of free CO_2 was almost eight times higher than N_2 .
- The composition of free N_2 , CO_2 and CH_4 appeared to be independent of particle sizes.
- The composition of free N_2 and CH_4 with respect to the CO_2 appeared to depend on the pressure level; the lower the pressure the lower their compositions.
- The CO_2 component appeared to desorb slower than N_2 and CH_4 .
- The highest excess of mixed gas was achieved at near atmospheric pressure.
- For similar ratios of gas composition, the excess of gas depended on its type.
- At high pressures, there was more adsorbed mass of CO_2 component in coal than N_2 or CH_4 .

CHAPTER EIGHT

Conclusions and recommendations

- The adsorbed mass of ternary mixed gas appeared to be independent of particle size.
- The adsorbed mass of N_2 , CO_2 , and CH_4 components appeared to strongly depend on pressure.
- The adsorbed mass of N_2 recovering in desorption appeared mainly to be at the expense of CO_2 .
- The amount of adsorbed mass of CO_2 and CH_4 components in coal appeared to depend on the composition of mixed gas. The lower the ratio of CO_2/CH_4 the higher the drop in their adsorbed mass.
- The Langmuir equation can be cautiously used to estimate the adsorbed mass of ternary mixed gas in desorption; it could over or under estimate the adsorbed mass of their components.
- A higher proportion of CH_4 in ternary mixed gas appeared to cause more residual gas in fragmented coals.

VIII.1.3. ENHANCING GAS DRAINAGE BY N_2 AND CO_2 GAS INJECTION

- Coal adsorbs more CO_2 than CH_4 in a confining environment and under axial load.
- The amount (composition) of CH_4 was marginally higher than CO_2 during the early stages of adsorption.
- The rate of CO_2 gas discharge was almost double that of CH_4 . Desorption of CO_2 increased by 16%, which was double that obtained without injecting N_2 .
- N_2 gas displaced CO_2 gas but CH_4 gas was not affected by the injection of N_2 .

CHAPTER EIGHT

Conclusions and recommendations

- The removal of CH_4 due to the injection of N_2 was only 20% at best. An injection of N_2 had a greater effect on the removal of CO_2 than on the removal of CH_4 .
- Injecting N_2 gas into coal created volumetric changes, although shrinkage was uni-axial.
- Perpendicular strain from injecting N_2 gas was greater than the parallel strain and was independent of the type of gas.
- Injecting N_2 gas appeared to relax the structure of the coal body such that the axial load dropped about 18% with 50/50 CO_2/CH_4 gas, 24% with CO_2 and 30% with CH_4 .
- The permeability of N_2 depended on the confining pressure and axial load, while the profiles of the linear strains were similar over the confining pressure due to the N_2 . Additionally, the axial and radial strain did not depend solely on the confining pressure, it was also affected by axial load.
- At the same confining pressure, the lower the axial load, the lower the axial strain and the higher the permeability of N_2 . Alternatively, the higher the axial load the lower the axial strain and permeability of N_2 .

VIII.2. RECOMMENDATIONS

This study has provided valuable information on the adsorption/desorption of gas in coal. The measurements of parameters such as adsorbed mass and permeability and the definition of a new procedure for testing gas has helped give a better understanding of the gas sorption process in coal. However, there are still other parameters involved in this process that require further research. The main issues to focus on are as follows:

CHAPTER EIGHT

Conclusions and recommendations

- Improving the sorption apparatus, especially the integrity of bombs, in order to avoid gas leakage and minimise the time require to weigh them. A detailed review and possible improvement to the gas sorption test procedure to make it more reliable, accurate, and easily repeatable.
- Further study on modelling the adsorbed mass of single and mixed gases, and an evaluation of models such as the extended Langmuir, IAS theory, and Dubinin-Astakhov among others.
- A detailed study of gas sorption in coal at pressures from 500 kPa down to atmospheric pressure. This study would improve our knowledge of how gas reacts at low pressures because it is often underestimated.

APPENDICES

Appendix 1 – Raw data form

Date: Hum Press B1 R1 B2 R2 Last Running %Press Days Status Bomb Gas Row Pressure Press Hours running Comment- Action										Date: Hum Press B1 R1 B2 R2 Last Running %Press Days Status Bomb Gas Row Pressure Press Hours running Comment- Action									
Date: Hum Press B1 R1 B2 R2 Last Running %Press Days Status Bomb Gas Row Pressure Press Hours running Comment- Action										Date: Hum Press B1 R1 B2 R2 Last Running %Press Days Status Bomb Gas Row Pressure Press Hours running Comment- Action									

Appendix 2 – Gas saturation degree

Gas pressure was monitored on daily basis in order to determine whether or not the saturation degree level (or equilibrium pressure) was sufficient. The saturation degree level was decided to be less than 5% in function of the pressure fluctuation over a period of time.

Table 0-1 shows an example of gas pressure changes over time. The column “Δ Time” was calculated dividing the length of the sorption period in eight segments, which in fact means equal number of spreadsheet rows (Equation 11).

Table 0-1

Δ Time (hours)	Bomb A (kPa)	Bomb H (kPa)	Δ Temp 1 (°C)	%BA	%BH	%T1
	0.00	0.00	0.00	0.00%	0.00%	0.00%
2.15	-282.48	0.90	-0.40	60.18%	-9.57%	-21.05%
8.93	-118.16	-4.10	0.30	25.17%	43.62%	15.79%
8.93	-31.29	-4.00	0.90	6.67%	42.55%	47.37%
22.25	-28.14	-6.40	0.50	5.99%	68.09%	26.32%
2.48	1.72	2.80	0.80	-0.37%	-29.79%	42.11%
8.93	0.00	3.30	0.80	0.00%	-35.11%	42.11%
8.93	-1.41	0.00	0.00	0.30%	0.00%	0.00%
6.24	-1.16	-1.80	0.40	0.25%	19.15%	21.05%

6.24 hrs ← 6.24 0.25% → **0.25%**

The column “Bomb A (kPa)” was calculated as the changes in gas pressure in each segment (Equation 10). The column “%BA”, which is the gas pressure fluctuation, was calculated according to the Equation 12. The coal reached an appropriate gas saturation level when the pressure fluctuation is less than 5% in the last 18 hours. The last 18 hrs could be either in one segment or in several of them. For instance, in the last 26.58 hrs (which is the sum of four segments, listed as 2.48, 8.93, 8.93 and 6.24 hrs), the gas pressure fluctuation was 0.37% which is less than the suggested 5% (Table 0-1).

(10) Pressure change
$$\Delta P = P(t_1) - P(t_0)$$

Where:

ΔP = pressure change in the time interval (9)

t_1 = pressure at final time of the interval (10)

t_0 = pressure at initial time of the interval (11)

(11) Time change $\Delta t = T/n$

Where:

T = sorption period (12)

n = number of segments, equal to 8 (13)

(12) Pressure change in % $\%P = \Delta P / (P_2 / P_1)$

Where:

P_2 = final pressure (14)

P_1 = initial pressure (15)

Figure 0-1 shows gas pressure changes against time in adsorption. Two requirements (minimum duration and gas pressure fluctuation) guarantee that the change of the gas pressure was stabilised over the period of time as indicated by the asymptotic profile of the graph to the time axis, as depicted in Figure 0-1.

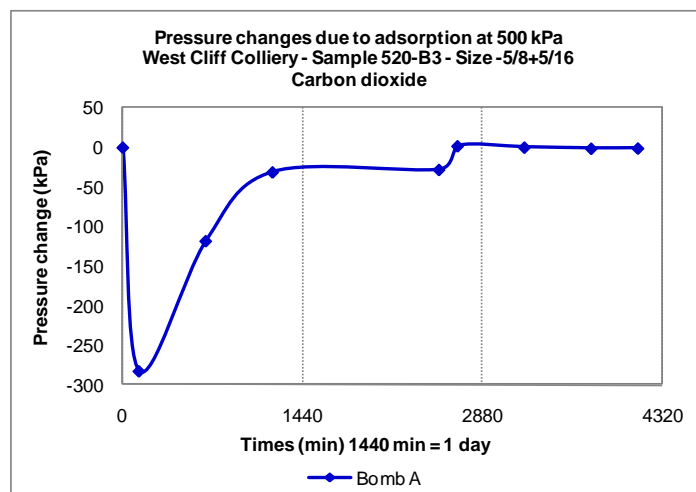


Figure 0-1 – Pressure changes against time

Appendix 3 – Soave-Redlich-Kwong Equation of state

Equilibrium pressure and gas mass was processed in order to obtain gas content in coal per unit of coal mass. The gas content volume was calculated by Soave-Redlich-Kwong equation of state (SRK EOS) for real gases (Soave 1972, Redlich and Kwong 1949). The SRK equation represents an attempt to take molecular geometry and polarity into account. It is widely used especially in the petrochemical industries.

The formulas involved in the volume calculations are the followings:

$$(13) \text{ Soave-Redlich-Kwong EOS} \quad P = (RT / (\bar{v} - b)) - (\alpha a / \bar{v} (\bar{v} + b))$$

Where:

$$R = \text{universal gas constant} \quad (16)$$

$$T = \text{absolute temperature} \quad (17)$$

$$\bar{v} = \text{specific molar volume} \quad (18)$$

$$b = \text{volume correction} \quad (19)$$

$$\alpha = \text{function} (\omega, T) \quad (20)$$

$$a = \text{molecular interaction parameter} \quad (21)$$

The function α is used for fitting the vapour pressure data for hydrocarbons;

$$(14) \text{ Parameter } a \quad a = 0.42747 (R^2 T_c^2 / P_c)$$

$$(15) \text{ Parameter } b \quad b = 0.08664 (RT_c / P_c)$$

$$(16) \text{ Reduced temperature} \quad T_R = T / T_c$$

Where:

$$T_R = \text{reduced temperature} \quad (22)$$

$$T_c = \text{critical temperature} \quad (23)$$

$$P_c = \text{critical pressure} \quad (24)$$

(17) Parameter $\alpha = (1 + m(1 - \sqrt[2]{T_R}))^2$

(18) Parameter m $m = 0.048508 + 1.55171 \omega - 0.15613 \omega^2$

Where:

ω = acentric factor (25)

Appendix 4 – Adsorbed mass spreadsheet calculation

The following parameters are needed for calculating the adsorbed mass in coal; gas density, coal density, bomb volume, and bomb empty weight. Meanwhile, the variables involved in the adsorbed volume calculation are:

$$\delta = \text{gas density (gm/cc)} \quad (26)$$

$$\lambda = \text{coal density (gm/cc)} \quad (27)$$

$$V_{bomb} = \text{bomb volume (cc)} \quad (28)$$

$$W_0 = \text{empty bomb weight (gm)} \quad (29)$$

$$W_1 = \text{weight of bomb and coal (gm)} \quad (30)$$

$$W_2 = \text{weight of bomb and coal and gas (gm)} \quad (31)$$

$$W_{coal} = \text{weight of coal (gm)} \quad (32)$$

$$W_{gas} = \text{weight of gas (gm)} \quad (33)$$

$$V_{coal} = \text{coal volume (cc)} \quad (34)$$

$$V_{(f+a)} = \text{volume of free and adsorbed gas} \quad (35)$$

$$V_{not\ coal} = \text{free bomb volume not taken by coal (cc)} \quad (36)$$

$$V_0 = \text{actual volume of bomb (cc)} \quad (37)$$

$$V_1 = \text{free gas volume (cc)} \quad (38)$$

$$V_3 = \text{free gas volume in bomb with coal sample (cc)} \quad (39)$$

$$V_4 = \text{volume of gas adsorbed in coal (cc)} \quad (40)$$

$$V_5 = \text{gas volume adsorbed in 1 gm of coal (cc/gm)} \quad (41)$$

$$R_1 = \text{ratio of free gas volume over bomb volume} \quad (42)$$

$$(19) \text{ Coal weight (gm)} \quad W_{coal} = W_1 - W_0$$

$$(20) \text{ Gas weight (gm)} \quad W_{gas} = W_2 - W_1$$

(21) Coal volume (cc) $V_{coal} = W_{coal} / \lambda$

(22) Free and adsorbed volume (cc) $V_{(f+a)} = \text{col } \mathbf{AN} \rightarrow \mathbf{P real sheet}$

Note that the value of column **AN** should be taken in between rows 51 and 56, which are the volumes due to the applied gases (weighed at each incremental pressure step).

(23) Free bomb volume not taken by coal (cc) $V_{not\ coal} = V_0 - V_{coal}$

(24) Free gas volume (Ad) $V_1 = \text{column } \mathbf{G} \rightarrow \mathbf{P real sheet}$

(25) Free gas volume (D) $V_1 = \text{column } \mathbf{AN} \rightarrow \mathbf{P real sheet}$

Note that the value of column **G** (adsorption) should be taken in between rows 44 and 50, which are the gas volumes calculated at equilibrium pressure. However, in desorption, the value of column **AN** should be taken in between rows 86 and 113, which are the volumes due to the applied gases (weighed at each incremental pressure step).

Variables $V_{(f+a)}$ and V_1 were calculated according to Appendix 3.

(26) Volume of adsorbed gas in coal (cc) $V_4 = V_{(f+a)} - V_1$

(27) Volume of adsorbed gas per gram of coal (cc/gm) $V_5 = V_4 / W_{coal}$

Determination of the Gas Content of Coal by Gravimetric Technique						Bomb Weight (W0)	Coal Density	Gas Density NTP (g/cc)	Mine
						1520.524	1.41	0.00065911	Westcliff
Weight of Bomb & Coal (W1) (gm)	Weight of Bomb & Coal & Gas (W2) (gm)	Weight of Bomb & Coal & Gas (W2) (gm)	Weight of Coal in Bomb (W1 - W0) (gm)	Weight of Gas in Bomb (W2 - W1) (gm)	Vol of Coal in Bomb (cc)	Vol of Gas in Bomb (Free & Adsorbed)	Bomb Pressure (Kpa)		
							a	b	
							Gauge	Absolute	
1690.538	-	-	170.014	-	120.577	-	0	101.325	
1690.538	1694.761	1694.761	170.014	4.223	120.577	6407.125	142.84	244.165	
1690.538	1695.687	1695.687	170.014	5.149	120.577	7812.050	546.25	647.575	
1690.538	1696.433	1696.433	170.014	5.895	120.577	8943.879	929.09	1030.415	
1690.538	1699.003	1699.003	170.014	8.465	120.577	12843.076	2210.10	2311.425	
1690.538	1701.019	1701.019	170.014	10.481	120.577	15901.746	3200.90	3302.225	
1690.538	1702.985	1702.985	170.014	12.447	120.577	18884.556	4157.90	4259.225	

Seam	Location	Gas	Bomb No.				
Bulll	520-B3	CH4	B4-1				
Actual Vol of Bomb (NTP) (V0) (cc)	Free Vol of Bomb not Taken by Coal (cc)	Free Gas Vol in Bomb at (P) with Coal Sample in Bomb (cc)	V1/V0	Free Vol of Gas at (P) as Obtained from Calibration Curve (V1) (cc)	Vol of Gas Adsorbed in Coal at (NTP)	Vol of Gas Adsorbed in 1gm of Coal (cc/gm)	
383.466	262.889	-		-			
383.466	262.889	398.076	0.000	0.000	6009.049	35.344	
383.466	262.889	1513.409	0.000	0.000	6298.641	37.048	
383.466	262.889	2559.542	0.000	0.000	6384.337	37.552	
383.466	262.889	5976.059	0.000	0.000	6867.017	40.391	
383.466	262.889	8534.058	0.000	0.000	7367.688	43.336	
383.466	262.889	10938.578	0.000	0.000	7945.978	46.737	

Appendix 5 – Langmuir equation

Langmuir isotherm was used as gas sorption model throughout our study for single and mixed gases. Langmuir (1918) has made three main assumptions in order to simplify the adsorption expression:

- Adsorption takes place only at specific localised sites on the surface and the saturation coverage corresponds to complete occupancy of these sites. In other words, the surface of the adsorbent is uniform, that is, all the adsorption sites are equal;
- Adsorbed molecules do not interact;
- At the maximum adsorption, only a monolayer is formed, molecules of adsorbate do not deposit on other already adsorbed molecules of adsorbate, only on the free surface of the adsorbent.

The Langmuir equation can be applied with reasonable accuracy to a surprisingly large number of cases of adsorption on planes surfaces. Due to the assumptions made in its derivation it should not be considered as a general equation for the adsorption isotherm. According to Langmuir (1933), the cases where this equation is most likely to apply are those in which the adsorption occurs only in elementary spaces which are so separated from one another that the ad atoms in the separate spaces do not exert appreciable forces on one another.

The main formulas involved in the Langmuir equations are:

(28) Langmuir equation ***adsorption rate*** = $d\theta/dt = k_a p (1 - \theta)$

Where:

dθ = differential coverage of the surface (43)

$$dt = \text{differential time} \quad (44)$$

$$k_a = \text{adsorption constant} \quad (45)$$

$$p = \text{gas pressure} \quad (46)$$

$$\theta = \text{surface coverage} \quad (47)$$

$$(29) \text{ Desorption rate} \quad \text{desorption rate} = d\theta/dt = k_d\theta$$

$$(30) \text{ Desorption constant} \quad k_a p (1 - \theta) = k_d$$

$$(31) \text{ Surface coverage} \quad \theta = Kp/(1 + Kp), \quad K = K_a/K_d$$

Where:

$$k_d = \text{desorption constant} \quad (48)$$

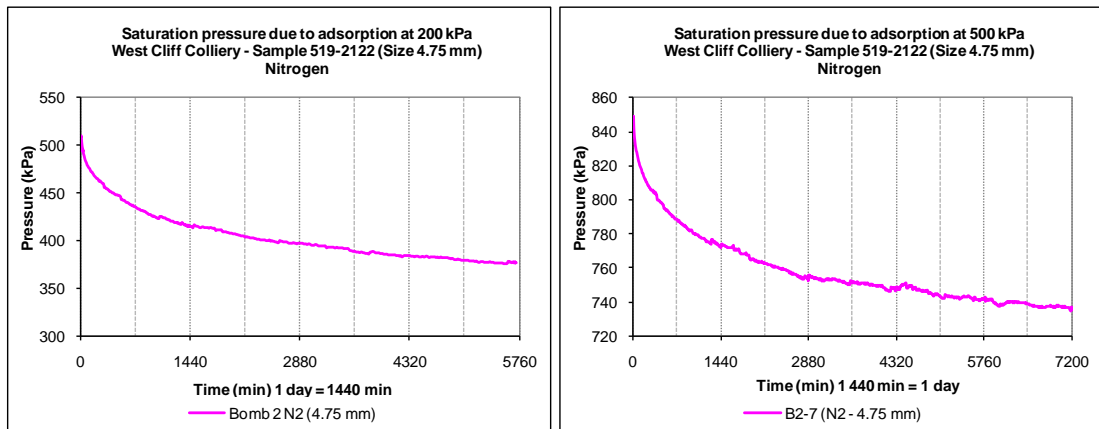
$$(32) \text{ Langmuir equation} \quad P/V = P/V_L + P_L/V_L$$

Where:

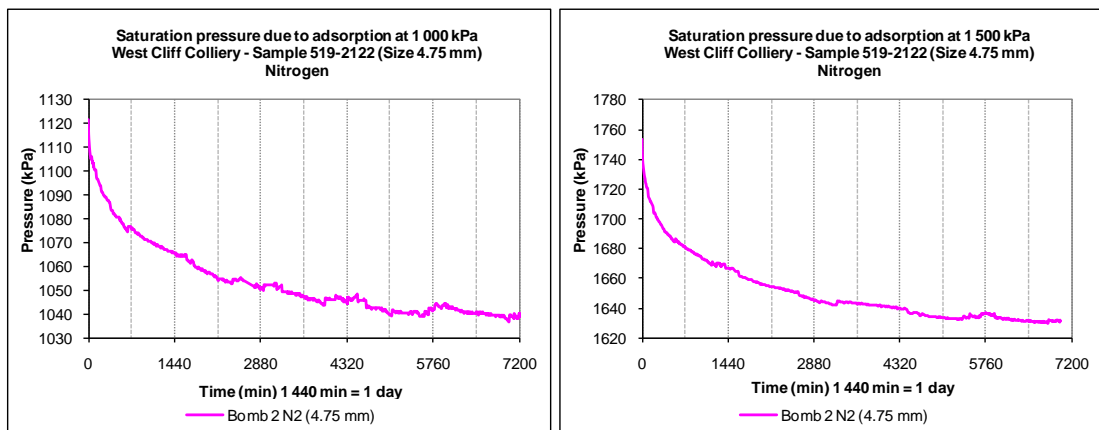
$$V_L = \text{maximum amount of gas stored by coal} \quad (49)$$

$$P_L = \text{pressure at half the Langmuir volume} \quad (50)$$

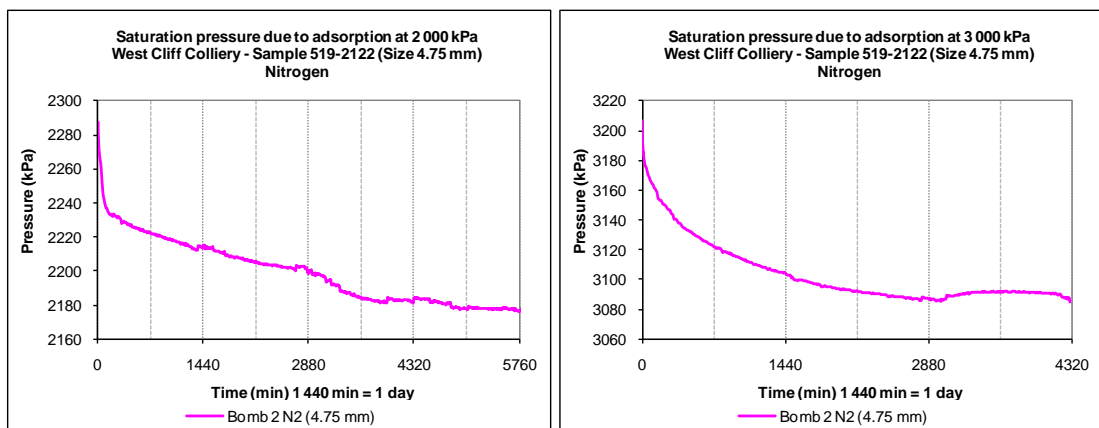
Appendix 6 – N₂ saturation time in adsorption – Sample B2-7 (4.75 mm)



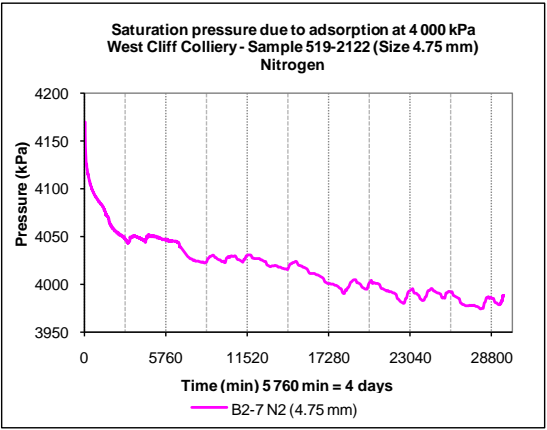
Saturation pressure due to adsorption at 200 and 500 kPa pressure levels



Saturation pressure due to adsorption at 1 000 and 1 500 kPa pressure levels

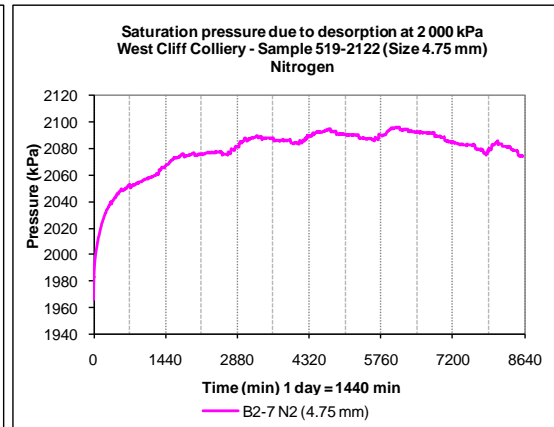
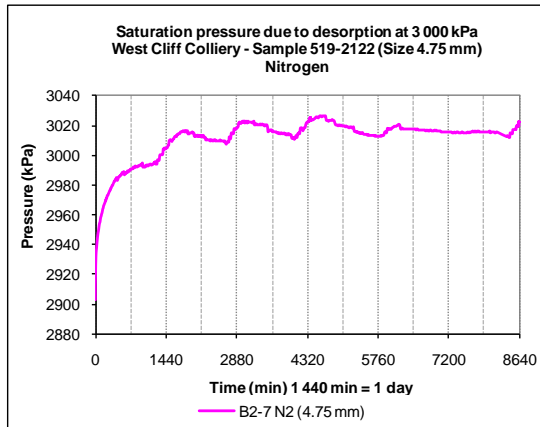


Saturation pressure due to adsorption at 2 000 and 3 000 kPa pressure levels

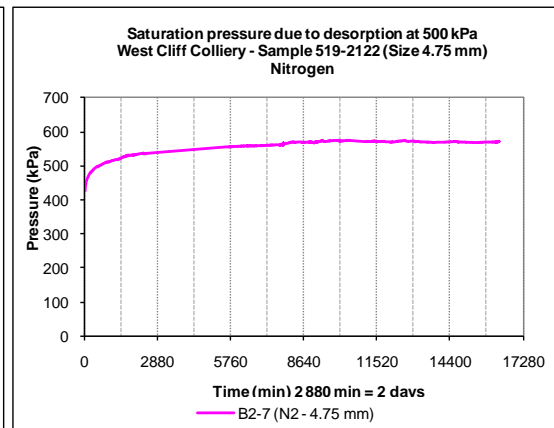
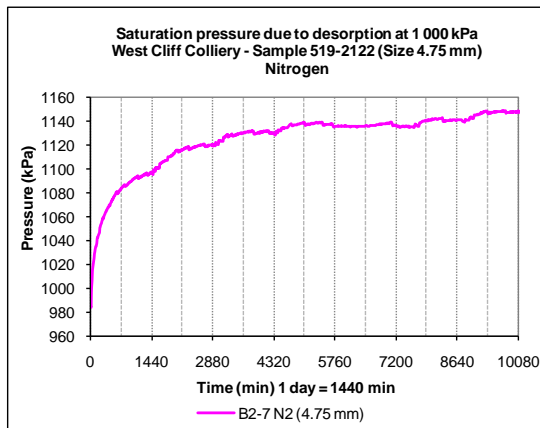


Saturation pressure due to adsorption at 4 000 kPa pressure level

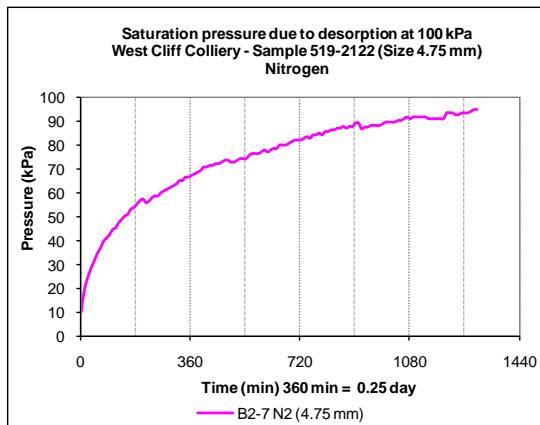
Appendix 7 – N₂ saturation time in desorption – Sample B2-7 (4.75 mm)



Saturation pressure due to desorption at 3 000 and 2 000 kPa pressure levels

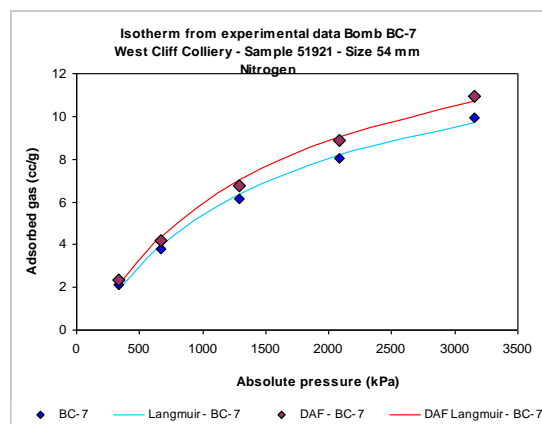
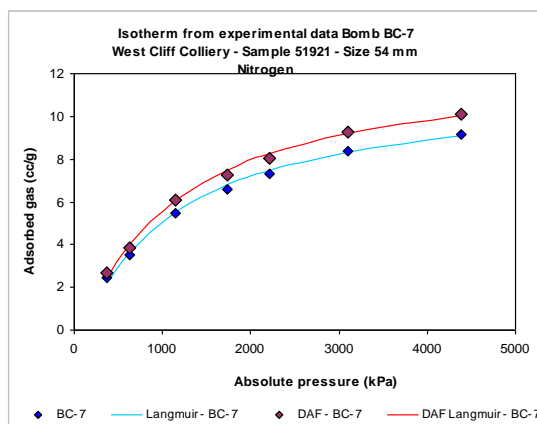


Saturation pressure due to desorption at 1 000 and 500 kPa pressure levels

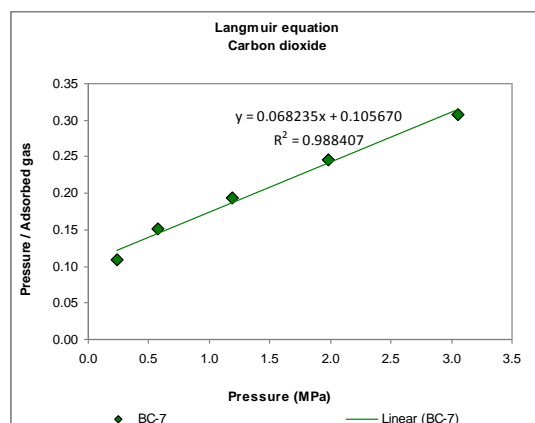
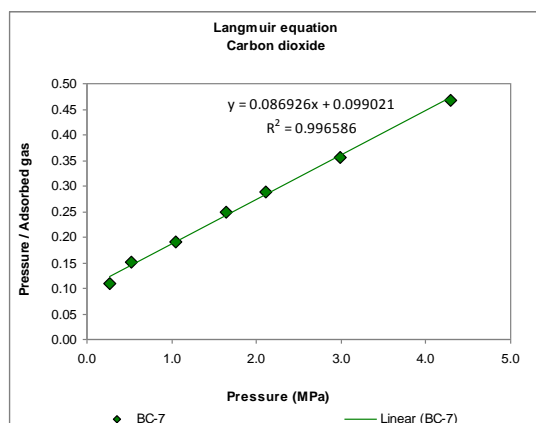


Saturation pressure due to desorption at 100 kPa pressure level

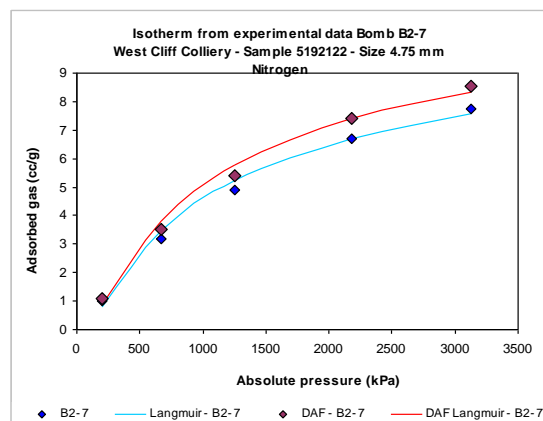
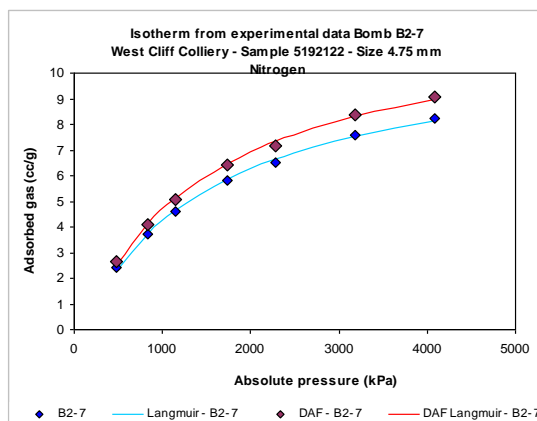
Appendix 8 – N₂ adsorbed mass in adsorption and desorption



N₂ adsorbed mass in adsorption and desorption – Sample BC-7

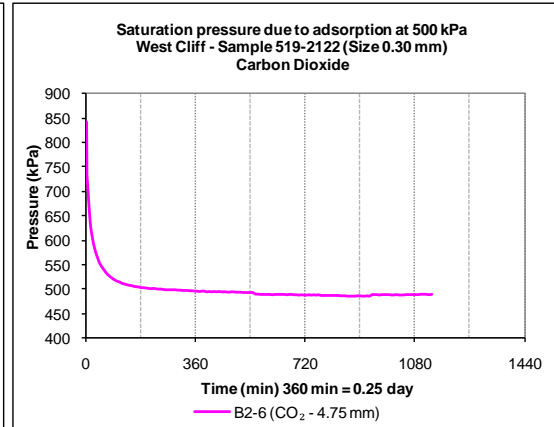
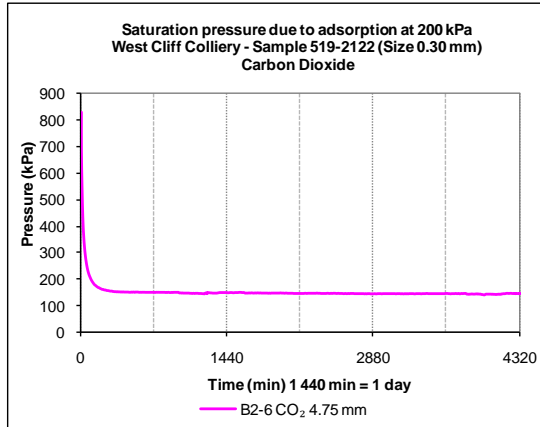


Langmuir equation in adsorption and desorption – Sample BC-7

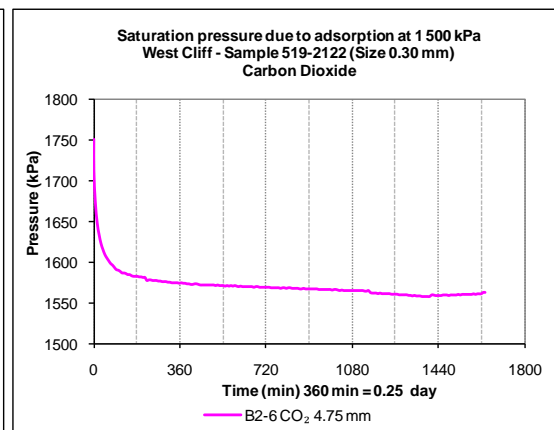
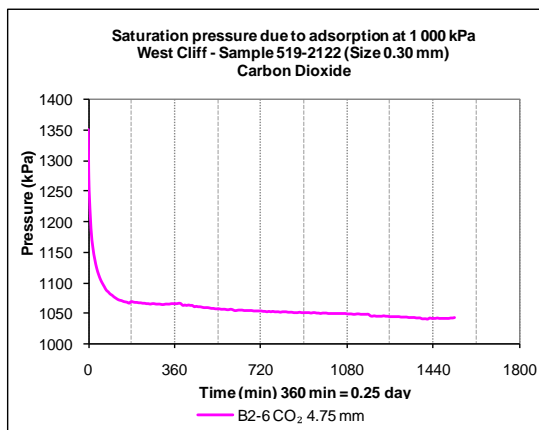


N₂ adsorbed mass in adsorption and desorption – Sample B2-7

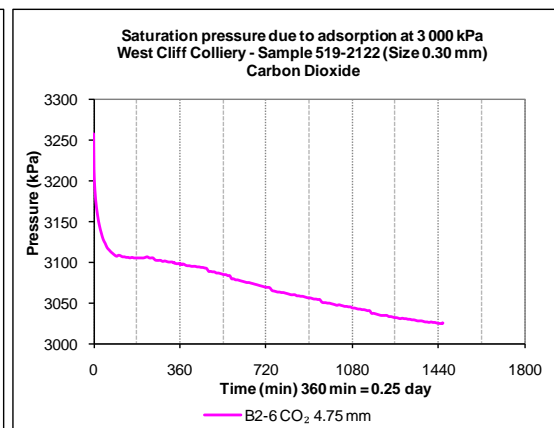
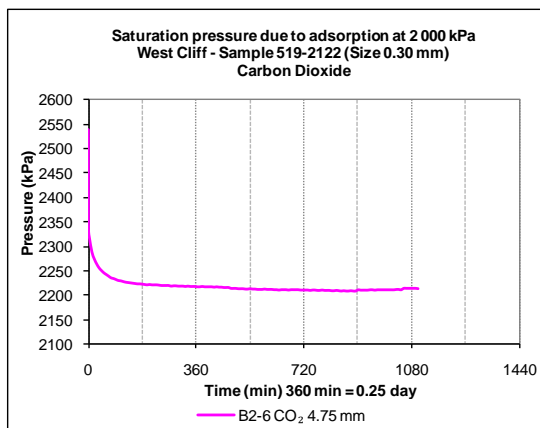
Appendix 9 – CO₂ saturation time in adsorption – Sample B2-6 (0.30 mm)



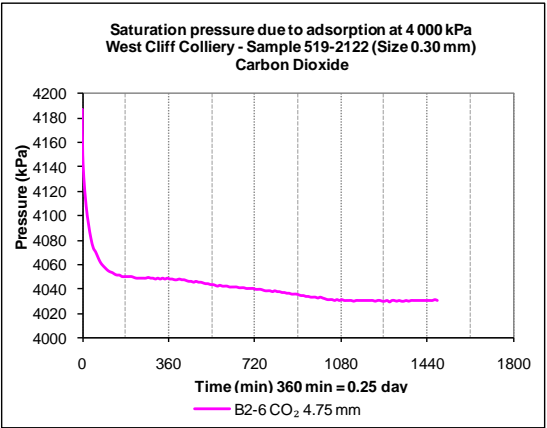
Saturation pressure due to adsorption at 200 and 500 kPa pressure levels



Saturation pressure due to adsorption at 1 000 and 1 500 kPa pressure levels

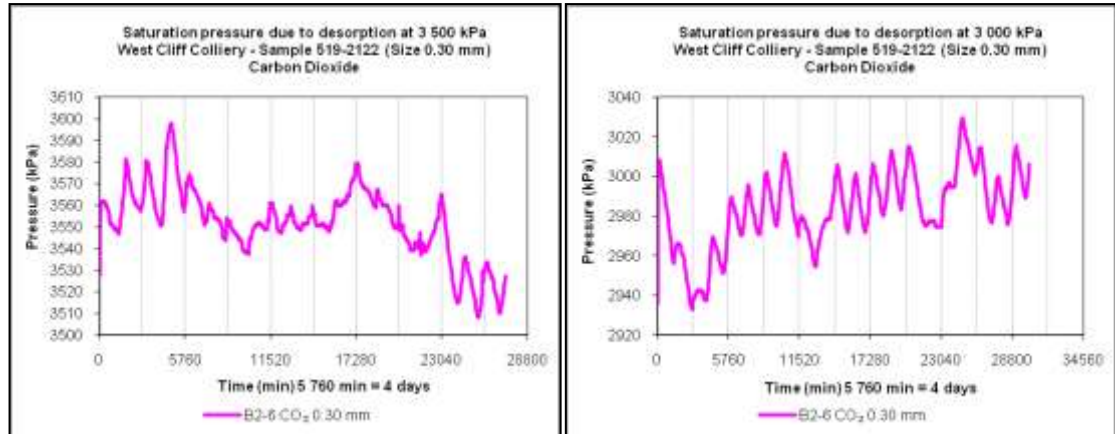


Saturation pressure due to adsorption at 2 000 and 3 000 kPa pressure levels

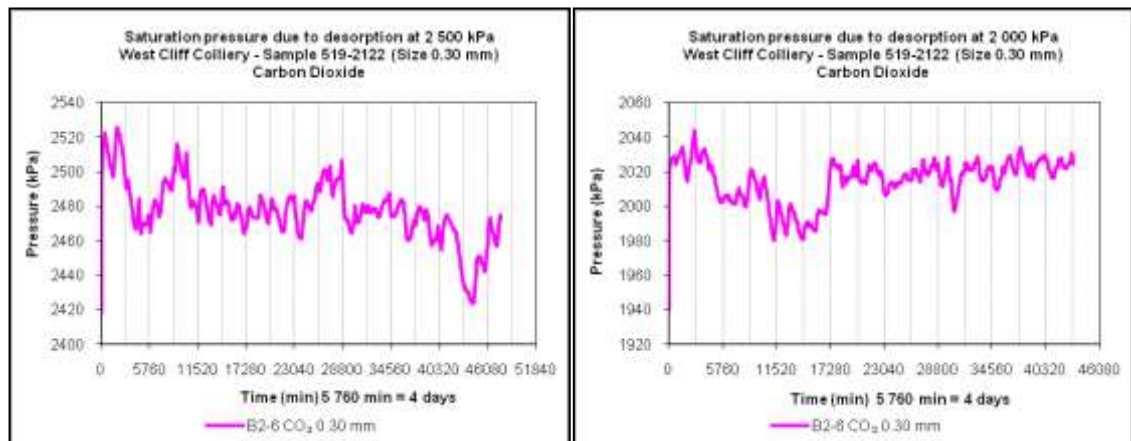


Saturation pressure due to adsorption at 4 000 kPa pressure level

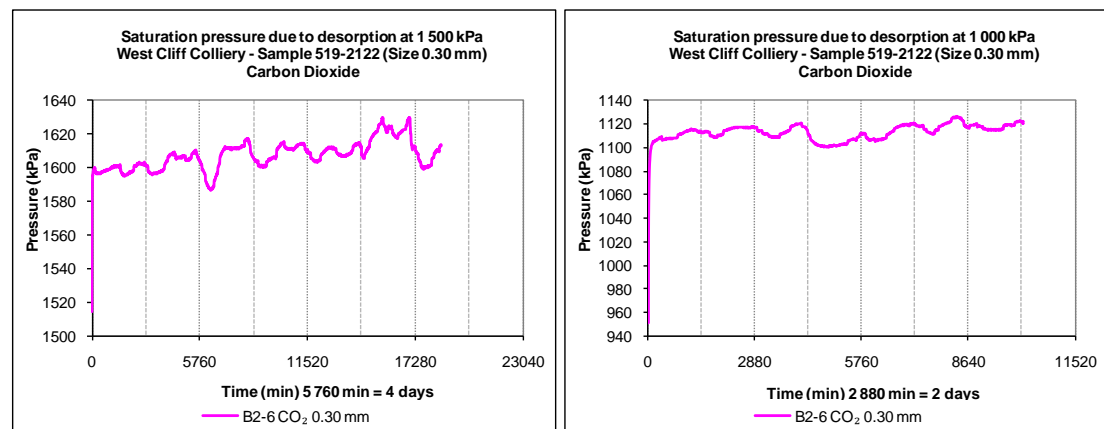
Appendix 10 – CO₂ saturation time in desorption – Sample B2-6 (0.30 mm)



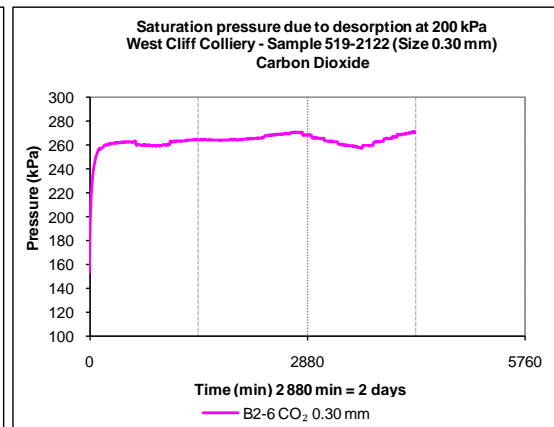
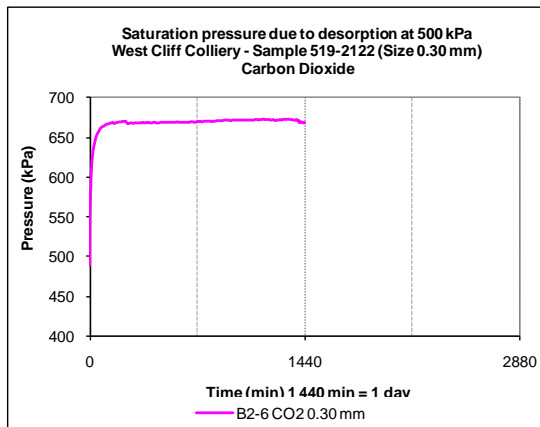
Saturation pressure due to desorption at 3 500 and 3 000 kPa pressure levels



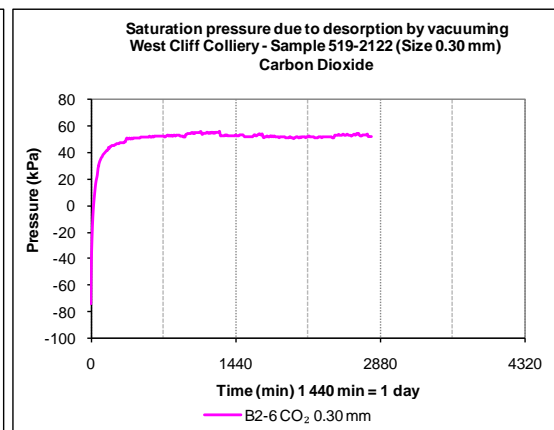
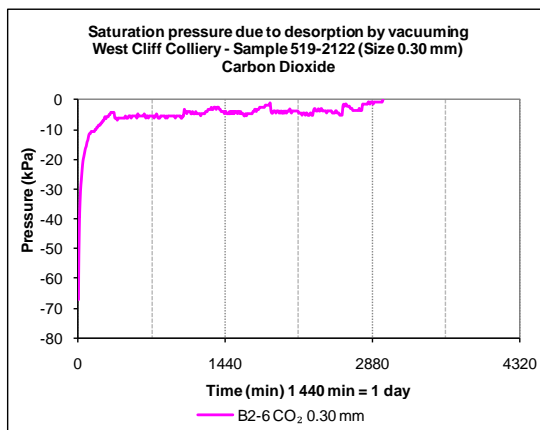
Saturation pressure due to desorption at 2 500 and 2 000 kPa pressure levels



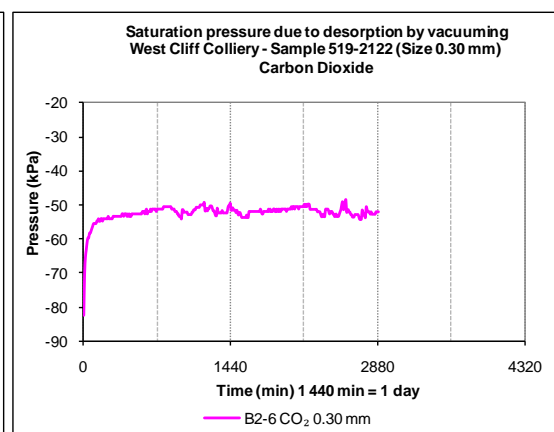
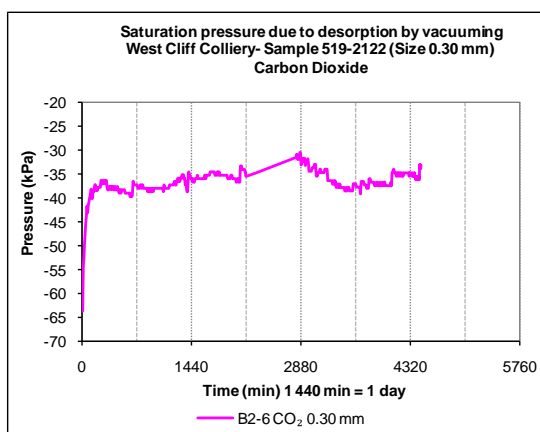
Saturation pressure due to desorption at 1 500 and 1 000 kPa pressure levels



Saturation pressure due to desorption at 500 and 200 kPa pressure levels

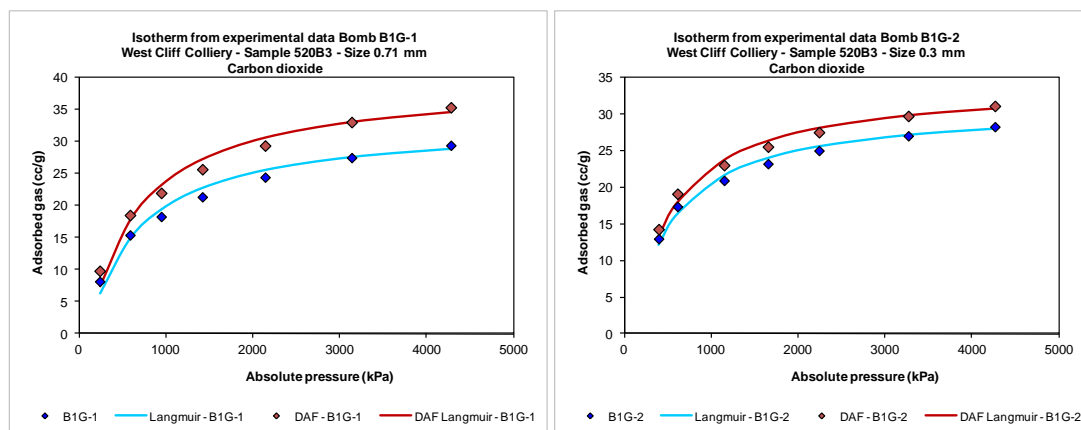


Saturation pressure due to desorption by vacuuming at atmospheric pressure levels

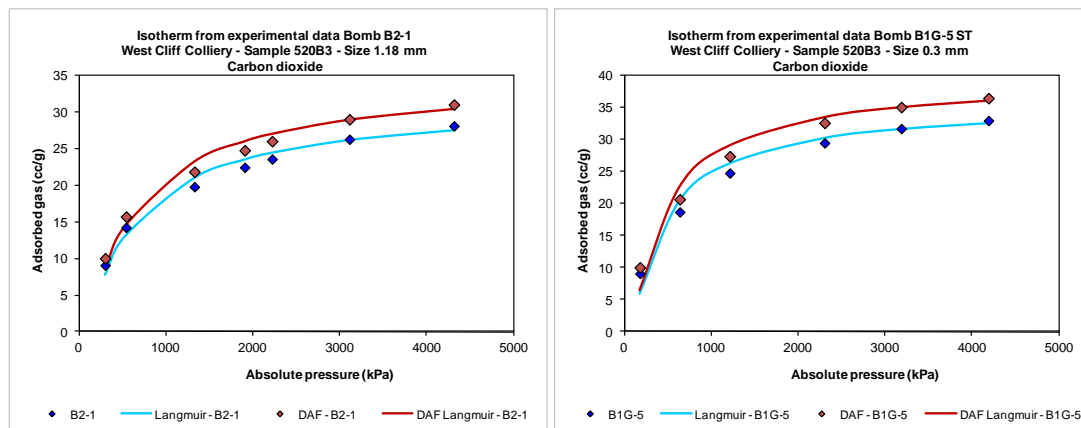


Saturation pressure due to desorption by vacuuming at atmospheric pressure levels

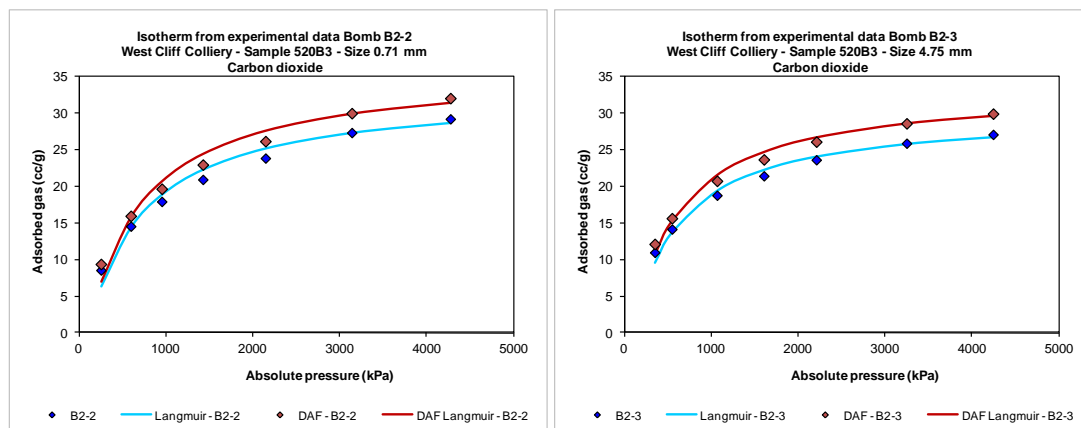
Appendix 11 – CO₂ sorption capacity in adsorption



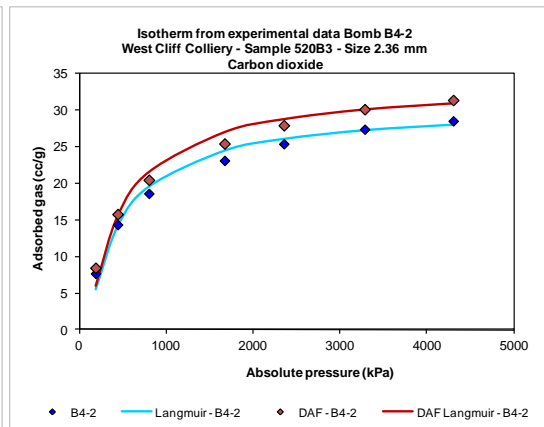
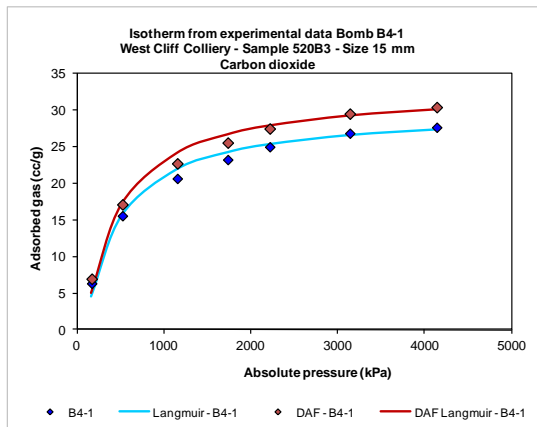
CO₂ sorption capacity in adsorption – Sample B1G-1 and B1G-2



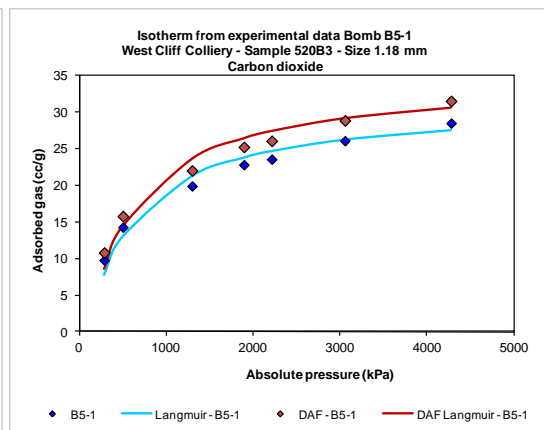
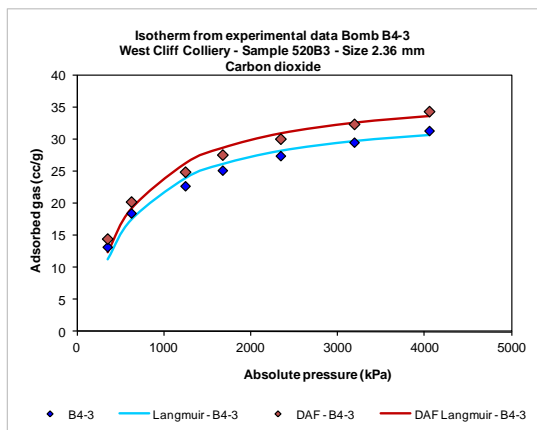
CO₂ sorption capacity in adsorption – Sample B2-1 and B1G-5



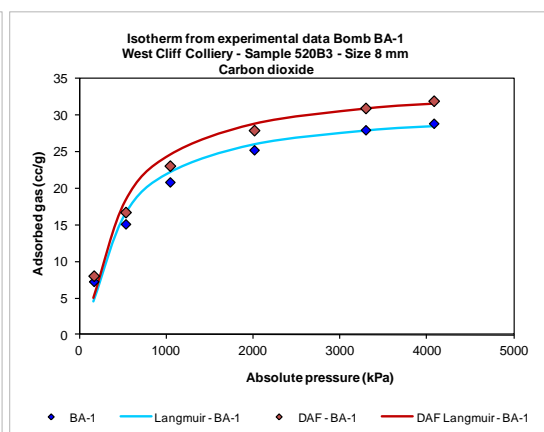
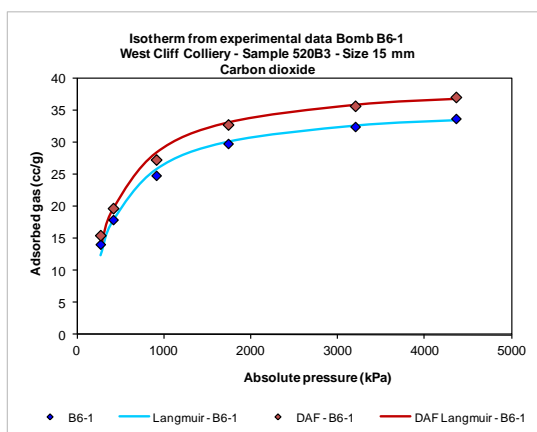
CO₂ sorption capacity in adsorption – Sample B2-2 and B2-3



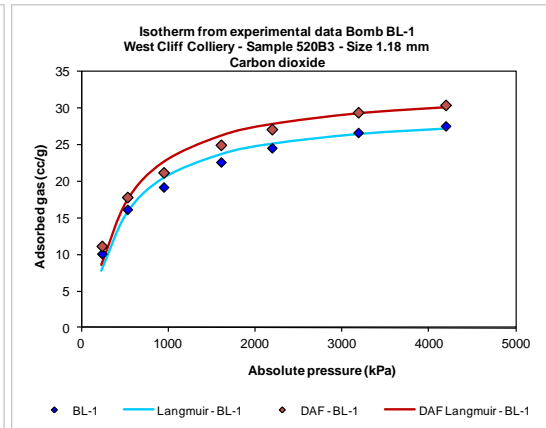
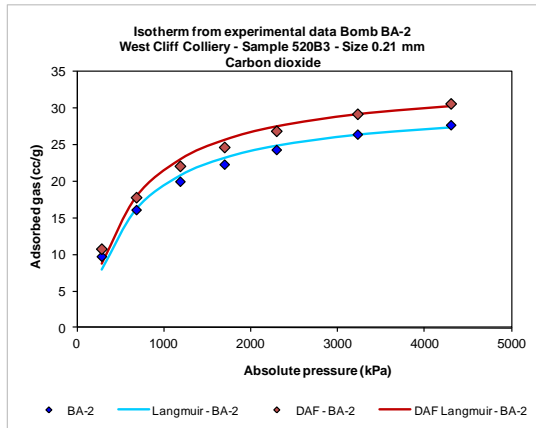
CO₂ sorption capacity in adsorption – Sample B4-1 and B4-2



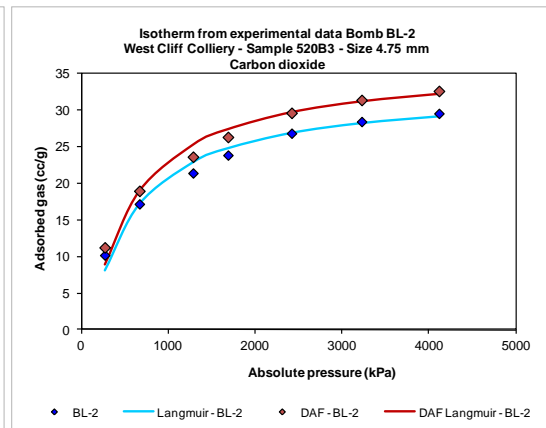
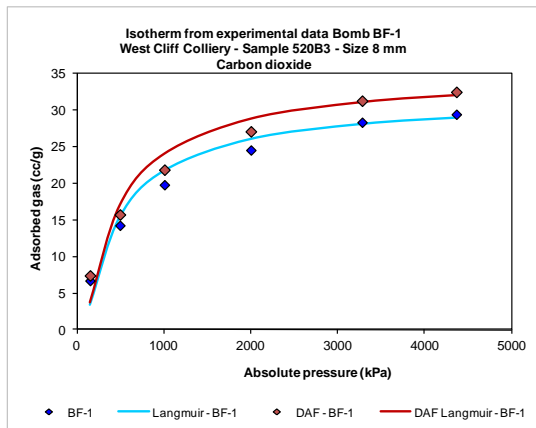
CO₂ sorption capacity in adsorption – Sample B4-3 and B5-1



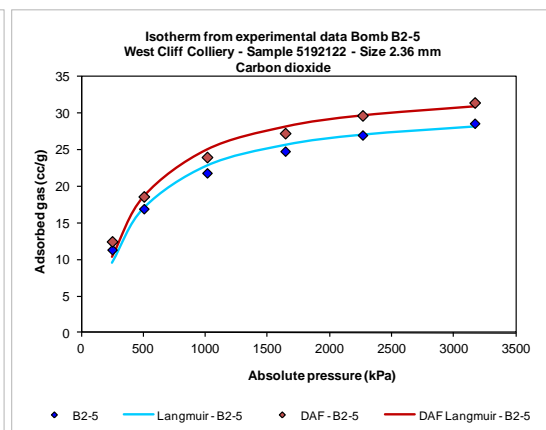
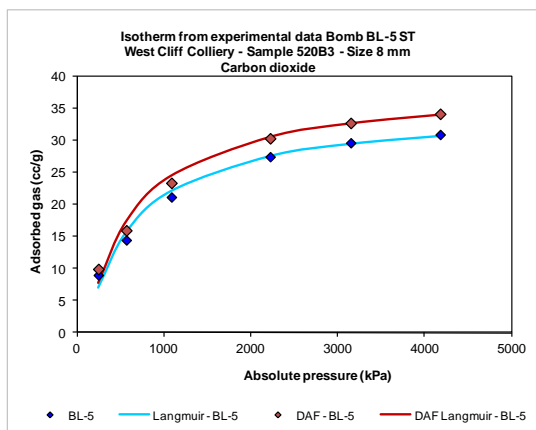
CO₂ sorption capacity in adsorption – Sample B6-1 and BA-1



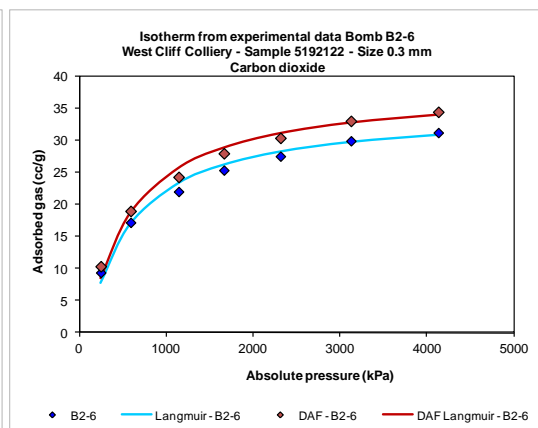
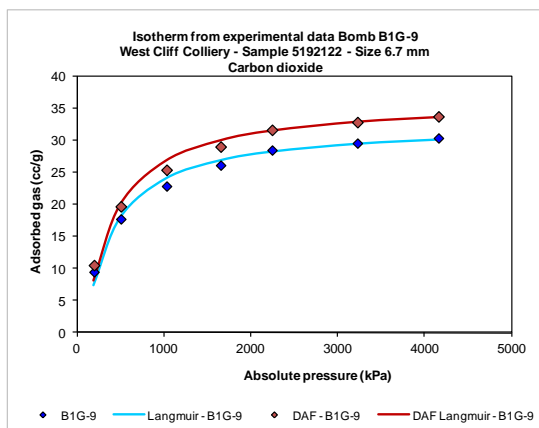
CO₂ sorption capacity in adsorption – Sample BA-2 and BL-1



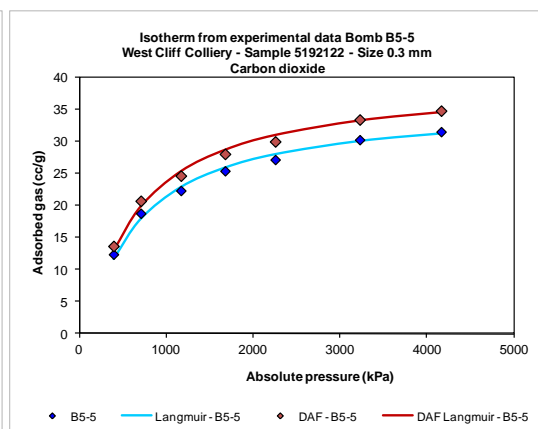
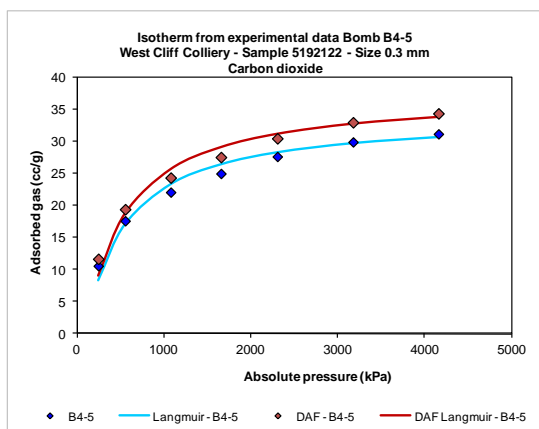
CO₂ sorption capacity in adsorption – Sample BF-1 and BL-2



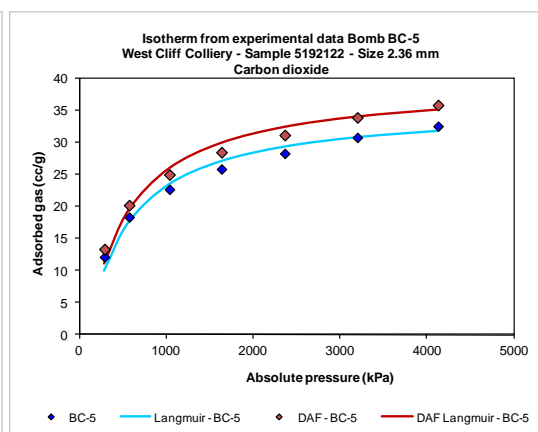
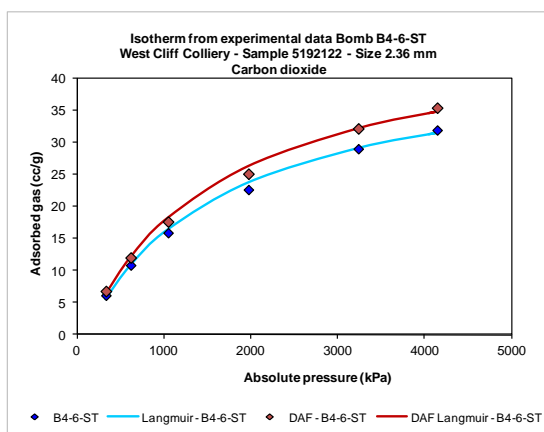
CO₂ sorption capacity in adsorption – Sample BL-5 and B2-5



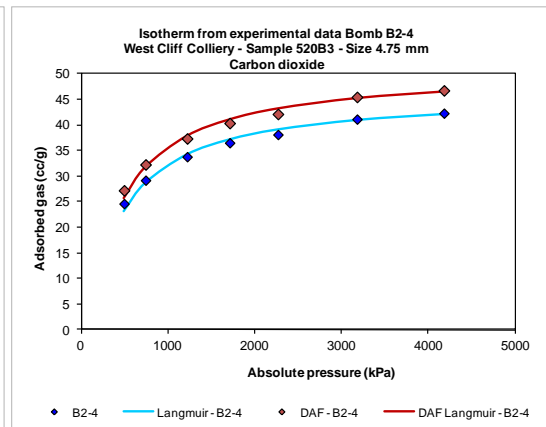
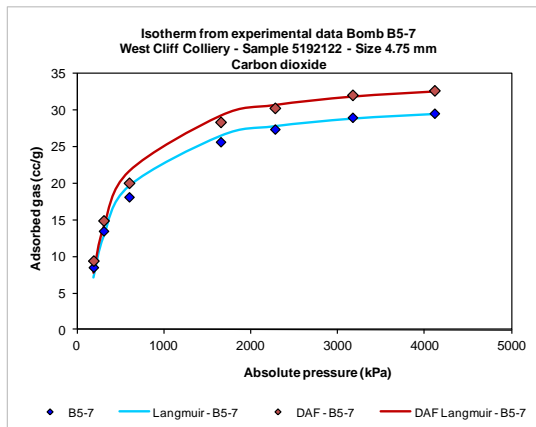
CO₂ sorption capacity in adsorption – Sample B1G-9 and B2-6



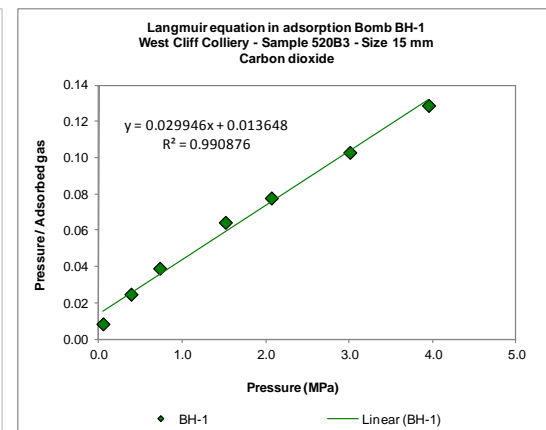
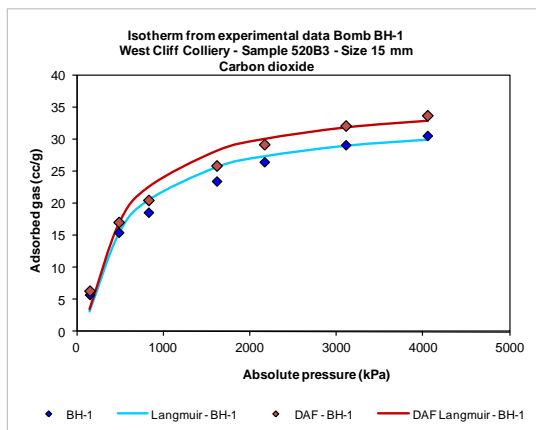
CO₂ sorption capacity in adsorption – Sample B4-5 and B5-5



CO₂ sorption capacity in adsorption – Sample B4-6 and BC-5

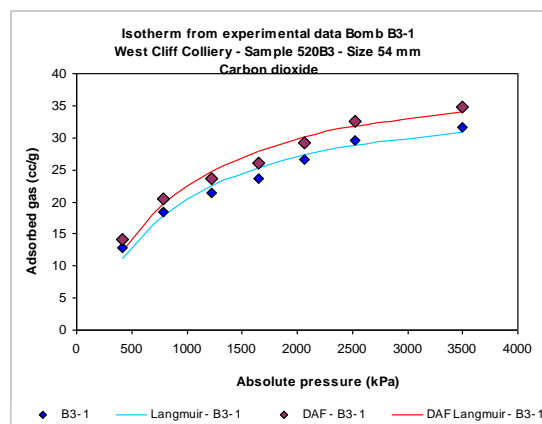
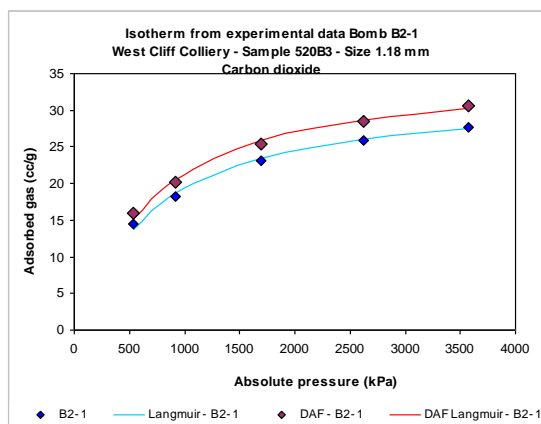


CO₂ sorption capacity in adsorption – Sample B5-7 and B2-4

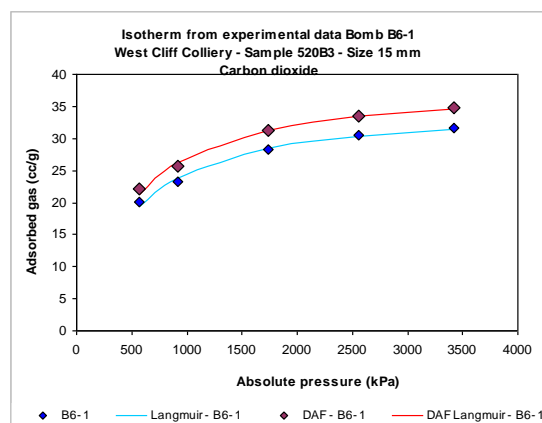
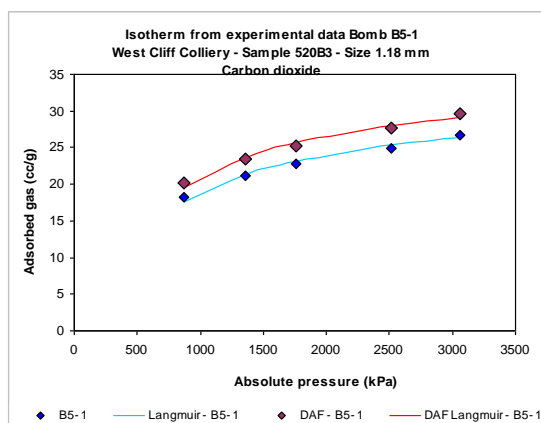


CO₂ sorption capacity – Sample BH-1 -- Langmuir equation – Sample BH-1

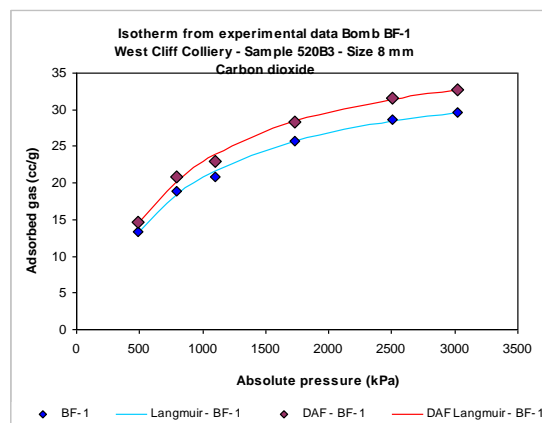
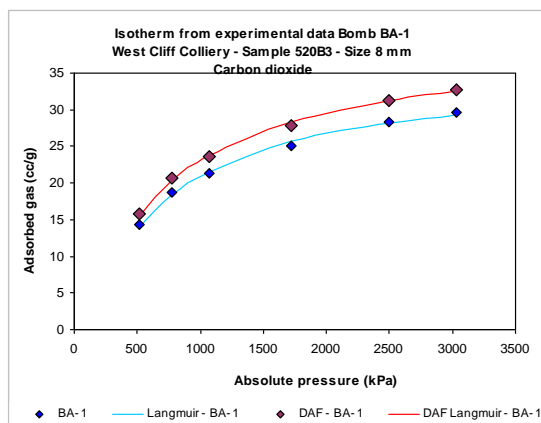
Appendix 12 – CO₂ adsorbed mass in desorption



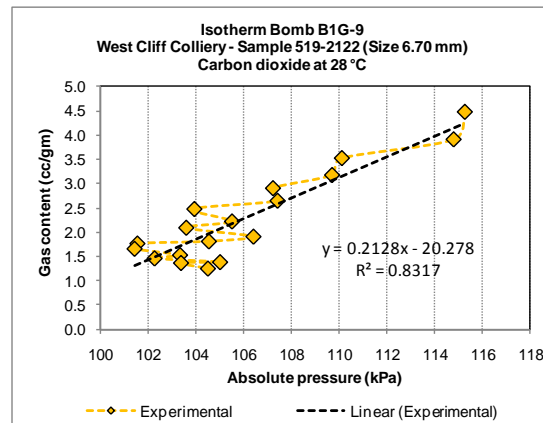
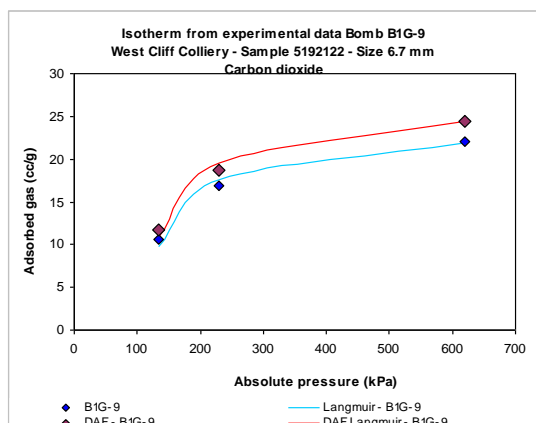
CO₂ adsorbed mass in desorption – Sample B2-1 and B3-1



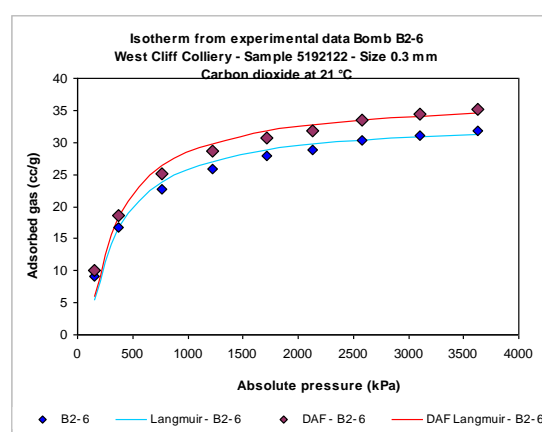
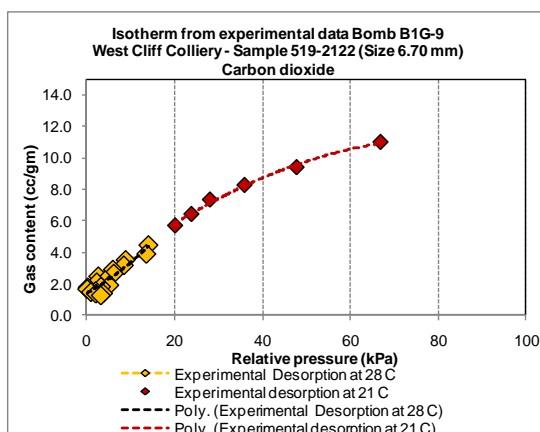
CO₂ adsorbed mass in desorption – Sample B5-1 and B6-1



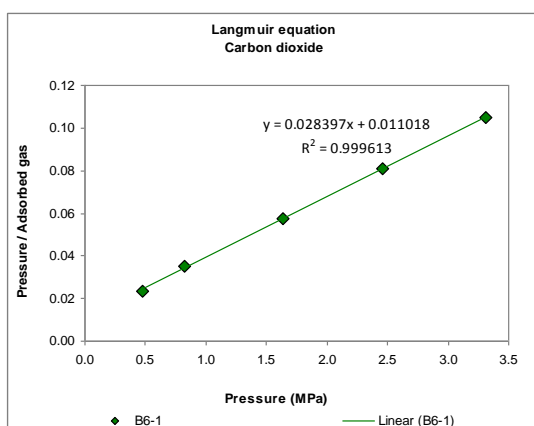
CO₂ adsorbed mass in desorption – Sample BA-1 and BF-1



CO₂ adsorbed mass in desorption – Sample B1G-9

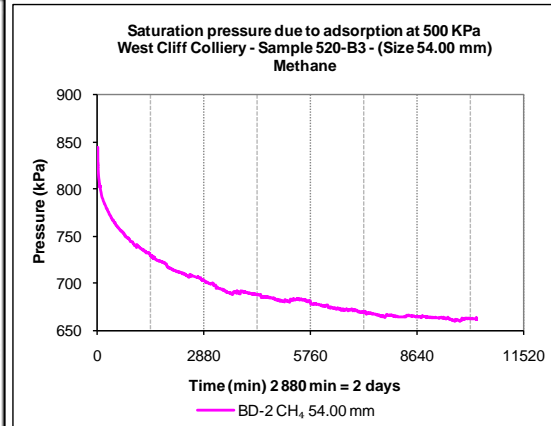
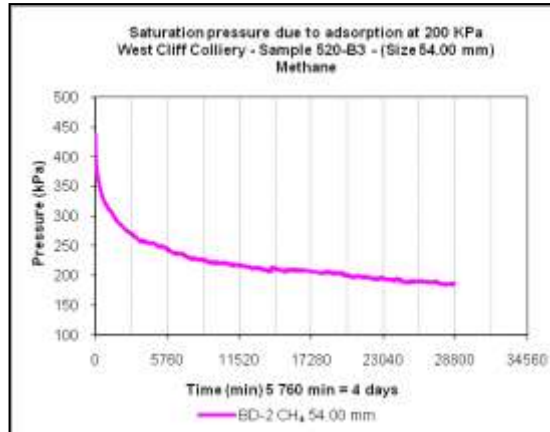


CO₂ adsorbed mass in desorption – Sample B1G-9 and B2-6

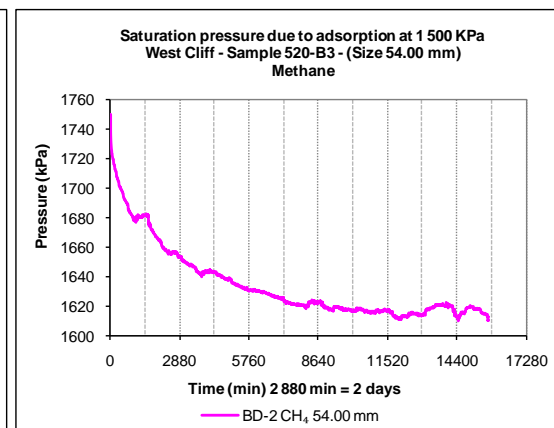
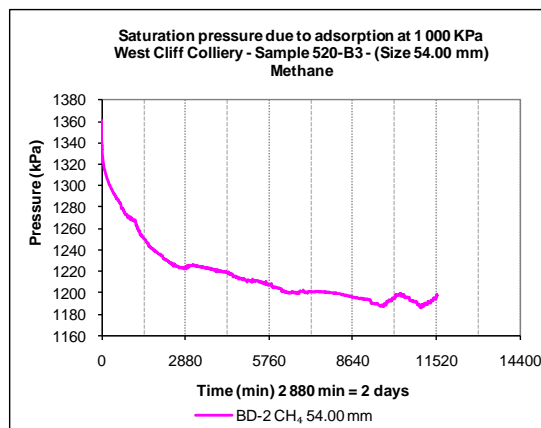


Langmuir equation in desorption – Sample B6-1

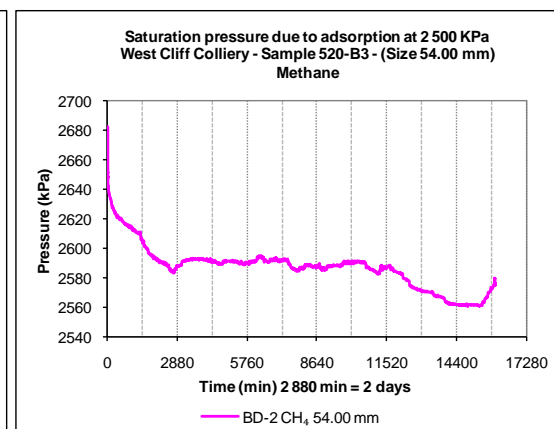
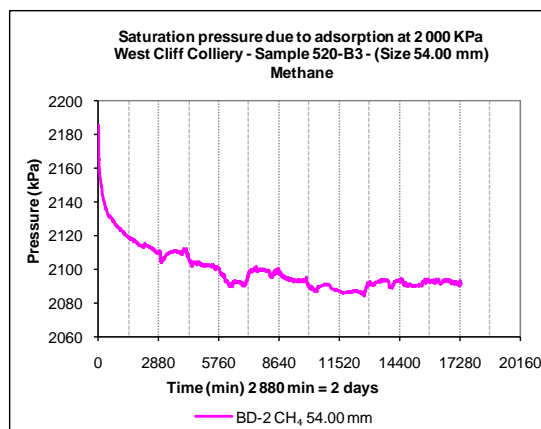
Appendix 13 – CH₄ saturation time in adsorption – Sample BD-2 (54.00 mm diameter)



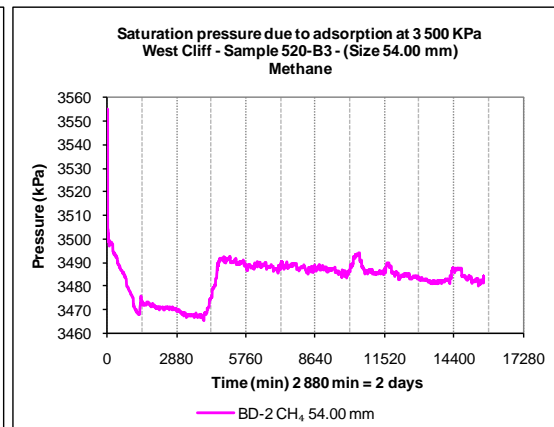
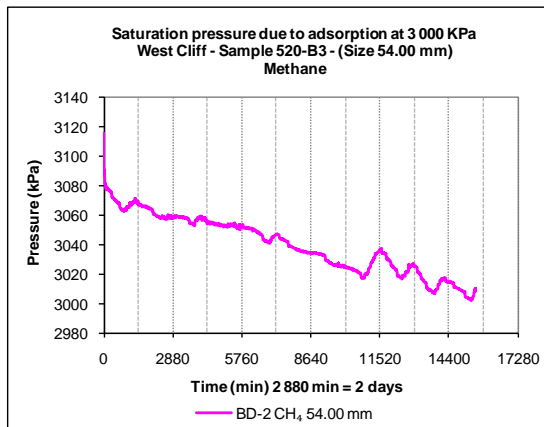
Saturation pressure due to adsorption at 200 and 500 kPa pressure levels



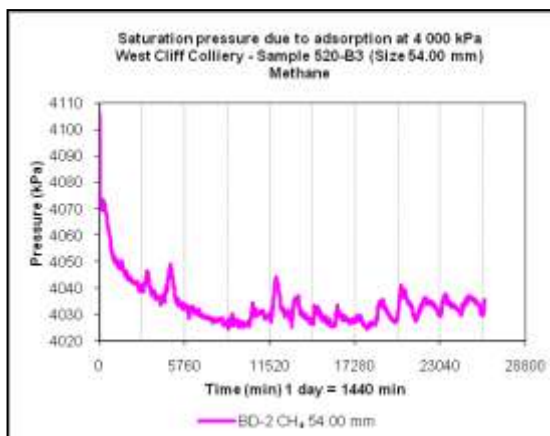
Saturation pressure due to adsorption at 1 000 and 1 500 kPa pressure levels



Saturation pressure due to adsorption at 2 000 and 2 500 kPa pressure levels

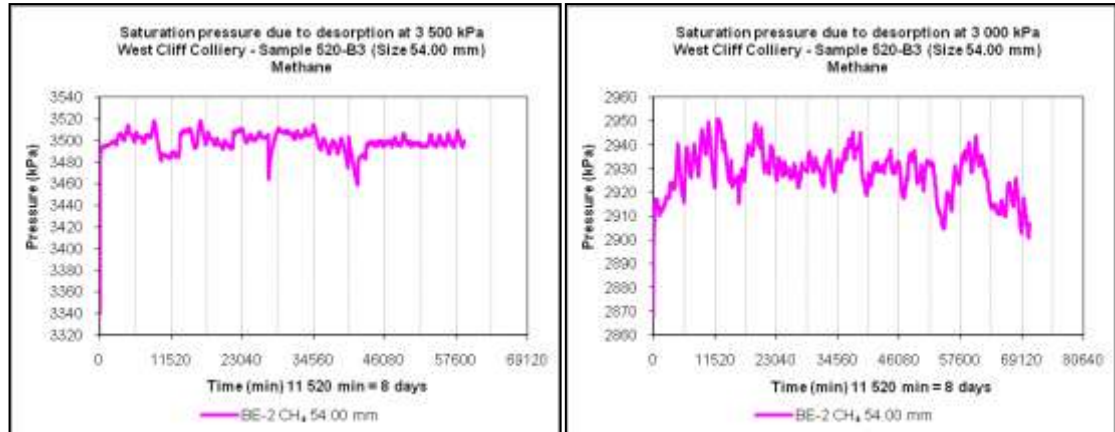


Saturation pressure due to adsorption at 3 000 and 3 500 kPa pressure levels

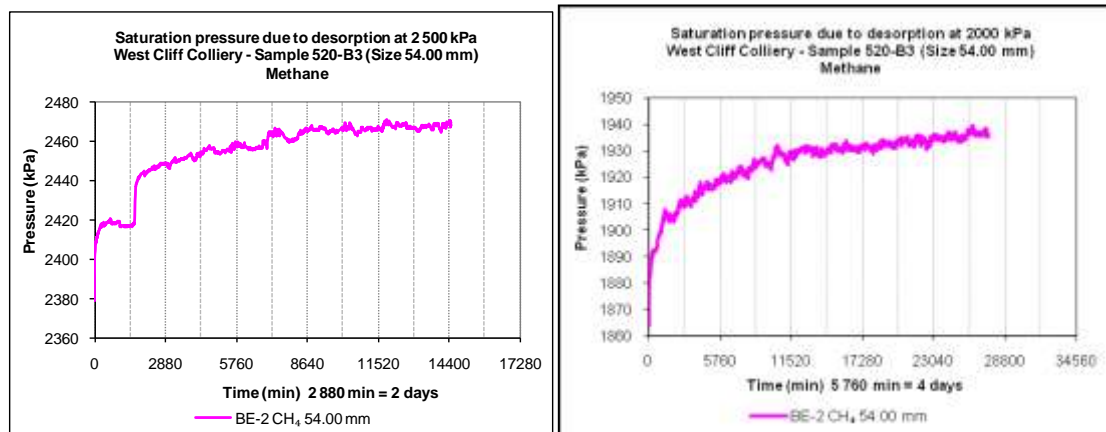


Saturation pressure due to adsorption at 4 000 kPa pressure level

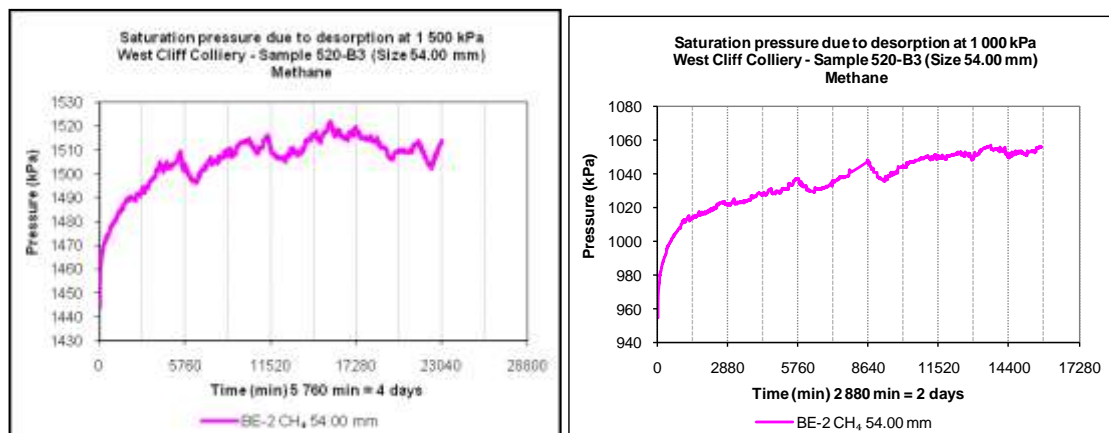
Appendix 14 – CH₄ saturation time in desorption – Sample BE-2 (54.00 mm diameter)



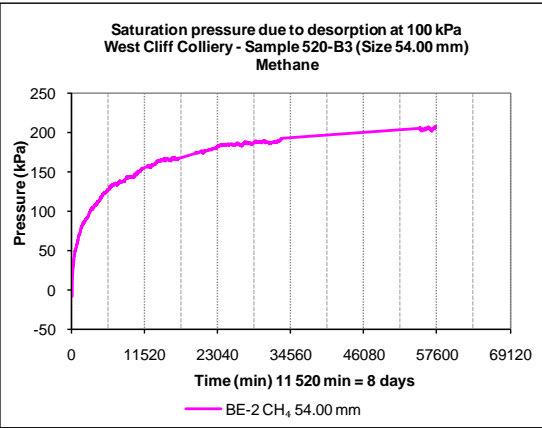
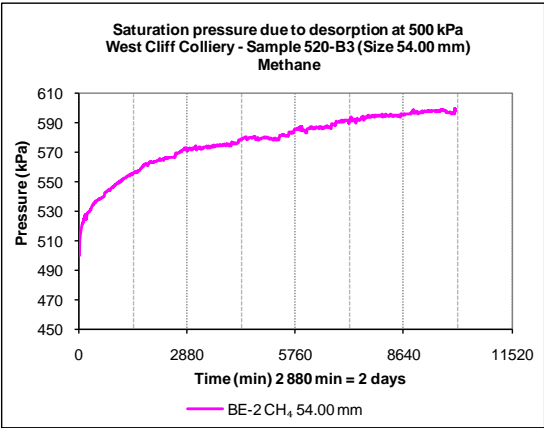
Saturation pressure due to desorption at 3 500 and 3 000 kPa pressure levels



Saturation pressure due to desorption at 2 500 and 2 000 kPa pressure levels

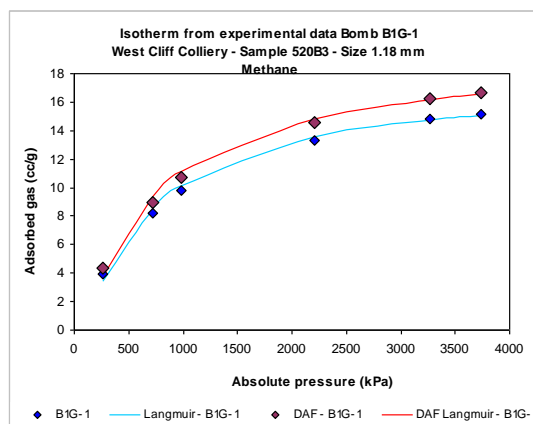
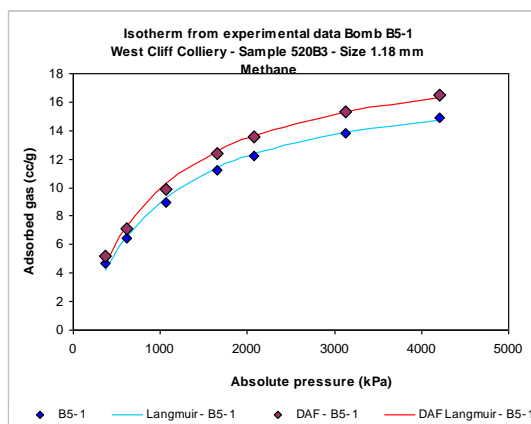


Saturation pressure due to desorption at 1 500 and 1 000 kPa pressure levels

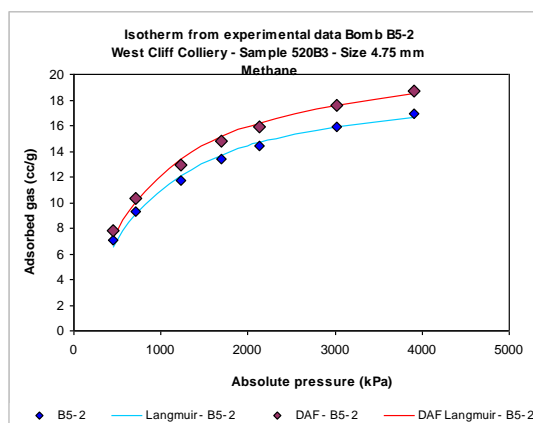
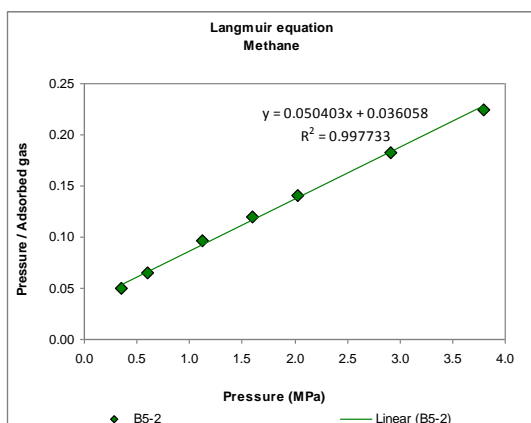


Saturation pressure due to desorption at 500 and 100 kPa pressure levels

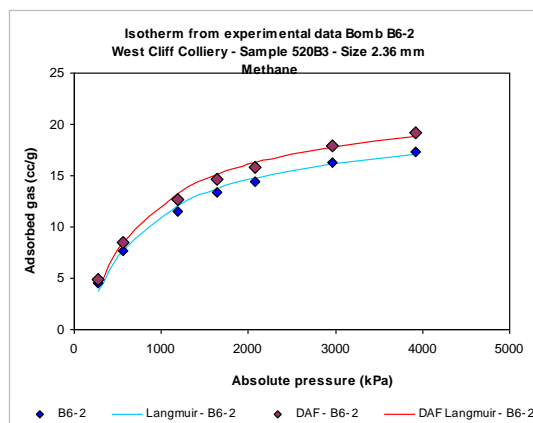
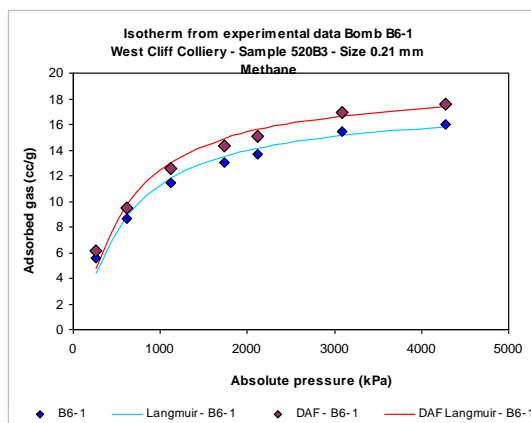
Appendix 15 – CH₄ adsorbed mass in adsorption



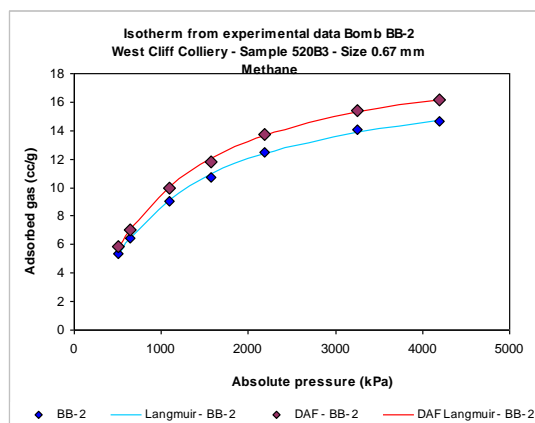
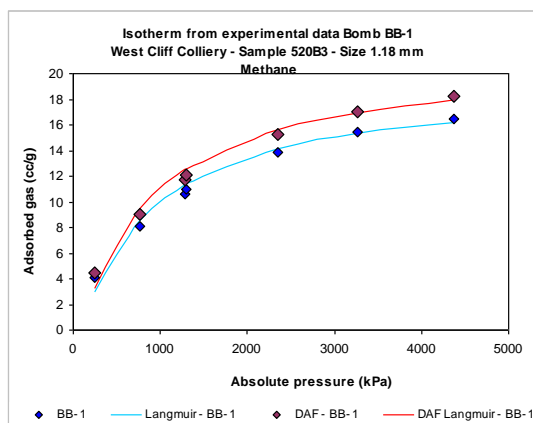
CH₄ adsorbed mass in adsorption – Sample B5-1 and B1G-1



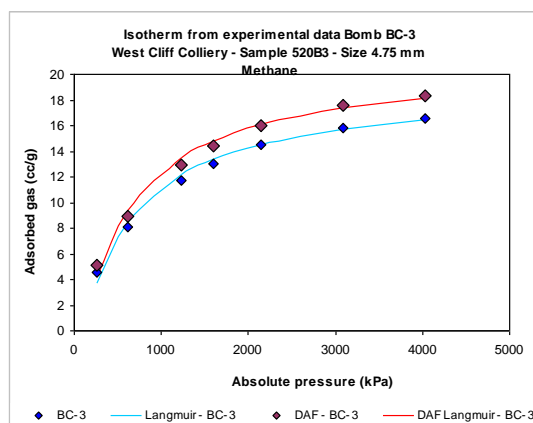
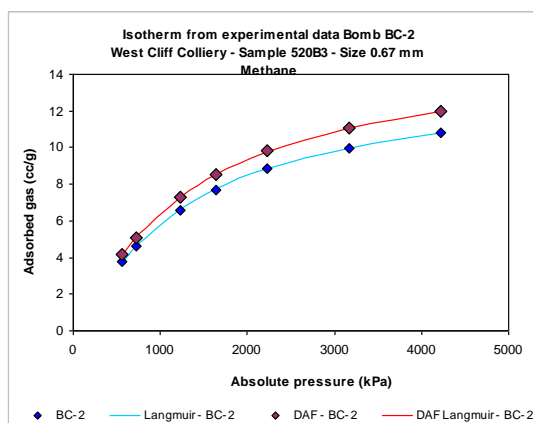
CH₄ adsorbed mass in adsorption – Sample B5-2



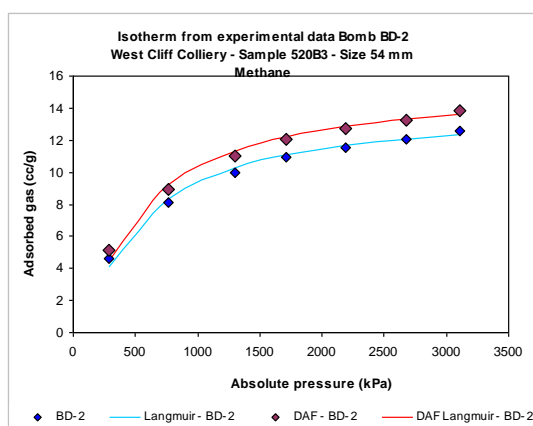
CH₄ adsorbed mass in adsorption – Sample B6-1 and B6-2



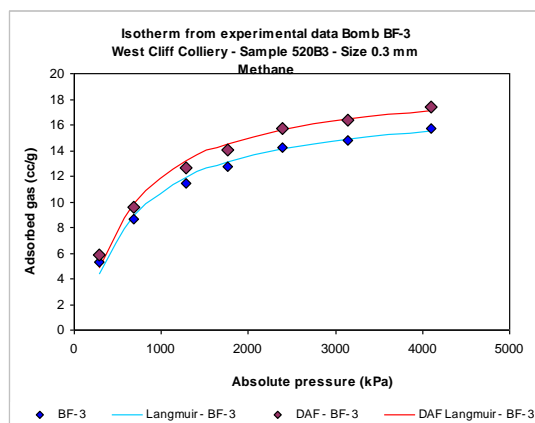
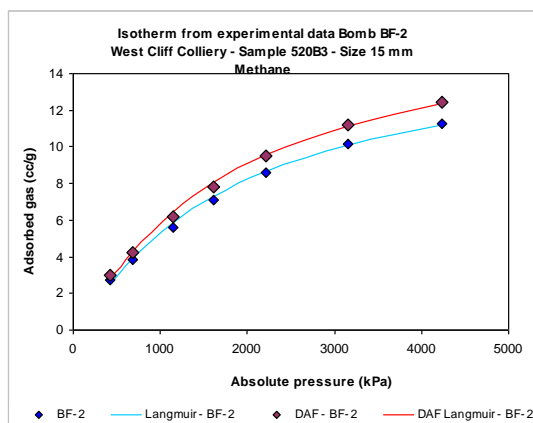
CH₄ adsorbed mass in adsorption – Sample BB-1 and BB-2



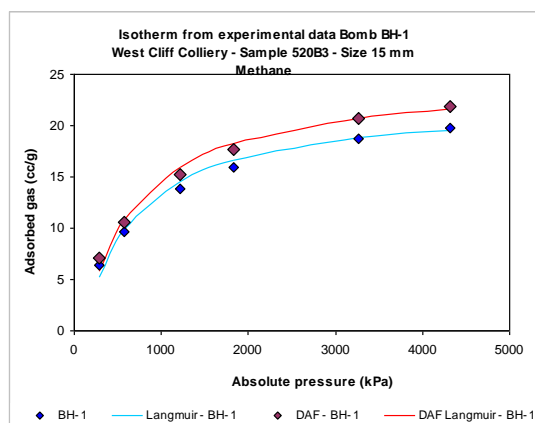
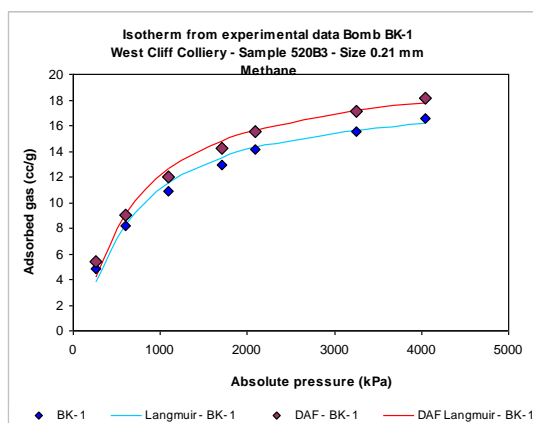
CH₄ adsorbed mass in adsorption – Sample BC-2 and BC-3



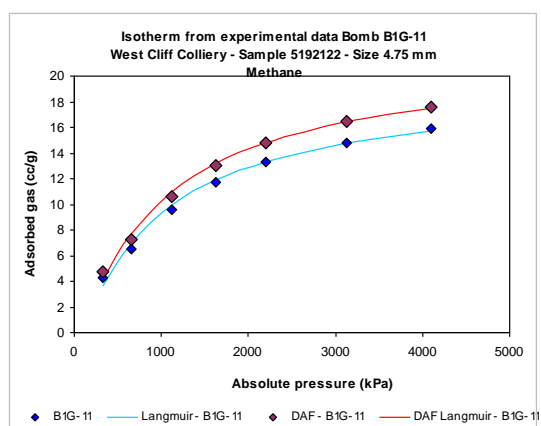
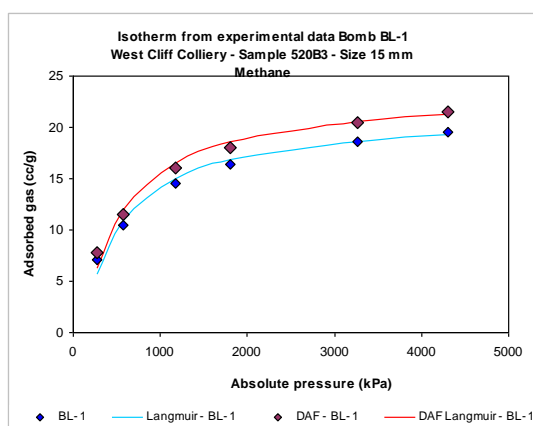
CH₄ adsorbed mass in adsorption – Sample BD-2



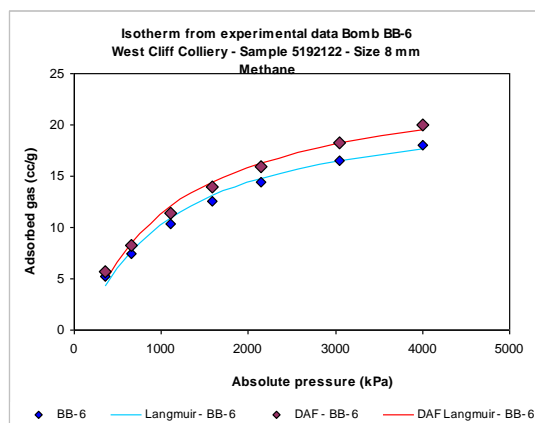
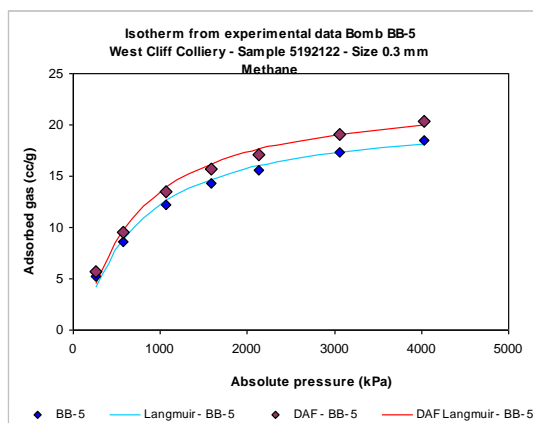
CH₄ adsorbed mass in adsorption – Sample BF-2 and BF-3



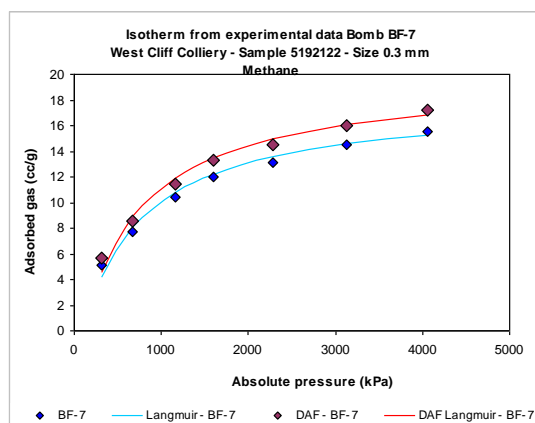
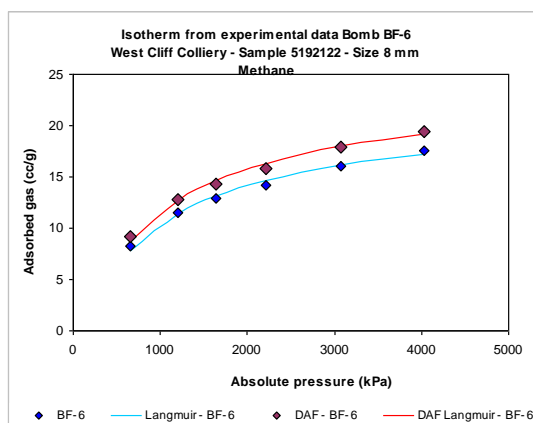
CH₄ adsorbed mass in adsorption – Sample BK-1 and BH-1



CH₄ adsorbed mass in adsorption – Sample BL-1 and B1G-11

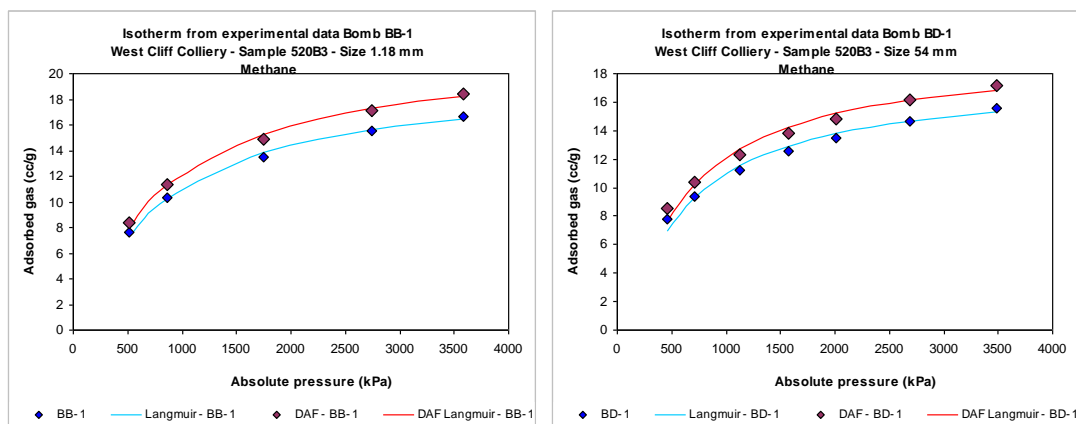


CH₄ adsorbed mass in adsorption – Sample BB-5 and BB-6

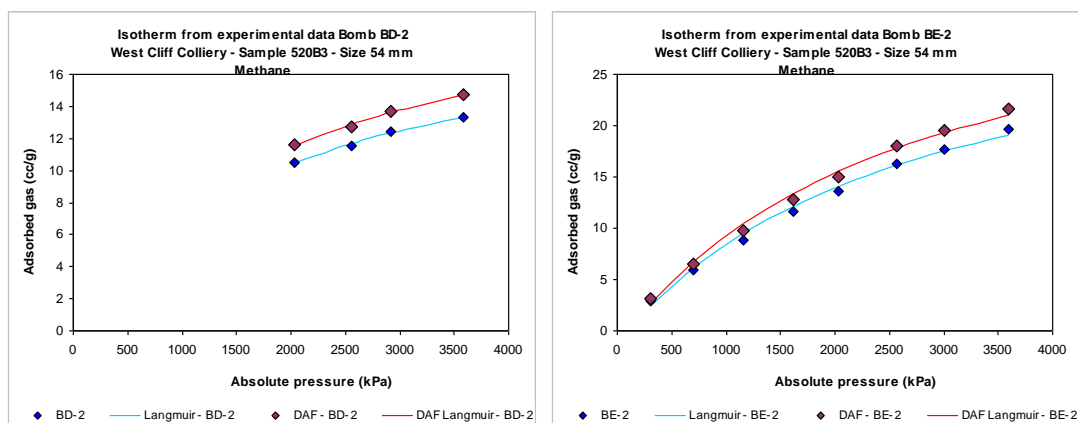


CH₄ adsorbed mass in adsorption – Sample BF-6 and BF-7

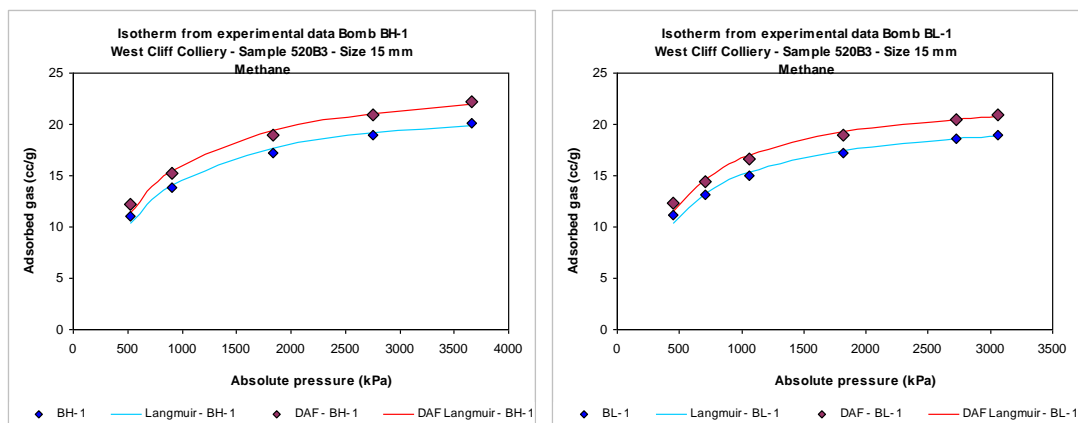
Appendix 16 – CH₄ adsorbed mass in desorption



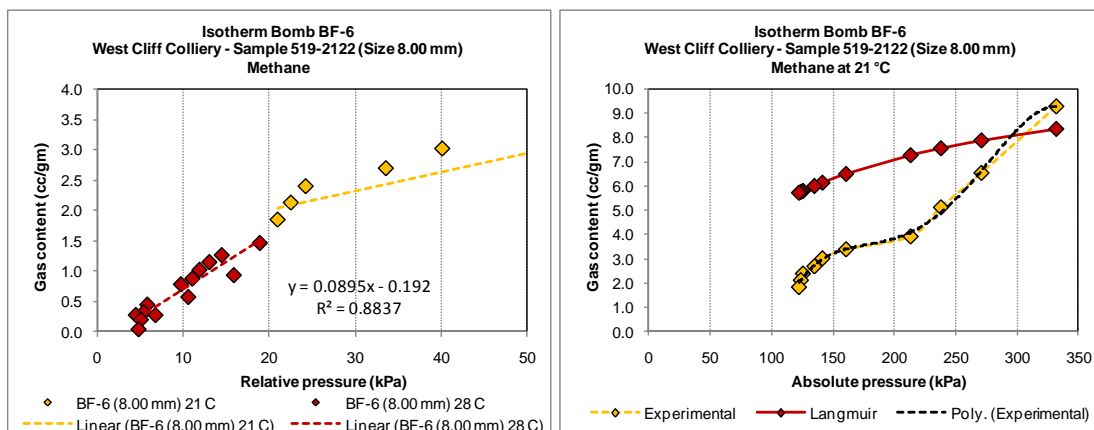
CH₄ adsorbed mass in desorption – Sample BB-1 and BD-1



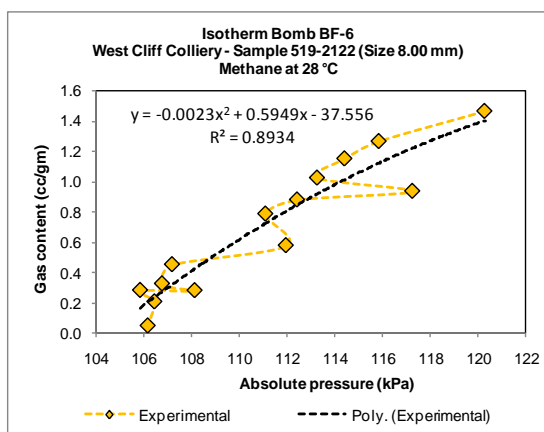
CH₄ adsorbed mass in desorption – Sample BD-2 and BE-2



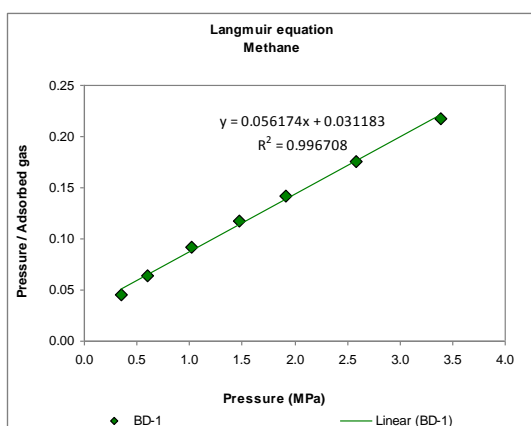
CH₄ adsorbed mass in desorption – Sample BH-1 and BL-1



CH₄ adsorbed mass in desorption – Sample BF-6

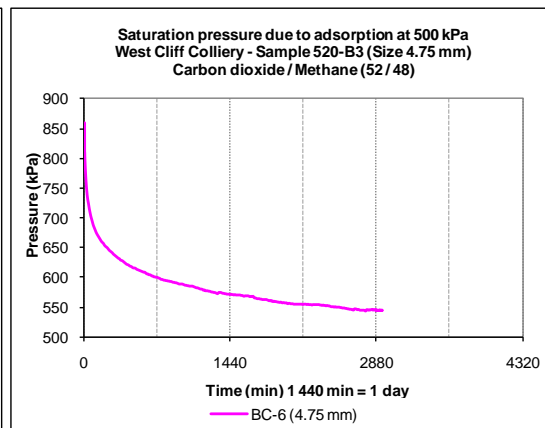
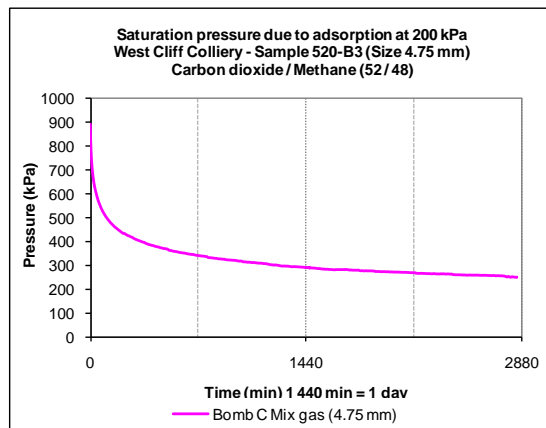


CH₄ adsorbed mass in desorption – Sample BF-6

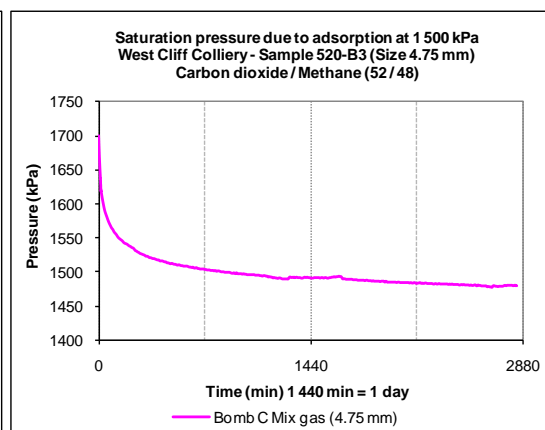
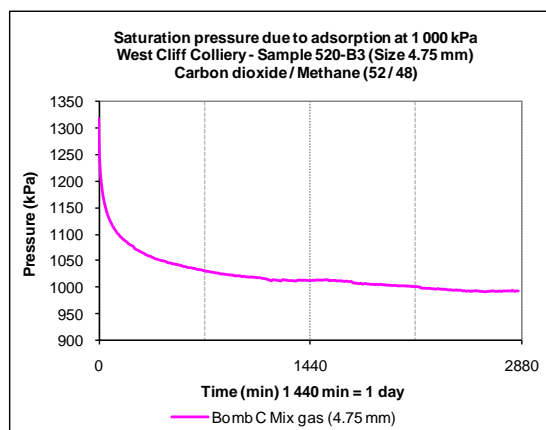


Langmuir equation in desorption – Sample BD-1

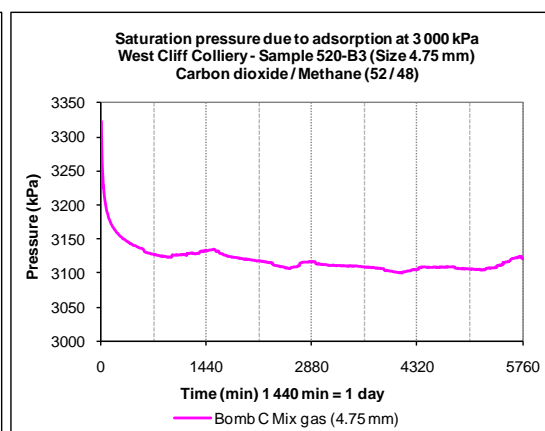
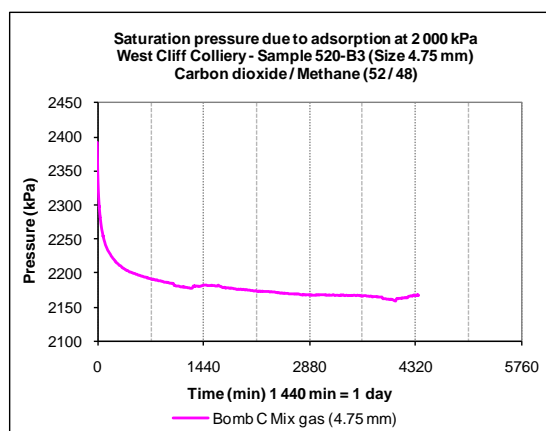
Appendix 17 – Binary mixed gas saturation time in adsorption – Sample BC-6 (4.75 mm)



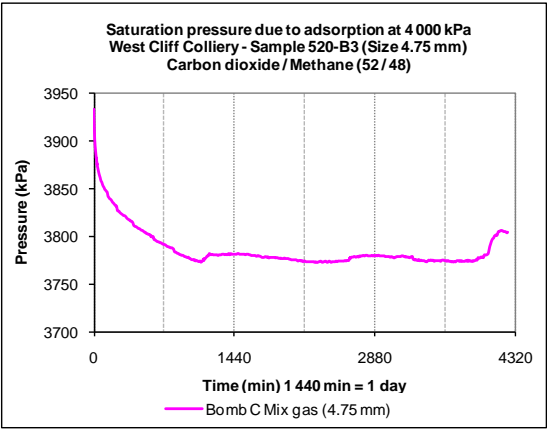
Saturation pressure due to adsorption at 200 and 500 kPa pressure levels



Saturation pressure due to adsorption at 1 000 and 1 500 kPa pressure levels

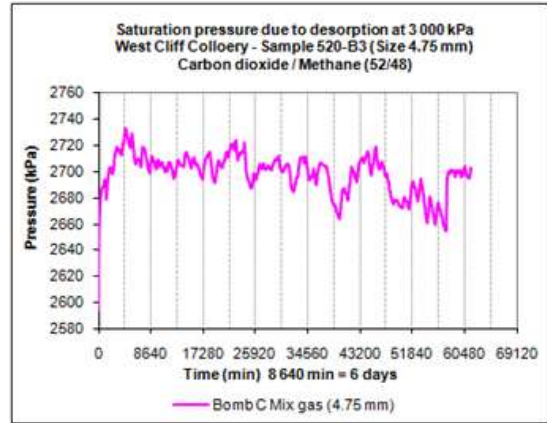
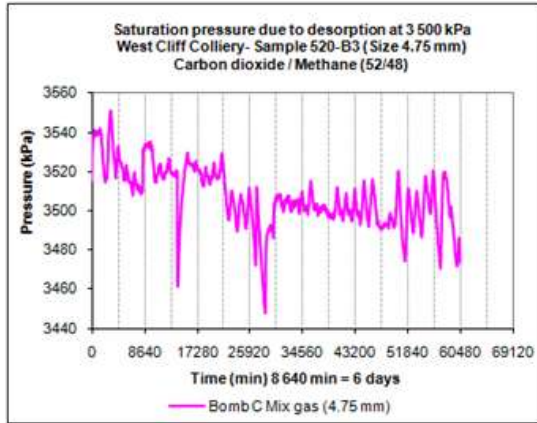


Saturation pressure due to adsorption at 2 000 and 3 000 kPa pressure levels

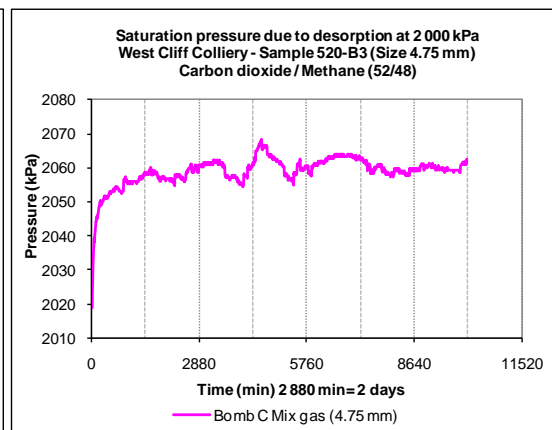
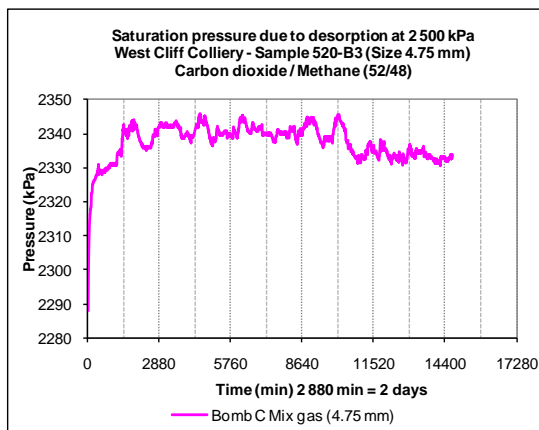


Saturation pressure due to adsorption at 4 000 kPa pressure level

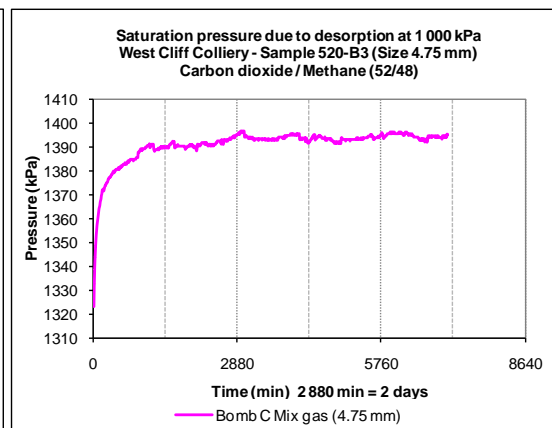
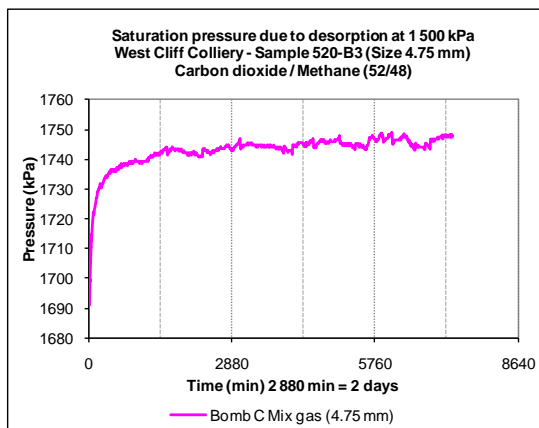
Appendix 18 – Binary mixed gas saturation time in desorption – Sample BC-6 (4.75 mm)



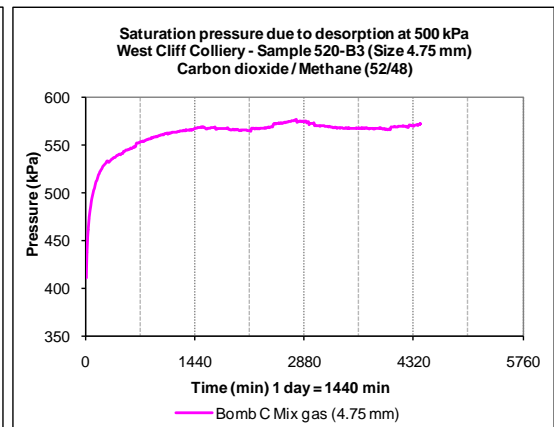
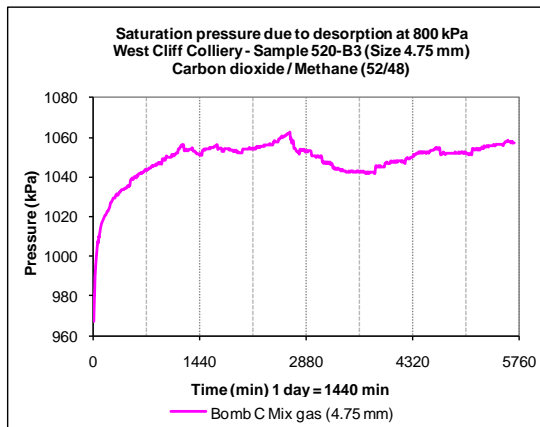
Saturation pressure due to desorption at 3 500 and 3 000 kPa pressure levels



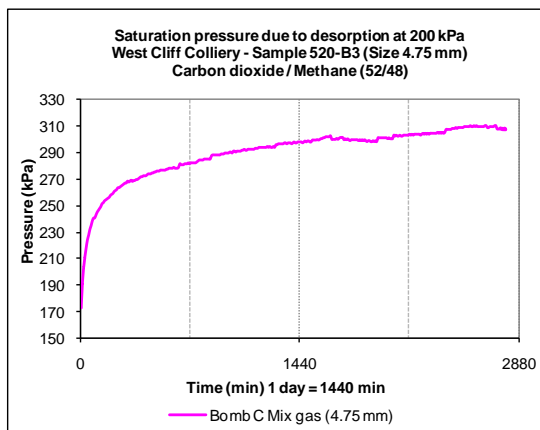
Saturation pressure due to desorption at 2 500 and 2 000 kPa pressure levels



Saturation pressure due to desorption at 1 500 and 1 000 kPa pressure levels

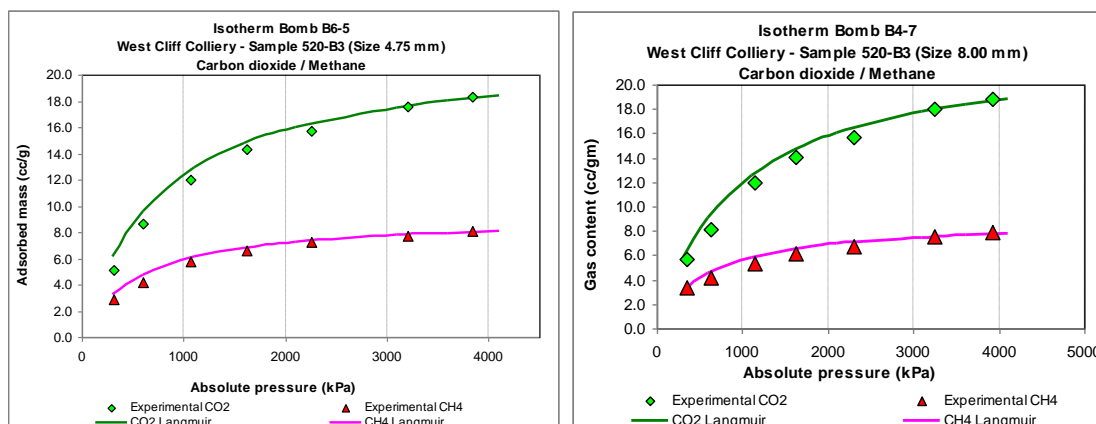


Saturation pressure due to desorption at 800 and 500 kPa pressure levels

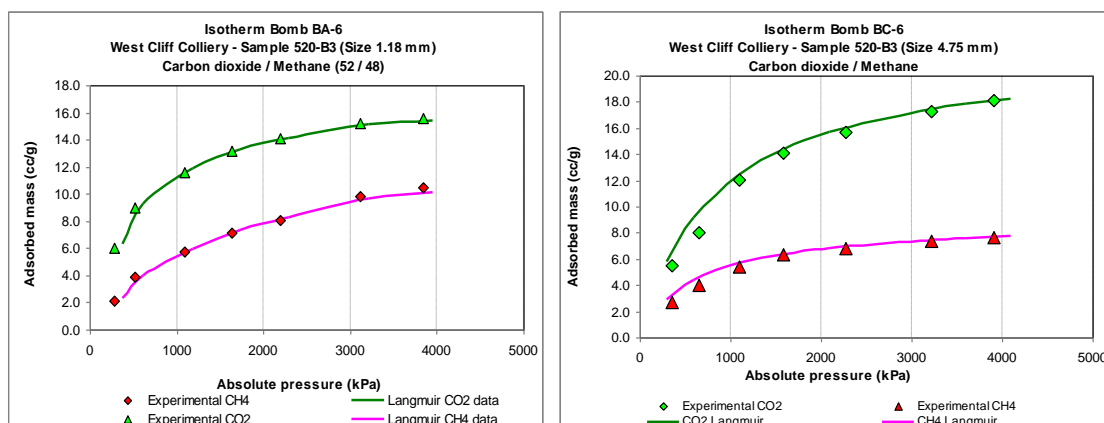


Saturation pressure due to desorption at 200 kPa pressure level

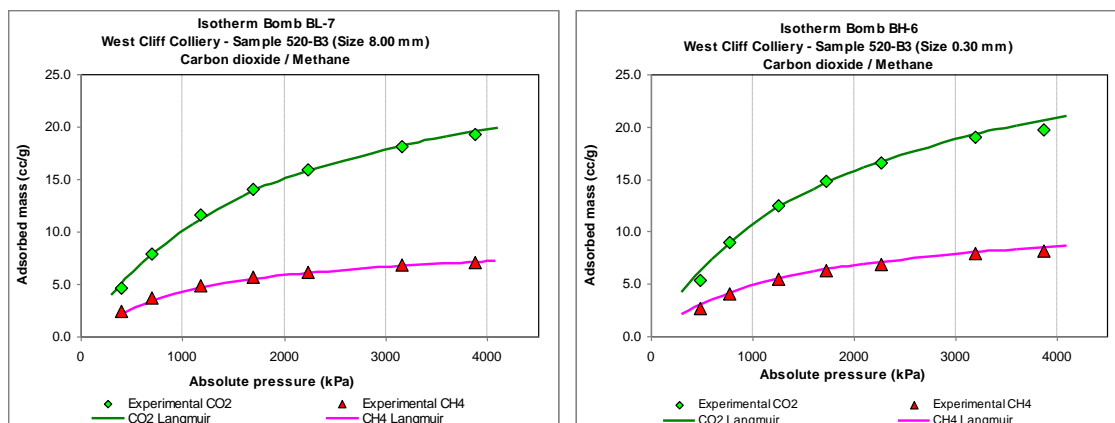
Appendix 19 – Binary CO₂/CH₄ mixed adsorbed mass in adsorption



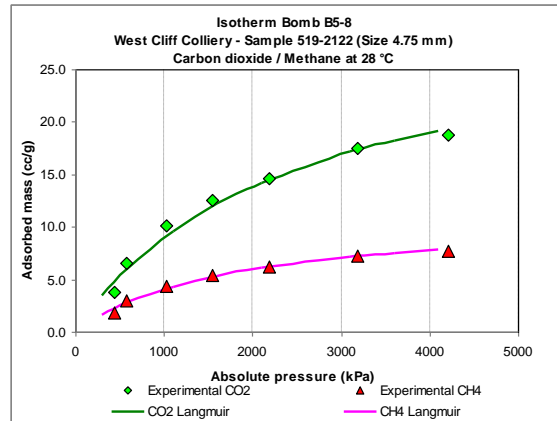
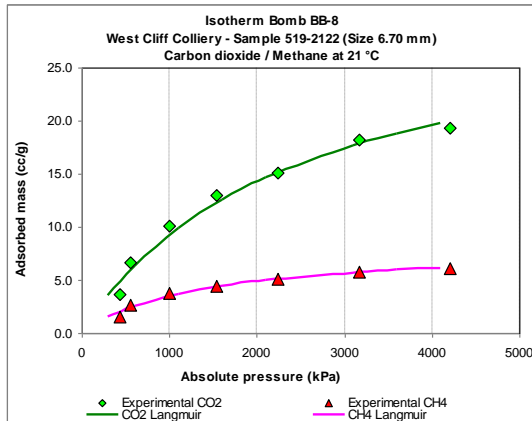
CO₂ and CH₄ adsorbed mass in adsorption – Sample B6-5 and B4-7



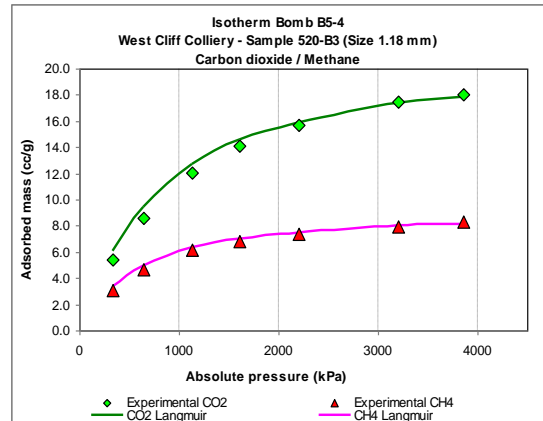
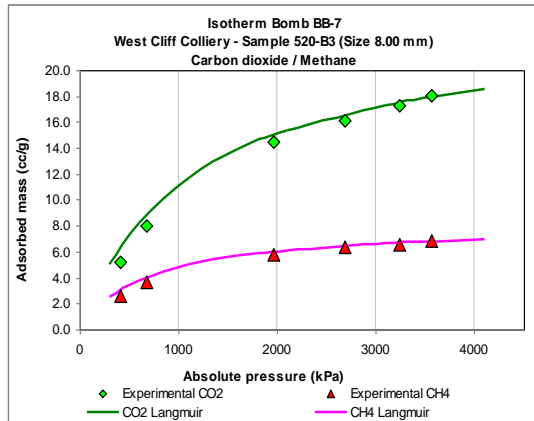
CO₂ and CH₄ adsorbed mass in adsorption – Sample BA-6 and BC-6



CO₂ and CH₄ adsorbed mass in adsorption – Sample BL-7 and BH-6

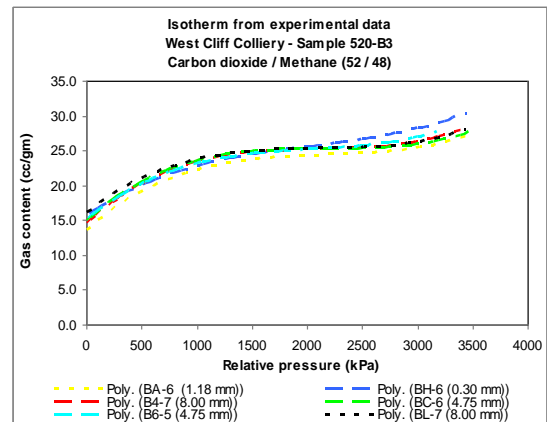
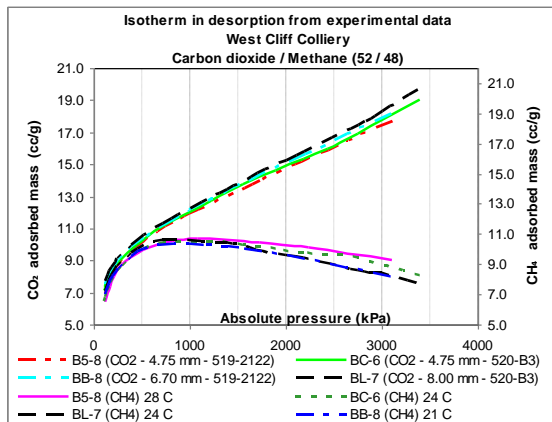


CO₂ and CH₄ adsorbed mass in adsorption – Sample BB-8 and B5-8

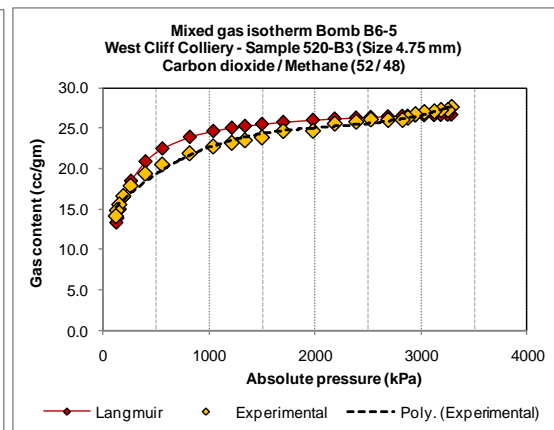
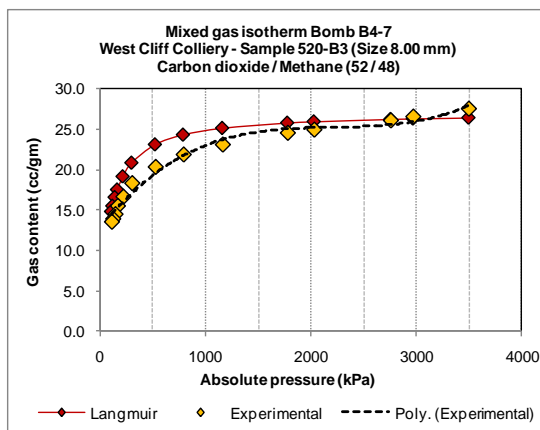


CO₂ and CH₄ adsorbed mass in adsorption – Sample BB-7 and Sample B5-4

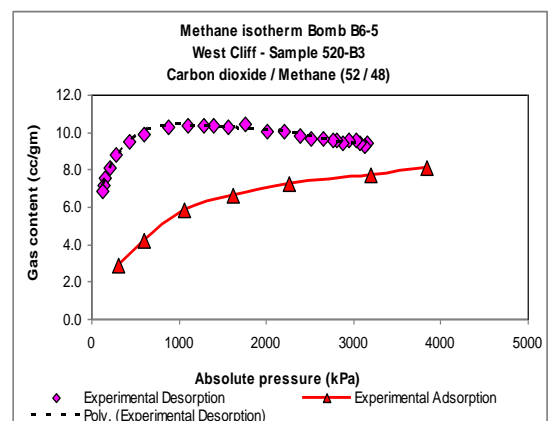
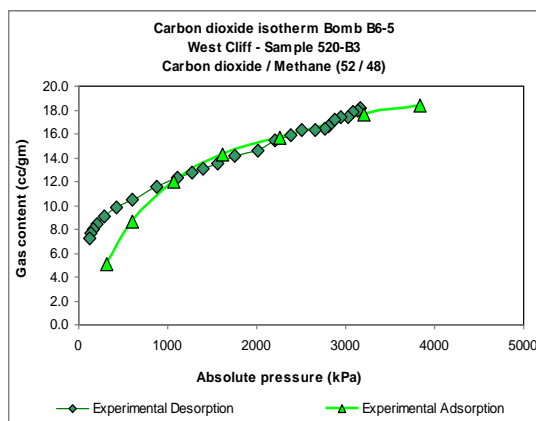
Appendix 20 – Binary CO₂/CH₄ mixed adsorbed mass in desorption



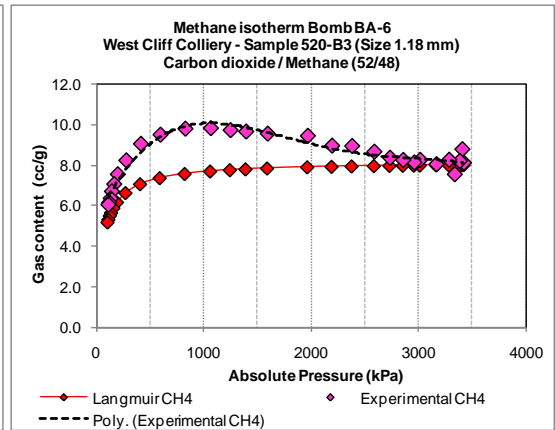
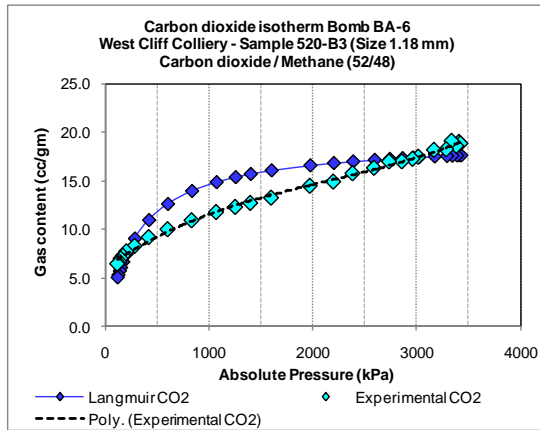
CO₂ and CH₄ components and mixed gas adsorbed mass in desorption



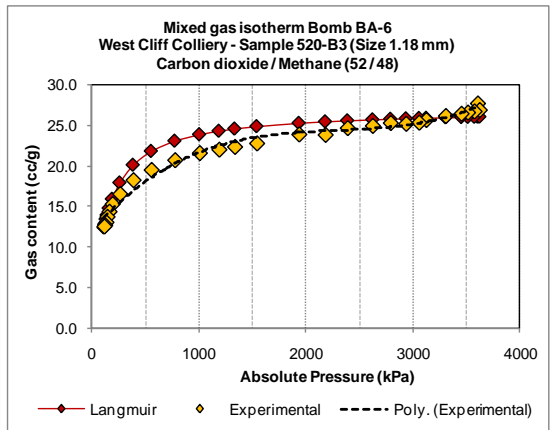
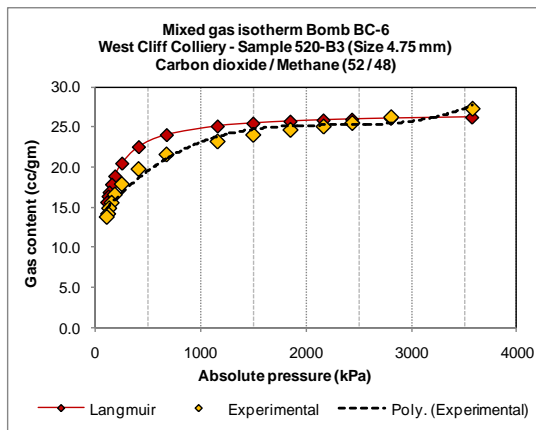
Mixed adsorbed mass in desorption – Sample B4-7 and B6-5



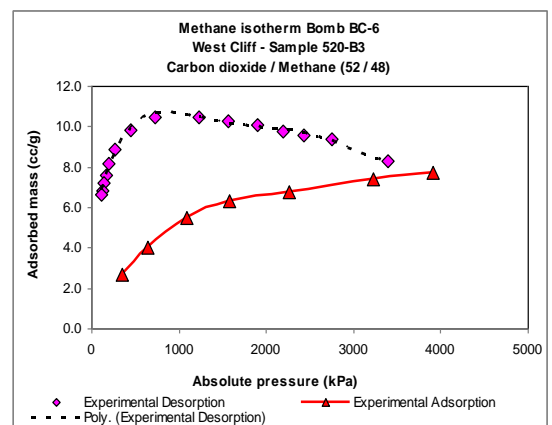
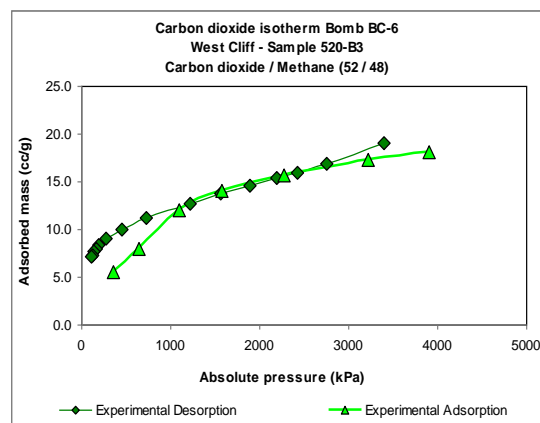
CO₂ and CH₄ adsorbed mass in desorption – Sample B6-5



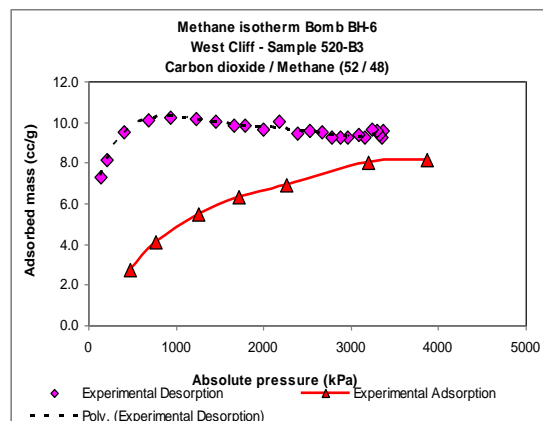
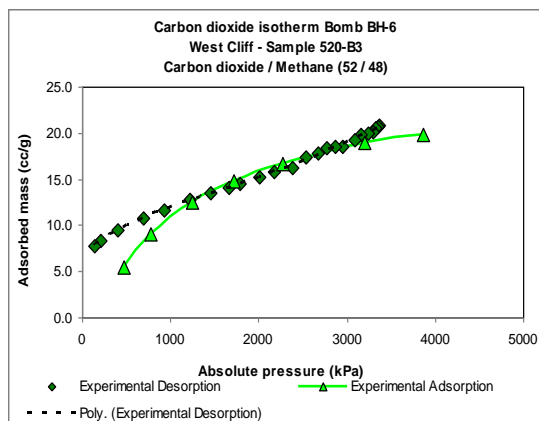
CO₂ and CH₄ adsorbed mass in desorption – Sample BA-6



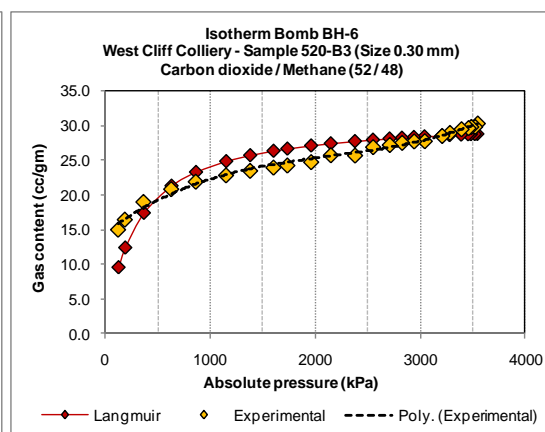
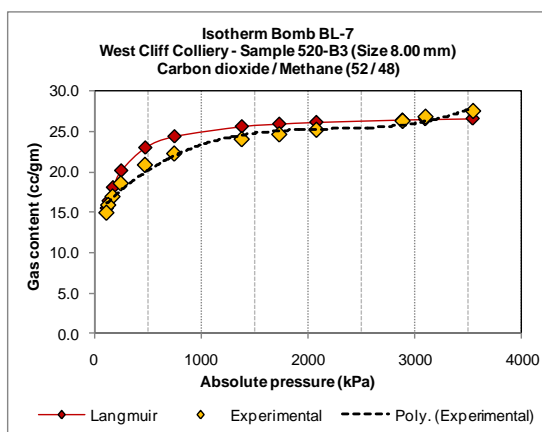
Mixed adsorbed mass in desorption – Sample BC-6 and BA-6



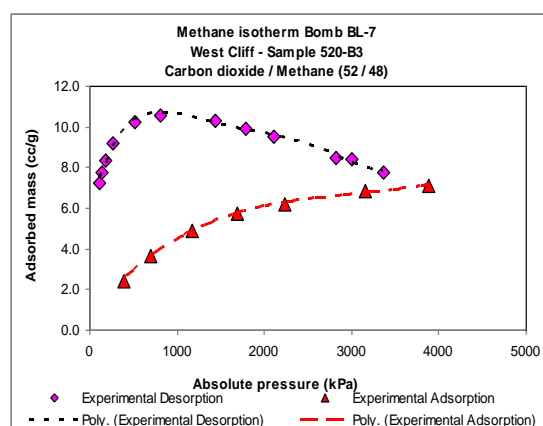
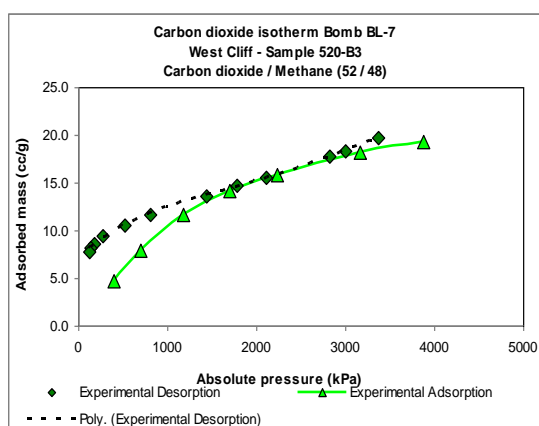
CO₂ and CH₄ adsorbed mass in desorption – Sample BC-6



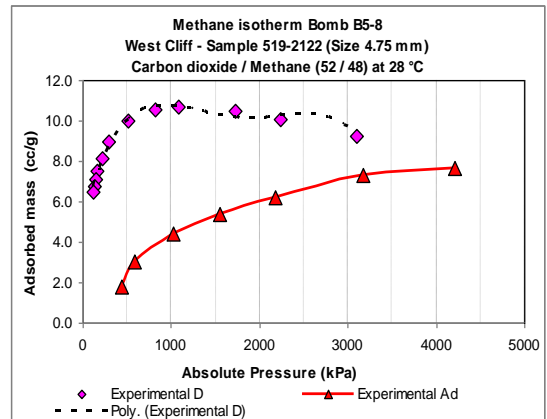
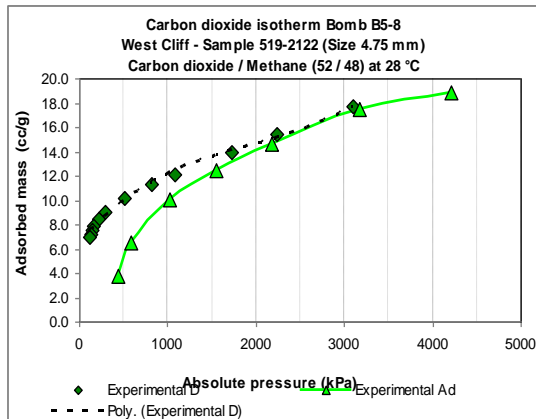
CO₂ and CH₄ adsorbed mass in desorption – Sample BH-6



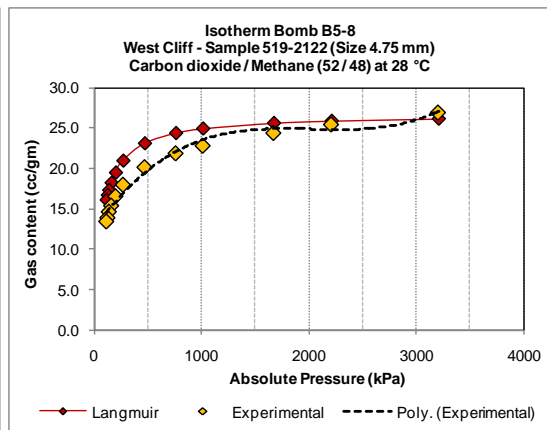
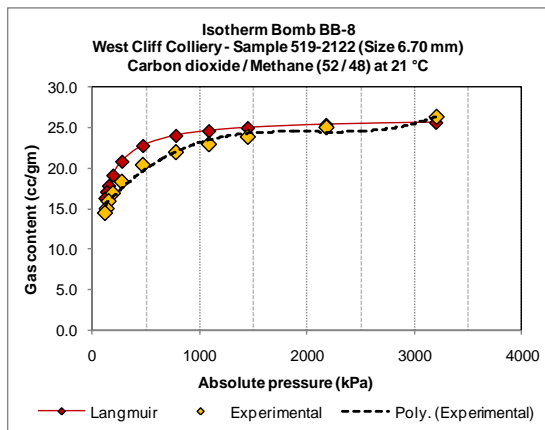
Mixed adsorbed mass in desorption – Sample BH-6 and BL-7



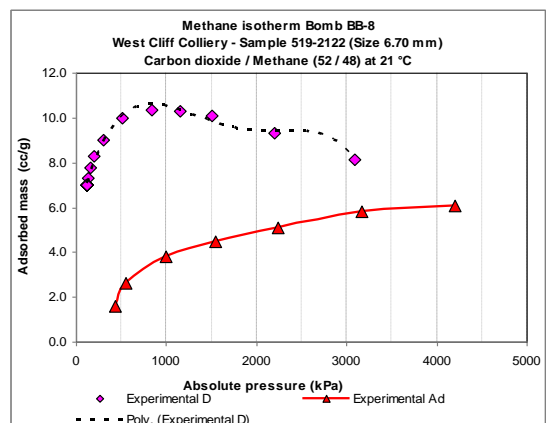
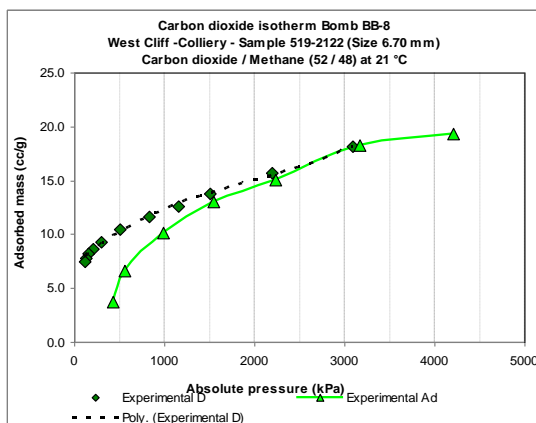
CO₂ and CH₄ adsorbed mass in desorption – Sample BL-7



CO₂ and CH₄ adsorbed mass in desorption – Sample B5-8

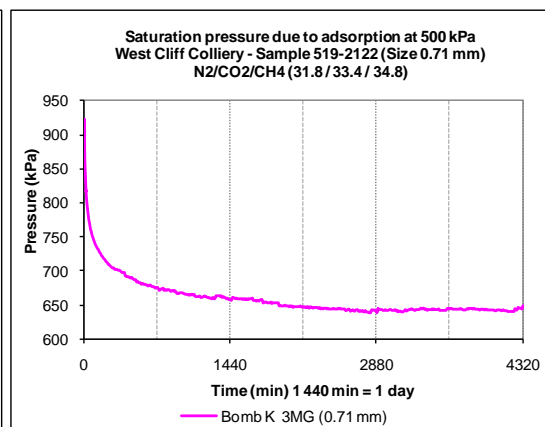
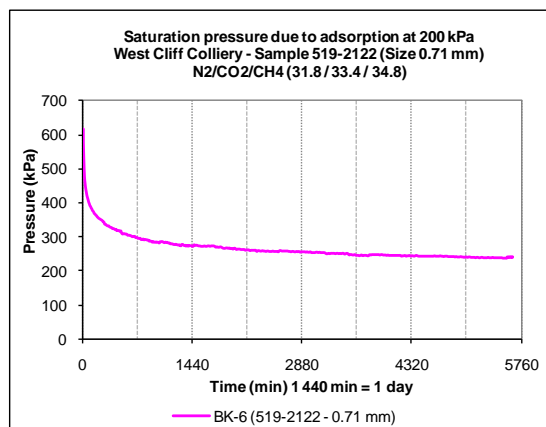


Mixed adsorbed mass in desorption – Sample B5-8 and BB-8

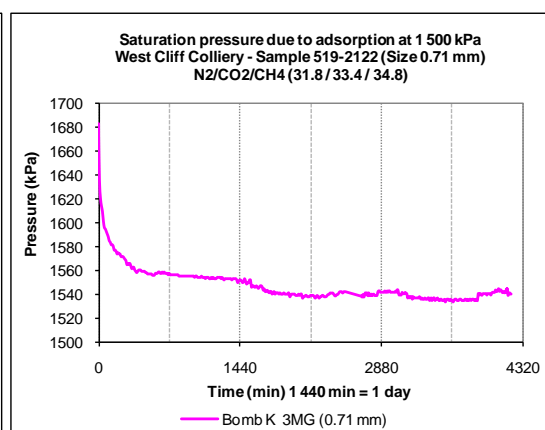
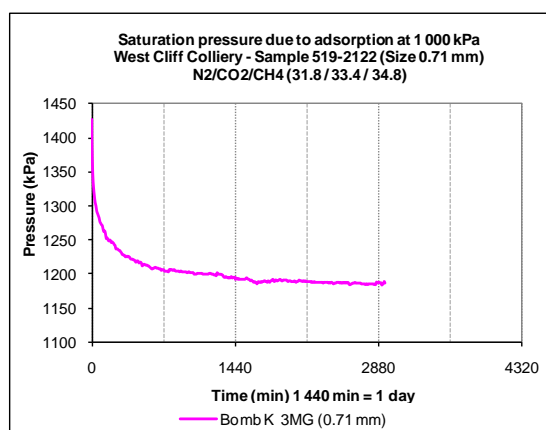


CO₂ and CH₄ adsorbed mass in desorption – Sample BB-8

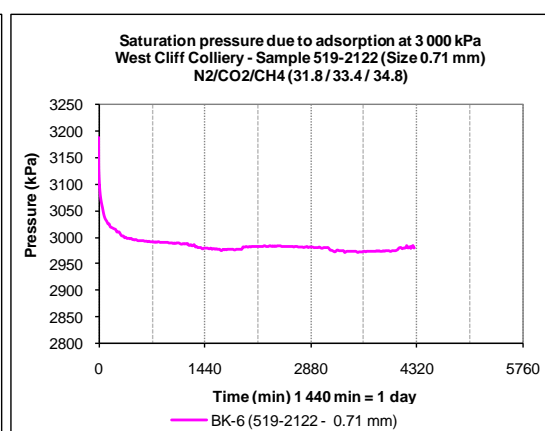
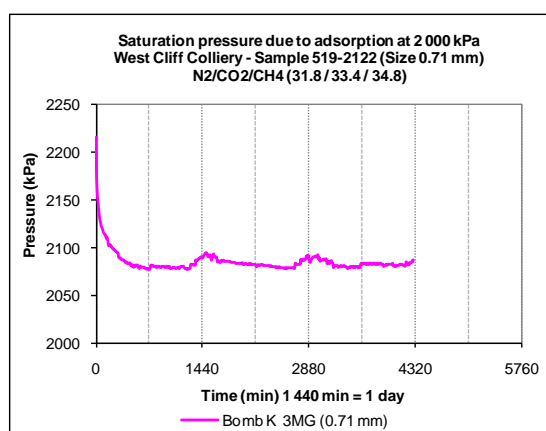
APPENDIX 21 - Ternary N₂/CO₂/CH₄ mixed gas saturation time in adsorption - Sample BK-6 (0.71 mm)



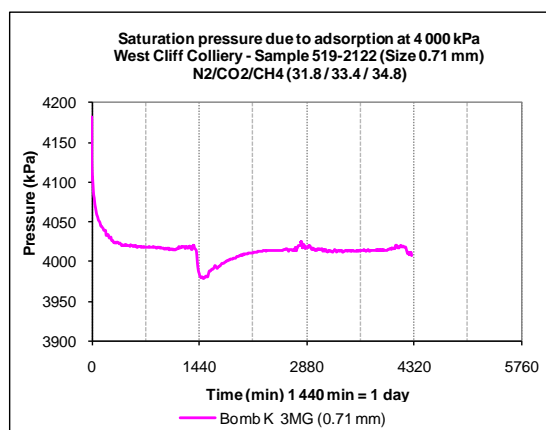
Saturation pressure due to adsorption at 200 and 500 kPa pressure levels



Saturation pressure due to adsorption at 1 000 and 1 500 kPa pressure levels

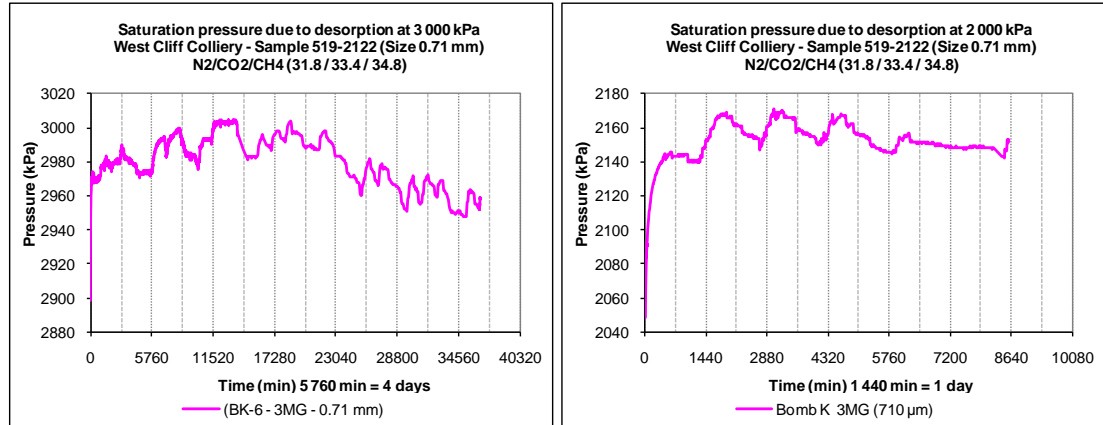


Saturation pressure due to adsorption at 2 000 and 3 000 kPa pressure levels

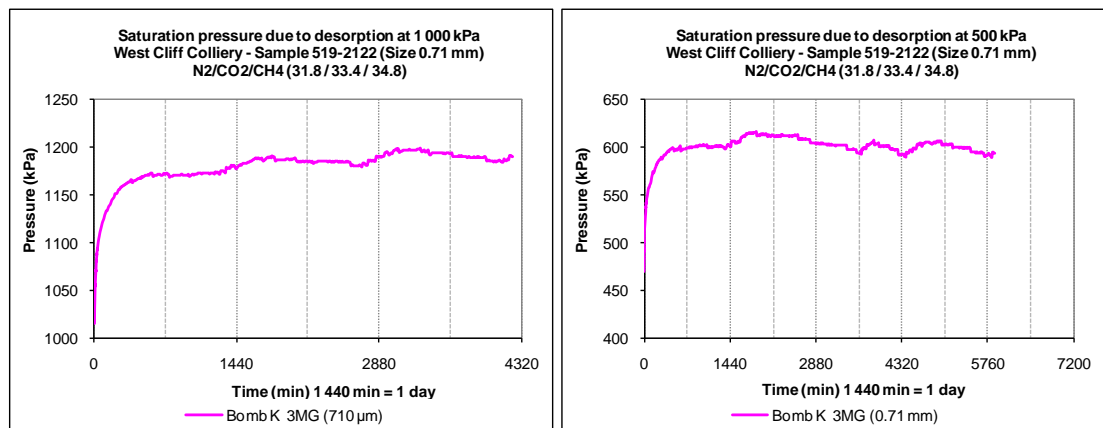


Saturation pressure due to adsorption at 4 000 kPa pressure levels

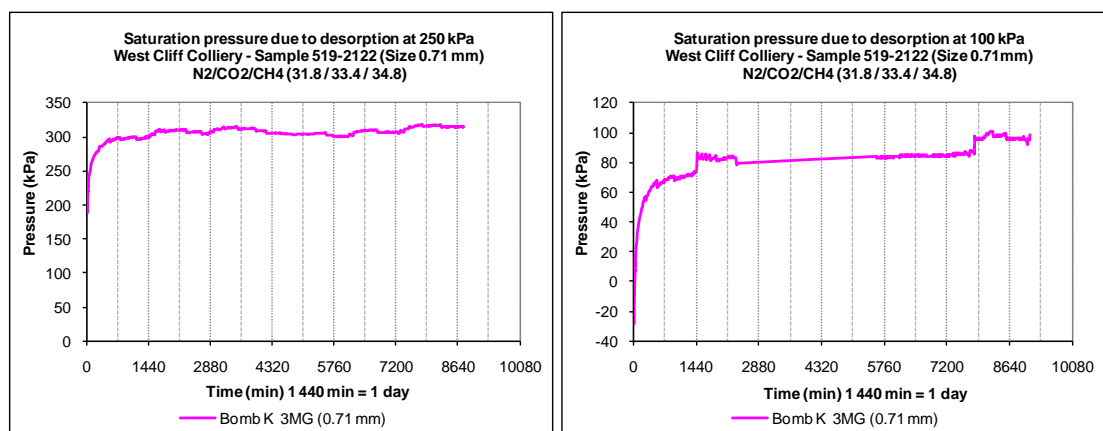
APPENDIX 22 - Ternary N₂/CO₂/CH₄ mixed gas saturation time in desorption - Sample BK-6 (0.71 mm)



Saturation pressure due to desorption at 3 000 and 2 000 kPa pressure levels

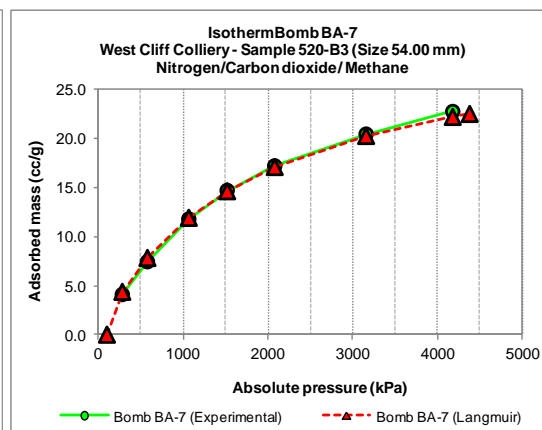
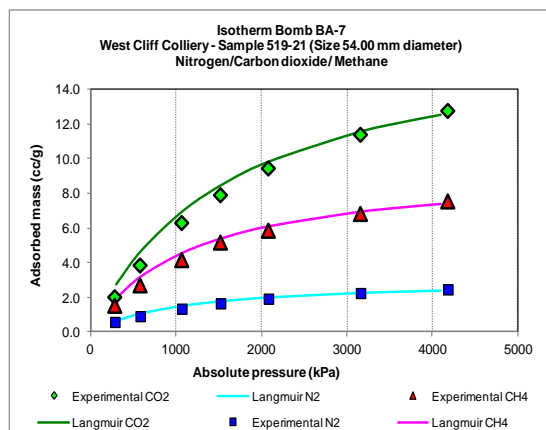


Saturation pressure due to desorption at 1 000 and 500 kPa pressure levels

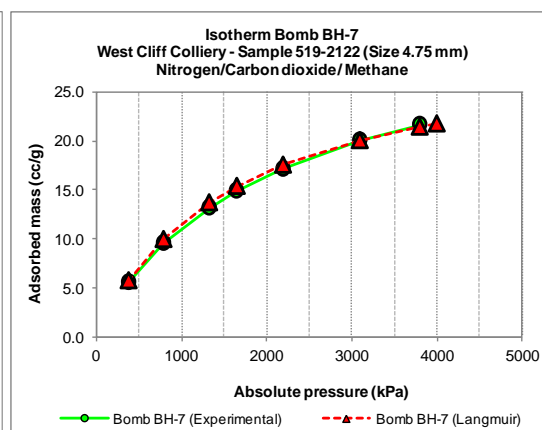
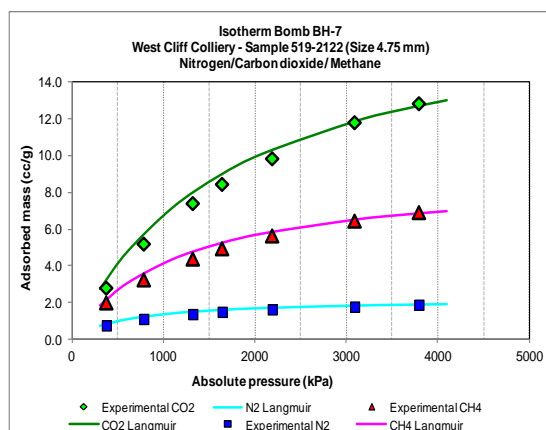


Saturation pressure due to desorption at 250 and 100 kPa pressure levels

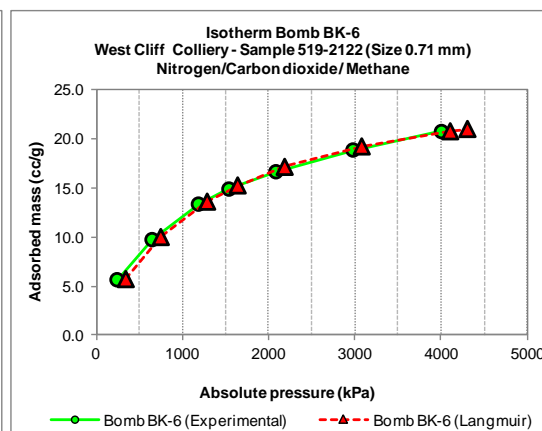
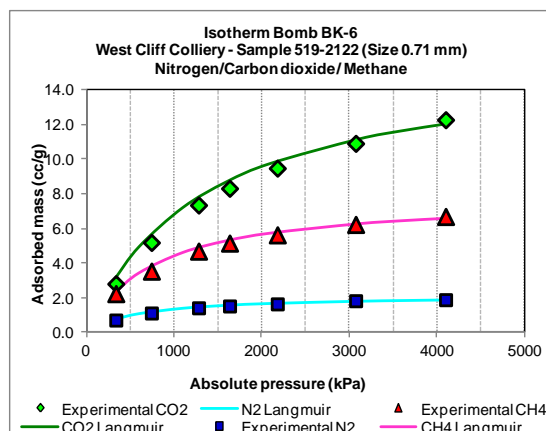
APPENDIX 23 – Ternary N₂/CO₂/CH₄ mixed adsorbed mass in adsorption



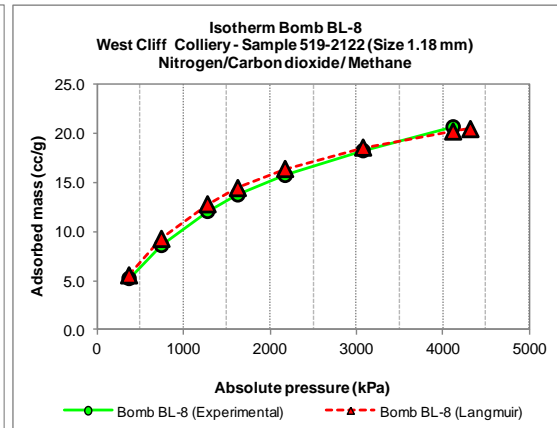
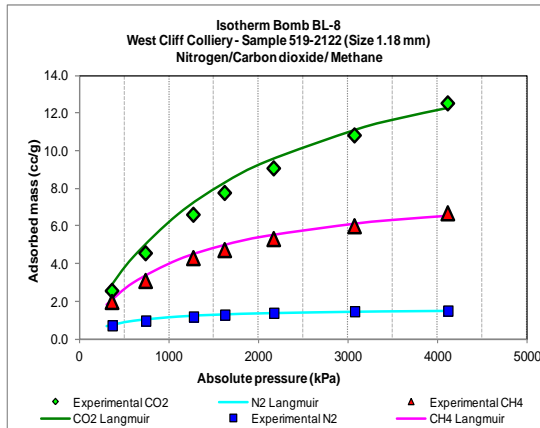
N₂, CO₂, CH₄ gas and their mixed adsorbed mass in adsorption – Sample BA-7



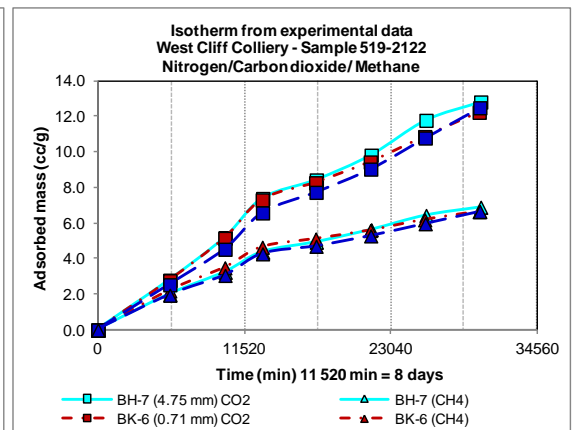
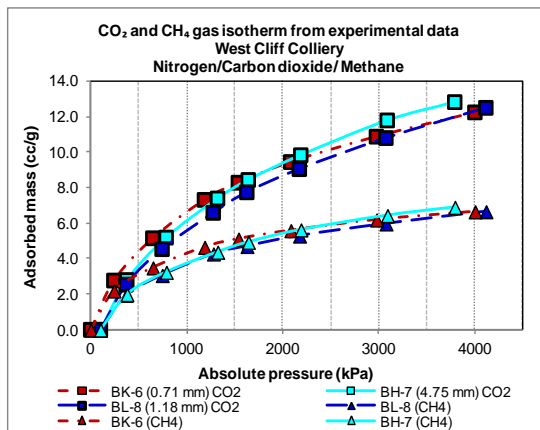
N₂, CO₂, CH₄ gas and their mixed adsorbed mass in adsorption – Sample BH-7



N₂, CO₂, CH₄ gas and their mixed adsorbed mass in adsorption – Sample BK-6

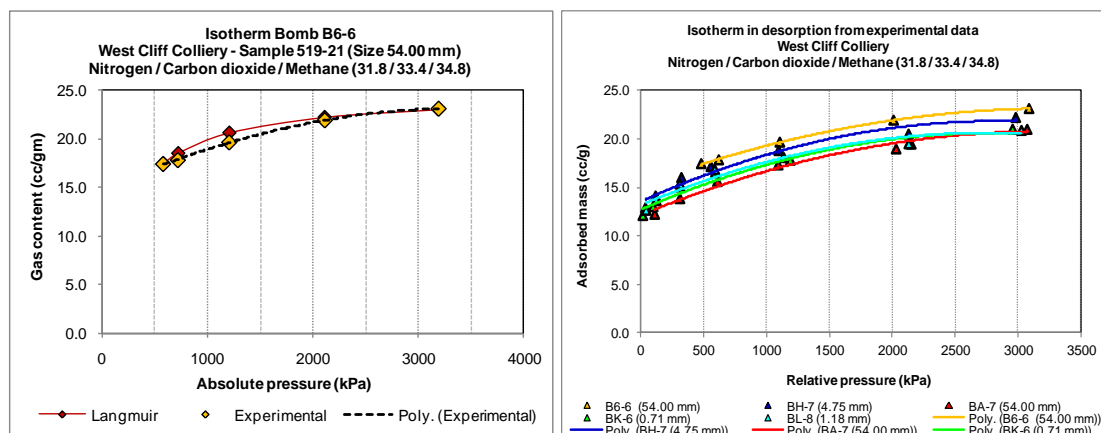


N₂, CO₂, CH₄ gas and their mixed adsorbed mass in adsorption – Sample BL-8

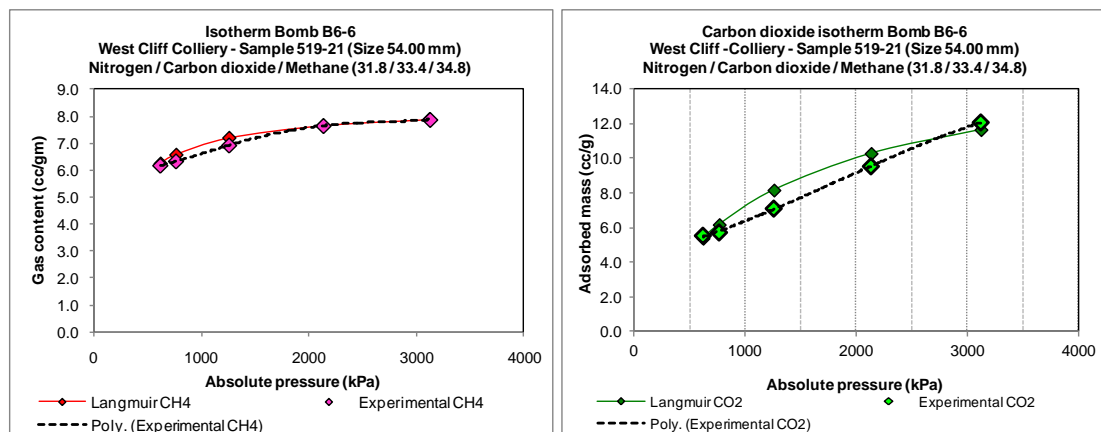


CO₂ and CH₄ adsorbed mass against pressure and time

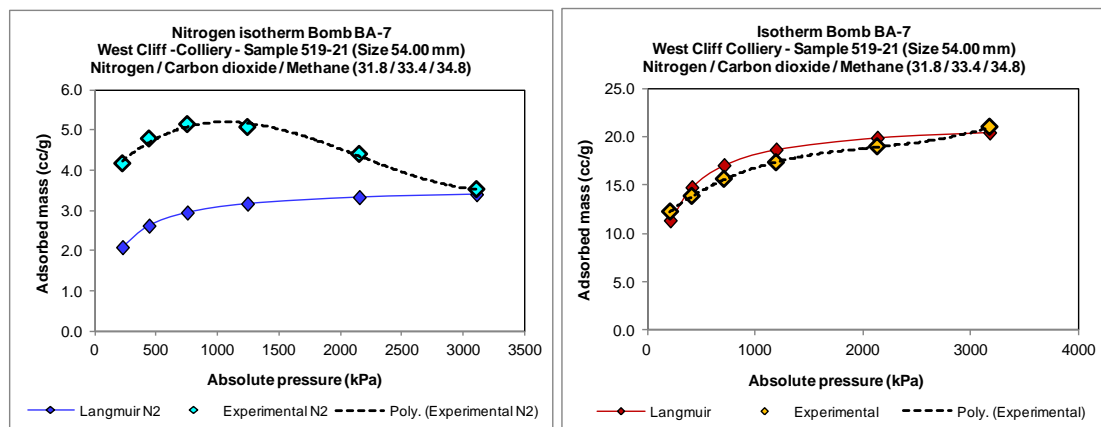
APPENDIX 24 – Ternary N₂/CO₂/CH₄ mixed adsorbed mass in desorption



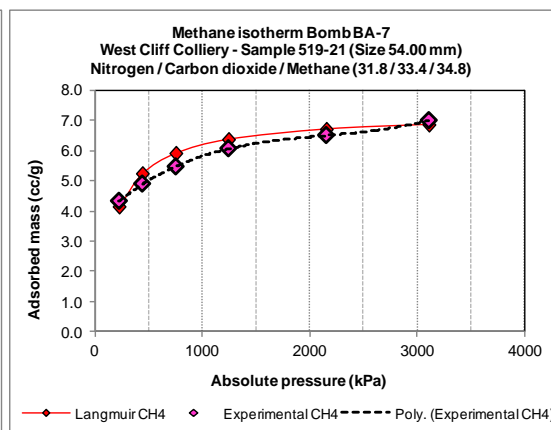
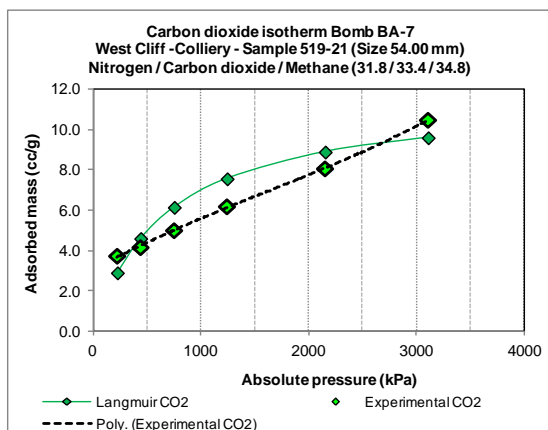
Mixed gas adsorbed mass in desorption



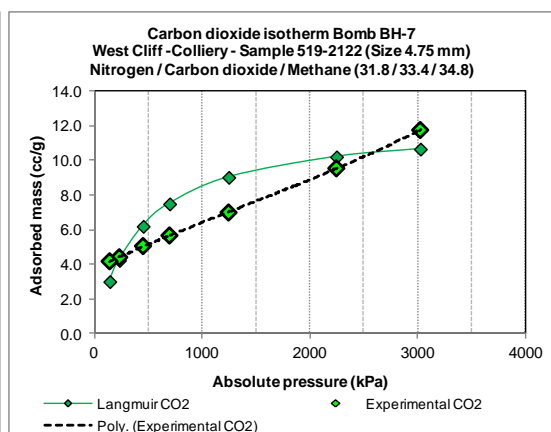
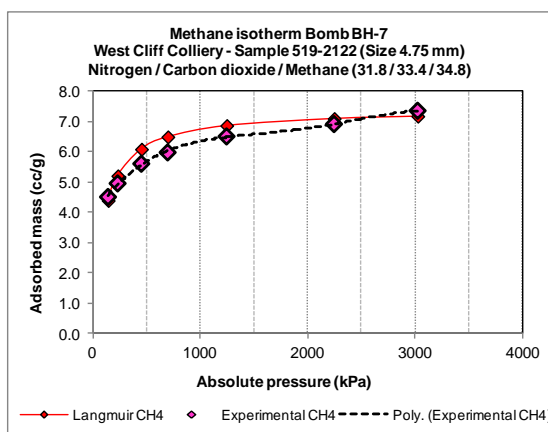
CO₂ and CH₄ components adsorbed mass in desorption – Sample B6-6



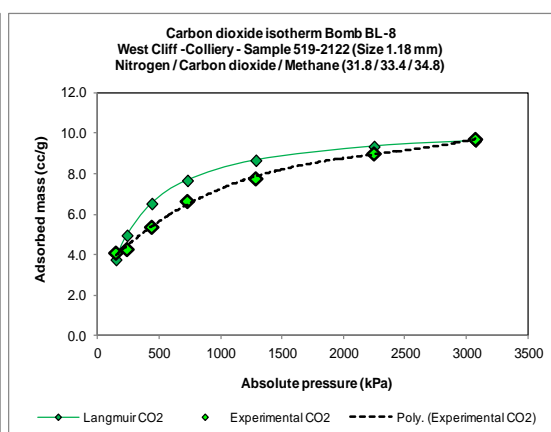
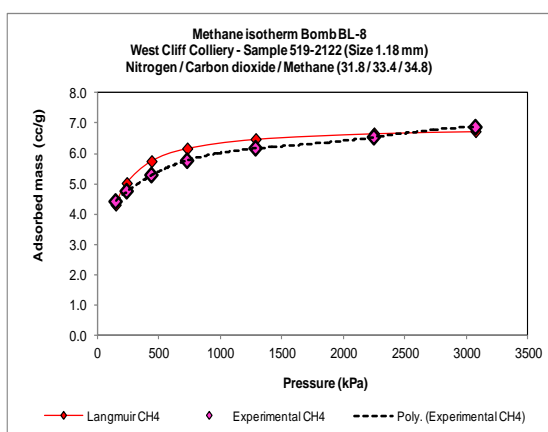
N₂ and mixed adsorbed mass in desorption – Sample BA-7



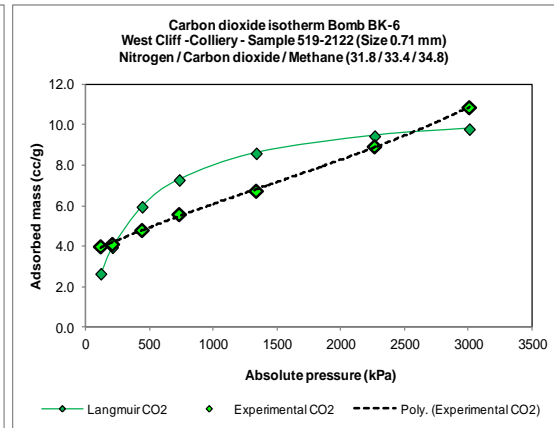
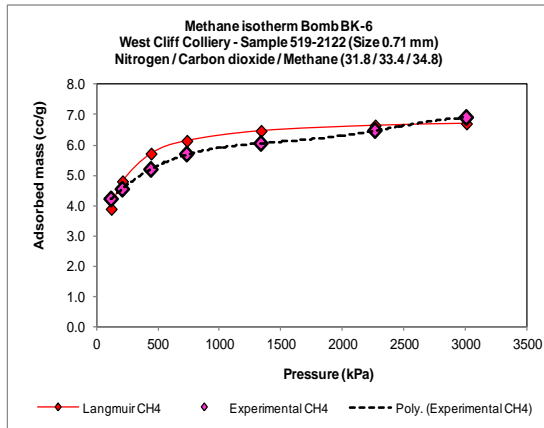
CO₂ and CH₄ components adsorbed mass in desorption – Sample BA-7



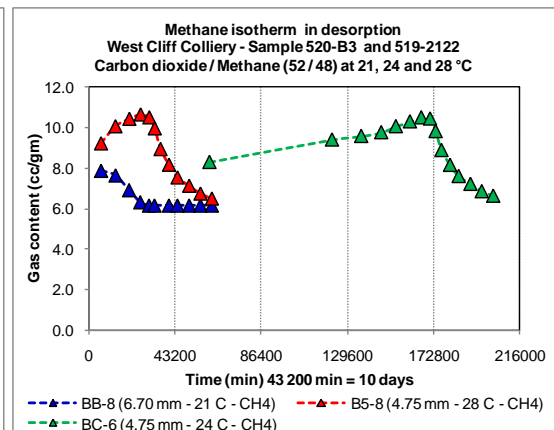
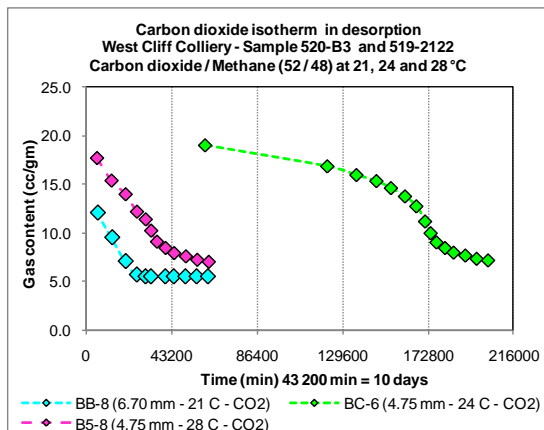
CO₂ and CH₄ components adsorbed mass in desorption – Sample BH-7



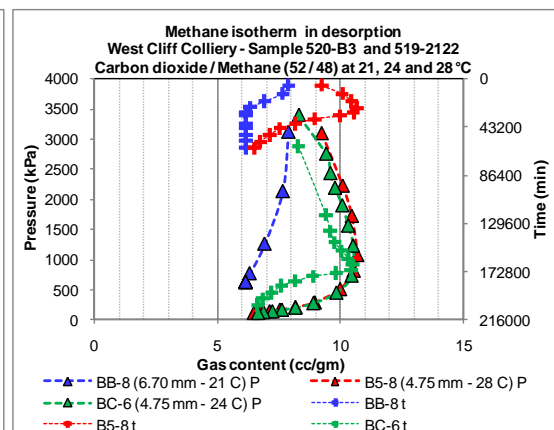
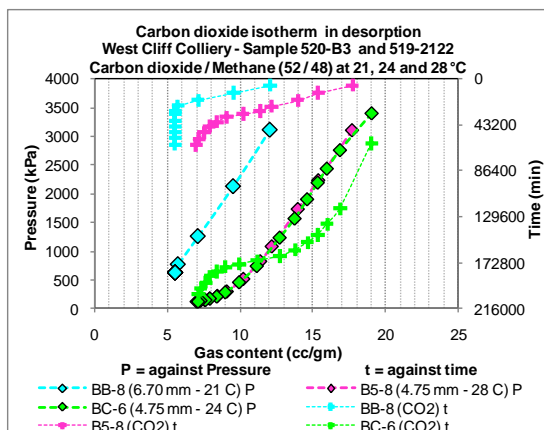
CO₂ and CH₄ components adsorbed mass in desorption – Samples BL-8



CO₂ and CH₄ components adsorbed mass in desorption – Samples BK-6



CO₂ and CH₄ adsorbed mass acting individually against time, in desorption



CO₂ and CH₄ adsorbed mass acting individually against time and pressure, in desorption

REFERENCES

- Alcaniz-Mongue, J., A. Linares-Solano and B. Rand (2001). "Mechanism of adsorption of water in carbon micropores as revealed by a study of activated carbon fibers." J. Phys. Chem. Ref. Data **106**(12): 3209–3216.
- Allardice, D. J. and D. G. Evans (1971). "The brown coal/water system: Part 2. Water sorption isotherms on bed-moist Yallourn brown coal" Fuel **50**: 236–253.
- Armstrong, M., P. Hatherly and S. Thomson (2006). Determining the Controls for Strata Gas and Oil Distribution within Sandstone Reservoirs Overlying the Bulli Seam. Proceedings of Coal Operators Conference. Wollongong, NSW, Australia.
- Arri, L. E. and D. Yee (1992). Modeling Coaled Methane Production with Binary Gas Sorption. SPE Paper 24363, Casper, WY.
- Aziz, N., A. Hutton and B. Indraratna (1996). The effect of gas pressure on coal strength. 15th international ground control conference, August 13-15. Golden Colorado, USA: 209-226.
- Aziz, N. and W. Ming-Li (1999). "The effect of sorbed gas on the strength of coal - an experimental study." Geotechnical and Geological Engineering **17**: 387-402.
- Black, D. and N. Aziz (2009). Reducing Coal Mine GHG Emissions Through Effective Gas Drainage and Utilisation. Underground Coal Operators' Conference.
- Bratek, K., W. Bratek, I. Gerus-Piasecka, S. Jasienko and P. Wilk (2002). "Properties and structure of different rank anthracites." Fuel **81**: 97–108.
- Brennan, J. K., T. J. Bandosz, K. T. Thomson and K. E. Gubbins (2001). "Water in porous carbons." Elsevier, Colloids and Surfaces A: Physicochemical and Engineering Aspects **187–188**: 539–568.

Brunauer, S. (1945). The adsorption of gases and vapors. New York, Oxford University Press.

Busch, A. and Y. Gensterblum (2011). "CBM and CO₂-ECBM related sorption processes in coal: A review." International Journal of Coal Geology **87**: 49–71.

Busch, A., Y. Gensterblum, B. M. Kroos and R. Littke (2004). "Methane and carbon dioxide adsorption–diffusion experiments on coal: upscaling and modeling." Int. J. Coal Geol(60): 151–168.

Busch, A., Y. Gensterblum and B. M. Krooss (2007). "High-pressure sorption of nitrogen, carbon dioxide and their mixtures on Argonne premium coals." Energy and Fuels **21**: 1640–1645.

Busch, A., Y. Gensterblum, B. M. Krooss and N. Siemons (2006). "Investigation of high-pressure selective adsorption/desorption behaviour of CO₂ and CH₄ on coals: An experimental study." International Journal of Coal Geology **66**: 53– 68.

Busch, A., Y. Gensterblum and B. M. Kross (2003). "Methane and CO₂ sorption and desorption measurements on dry Argonne premium coals: pure components and mixtures." Int. J. Coal Geol **55**: 205-224.

Busch, A., Y. Gensterblum, N. Siemons, B. M. Krooss, H. J. M. F. van Bergen and P. D. Pagnier (2003). Investigation of Preferential Sorption Behaviour of CO₂ and CH₄ on Coal by High Pressure Adsorption/Desorption Experiments with Gas Mixtures, Paper No. 0350. International Coalbed Methane Symposium, University of Alabama. Tuscaloosa, Alabama, May 5-9 2003.

Ciu, X., R. M. Bustin and D. Gregory (2004). "Selective transport of CO₂, CH₄, and N₂ in coals: insights from modelling of experimental gas adsorption data." Fuel **83**: 293-303.

Clarkson, C. R. and R. M. Bustin (1996). "Variation in micropore capacity and size distribution with composition in bituminous coal of the Western Canadian Sedimentary Basin: Implications for coalbed methane potential." Fuel **75**(13): 1483-1498.

Clarkson, C. R. and R. M. Bustin (2000). "Binary gas adsorption/desorption isotherms: effect of moisture and coal composition upon carbon dioxide selectivity over methane." International Journal of Coal Geology **42**: 241–271.

Condon, J. B. (2006). "Surface Area and Porosity Determinations by Physisorption." Elsevier, Amsterdam.

Cram, K. (2008). New South Wales Coal Statistics 2007-2008, Coal services Pty. Limited data source 2007-2008. Corrimal, NSW, Australia.

Crosdale, P. J. (1998). Degassing of Methane and Carbon dioxide: Prediction of gas composition. ACARP Project C5037, James Cook University.

Crosdale, P. J. (1999). Mixed methane/carbon dioxide sorption by coal: new evidence in support of pore-filling models. Proceedings International Coalbed Methane Symposium, Tuscaloosa, Alabama.

Crosdale, P. J. and B. B. Beamish (1993). In Proceedings, New Developments in Coal Seam Development Symposium, Brisbane.

Cui, X., R. M. Bustin and D. Gregory (2004). "Selective transport of CO₂, CH₄, and N₂ in coals: insights from modelling of experimental gas adsorption data." Fuel 2004, 83, 293-303.

Curl, S. J. (1978). Methane production in coal mines. London, International Energy Agency of Coal Research: Report No ICTIS/TR04.

Day, S., G. Duffy, R. Sakurovs and S. Weir (2007). "Effects of coal properties on sorption capacity under supercritical conditions." International Journal of Greenhouse Gas Control **doi:10.1016/S1750-5836(07)00120-X**.

Day, S., R. Fry and R. Sakurovs (2008). "Swelling of Australian coals in supercritical CO₂." International Journal of Coal Geology **74**: 41–52.

Day, S., R. Sakurovs and S. Weir (2008). "Supercritical gas sorption on moist coals." International Journal of Coal Geology **74**: 203–214.

Dubinin, M. M. and V. A. Astakhov, Eds. (1971). Description of adsorption equilibria of vapors on zeolites over wide ranges of temperature and pressure. Advances in Chemistry Series, No. 102, American Chemical Society Publications. Washington, DC.

Ettinger, I., I. Eremin, B. Zimakov and M. Yanovskaya (1966). "Natural factors influencing coal sorption properties. I: Petrography and sorption properties." Fuel **45**: 267-275.

Faiz, M., A. Saghafi, N. Sherwood and I. Wang (2007). "The influence of petrological properties and burial history on coal seam methane reservoir characterisation, Sydney Basin, Australia." International Journal of Coal Geology **70**(1-3): 193-208.

Faiz, M., L. Stalker, N. Sherwood, A. Saghafi, M. Wold, S. Barclay, J. Choudhury, W. Barker and I. Wang (2003). "Bio-enhancement of coal bed methane resources in the southern Sydney Basin." Journal of the Australian Petroleum Production and Exploration Association **43**: 595-610.

Faiz, M. M., N. I. Aziz, A. C. Hutton and B. Jones (1992). Porosity and gas sorption capacity of some eastern Australian coals. Proceedings of the Symposium on coalbed methane research and development in Australia. B. Beamish, Gamson, P. (Eds.). James Cook University of North Queensland, Townsville, Queensland, Australia. **4**: 9–20.

Faiz, M. M. and A. C. Hutton (1995). Geological controls on the distribution of CH₄ and CO₂ in coal seam gas of the Southern Coalfield, NSW, Australia. Proceedings of the International Symposium-cum-workshop on management and control of high gas emissions and outbursts in underground coal mines. R. D. Lama (ed). Wollongong, NSW, Australia: 375–383.

Faiz, M. M. and A. C. Hutton (1997). "Coal seam gas in the southern Sydney Basin, New South Wales." Journal of the Australian Petroleum Exploration Association **37**(1): 415–428.

Fitzgerald, J. E., Z. Pan, M. Sudibandriyo, R. L. J. Robinson, K. A. M. Gasem and S. Reeves (2005). "Adsorption of methane, nitrogen,

carbon dioxide and their mixtures on wet Tiffany coal." Fuel **84**(18): 2351-2363.

Florentin, R., N. Aziz, D. Black and L. Nghiem (2009). Sorption Characteristics of Coal, Particle Size, Gas Type and Time. Proceedings of Coal Operators Conference, 12-13 February. Wollongong, NSW, Australia: 208-216.

Florentin, R., N. Aziz, D. Black and L. Nghiem (2010 c). Binary Carbon Dioxide/Methane Adsorption on Fragmented Coals – A Laboratory Study. Proceedings of the 17th Congress of Turkey, 2-4 June. Zonguldak, Turkey: 369-381.

Gamson, P. D. and B. B. Beamish (1992). Coal type, microstructure and gas flow behaviour of Bowen Basin coals. Proceedings of the Symposium on coalbed methane research and development in Australia. James Cook University of North Queensland, Townsville, Queensland, Australia. **4**: 43–66.

Gan, H., S. P. Nandi and P. L. Walker, Jr. (1972). "Nature of the porosity in American coals." Fuel **51**: 272-277.

Goodman, A. L., A. Busch, G. J. Duffy, J. E. Fitzgerald, K. A. M. Gasem, Y. Gensterblum, B. M. Krooss, J. Levy, E. Ozdemir, Z. Pan, R. L. J. Robinson, K. Schroeder, M. Sudibandriyo and C. M. White (2004). "An Inter-laboratory Comparison of CO₂ Isotherms Measured on Argonne Premium Coal Samples." Energy Fuels **18**(4): 1175–1182.

Gray, I. (1987). "Reservoir Engineering in Coal Seams: Part 1 – The Physical Process of Gas Storage and Movement in Coal Seams, SPE 12514." SPE Reservoir Engineering **2**(1): 28-34.

Gregg, S. J. and K. S. W. Singh (1982). Adsorption, Surface Area and Porosity. London, 2nd ed, Academic Press.

Gunter, W. D., B. Wiwchar and E. H. Perkins (1997). "Aquifer disposal of CO₂-rich greenhouse gases; extension of the time scale of experiment for CO₂-sequestering reactions by geochemical modelling." Mineralogy and Petrology **59**(1-2): 121-140.

Gunther, J. (1965). "Study of the gas coal relationship." Rev. Ind. Min. **Vol. 47**(10).

Hall, F. E., C. Zhou, K. A. M. Gasem, R. L. J. Robinson and D. Yee (1994). Adsorption of Pure Methane, Nitrogen, and Carbon Dioxide and Their Binary Mixtures on Wet Fruitland Coal, SPE Paper 29194. Eastern Regional Conference and Exhibition. Charleston, WV: 329–344.

Hanzawa, Y., K. Kaneko, N. Yoshizawa, R. W. Pekala and M. S. Dresselhaus (1998). "The pore structure determination of carbon aerogels." Adsorption **4**: 187–195.

Hargraves, A. J. (1963). Instantaneous outbursts of coal and gas, The University of Sydney. **PhD thesis**: 323, unpublished.

Harpalani, S. (2005). Gas flow characterization of Illinois coal - Final technical report. Support by the Illinois Department of Commerce and Economic Opportunity through the Office of Coal Development and the Illinois Clean Coal Institute, ICCI Project Number: 03-1/7.1B-2.

Harpalani, S. and G. Chen (1995). "Estimation of changes in fracture porosity of coal with gas emission." Fuel **74**(10): 1491-1498.

Harpalani, S. and G. Chen (1995). "Estimation of changes in fracture porosity of coal with gas emission." Fuel **Vol. 74**(10): pp. 1491-1498.

Harpalani, S., B. K. Prusty and P. Dutta (2006). "Methane/CO₂ Sorption Modelling for Coalbed Methane production and CO₂ sequestration." Energy and Fuels **20**(4): 1591-1599.

Harpalani, S. and R. A. Schraufnagel (1990). Influence of Matrix Shrinkage and Compressibility on Gas Production From Coalbed Methane Reservoirs, paper SPE 20729. SPE Annual Technical Conference and Exhibition. New Orleans, Louisiana, 23-26 September. .

Iiyama, T., K. Nishikawa, T. Suzuki and K. Kaneko (1997). "Study of the structure of a water molecular assembly in a hydrophobic nanospace at low temperature with in situ X-ray diffraction." Chemical Physics Letters **274**: 152–158.

ISRM (1981). The complete ISRM suggested methods for rock characterisation, testing and monitoring, E T Brown (Ed), Pergamon Press, UK.

Janowsky, U. (1984). Experimentelle Untersuchungen zum Strömungs-und Sorptionsverhalten von Wasser und Gasen in Steinkohle und Ableitung eines Porenmodells. Diss., 144p, University of Essen, Essen.

Jolly, Morris and Hinsley (1968). "An investigation into the relationship between the methane sorption capacity of coal and gas pressure." The Mining Engineering, No. 94, July 1968, Trans. AIME Vol. 127.

Karge, H., J. Weitkamp and D. M. Ruthven (2008). "Fundamentals of adsorption equilibrium and kinetics in microporous solids, adsorption and diffusion. Molecular Sieves—Science and Technology." Springer Berlin/Heidelberg: 1–43.

Kelemen, S. R. and L. M. Kwiatak (2009). "Physical properties of selected block Argonne Premium bituminous coal related to CO₂, CH₄, and N₂ adsorption." International Journal of Coal Geology 77(2-9).

Kelemen, S. R., L. M. Kwiatak and A. G. K. Lee (2006). Swelling and Sorption Response of Selected Argonne Premium Bituminous Coals to CO₂, CH₄, and N₂, Paper No. 0604. International Coalbed Methane Symposium, University of Alabama. Tuscaloosa, AL, 2006.

King, G. R. and T. M. Ertekin (1989). A survey of mathematical models related to methane production from coal seams, Part 1: Empirical and equilibrium sorption models. Proc. 1989 Coalbed Methane Symposium, Univ. Alabama April 17-20, 1989: 125-138.

Koperna, G., A. Oudinot, G. R. McColpin, J. Heath, N. Liu, A. Wells and G. Young (2009). CO₂-ECBM/Storage Activities at the San Juan Basin's Pump Canyon test site, SPE 124002. International CBM Symposium, Alabama, 2009.

Krooss, B. M., F. van Bergen, Y. Gensterblum, N. Siemons, H. J. M. Pagnier and P. David (2002). "High-pressure methane and carbon

dioxide adsorption on dry and moisture-equilibrated Pennsylvanian coals." International Journal of Coal Geology **51**: 69–92.

Lama, R. D. (1988). "Adsorption and desorption of mixed gases on coal and their implications in mine ventilation." Fourth international mine ventilation congress: Brisbane, Qld, Australia, pp. 161-174.

Lama, R. D. (1995). Effect of stress, gas pressure and vacuum on permeability of Bulli coal samples. Proceedings of International Symposium on Management and Control of High Gas Emissions and Outbursts in Underground Coal Mines, 20-24 March. Wollongong, NSW, Australia: 293-301.

Lama, R. D. and H. Bartosiewicz (1982). Determination of gas content of coal seams. Seam gas drainage with particular reference to the working seam. A. J. e. Hargraves, The Australian Institute of mining and metallurgy, Illawara Branch, University of Wollongong: pp. 36-52.

Langmuir, I. (1918). "The adsorption of gases on plane surfaces of glass, mica and platinum." Journal of the American Chemical Society **40**(9): 1361-1403

Langmuir, I. (1918). "The adsorption of gases on plane surfaces of glass, mica and platinum." Journal of the American Chemical Society **40** (9): 1361-1403

Langmuir, I. (1933). Surface chemistry. Chem. Rev. Washington, DC, 13, 147.

Levine, J. R. (1996). "Model study of the influence of matrix shrinkage on absolute permeability of coal bed reservoirs." Coalbed Methane and Coal Geology, R Gayer and I. Harris (eds.), Geological Society Special Publication, **109**: 197-212.

Levy, J. H., S. J. Day and J. S. Killingley (1997). "Methane capacities of Bowen Basin coals related to coal properties." Fuel **76**: 813–819.

Mahajan, O. P. and P. L. Walker Jr., Eds. (1978). Porosity of coals and coal products. Analytical methods for coal and coal products, vol. 1, Academic Press. New York, 125–162.

Mazumder, S., N. Siemons and K. H. Wolf (2006). Differential Swelling and Permeability Change of Coal in Response to CO₂ Injection for Enhanced Coalbed Methane, Paper No. 0602. International Coalbed Methane Symposium, University of Alabama. Tuscaloosa, AL, 2006.

McCutcheon, A. L., W. A. Barton and M. A. Wilson (2003). "Characterisation of water adsorbed on bituminous coals." Energy Fuels **17**: 107–112.

Mills, K., R. Jeffreys, D. Black, T. Meyer, K. Carey and S. Goddard (2006). Developing methods for placing sand-propped hydraulic fractures for gas drainage in the Bulli seam. In proceedings of Coal Operators Conference, Coal 06, July 5-7. Wollongong, NSW, Australia: 190-199.

Moffat, D. H. and K. E. Weale (1955). "Sorption by coal of methane at high pressures." Fuel **Vol. 34**(4): pp. 449-462.

Moffat, D. H. and K. E. Weale (1955). "Sorption by coal of methane at high pressures." Fuel **34**(4): 449-462.

Myers, A. L. and J. M. Prausnitz (1965). "Thermodynamics of mixed-gas adsorption." AIChE Journal **11**(1): 121–127.

Nelson, C. R. (2000). Effects of Geologic Variables on Cleat Porosity Trends in Coalbed Gas Reservoirs. SPE/CERI Gas Technology Symposium. 3-5 April 2000, Calgary, Alberta, Canada, Society of Petroleum Engineers.

Ozdemir, E., B. I. Morsi and K. Schroeder (2003). "Importance of volume effects to adsorption isotherms of carbon dioxide on coals." Langmuir **19**: 9764–9773.

Ozdemir, E., B. I. Morsi and K. Schroeder (2004). "CO₂ adsorption capacity of Argonne premium coals." Fuel **83**(7-8): 1084-1094.

Pekot, L. J. and S. R. Reeves (2002). Modelling Coal Matrix Shrinkage and Differential Swelling with CO₂ Injection for Enhanced Coalbed Methane Recovery and Carbon Sequestration Applications.

U. S. D. Contract No. DE-FC26-00NT40924, Washington, DC (November 2002).

Pitard, F. F. (1989). Pierre Gy's Sampling Theory and Sampling Practice, CRC Press, Inc., Boca Raton, Florida.

Puri, R. and D. Yee (1990). Enhanced coalbed methane recovery, SPE Paper 20732. Presented at the 65th Annual Technical Conference and Exhibition of the SPE. New Orleans, LA: 193–202.

Redlich, O. and J. N. S. Kwong (1949). "On the Thermodynamics of Solutions. V. An Equation of State. Fugacities of Gaseous Solutions". Chem. Rev. **44**(2): 233-244.

Reeves, S., R. Gonzalez, K. A. M. Gasem, J. E. Fitzgerald, Z. Pan, M. Sudibandriyo and R. L. J. Robinson (2005). Measurement and Prediction of Single- and Multi-Component Methane, Carbon Dioxide and Nitrogen Isotherms for U.S. Coals, Paper No. 0527. International Coalbed Methane Symposium, University of Alabama. Tuscaloosa, AL, 2005.

Reeves, S. and A. Oudinot (2004). The Tiffany Unit N2 – ECBM Pilot: A Reservoir Modeling Study. Topical Report U.S. Department of Energy, DE-FC26-0NT40924.

Reznik, A. A., P. K. Singh and W. L. Foley (1984). "An analysis of the effect of CO₂ injection on the recovery of in-situ methane from bituminous coal: an experimental simulation." Soc. Pet. Eng. J. **24**: 521-528.

Robertson, E. P. and R. L. Christiansen (2005). Measurement of Sorption-Induced Strain. International Coalbed Methane Symposium, University of Alabama. Tuscaloosa, AL, 2005, Paper No. 0532.

Ruthven, D. M. (1984). Principles of Adsorption and Adsorption Processes, Wiley, New York.

Saghafi, A., M. Faiz and D. Roberts (2007). "CO₂ Storage and Gas Diffusivity Properties of Australian Coals from Sydney Basin." International Journal of Coal Geology **Volume 70**(1–3): 240–254.

Saghafi, A. and D. Roberts (2008). Measurement of CO₂ and CH₄ reservoir properties of coals from Westcliff mine, CSIRO Investigation report ET/IR 1033 R.

Sakurovs, R., S. Day and S. Weir (2009). "Causes and consequences of errors in determining sorption capacity of coals for carbon dioxide at high pressure." International Journal of Coal Geology **77**: 16–22.

Sakurovs, R., S. Day, S. Weir and G. Duffy (2007). "Application of a modified Dubinin–Radushkevich equation to adsorption of gases by coals under supercritical conditions." Energy & Fuels **21**: 992–997.

Sakurovs, R., S. Day, S. Weir and G. Duffy (2008). "Temperature dependence of sorption of gases by coals and charcoals." International Journal of Coal Geology (73): 250–258.

Salame, I. I. and T. J. Bandosz (1998). "Experimental study of water adsorption on activated carbons." Langmuir **15**(2): 587–593.

Seidle, J. P. and L. G. Huitt (1995). Experimental measurement of coal matrix shrinkage due to gas desorption and implications for cleat permeability increases. SPE International Meeting on Petroleum Engineering, Beijing, China.

Sereshki, F. (2005). Improving coal mine safety by identifying factors that influence the sudden release of gases in outburst prone zones, PhD thesis, University of Wollongong.

Setzmann, U. and W. Wagner (1991). "A New Equation of State and Tables of Thermodynamic Properties for Methane Covering the Range from the Melting Line to 625 K at Pressures up to 1000 MPa." J. Phys. Chem. Ref. Data **20**(6): 1061-1151.

Shi, J. Q. and S. Durucan (2003). "Gas Storage and Flow in Coalbed Reservoirs: Implementation of a Bidisperse Pore Model for Gas Diffusion in a Coal Matrix." SPE Res Eval & Eng **8**(2): 169-175. SPE-84342-PA.

Singh, A. K. (1968). Desorption studies of gases from coal. M.Sc. thesis, University of Alberta.

Smith, J. W. and R. J. Pallasser (1996). "Microbial origin of Australian coalbed methane." American Association of Petroleum geologists **80**: 807–891.

Soave, G. (1972). "Equilibrium Constants from a Modified Redlich-Kwong Equation of State." Chem. Eng. Sci. **27**(6): 1197-1203.

Span, R. and W. Wagner (1996). "A New Equation of State for Carbon Dioxide Covering the Fluid Region from the Triple-Point Temperature to 1100 K at Pressures up to 800 MPa." J. Phys. Chem. Ref. Data **25**(6): 1509-1596.

St. George, J. D. and M. A. Barakat (2001). "The change in effective stress associated with shrinkage from gas desorption in coal." International Journal of Coal Geology **45**: 105-113.

Stevenson, M. D., W. V. Pinczewski, M. L. Somers and S. E. Bagio (1991). Adsorption/Desorption of Multicomponent Gas Mixtures at In-Seam Conditions, SPE Paper 23026. SPE Asia-Pacific Conference. Perth, Western Australia: 741–755.

Van Bergen, F., C. Spiers, G. Floor and P. Bots (2009). "Strain development in unconfined coals exposed to CO₂, CH₄ and Ar: Effect of moisture." International Journal of Coal Geology **Vol. 77**: pp. 43-53.

Yang, R. T. (1987). Gas Separation by Adsorption Processes, Butterworth, Boston, MA.

Zuber, M. D., J. L. Saulsberry and D. P. Sparks (1996). Developing and managing the reservoir. J. L. In: Saulsberry, Schafer, P.S., Schraufnagel, R.A. Eds., A Guide to Coalbed Methane Reservoir Engineering. Gas and C. Research Institute Report No. GRI-94r0397, IL, pp. 7-1:7-26.